Using a Gliding Arc Plasmatron for CO_2 conversion

The future in industry?

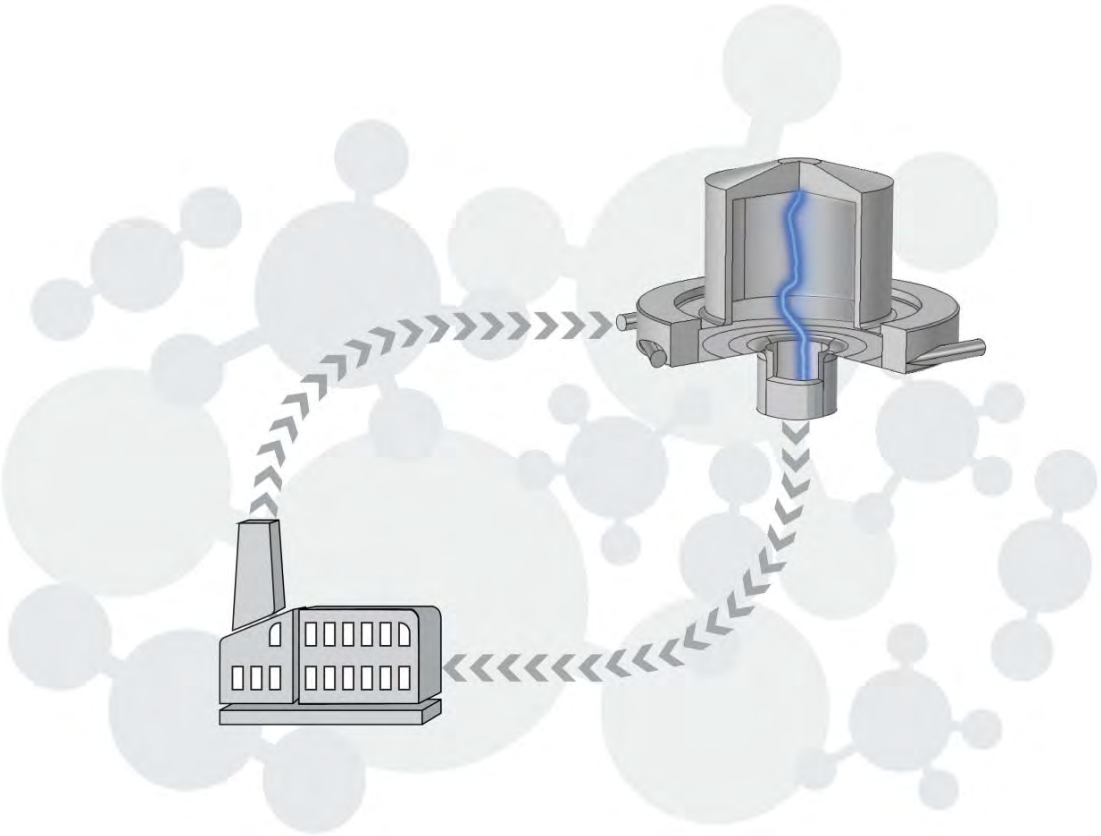

Proefschrift voorgelegd tot het behalen van de graad van
doctor in de wetenschappen aan de Universiteit Antwerpen te verdedigen door

Marleen Ramakers

Promotor: Prof. dr. Annemie Bogaerts

Universiteit Antwerpen

Faculteit Wetenschappen
Departement Chemie

Using a Gliding Arc Plasmatron for CO_2 conversion

The future in industry?

Gebruik van een Gliding Arc Plasmatron voor CO_2 conversie

De toekomst in de industrie?

Proefschrift voorgelegd tot het behalen van de graad
doctor in de wetenschappen: chemie
aan de Universiteit Antwerpen
te verdedigen door

Marleen Ramakers

Promotor: Prof. dr. Annemie Bogaerts
Antwerpen, 2019

Contents

CHAPTER 1 – Background **1**

1 What is plasma? 4

1.1 Thermal plasmas 6

1.2 Non-thermal plasmas 6

1.3 Warm plasmas 7

1.4 Plasma chemistry 8

1.5 CO_2 dissociation channels 10

2 Why plasma-based conversion is interesting? 13

3 Different kinds of plasma reactors 14

3.1 Dielectric barrier discharge (DBD) 14

3.2 Microwave (MW) discharge 15

3.3 Gliding arc (GA) discharge 16

4 Aim of the work and outline of the thesis 21

CHAPTER 2 – CO_2 conversion **25**

1 Description of the experiments 28

1.1 Gliding arc setup 28

1.2 Gas analysis 29

2 Description of the modeling work 31

3 Results and discussion 32

3.1 Effect of power and flow rate on CO_2 conversion, energy cost, and energy efficiency 32

3.2 Effect of the vortex flow on CO_2 conversion, energy cost, and energy efficiency 36
3.3 Comparison of our results with thermal conversion and energy efficiency 39
3.4 Comparison of our results with model calculations and explanation of the underlying mechanisms 41
3.5 Comparison of our results with other types of plasmas, as well as other novel CO_2 conversion technologies 44
4 Conclusions 50
Appendix *55*

CHAPTER 3 – Arc dynamics **67**
1 Description of the experiments 70
2 Description of the modeling work 74
3 Results and discussion 75
3.1 Arc behavior at different conditions 75
3.2 Arc dynamics—modeling results 83
3.3 Influence of arc behavior on CO_2 conversion 86
4 Conclusions 89
Appendix *91*

CHAPTER 4 – Combining CO_2 conversion and N_2 fixation **93**
1 Description of the experiments 96
1.1 Gliding arc setup 96
1.2 Product analysis 97
2 Description of the model 98

3 Results and discussion 99
3.1 CO_2 conversion, energy cost and energy efficiency 99
3.2 Analysis of the byproducts - NOx concentrations 102
3.3 Underlying mechanisms as revealed by computer simulations 112
3.4 Comparison of gliding arc plasmatron with dielectric barrier discharge 120
3.4.1 CO_2 conversion, energy cost and energy efficiency 120
3.4.2 Byproduct formation 123
4 Conclusions 127
Appendix *133*

CHAPTER 5 – Dry reforming **149**
1 Description of the experiments 152
2 Description of the model 153
3 Results and discussion 154
3.1 Measured conversion, energy efficiency, and energy cost 154
3.2 Measured product selectivities 158
3.3 Comparison of measured and calculated conversion and energy efficiency 160
4 Conclusions 163
Appendix *170*

CHAPTER 6 – Multi-reforming **177**
1 Results and discussion 180
1.1 Effect of applied current and gas flow rate 180
1.2 Effect of N_2 addition 186

2 Conclusions 189
Appendix *191*

CHAPTER 7 – The road to industry? 193
1 Techno-economic analysis 196
1.1 Methods 196
1.2 Results and discussion 197
1.3 Conclusions 206
2 Investigation routes for industrialization 207
Appendix *212*

SUMMARY 219

SAMENVATTING 223

PUBLICATIONS 227

CONFERENCE CONTRIBUTIONS 228

AWARDS 230

COLLABORATIONS 231

DANKWOORD – ACKNOWLEDGEMENTS 233

CHAPTER 1

Background

The problems associated with global warming are gaining more and more attention into public media. It is very clear that the impact of our human life changes climate, which has devastating consequences. Therefore, the world faces a huge challenge. This challenge lies within limiting the emission of greenhouse gases. Indeed, it is the enormous amount of greenhouse gases we dump into the atmosphere that causes global warming. People must be made aware, in order for a change in lifestyle, which avoids the emission of harmful greenhouse gases. However, not every emission can be avoided. For these unavoidable emissions we have to find a solution. The proposed solution is to convert CO_2 and CH_4, the two main greenhouse gases, into useful chemicals and fuels. This conversion is however not easy and requires a lot of energy due to the strong C=O bond. The technology that is investigated in this thesis to efficiently convert CO_2 is plasma-based conversion.

First, an introduction on plasmas will be given. Next, the question why plasma-based conversion might be an interesting conversion technology will be answered. Subsequently, different kinds of plasma setups will be described, with specific detail for the plasma setup used in this thesis. Finally, the aim of the work and outline of the thesis are given.

1 What is plasma?

Lightning is an example of naturally produced plasma, of which the appearance resembles the most to the plasma used in this thesis. However, there are many more examples of both natural and anthropogenic plasmas. They often get referred to as the 'fourth state of matter', next to solid, liquid and gas (see Figure 1). A plasma is a (partially) ionized gas, which consists of several reactive species, such as ions, electrons, radicals and excited species. The latter provide the most important characteristic of plasma: the emission of light.

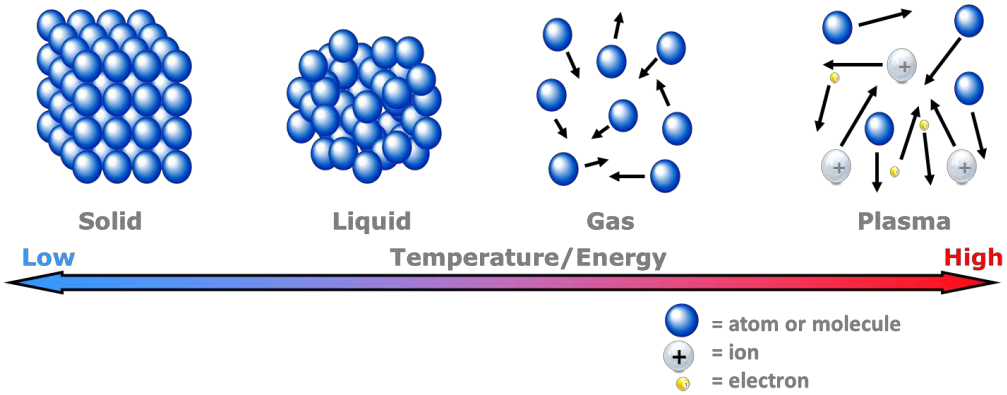

Figure 1 Plasma is the 'fourth state of matter', next to solid, liquid and gas.

Within the anthropogenic plasmas, we can distinguish two groups based on temperature, i.e., fusion (or high-temperature) plasmas and gas discharges (or low-temperature plasmas). For gas conversion technology we are more interested in the latter. This group can be divided into two sub-groups based on thermal equilibrium. The different species in a plasma (electrons, ions, neutrals) and their degrees of freedom (translational, rotational, vibrational, and electronic excitation) each are characterized by a certain temperature. If the temperature of these species is the same, it is called thermal plasma (LTE; local thermal equilibrium). When the temperatures differ, the discharge is called non-thermal plasma (non-LTE). These concepts are further explained in

the next sections. An overview of the different types of plasmas is made in Figure 2.

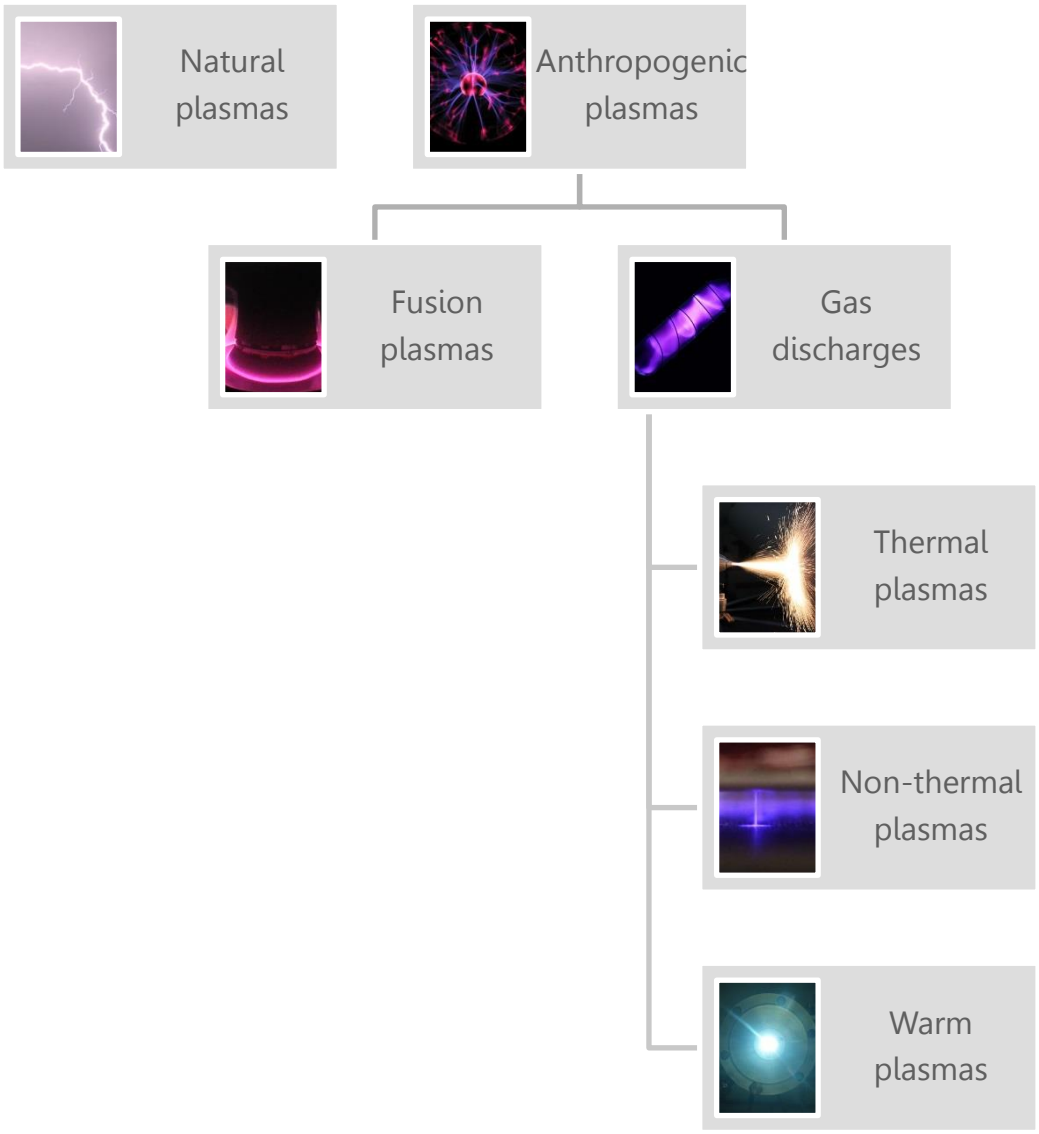

Figure 2 Overview of the different types of plasmas.

1.1 Thermal plasmas

Thermal plasmas are typically obtained by either a high temperature or a high gas pressure (leading to high temperature). The temperature depends on the ease of ionization and ranges from 4000 to 20,000 K.[1] The pressure affects the number of collisions that occur. During collisions between heavy particles (e.g., gas molecules or atoms) and electrons, the latter lose a small portion of the energy they previously received from the electric field during their mean free path in between collisions. Multiple of these collisions lead to an equilibrium between the electron and heavy particle temperature.

Due to the interesting characteristics, such as high temperature, high intensity of non-ionizing radiation and high-energy density, thermal plasmas are widely used. A few examples of such applications are metallurgy (e.g., welding and cutting), fine powder synthesis, coating technology and treatment of hazardous waste materials.[2]

However, the abovementioned characteristics make them in principle less suitable for efficient conversion. This is because chemical and ionization processes are determined by the temperature in thermal plasmas. The maximum energy efficiency of CO_2 conversion is thereby limited to the thermodynamic equilibrium efficiency of 47 % at 3500 K. In non-thermal plasmas on the other hand, reactions are determined by multiple temperatures, as further explained in the next section.

1.2 Non-thermal plasmas

Typical for a non-thermal plasma is that the electrons have a much higher temperature than the heavy particles. The presence of different species in a plasma, each with their own temperature, makes the distribution quite complex. However, generally there is a certain order. That is, the temperature of the electrons (T_e) is the highest. This is followed by the vibrationally excited molecules (T_v). The neutral species (T_0 or the gas temperature T_g), the ions (T_i), and the rotational degrees of freedom of

the molecules (T_r) share the lowest temperature. Hence, the distribution can be expressed as follows:[3]

$T_e >> T_v > T_r \approx T_i \approx T_0$

Most often the electron temperature is in the order of 1 eV (~ 10,000 K), while the gas temperature is much lower and in some cases can remain as low as room temperature. Due to the small mass of the electrons, it allows them to be easily accelerated by the applied electric field, resulting in a high electron temperature. This is in contrast with the heavy particles, which cannot be easily accelerated due to their large mass. During elastic collisions of heavy particles with electrons, the latter lose less energy due to the large mass difference and they can easily keep their high energy gained from the electric field.

The highly energetic electrons can, besides elastic collisions, also give rise to inelastic collisions. As example, the electron impact ionization reactions sustain the plasma by generating new electrons and ions. Electron impact dissociation (and excitation) reactions, on the other hand, create highly reactive (or energetic) gas species. Electrons are thus the initiators of the highly reactive chemical mixture, which is the key advantage of non-thermal plasma. In this way, unreactive gases such as CO_2 can be converted at room temperature by the highly energetic electrons. There is no need to heat the entire reactor or the gas, since the discharge and the associated reactions are initiated by applying an electric field. Because of this reason, lab-scale efficiencies of up to 90 % have already been reported in non-thermal plasmas.[3]

1.3 Warm plasmas

Whereas thermal plasma has a high electron density and a non-thermal discharge proves a high level of non-equilibrium, these properties can be combined in a warm plasma. These kinds of plasmas have a high power for efficient reactor productivity and a high degree of non-equilibrium to

selectively populate certain degrees of freedom, like vibrationally excited states (see section 1.5 below).[4] Warm discharges are non-equilibrium discharges, which are not only able to supply (re)active species, but also some controlled level of translational temperature. The translational gas temperature is still much lower than the electron temperature (non-equilibrium), but it is significantly higher than room temperature and reaches values up to 2000 – 3000 K. Hence, warm plasmas are able to create the advantage of non-equilibrium, and at the same time influence the chemical kinetics due to a higher gas temperature.

It is not the elevated temperature that makes these discharges most interesting for CO_2 conversion, but rather the characteristic electron energy distribution. This leads most of the electron energy into vibrational excitation of CO_2 as will be discussed in section 1.5 below. CO_2 dissociation through vibrational excitation is known as the most energy efficient and therefore most important dissociation channel.[3,5] Recent modeling studies suggest that the higher gas temperature is rather an unwanted effect.[6–8] Thus, the CO_2 conversion and energy efficiency might be further increased in "cooler" warm plasmas.

1.4 Plasma chemistry

Reactions take place by collision of the plasma species. These collisions can be either elastic or inelastic collisions. In the first case the internal energy of the colliding plasma species stays unchanged and the kinetic energy is conserved. In the second case the collision results in an energy transfer from kinetic energy into internal energy.

As previously mentioned, a plasma consists of many species such as molecules, atoms, radicals, ions, electrons, excited species and photons. These species can interact with each other in various ways and at different time scales. The most important plasma chemical processes are shown in Figure 3.

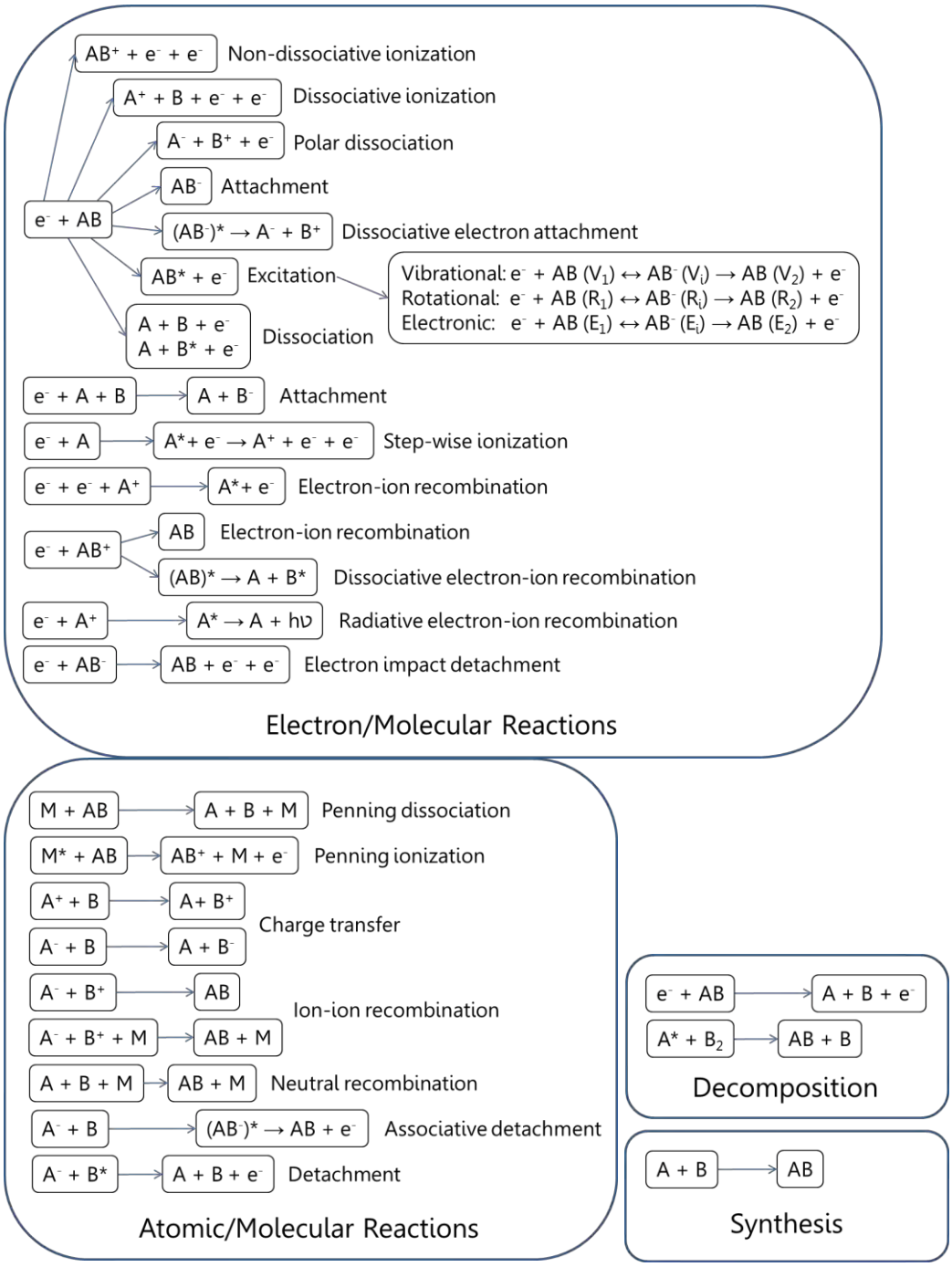

Figure 3 Overview of the main plasma chemical processes. A and B represent atoms and M stands for a temporary collision partner.[3]

First, primary processes such as (electron impact) ionization, excitation, dissociation and charge transfer, generate active species, i.e., radicals, excited species and ions. These reactions occur on a very fast time scale (~ ns). Subsequently, chemical reactions between the primary species, i.e., electrons, radicals, excited molecules and ions, take place as a secondary process within ~ 10 ms.

1.5 CO_2 dissociation channels

The energy added to the plasma, in the form of an electric field, can be transferred by electrons to CO_2 through different channels. It is distributed between elastic energy losses and different channels of excitation, ionization and dissociation. The fraction of energy transferred to the different channels of excitation, ionization and dissociation of CO_2 is presented as a function of the reduced electric field (E/n) in Figure 4.[9] The reduced electric field is the ratio of the electric field in the plasma over the neutral gas density. Each type of plasma has distinctive values of reduced electric field. A dielectric barrier discharge (DBD), which is one of the most commonly studied non-thermal plasma types for CO_2 conversion (see section 3.1 below), has a reduced electric field typically above 200 Td (Townsend; 1 Td = 10^{-21} Vm^2). Microwave (MW) and gliding arc (GA) discharges, on the other hand, typically have values of about 50 Td. They are both categorized as warm plasmas, as will be explained in the next section.

As can be seen in Figure 4, the reduced electric field has a large influence on the distribution of the electron energy among the different channels. In the typical range of MW and GA plasmas (about 50 Td), 90 % of the energy goes into vibrational excitations and only 10 % goes into electronic excitation. Above 200 Td, which is the typical range of a DBD, 70 – 80 % of the electron energy goes into electronic excitation, about 5 % is used for dissociation, 5 % is transferred to ionization (increasing with E/n), while only 10 % goes into vibrational excitation (decreasing

with E/n). The addition of other gases (e.g., Ar, He, N_2, H_2O, H_2, CH_4, etc.) has an influence on the distribution of these channels.[10]

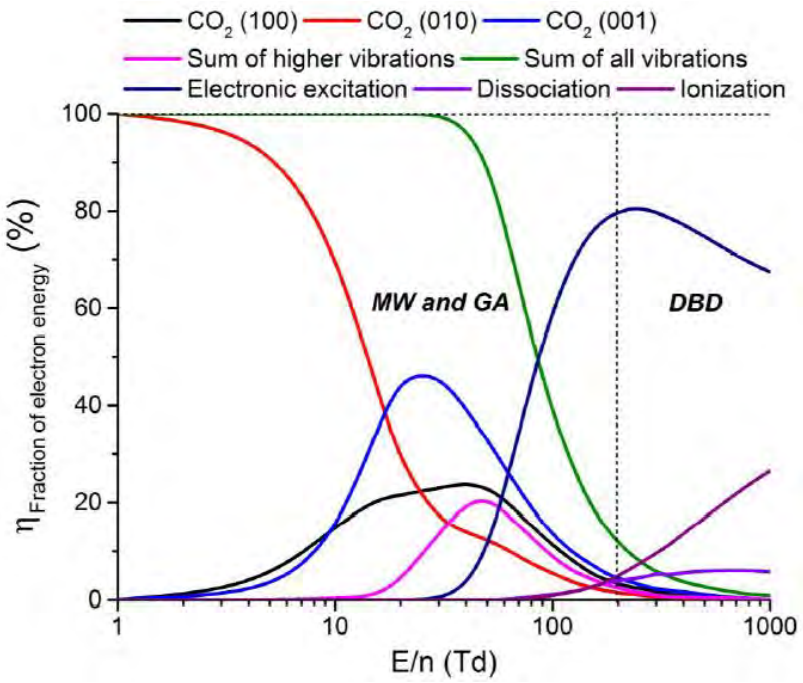

Figure 4 Fraction of electron energy transferred to different channels of excitation, ionization and dissociation of CO_2 as a function of the reduced electric field (E/n). The typical E/n regions for MW, GA and DBD plasma are indicated.[9,11]

The distribution of energy into the different channels, especially the fraction going into vibrational excitation, is important. Indeed, it is known that the vibrational levels of CO_2 play an important role in the efficient dissociation of CO_2. A schematic diagram of some CO_2 electronic and vibrational levels is shown in Figure 5.

For direct electron impact dissociation, an electron needs at least 7 eV to excite CO_2 into a dissociative electronic state, which leads to its dissociation into CO and O. In this way, there is a larger amount of energy spent than the theoretical value necessary for breaking a C=O bond (i.e., 5.5 eV). A more efficient pathway for dissociation is possible based on vibrational excitation of CO_2. It starts with electron impact

vibrational excitation of the lowest vibrational levels. This is followed by vibrational-vibrational (VV) collisions. By this so-called ladder climbing, the higher vibrational levels gradually get populated. Eventually, this leads to the dissociation of the CO_2 molecule (see Figure 5). This pathway is more efficient for dissociating CO_2 since it only needs the minimum amount of 5.5 eV for bond breaking.[9]

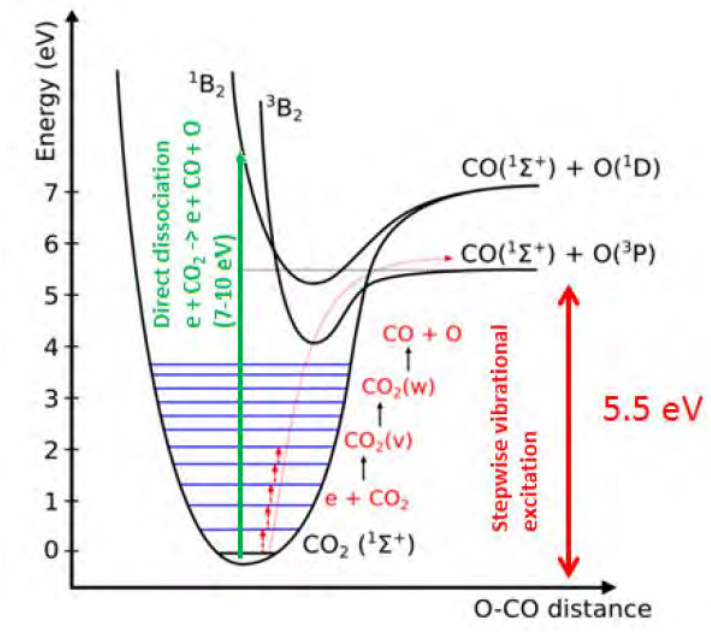

Figure 5 Schematic diagram of some CO_2 electronic and vibrational levels. This diagram shows that much more energy is needed for direct electronic dissociation than for stepwise vibrational excitation, i.e., so-called ladder climbing. Taken from reference 9.

2 Why plasma-based conversion is interesting?

As elaborated above, a plasma contains a variety of species, which can activate efficient conversion routes that are not possible within thermal chemistry. Compared to the latter, it is not necessary to heat the entire reactor or the gas, because the discharge and the associated reactions are easily initiated by applying an electric field. This is a first reason for the increasing interest in plasma-based conversion. Because plasma is an electricity-driven process, it has the potential to use renewable energy sources, such as wind, solar and hydroelectric energy, as power source. The current transition to renewable energy gives plasma a clean electricity source.

Because renewable energy supply is intermittent in nature, this causes an imbalance between the energy production and consumption. Therefore, industry faces specific grid balancing challenges to further integrate renewable energy in its systems.[12] In turn, plasma has the potential to address these issues. It can be easily switched on and off, giving plasma the ability to follow an irregular and intermittent energy supply in a flexible manner. This creates an on-demand storage of energy in a chemical form and a better integration of renewable energy in the chemical industry.[13]

Besides the flexibility due to fast switching on and off, plasma-based gas conversion is a flexible technique, because plasma reactors are modular. Depending on the size of the plant and the quantity of the treated gas, multiple plasma reactors can be placed in parallel to reach the ideal scale. The simple scalability by numbering up the reactors, from watt to megawatt applications is already demonstrated by the successful development of ozone generators.[14] Additionally, the investment cost for the reactors is low (with the largest cost being due to the power supply), because they do not rely on rare-earth materials.[15]

3 Different kinds of plasma reactors

There are a lot of different kinds of plasma reactors, but three setups are most often used for studying CO_2 conversion, i.e., dielectric barrier discharges (DBD), microwave (MW), and gliding arc (GA) discharges. Other, less common types are radiofrequency, corona, atmospheric pressure glow, spark and nanosecond pulsed discharges. A typical example of a non-thermal plasma is the DBD, where the gas is more or less at room temperature, while the electrons have temperatures of 2 - 3 eV (~ 20,000 – 30,000 K). MW and GA discharges are examples of warm plasmas (see above). The gas temperature reaches up to 1000 - 3000 K, and the electron temperature is typically up to a few eV. The characteristic features and operation conditions of the three major plasma types for CO_2 conversion are explained in the following sections.

3.1 Dielectric barrier discharge (DBD)

The most popular and intensively studied plasma reactor is a dielectric barrier discharge (DBD). It has been known for more than a century and is already used on industrial scale for ozone generation.[14] Typically, a DBD is designed as two plane-parallel or concentric metal electrodes, with in between at least one dielectric barrier (e.g., glass, quartz, ceramic material or polymers).[4,14,16,17] The dielectric barrier restricts the electric current and prevents the formation of arcs.[17] The gas flows through the gap between both electrodes, which can vary from less than a mm to several cm.[4,16] Typical examples of DBD configurations are shown in Figure 6. DBDs generally operate at atmospheric pressure (or close by; 0.1 - 10 atm). An alternating voltage (amplitude = 1 – 100 kV) with a frequency of a few Hz to MHz is applied to the electrodes to initiate and maintain the plasma.

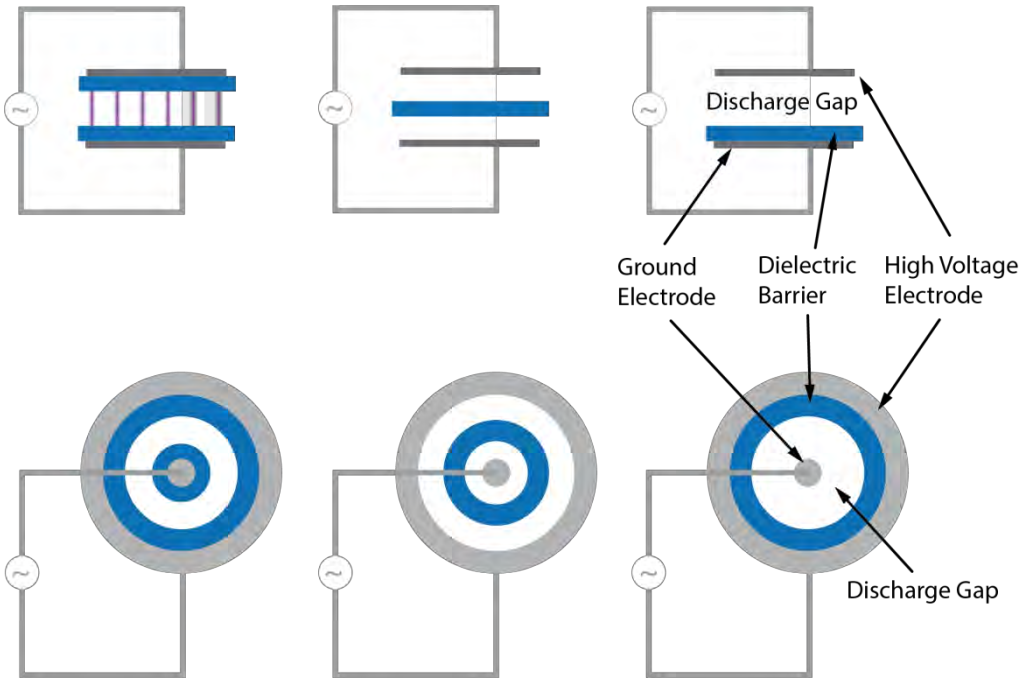

Figure 6 Typical planar (top) and cylindrical (bottom) dielectric barrier discharge configurations. Taken from reference 11.

3.2 Microwave (MW) discharge

Microwave discharges are warm plasmas and operate according to a different principle. The setup does not require electrodes and instead the electric power is applied as microwaves, i.e., electromagnetic radiation with a frequency in the range of 300 MHz to 10 GHz. There are many different types of MW plasmas, e.g., cavity induced plasmas, free expanding atmospheric plasma torches, electron cyclotron resonance plasmas, surface wave discharges, etc. The surface wave discharge is most commonly used for CO_2 conversion research. In this configuration, the gas flows through a quartz tube, which intersects with a rectangular wave guide where the discharge is initiated. This system is shown in Figure 7. Along the interface between the quartz tube and the plasma column, the microwaves propagate and the wave energy is absorbed by the plasma. The wavelength (typically 815 MHz or 2.45 GHz) and the

short period of the exciting microwave field characterize these surface wave discharges. They can operate both at reduced and atmospheric pressure, but when the pressure rises above 0.1 atm, the discharge approaches a LTE state.[3,16–18]

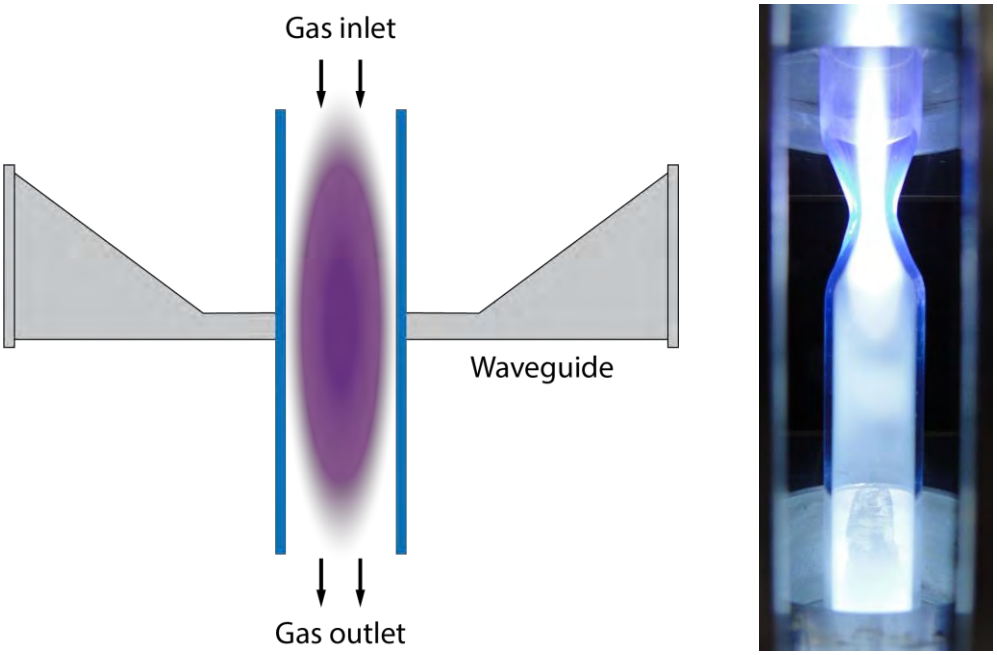

Figure 7 Schematic view (left) and picture (right; courtesy of DIFFER) of a MW discharge. Taken from reference 11.

3.3 Gliding arc (GA) discharge

As another example of a warm plasma, the gliding arc discharge combines the advantages of thermal and non-thermal plasmas.[4] It is a transient type of arc discharge. The periodic discharge passes during one cycle from an arc stage to a non-equilibrium discharge, which is a very sophisticated physical phenomenon.[4]

A classical gliding arc reactor typically consists of two plane diverging electrodes between which the gas flows. An arc is formed at the narrowest gap when a potential difference is applied between both electrodes. The gas flow drags the arc towards rising inter-electrode

distance, until it extinguishes, followed by the ignition of a new arc at the shortest inter-electrode gap. The length of the arc increases with the voltage, until it exceeds its critical value (l_{crit}). At that moment, the supplied energy is no longer sufficient to sustain the plasma in its LTE state, with a transition to a non-LTE state as a result. The discharge rapidly cools down to gas temperature. However, a high electron temperature (T_e ~ 1 eV, which is most suitable for efficient vibrational excitation of CO_2) maintains the plasma conductivity. The gliding arc further elongates under non-LTE conditions until a new critical length is reached ($l \sim 3 \cdot l_{crit}$), which leads to extinction of the discharge. Subsequently, the evolution repeats from the initial breakdown. Up to 75 - 80 % of the energy can be dissipated in the non-LTE zone of the gliding arc during a cycle. This effect stimulates chemical reactions in regimes, which are quite different from conventional thermal reaction chemistry. The transition to the non-LTE phase can occur in the order of nanoseconds, when the GA is operated at low currents ($I \leq 1$ A).[4] This results in a GA operating in the non-LTE regime almost immediately after ignition, thus a higher fraction of the discharge energy can be consumed by the non-LTE phase.[19,20]

Most of the studies on CO_2 conversion performed with gliding arc plasmas are carried out with classical gliding arc reactors. The latter configuration, however, has a few disadvantages. Indeed, it is incompatible with various industrial systems, because of its 2D geometry. Furthermore, the gas treatment is non-uniform, because only a limited fraction of the gas passes through the arc, and the residence time inside the plasma is short. To overcome these drawbacks, a three-dimensional gliding arc reactor with specific gas flow configuration, also called gliding arc plasmatron (GAP), was developed by Nunnally et al.[21] Figure 8 shows the difference between these two types of gliding arc discharges.

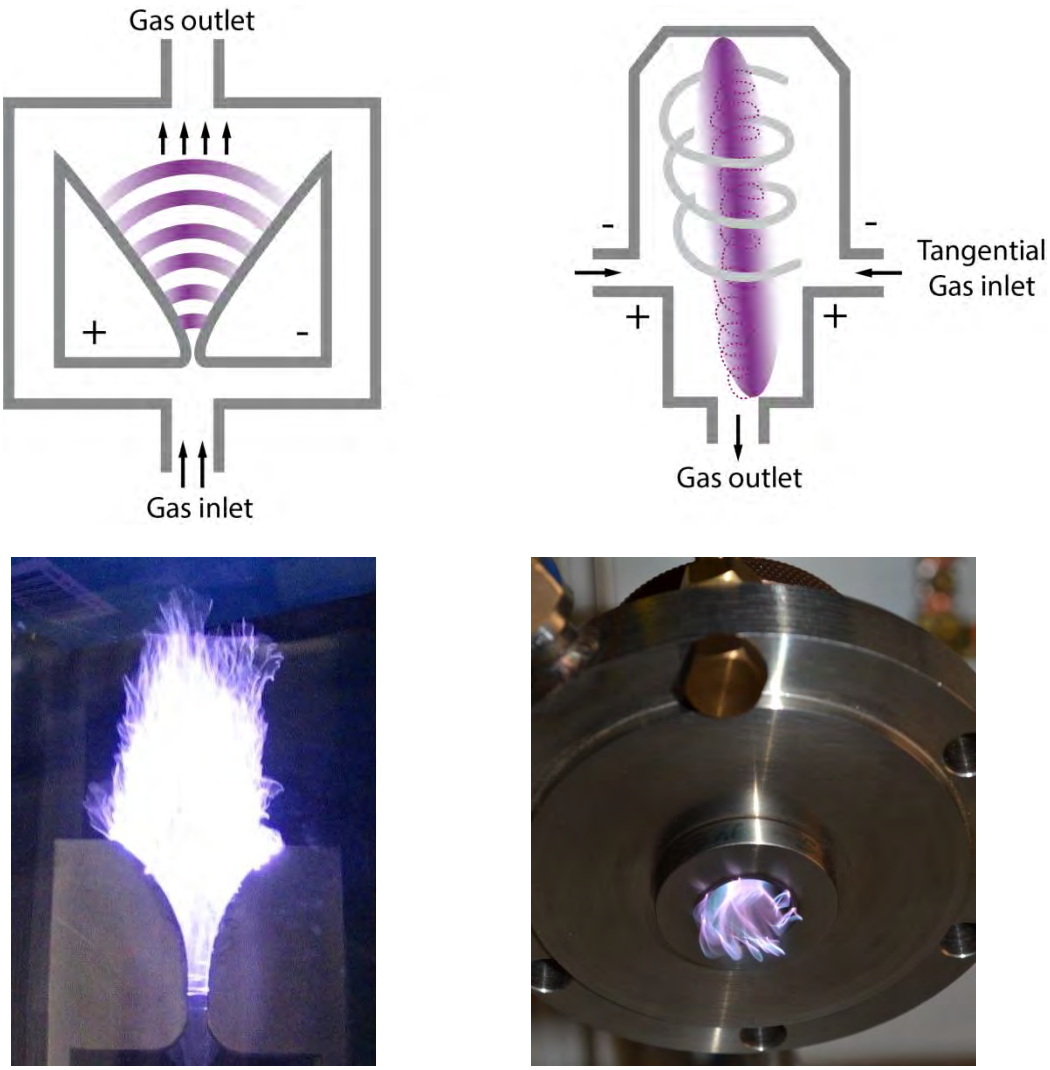

Figure 8 Schematic representation and picture of the classical GA (left; courtesy of University of Manchester), and the GAP (right). Taken from reference 11.

The reactor design of the GAP is very promising, because it can be implemented in industry and the specific gas flow configuration ensures the gas treatment to be more uniform, while it forces a longer residence time inside the plasma arc. In this reactor, the gas flow enters through a tangential inlet, so that a vortex flow is obtained (see Figure 9). A potential difference is applied between the cathode and anode, creating

an arc discharge. Depending on the electrode configuration, more specifically the diameter of the reactor body (acting as cathode) and the outlet of the reactor (acting as anode), two vortex flow patterns can be obtained: forward vortex flow (FVF) or reverse vortex flow (RVF). When the anode diameter is equal to the cathode diameter, the gas flow enters and follows a spiral trajectory both toward the bottom and the top of the reactor. The reactor outlet is found at the bottom of the reactor, so part of the gas will leave the reactor in a so-called FVF. On the other hand, when the anode diameter is smaller than the cathode diameter, the incoming gas cannot immediately exit the reactor, and it will first be forced upwards in the cathodic part of the reactor. Due to friction and inertia it loses rotational speed, so when arriving at the top of the reactor; it will start to move in a smaller vortex towards the bottom, that is, reverse direction, so that it can now exit the reactor at the bottom. The arc plasma is stabilized in the center of the reactor by this vortex flow and the reverse vortex gas flow is actually forced to go through the plasma (see Figure 9).

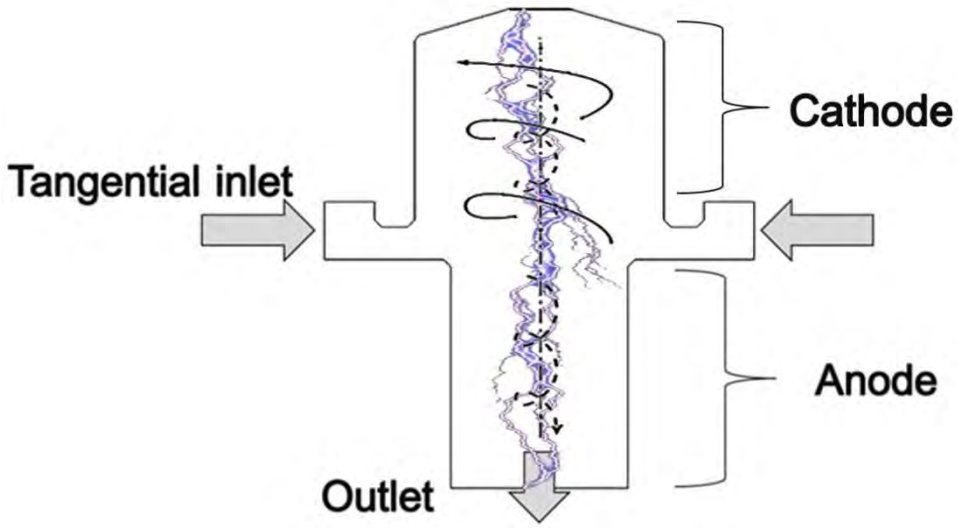

Figure 9 Schematic picture of the gliding arc plasmatron in reverse vortex flow configuration. Both the forward and reverse vortex flows are indicated (with full and dashed spirals, respectively). This vortex flow configuration stabilizes the arc discharge (indicated in purple) in the center of the reactor and forces the reverse gas flow to go through the plasma.

Figure 10 presents a photograph of the gliding arc plasma, illustrating that it is stabilized in the center of the reactor and clearly showing where the arc is attached to the electrodes.

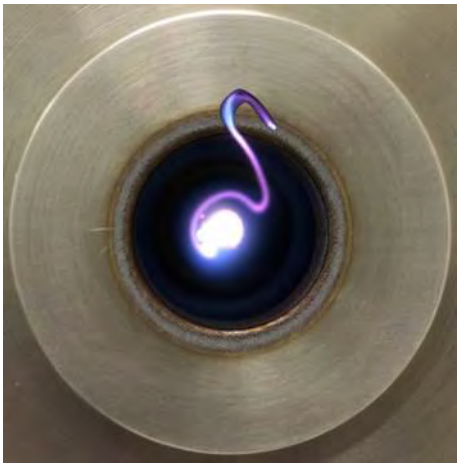

Figure 10 Photo of the outlet of the GAP (anode), showing the arc discharge. The arc is stabilized in the middle of the reactor, where it is attached to the cathode and anode.

4 Aim of the work and outline of the thesis

In this thesis we study the conversion of CO_2 in a gliding arc plasmatron (GAP) with the eye on future industrial implementation. We focus on the successive steps necessary for real-life application, trying to bridge the gap between university and industry.

As a first step, pure CO_2 splitting is investigated in Chapter 2. We describe the effect of the flow rate, applied power and reactor configuration on the performance of CO_2 conversion and energy efficiency. A comparison with thermal conversion, other plasma types and other novel CO_2 conversion technologies is made, to find out whether the GAP can provide a significant contribution to the much-needed efficient conversion of CO_2. With the help of modeling results, we elaborate on the underlying mechanisms.

In Chapter 3 we visualize the gliding arc plasma with a high-speed camera for different reactor configurations and in a wide range of operating conditions, to study the arc dynamics. This allows us to provide a complete image of the behavior of the gliding arc and to correlate this with the CO_2 conversion and energy efficiency measured in Chapter 2.

Waste streams in industry are typically not pure and therefore we investigate in Chapter 4 the effect of an additional gas, i.e., N_2. On one hand, we focus on the effect of N_2 on the CO_2 conversion and its energy efficiency. On the other hand, we also investigate whether CO_2 conversion can be combined with N_2 fixation, i.e., the conversion of N_2 molecules into simple nitrogen compounds that form the building blocks for life on Earth. By evaluating both processes and combining experimental work with chemical reaction kinetics simulations, we can evaluate whether it is possible to combine these two processes or whether (pre- or post-) separation is necessary. Furthermore, we also compare our

results with those obtained in a DBD reactor, in order to compare the different chemical processes in these two different types of plasma.

In Chapter 5, we combine CO_2 and CH_4 conversion, in order to form more complex molecules and fuels. Experiments are performed with various amounts of CH_4 added (0 – 25 %) to investigate how this influences the conversion and product distribution.

Chapter 5 reveals that the reaction of CO_2 with CH_4 is a desirable process for industry, to make complex molecules and fuels out of two greenhouse gases. However, to make this technique more applicable to industry, we would like to take the inlet gases directly from the exhaust gases of large CO_2 producers. It is easy to imagine that these exhaust gases are not pure and they often contain other gases that might influence the conversion efficiency. Therefore, a first step to more complicated mixtures is adopted in Chapter 6, where we present the results of experiments in a CO_2 - CH_4 - N_2 mixture with a 1/1/8 ratio. These experiments reveal the effect of N_2 on the dry reforming reaction and the influence of the flow rate and applied power.

Finally, Chapter 7 evaluates the performance of our GAP qualitatively, based upon the experience obtained over the past years, as well as quantitatively, based on a techno-economic assessment of CO_2 conversion. It also addresses new investigation routes, which should be made to proceed the GAP in its way to industry.

References

1 S. Samal, *J. Clean. Prod.*, 2017, **142**, 3131–3150.

2 E. Gomez, D. A. Rani, C. R. Cheeseman, D. Deegan, M. Wise and A. R. Boccaccini, *J. Hazard. Mater.*, 2009, **161**, 614–626.

3 A. Fridman, *Plasma Chemistry*, Cambridge University Press, New York, 2008.

4 A. Fridman, A. Chirokov and A. Gutsol, *J. Phys. D*, 2005, **38**, R1–R24.

5 T. Kozák and A. Bogaerts, *Plasma Sources Sci. Technol.*, 2014, **23**, 045004.

6 T. Kozák and A. Bogaerts, *Plasma Sources Sci. Technol.*, 2015, **24**, 015024.

7 A. Berthelot and A. Bogaerts, *J. Phys. Chem. C*, 2017, **121**, 8236–8251.

8 A. Bogaerts, A. Berthelot, S. Heijkers, S. Kolev, R. Snoeckx, S. Sun, G. Trenchev, K. Van Laer and W. Wang, *Plasma Sources Sci. Technol.*, 2017, **26**, 063001.

9 A. Bogaerts, T. Kozák, K. van Laer and R. Snoeckx, *Faraday Discuss.*, 2015, **183**, 217–232.

10 A. Janeco, N. R. Pinhão and V. Guerra, *J. Phys. Chem. C*, 2015, **119**, 109–120.

11 R. Snoeckx and A. Bogaerts, *Chem. Soc. Rev.*, 2017, **46**, 5805–5863.

12 A. Bogaerts and E. C. Neyts, *ACS Energy Lett.*, 2018, **3**, 1013–1027.

13 G. J. van Rooij, H. N. Akse, W. A. Bongers and M. C. M. van de Sanden, *Plasma Phys. Control. Fusion*, 2018, **60**, 014019.

14 U. Kogelschatz, *Plasma Chem. Plasma Process.*, 2003, **23**, 1–46.

15 R. Snoeckx and A. Bogaerts, *Chem. Soc. Rev.*, 2017, **46**, 5805–5863.

16 A. Bogaerts, E. Neyts, R. Gijbels and J. van der Mullen, *Spectrochim. Acta, Part B*, 2002, **57**, 609–658.

17 C. Tendero, C. Tixier, P. Tristant, J. Desmaison and P. Leprince, *Spectrochim. Acta - Part B*, 2006, **61**, 2–30.

18 H. Conrads and M. Schmidt, *Plasma Sources Sci. Technol.*, 2000, **9**, 441–454.

19 S. R. Sun, H. X. Wang, D. H. Mei, X. Tu and A. Bogaerts, *J. CO2 Util.*, 2017, **17**, 220–234.

20 W. Wang, B. Patil, S. Heijkers, V. Hessel and A. Bogaerts, *ChemSusChem*, 2017, **10**, 2145–2157.

21 T. Nunnally, K. Gutsol, A. Rabinovich, A. Fridman, A. Gutsol and A. Kemoun, *J. Phys. D. Appl. Phys.*, 2011, **44**, 274009.

CHAPTER 2

CO_2 conversion

This chapter is published as

Marleen Ramakers, Georgi Trenchev, Stijn Heijkers, Weizong Wang, and Annemie Bogaerts, Gliding Arc Plasmatron: Providing an Alternative Method for Carbon Dioxide Conversion, *ChemSusChem* **2017**, *10*, 2642 – 2652.

In this chapter, we investigate pure CO_2 splitting in a GAP. We provide a detailed experimental study, supported by modeling, of the CO_2 conversion, as well as the energy cost and efficiency in a GAP. We perform a comparison with thermal conversion, other plasma types and other novel CO_2 conversion technologies to find out whether this novel plasma reactor can provide a significant contribution to the much-needed efficient conversion of CO_2. Furthermore, we indicate how the performance of the GAP can still be improved by further exploiting its non-equilibrium character. Hence, it is clear that the GAP is very promising for CO_2 conversion.

1 Description of the experiments

1.1 Gliding arc setup

The experiments were performed with a GAP, as developed by Nunnally et al.[1] The concept of this reactor is explained in detail in Chapter 1. To compare the performance of the reverse vortex flow (RVF) and forward vortex flow (FVF) configurations, we used four different stainless steel electrodes, that is, a high voltage electrode and three grounded electrodes. The high voltage electrode, which acts as the cathode, has a length of 20.30 mm and a diameter of 17.50 mm. All grounded electrodes, acting as anode, have the same length (16.30 mm) but their diameter is 7.08, 14.20, and 17.50 mm, respectively. There is a 3 mm gap between the cathode and anode. These dimensions gave rise to a reactor volume of 6.22, 6.93, and 7.43 cm^3, respectively, but the arc volume was only about 0.13 cm^3. A photograph and diagram of the entire experimental system is shown in Figure 1.

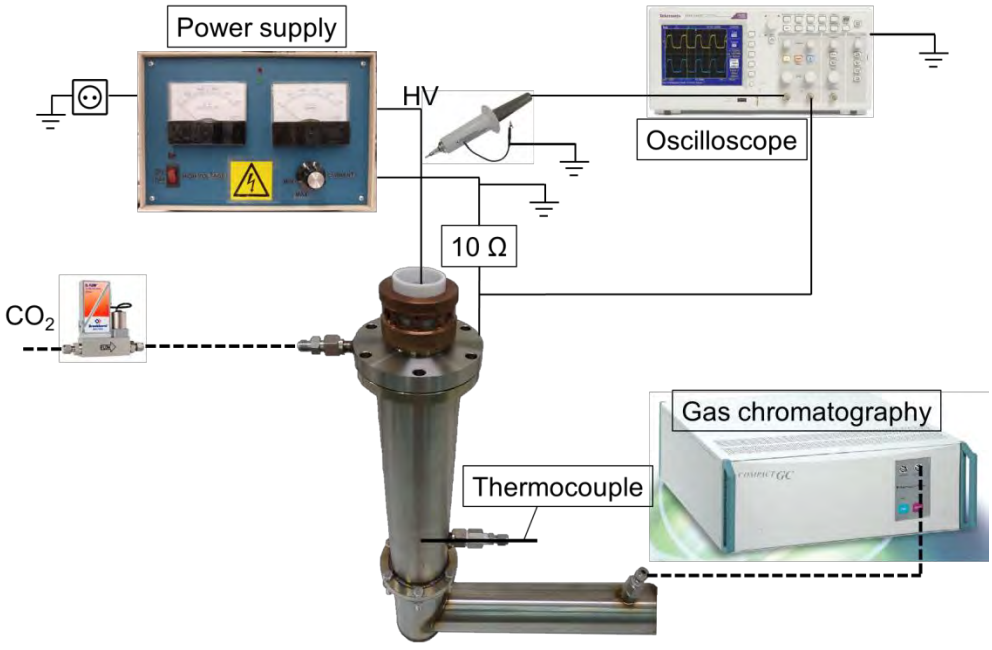

Figure 1 Schematics of the entire experimental system.

A mass-flow controller (Bronkhorst) was used to insert CO_2 into the GAP. The CO_2 flow rate was varied between 10 and 22 L/min. CO_2 with a purity of 99.5% was used and no preheating of the gas occurred. The pressure in the reactor is slightly higher than atmospheric pressure (1.25 bar). The reactor was powered by a custom build DC current source type power supply. The plasma voltage and current were measured by a high-voltage probe (Tektronix P6015A) and a current sense resistor of 10 Ω, respectively. The electrical signals were sampled by a two-channel digital storage oscilloscope (Tektronix TDS2012C). The current was varied between 0.04 and 0.38 A. The plasma power (P_{plasma}) was calculated as follows:

$$P_{plasma} = 1/T \int_0^{t=T} V_{plasma} \times I_{plasma} dt \quad (1)$$

where P is the power in watts, T is the period, V is the voltage in volts, and I is the current in amps. In the reactor tube, which was placed after the GAP, a thermocouple was inserted to measure the temperature of the effluent stream. The output gas composition was analyzed online by gas chromatography.

1.2 Gas analysis

The feed and product gases were analyzed by a three-channel compact gas chromatograph (CGC) from Interscience. This device has three different ovens, each with their own column and detector. A Molsieve 5A and Rt-Q-Bond column were used to separate O_2 and CO, which were detected with a thermal conductivity detector (TCD). The other channel was equipped with a Rt-Q-Bond column and TCD for the measurement of CO_2.

The conversion of CO_2 (X_{CO_2}), was defined as:

$$X_{CO_2}\ (\%) = \frac{\dot{n}_{CO_2(in)} - \dot{n}_{CO_2(out)}}{\dot{n}_{CO_2(in)}} \times 100\ \% \quad (2)$$

where $\dot{n}_{CO_2(in)}$ and $\dot{n}_{CO_2(out)}$ are the molar flow rate of CO_2 without and with plasma, respectively. As the method mentioned above does not account for the gas expansion due to CO_2 splitting, a correction factor was used, which is explained in the appendix.

To calculate the energy efficiency of CO_2 conversion, the specific energy input (SEI) in the plasma was defined as:

$$SEI\ (kJ/L) = \frac{Plasma\ power\ (kW)}{Flow\ rate\ (L/min)} \times 60\ s/min \quad (3)$$

The energy cost (EC) for converting CO_2 was calculated as:

$$EC_{CO_2}(kJ/L) = \frac{SEI(kJ/L)}{X_{CO_2}} \quad (4)$$

Likewise, the energy efficiency (η), was calculated as follows:

$$\eta\ (\%) = \frac{\Delta H_R(kJ/mol) \times X_{CO_2}(\%)}{SEI(kJ/L) \times 22.4\ L/mol} \quad (5)$$

where ΔH_R is the reaction enthalpy of CO_2 splitting (i.e., 279.8 kJ/mol), X_{CO_2} is the amount of CO_2 converted, SEI is defined above and 22.4 L/mol is the molar volume at 0 °C and 1 atm.

Every experiment was performed three times. Subsequently, a propagation of uncertainty was applied to the results to calculate the error bars.

2 Description of the modeling work

To understand the effect of the different electrode configurations, Georgi Trenchev (also PhD student within PLASMANT) calculated the 3D gas flow pattern in the different reactor setups, with COMSOL Multiphysics Simulation Software, based on solving the Navier–Stokes equations, assuming a turbulent flow. Details on this model can be found in the supporting information of reference 2.

To describe the plasma chemistry of CO_2 conversion in the GAP, and to elucidate the underlying mechanisms, Stijn Heijkers (another PhD student within PLASMANT) used a 0D plasma chemistry model. This model allows to describe the behavior of a large number of species, and incorporate a large number of chemical reactions, with limited computational effort. In this 0D chemical kinetics model, called ZDPlaskin, balance equations were used to calculate the time-evolution of the species densities, taking into account the various production and loss terms by chemical reactions. From these species densities the CO_2 conversion can be obtained, and in combination with the plasma power and gas flow rate (and thus the SEI), this also yields the energy cost and energy efficiency, in the same way as explained above (see Equations (4) and (5)). Besides that, the model also calculates the gas temperature, the electron density, and electron temperature. The model is described in more detail in the supporting information of reference 2.

3 Results and discussion

First, we will present and discuss the experimental results for different values of plasma power and flow rate. Next, we will illustrate the effect of the vortex flow for the three different configurations (i.e., anode diameters). These results will be compared with the theoretical thermal conversion and energy efficiency. Subsequently, we will compare the experimental results with model predictions, and we will use the model for a detailed analysis of the underlying plasma chemistry. Finally, we will benchmark our results with different plasma setups and make a comparison with other novel CO_2 conversion technologies.

3.1 Effect of power and flow rate on CO_2 conversion, energy cost, and energy efficiency

The experiments were conducted for five different flow rates and eight different values of plasma power. We show here the results for the configuration with anode diameter of 14.20 mm. The results for the other configurations can be found in the appendix.

Figure 2(a) shows the conversion plotted as a function of plasma power for the five different flow rates. The values are in the order of 1 – 6 %. Below 225 W the arc is in a so-called low-current regime around 50 mA, whereas above 475 W a so-called high-current regime is obtained, with current values between 260 and 380 mA. In between these two regimes, no stable plasma could be formed with this power supply. If we compare these two regimes, it is obvious that the conversion is lower in the low-current regime than in the high-current regime. This can of course be explained by the lower current and plasma power. A lower current simply means fewer electrons, which can be used to split CO_2. In addition, also the power is lower, so less energy is available to convert CO_2. However, if the plasma power increases in its own regime, this has no significant effect on the CO_2 conversion. Instead, the extra energy available will be used to heat up the gas, as is shown in Figure 2(d).

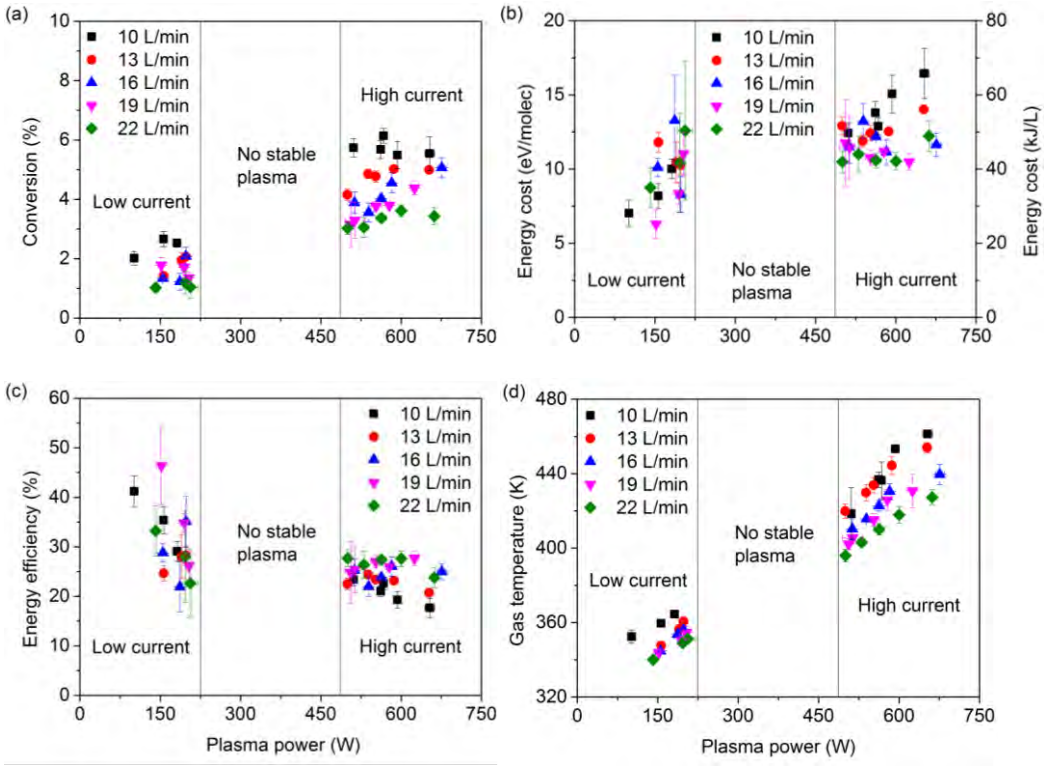

Figure 2 Conversion (a), energy cost (b), energy efficiency (c), and gas temperature of the effluent stream (d) as a function of plasma power for five different flow rates, for the configuration with anode diameter of 14.20 mm.

In contrast to the plasma power, the gas flow rate has a visible effect on the CO_2 conversion: the lower the flow rate, the higher the conversion, both in the low- and high-current regime. This is obviously owed to the longer residence time of the gas in the plasma. Further decreasing the flow rate to increase the conversion is, however, not possible in our setup, because a minimum flow rate is necessary to obtain a good vortex flow. Furthermore, the increase in conversion facilitated by lowering the flow rate overall results in less CO_2 converted, in liters per minute. This is less interesting from industrial point of view. We are thus limited in varying the flow rate, but the residence time, and therefore probably also the conversion, might be further increased by increasing the length of the cathode.

Figure 2(b) and 2(c) show the energy cost and energy efficiency, respectively. The measurements in the low-current regime seem to follow a random order and have a larger error than the ones in the high-current regime. This can be explained by the fact that the plasma power fluctuates more in the low-current regime. Moreover, it is clear that in some cases the energy cost is lower and the energy efficiency is higher in the low-current regime than in the high-current regime. However, the corresponding conversion in these cases is quite low (see Figure 2(a)), so these cases are overall not so interesting. In the high-current regime there is no significant change in the energy cost or in the energy efficiency when increasing the plasma power. In general, the energy cost is slightly lower and the energy efficiency is slightly higher for higher flow rates at constant plasma power. All these trends can be explained from Equations (4) and (5) in section 1.2. The values of energy cost and energy efficiency are in the range of 42 - 66 kJ/L (or 10.5 - 16.4 eV/molec) and 18 – 28%, respectively.

We are not able to measure the gas temperature inside the arc, but we measured the temperature of the effluent stream (Figure 2(d)), and it shows the same trends as the conversion. The temperature rises more or less linearly with the plasma power, which is logical because more energy is available to heat up the gas. Furthermore, at constant plasma power, the gas temperature is slightly higher at lower flow rate, because of the longer residence time of the gas in the plasma, giving more time to heat up the gas. The temperature values inside the plasma are of course much higher, and the gas cools down significantly when leaving the reactor, but the temperature of the effluent stream can still reach values up to 450 K, which offers opportunities in the future to insert a catalyst in the reactor tube, for so-called plasma catalysis when mixing CO_2 with a suitable hydrogen source to realize more selective CO_2 conversion into targeted value-added chemicals.

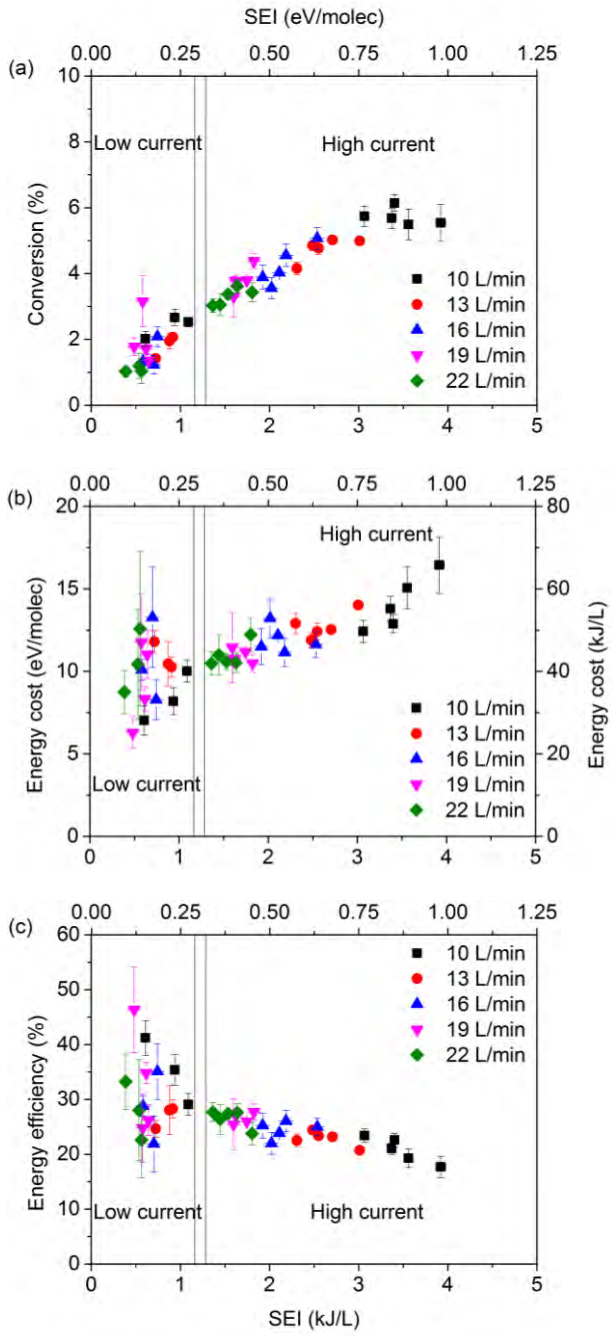

Figure 3 Conversion (a), energy cost (b), and energy efficiency (c) as a function of SEI for five different flow rates, for the configuration with anode diameter of 14.20 mm. The SEI is not only expressed in kJ/L, but also in eV/molec, which is commonly done in plasma research.

In Figure 3, we combine all data of Figure 2 by plotting the results as a function of the specific energy input (SEI) for the five different flow rates investigated. The SEI is indeed a very important parameter in plasma-based CO_2 conversion, as it combines the effect of power and gas flow rate (see Equation (3) in section 1.2). The SEI values are depicted in the figure both in eV/molec, which is of interest from the point of view of the plasma chemistry, to explain the good energy efficiency (see below), as well as in kJ/L, which is of more practical interest for the applications. Again the low- and high-current regime can be distinguished. The conversion increases more or less linearly with rising SEI, which is logical as more energy per molecule is available to convert CO_2. Because the conversion rises slightly less than the rise in SEI (i.e., slope ≈ 0.7), the energy cost slightly rises, and the energy efficiency slightly decreases, as a function of the SEI, which can be explained from Equations (4) and (5) in section 1.2.

3.2 Effect of the vortex flow on CO_2 conversion, energy cost, and energy efficiency

As explained above in the description of the experiments, the outlet of the reactor, which acts as the anode, is replaceable, and this will affect the vortex flow pattern. Hence, we want to investigate whether the latter will also affect the CO_2 conversion. For this comparison, diameters of 7.08, 14.20, and 17.50 mm are examined. Figure 4 shows the conversion (a), as well as energy cost (b), and energy efficiency (c) as a function of the SEI for the three studied configurations, for all combinations of gas flow rate and plasma power investigated. It is clear that the highest conversion (i.e., almost 9 %) can be reached in the configuration with anode diameter of 7.08 mm and it decreases with increasing anode diameter. For each configuration, the conversion increases with rising SEI, as explained in the previous section.

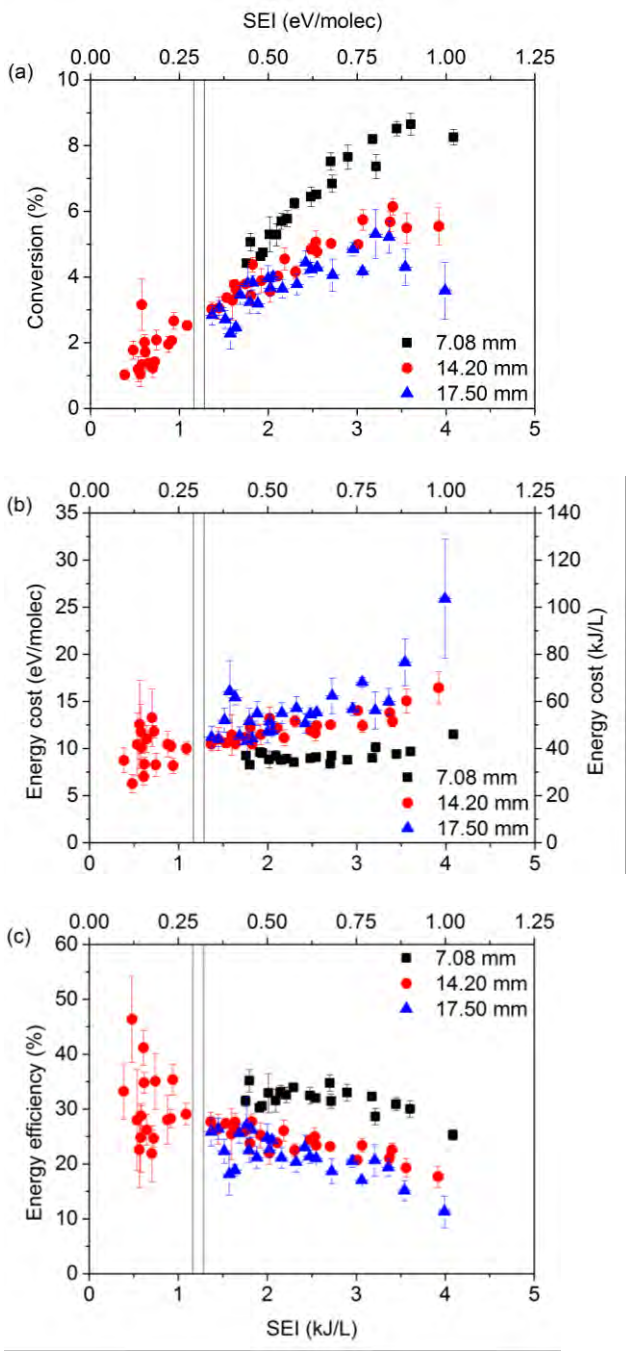

Figure 4 Conversion (a), energy cost (b), and energy efficiency (c) as a function of the SEI for the three studied configurations, with three different anode diameters, as indicated by the legend.

For SEI values below 1 kJ/L (low-current regime), results could only be obtained for the configuration with anode diameter of 14.20 mm. The reason is that the power supply could not sustain a stable discharge for the other configurations in this regime. It is clear from Figure 4(b), (c) that the energy cost in this case is slightly lower and the energy efficiency is slightly higher than the lowest/highest values, respectively, obtained with an anode diameter of 7.08 mm. However, the corresponding conversion is very low, making this regime overall not very suitable. Above 1.5 kJ/L (high-current regime), the energy cost obtained in the configuration with anode diameter of 7.08 mm is again the lowest and the energy efficiency is again the highest. In general, the energy cost and efficiency stay more or less constant or slightly increase/decrease, respectively, with increasing SEI, depending on how much the conversion rises with SEI, as explained in the section above (see again Equations (4) and (5) in section 1.2). Overall, we can conclude that the configuration with the smallest anode diameter gives the best performance for both the CO_2 conversion and energy cost/efficiency, reaching values of 8.6 % conversion at an energy cost of 39 kJ/L (or 9.7 eV/molec) and an energy efficiency of 30%. The best energy efficiency reached with this configuration is 35 %, corresponding to an energy cost of 33 kJ/L (or 8.3 eV/molec), but the conversion in this case is slightly lower, that is, 5.1 %.

The reason why the configuration with the smallest diameter gives the best results is that the reverse vortex flow (RVF) is most strongly pronounced, whereas in the configuration with the largest diameter, the RVF is almost non-existent. This is further elaborated in detail in the appendix, based on gas-flow calculations for the different setups. The RVF forces a higher residence time of the gas in the reactor, and thus, in the arc discharge. Also, it provides thermal insulation of the discharge from the side walls, as the mass transfer always takes place from the walls to the plasma. This improves the ionization, excitation, and

dissociation efficiency in the plasma, as it lowers the thermal losses due to cooling by the walls.

3.3 Comparison of our results with thermal conversion and energy efficiency

To evaluate the performance of the GAP for CO_2 conversion, we compare our results with the calculated theoretical conversion and energy efficiency for a temperature range of 300 – 5000 K, in case of pure thermal CO_2 conversion. A detailed description of the calculation of this conversion and energy efficiency, as well as of the SEI values in this case, can be found in the supporting information of reference 2.

The thermal conversion and corresponding energy efficiency are plotted as a function of the applied SEI in Figure 5. The CO_2 conversion and energy efficiency obtained in our GAP for the configuration with anode diameter of 7.08 mm are also plotted for comparison. It is obvious that the SEI applied to the GAP is typically below 4 kJ/L or 1 eV/molec (see also Figure 3 and 4), but in Figure 5 we show the results for the thermal calculations up to much higher SEI values, just to illustrate that the thermal conversion and energy efficiency at the typical SEI values as used in our GAP are virtually negligible, and only evolve to higher values above 4 kJ/L (or 1 eV/molec).

To summarize, Figure 5 clearly demonstrates that both the conversion and especially the energy efficiency of CO_2 splitting in the GAP are much higher than for pure thermal conversion, in which the values are still negligible in the range of SEI values applied to the GAP. This better performance of the GAP can be explained by the non-equilibrium properties of the gliding arc plasma, as the electrons have a higher temperature than the gas (i.e., ca. 1.68 eV or 19,500 K vs. up to 3000 K for the gas), and these highly energetic electrons induce different chemical reactions. These chemical reactions will be further elaborated in the next section.

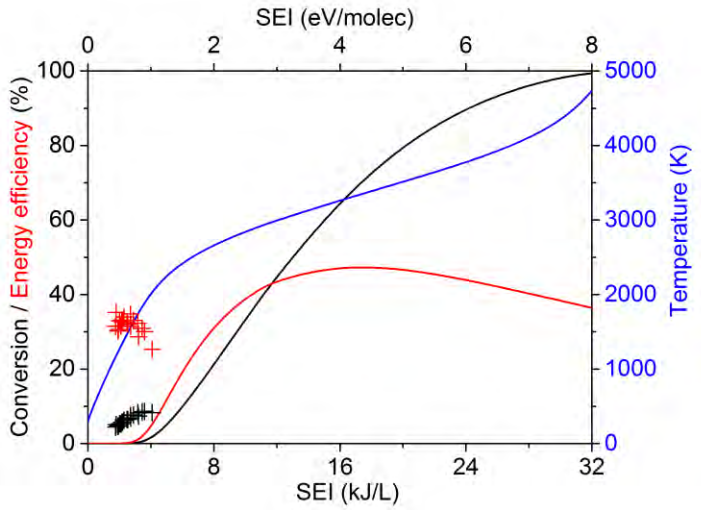

Figure 5 Calculated theoretical thermal conversion (left y-axis), energy efficiency (left y-axis), and corresponding temperature (right y-axis) as a function of specific energy input for pure CO_2 at a pressure of 1 atm, and comparison to our results (crosses) obtained in the GAP for the configuration with anode diameter of 7.08 mm.

The temperature for thermal conversion is also indicated in Figure 5 (blue curve, right y-axis). At a temperature of 3000 K, which is calculated to be the temperature in the arc, the SEI is about 12 kJ/L, yielding a thermal conversion of about 45 % and an energy efficiency of about 44 % (see Figure 5: black and red curve, respectively). In our GAP only a fraction of about 15 % of the introduced CO_2 gas (see Chapter 4 and 5) passes through the plasma arc. Based on the fact that the arc temperature is calculated to be 3000 K, and that temperature yields a thermal conversion of 45 %, and keeping in mind that the treated gas fraction is only 15 %, we estimate an overall thermal conversion of 6.75 % in our GAP. In our experiments, we obtained slightly higher conversions, around 8%. This indicates that also other processes are important in certain parts of the arc, where the temperature is somewhat lower, yielding a somewhat higher than pure thermal conversion. This is also shown from simulations (see next section). From these simulations, it is however also clear that the vibrational and gas temperature are quite similar, which indicates that most CO_2 conversion is near thermal.

3.4 Comparison of our results with model calculations and explanation of the underlying mechanisms

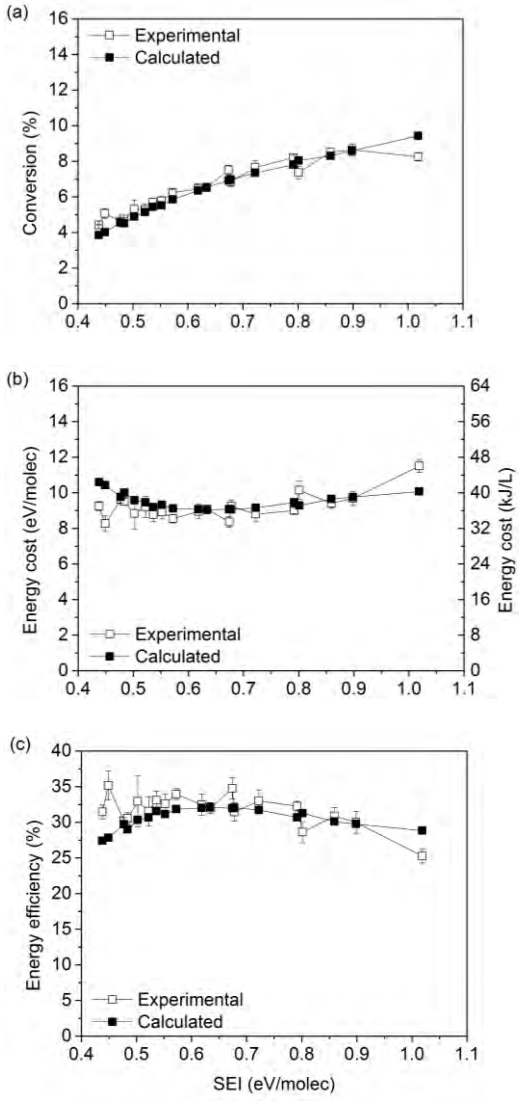

Figure 6 Calculated (full symbols) and measured (open symbols) conversion (a), energy cost (b) and energy efficiency (c) as a function of SEI, for the configuration with anode diameter of 7.08 mm. Note that some discontinuities are observed in the data as a function of SEI. The reason is that the SEI is composed of plasma power and gas flow rate, and different combinations of plasma power and gas flow rate can give rise to the same SEI, but can also yield slightly different conversion, energy cost, and energy efficiency. Calculations performed by S. Heijkers within PLASMANT.

Figure 6 illustrates the calculated conversion (a), energy cost (b), and energy efficiency (c), as a function of SEI, for the GAP configuration with anode diameter of 7.08 mm, in comparison with the experimental data. The same rising trend is observed for the conversion, whereas the energy cost and efficiency do not vary a lot within the entire range of SEI values, similar to the experimental data. Moreover, also the absolute values are in good agreement, certainly when taking into account the complexity of the plasma chemistry and the assumptions inherent to a 0D model. This good agreement, in addition to the realistic values calculated by this model for the gas temperature, electron density, and temperature, indicates that the model provides a realistic picture of the plasma chemistry in the GAP, and can thus be used to investigate the underlying mechanisms of the CO_2 conversion.

In Figure 7, we plot the relative contributions of the various CO_2 dissociation processes to the overall CO_2 conversion, as a function of the SEI, as predicted by the model. Electron impact dissociation of CO_2, either from the ground state ($CO_2(g)$) or from the vibrational levels ($CO_2(v)$), appears to be the main dissociation mechanism. At the lowest SEI values investigated, electron impact dissociation from the CO_2 ground state contributes up to 50 % to the CO_2 dissociation, but this value drops to 33 % at the highest SEI values, whereas the contribution of electron impact dissociation from vibrationally excited CO_2 is about 30 - 35 % at all SEI values investigated. The role of CO_2 dissociation upon collision of O atoms or any other molecule (indicated as M) with CO_2 molecules in vibrational levels slightly rises with SEI, and the relative contribution reaches about 24 and 7%, respectively, at the highest SEI values investigated. It is important to mention that electron impact dissociation from the CO_2 ground state is less energy efficient, as it requires more energy than strictly needed for dissociation (see below), whereas the dissociation processes from vibrationally excited CO_2 provide a more energy-efficient channel. The latter is especially true for the collisions of vibrationally excited CO_2 with O atoms, as the O atom

formed upon dissociation of CO_2 in one of the other processes can be used to dissociate an extra CO_2 molecule. Figure 7 thus illustrates that CO_2 conversion in the GAP already proceeds in an energy-efficient way, compared for instance to a DBD, in which electron impact dissociation from the ground state is the main mechanism;[3–5] however, that there is still room for improvement if we can further enhance the contributions of the processes involving vibrationally excited CO_2. More details on the calculated vibrational distribution function can be found in the appendix.

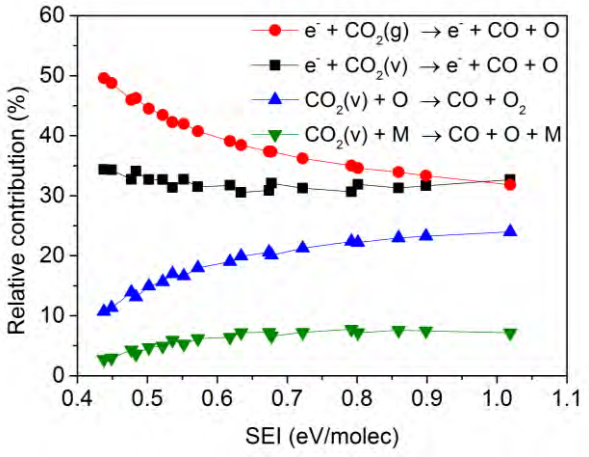

Figure 7 Calculated relative contribution of the various CO_2 dissociation processes to the overall CO_2 conversion, as a function of the SEI. Calculations performed by S. Heijkers within PLASMANT.

The important role of the vibrational levels for energy-efficient CO_2 conversion in the GAP is in line with observations made for a classical gliding arc[6] and a MW plasma.[4,7,8] Indeed, the electron temperature in the GAP is about 1.68 eV, which is suitable for populating the lowest vibrational levels of CO_2. Subsequently, collisions between vibrationally excited CO_2 molecules, also called vibration–vibration relaxation, will gradually populate the higher vibrational levels, which will easily dissociate into CO and O atoms (either due to electron impact or upon collision with another O atom or any molecule; see Figure 7 above). This so-called ladder-climbing process is schematically illustrated in Figure 5 in Chapter 1.

This process is very energy efficient, and thus it explains the good energy efficiency of the GAP, in contrast to, for instance, a DBD plasma, where the CO_2 conversion almost exclusively proceeds through electron impact electronic excitation from the ground state, as mentioned above. As seen from Figure 5 in Chapter 1, this process requires about 7 – 10 eV, which is more than the C=O bond energy of 5.5 eV. This extra energy can be considered as waste, and the latter explains why the energy efficiency of the DBD is lower than for the GAP (or MW plasma); see also next section. The ladder climbing process, as well as the other processes illustrated in Figure 7 above, also explains why the energy cost of the GAP is lower, and the energy efficiency higher, compared to thermal dissociation. Indeed, in the GAP, the electrons heated by the applied power will selectively activate the CO_2 molecules, by vibrational excitation as well as electronic excitation, whereas the other degrees of freedom do not need to be activated, as is the case in thermal dissociation, in which the entire gas must be heated for the conversion to take place.

3.5 Comparison of our results with other types of plasmas, as well as other novel CO_2 conversion technologies

To give an overview of where our results should be positioned in the rapidly expanding field of plasma-based CO_2 conversion, we plot in Figure 8 the energy efficiency of CO_2 splitting versus the conversion in different types of plasmas. The results are shown for all pressures, with open symbols indicating low pressure and solid symbols indicating atmospheric pressure or higher.

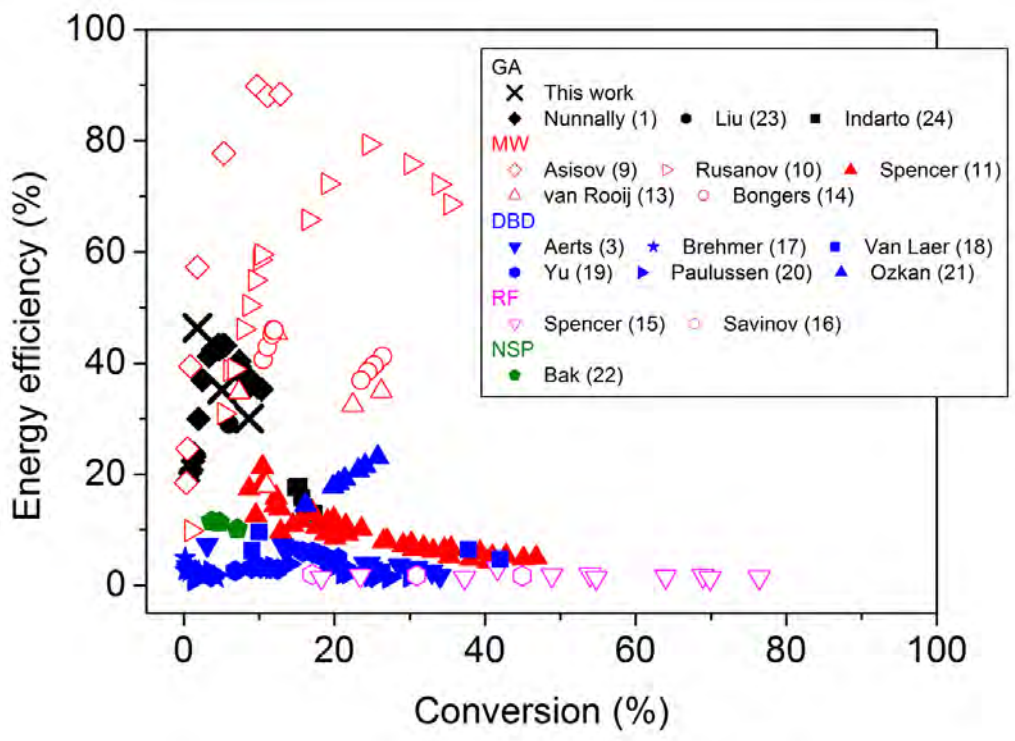

Figure 8 Energy efficiency versus conversion in different types of plasmas used for CO_2 conversion, and comparison with our data. The results are shown for all pressures, with open symbols indicating low pressure and solid symbols indicating atmospheric pressure or higher.

If we compare our data (indicated with black crosses) with the results of other experiments, we can conclude that in terms of energy efficiency, the GAP is very promising. Only Asisov et al.[9] and Rusanov et al.[10] obtained higher energy efficiency (i.e., up to 90 and 80 %, respectively) with their MW plasma reactors. However, the discharge used by Asisov et al. was organized in a supersonic flow and the setup operated at a reduced pressure of 0.05 – 0.2 atm. Rusanov et al. also made use of a setup operating at reduced pressure (50 – 200 torr or 0.06 – 0.26 atm), and it was reported that the energy efficiency dramatically drops to values of about 5 – 20% when the pressure rises to 1 atm.[11,12] The excellent energy efficiencies obtained by Asisov et al. and Rusanov et al., back in 1981 and 1983, have not yet been reproduced since then. However, similar energy

efficiencies as in our GAP were reached more recently with a MW reactor by van Rooij et al.[13] and Bongers et al.[14] They both obtained a higher conversion (i.e., up to 26 %) than in our case, but again these experiments were conducted at reduced pressures of 200 mbar (0.2 atm) and 150 - 600 mbar (0.15 – 0.60 atm), respectively. If the pressure would be increased, the conversion and energy efficiency would again be lower, and the plasma would also be less stable. Moreover, the energy cost of the pumping system should also be accounted for, when operating at reduced pressure, and this would lower the overall energy efficiency.

As seen in Figure 8, both studies performed in radiofrequency (RF) plasma at low pressure show lower energy efficiency than in our GAP. This can be explained by the fact that the optimum operating conditions for vibrational excitation of CO_2, that is, having a specific energy input of ≈ 1 eV/molec, an electron temperature of ≈ 1 eV and an ionization degree (n_e/n_0) ≥ 10^{-6} are not met in this type of plasma.[15,16]

Because operation at atmospheric pressure is generally more compatible with industrial applications, it is better to compare with results obtained at 1 atm (or higher), as plotted with solid symbols in Figure 8. In a MW plasma, the energy efficiency is then typically lower, that is, in the range of 5 – 20 %.[11] In this specific case, the conversion is higher than in our GAP. However, these experiments were conducted at a higher power (up to 2 kW).

We also plot in Figure 8 the results obtained in a DBD, which is very often used for CO_2 conversion. It is clear that the energy efficiency of the studies conducted with DBD[3,17–21] are much lower than our results. This is again due to the non-ideal operating conditions, as the SEI and electron temperature are typically higher than 1 eV/molec and 1 eV, respectively. Therefore, the energy-efficient vibrational excitation is not favored.

The energy efficiency obtained with a nanosecond-pulsed (NSP) discharge by Bak et al.[22] is also lower than in our case, at slightly lower

conversion values. In this configuration, the pressure reached values from 2.4 to 5.1 atm. This can explain the lower energy efficiency. Moreover, in this type of plasma the average electron energy is rather high. Therefore, the excitation and auto-dissociation of CO_2 (10.5 eV) is the dominant reaction path instead of the vibrational excitation-dissociation pathway, which is more efficient.

Finally, if we compare our results with data obtained in other gliding arc plasmas, we can distinguish two groups, that is, on one hand the results obtained by Nunnally et al.[1] and Liu et al.[23], which are similar to our results, and on the other hand the data of Indarto et al.[24] The difference between these two groups is the flow configuration that was used. Nunnally et al.[1] and Liu et al.[23] used a vortex flow, like in our case, whereas the results of Indarto et al.[24] were obtained in a classical gliding arc configuration. This comparison clearly shows that a vortex flow increases the energy efficiency of CO_2 conversion, because it stabilizes the plasma in the middle of the reactor and the gas flow is forced to go through the plasma, whereas the heat lost to the reactor walls is minimized.

In general, we can conclude that the energy efficiency is typically much higher in a gliding arc discharge as well as in MW plasmas than in the other plasma types. This can be explained by the fact that the electron energy is in the order of 1 eV in gliding arc and MW discharges, and therefore vibrational excitation of the CO_2 molecules is favored, whereas the electron energy in other plasma types such as DBD, RF, and NSP discharges is typically somewhat higher, yielding mainly electronic excitation of CO_2, leading to a waste of energy, as explained in the previous section. To summarize, we can conclude from Figure 8 that the GAP performs better at atmospheric pressure in terms of energy efficiency than all the other plasma types.

Plasma technology is obviously not the only technology of interest for CO_2 conversion. Therefore, it is necessary to compare our plasma process with other alternatives for the production of fuels from sunlight. One of the primary indicators used to compare different technologies is the solar-to-fuel energy conversion efficiency ($\eta_{solar\text{-}to\text{-}fuel}$). This is a measure of how well solar energy is converted to chemical energy of the fuel. If we assume that the electricity needed for our plasma process is produced by solar panels, which have an efficiency of 25 %,[25] we currently can reach a solar-to-fuel efficiency of 11.5 % (based on plasma power, which is about 80 % of the power input and not including the separation cost). We are aware that CO is not a mainstream fuel. However, it has a heating value and can therefore be used to define a solar-to-fuel efficiency in a correct manner. The splitting of CO_2 by means of plasma can be seen as an efficient source of CO, to produce fuels in combination with H_2. On the other hand, when CO_2 is mixed with a hydrogen source in the plasma, syngas and other (liquid) fuels can be produced directly. Moreover, if we add a catalyst to the system to improve the selectivity, synergies due to plasma and catalyst may arise, as explained in reference 26. This opens up an array of interesting investigation routes.

Using electrocatalysts for the solar conversion of CO_2 to CO is a competitive technology that also uses electricity for the production of fuels with a $\eta_{solar\text{-}to\text{-}fuel}$ = 13.4 %.[27] Next to electrochemical conversion, there are also thermocatalytic routes, for example:

- $CO_2 + H_2 \rightarrow CO + H_2O$
- $CO_2 + H_2 \rightarrow HCOOH$
- $CO_2 + 3\ H_2 \rightarrow CH_3OH + H_2O$
- $2\ CO_2 + 6\ H_2 \rightarrow CH_3OCH_3 + 3\ H_2O$

Other novel conversion technologies, like photocatalytic and solar thermochemical conversion, use direct sunlight to produce fuels. Theoretically, the solar-to-fuel efficiency of photocatalytic

CO_2 conversion is limited to a maximum of 17 % owing to the band gap energy of the photocatalyst, which should be at least 1.33 eV and a value between 2 - 2.4 eV would be optimal.[28] However, the solar energy-conversion efficiencies obtained to date with metal oxides, such as TiO_2, for full spectrum illumination are lower (< 2 %).[29] For the solar thermochemical approach, theoretical $\eta_{\text{solar-to-fuel}}$ values exceeding 30 % are often assumed, but solar-to-fuel energy conversion efficiencies above 10 % are still pending experimental demonstration with robust and scalable solar reactors.[29–31] A value of 20 % is likely needed for solar fuels to be cost competitive.[32]

Both our experiments and simulations indicate that there is still room for improvement of the GAP and we should be able to reach even higher values in the future. Also, the overall energy efficiency can be improved when the efficiency of solar panels can be further enhanced or by producing the electricity needed for the plasma process with another renewable energy source. The latter option is not possible for photochemical and solar thermochemical technologies since their primary source of energy originates from sunlight.

4 Conclusions

In this chapter, we have investigated the performance of a novel type of gliding arc, the gliding arc plasmatron (GAP), for the conversion of CO_2, and we evaluated it in terms of its energy cost and efficiency for a wide range of conditions of plasma power and gas flow rate, and for different anode diameters of the setup. The best performance, in terms of both conversion and energy cost/efficiency, was reached in the configuration with the smallest anode diameter of 7.08 mm. The highest conversion of 8.6 % was obtained at an energy cost of 39 kJ/L (or 9.7 eV/molec) and an energy efficiency of 30 %, whereas the highest energy efficiency in this configuration was 35 %, corresponding to an energy cost of 33 kJ/L (or 8.3 eV/molec), but at a somewhat reduced conversion of 5.1 %. The reason that the configuration with the smallest anode diameter yields the best results can be understood from gas flow calculations, which demonstrate that the reverse vortex flow (RVF) is most strongly pronounced in this case. This RVF is indeed important for obtaining the highest CO_2 conversion, because it stabilizes the plasma in the middle of the reactor, as supported by 3D plasma simulations (performed by G. Trenchev within our group), and the gas flow is forced to go through the plasma, while the heat lost to the reactor walls is minimized.

In general, we can conclude that the GAP is very promising for CO_2 conversion, but we believe there is still room for improvement, since the conversion is still quite low. We compared our results with the conversion and energy efficiency of thermal CO_2 splitting, as well as with results of other types of plasmas and novel CO_2 conversion technologies. It is very striking that the conversion and energy efficiency are higher in the GAP compared to thermal CO_2 conversion, owing to the non-equilibrium properties of the plasma, as the chemistry of the conversion process is induced by energetic electrons. Also when compared to other types of plasmas, it is clear that the GAP is one of the most promising candidates for CO_2 conversion, as this type of discharge operates at

atmospheric pressure and produces electrons with a typical energy in the order of 1 eV, which can vibrationally excite the CO_2 molecules, so that they can split into CO and O_2 in an energy-efficient way through the ladder-climbing process.

Our results indicate that the conversion rises upon lowering the flow rate because of the longer gas residence time in the reactor. However, we are limited in varying the flow rate in the current reactor setup, because a minimum flow rate is necessary to obtain a good vortex flow. Another way to increase the residence time in the reactor would be to increase the length of the cathode. This was tested for three different cathode lengths in pure CO_2. Increasing the cathode length gave an increase in conversion and had no effect on the energy efficiency. A longer cathode ensures that the arc is longer, which provides a longer residence time of the gas in the plasma, but also requires more power to maintain the plasma. The increased plasma power can thus also explain the increase in conversion. Using the current power supply, a higher power requirement due to a longer cathode can cause plasma instability in certain gas mixtures. For this reason, we did not use a longer cathode in Chapters 4 – 6, but instead used a shorter one to easily obtain a stable plasma.

Finally, we supported our experimental data with model calculations for the plasma chemistry, performed by S. Heijkers within PLASMANT, and obtained good agreement for the CO_2 conversion, energy cost, and energy efficiency. This indicates that we can use the model to elucidate the underlying plasma chemical processes of CO_2 conversion in the GAP. It is clear that vibrationally excited CO_2 significantly contributes to the CO_2 dissociation, and this can explain the good energy efficiency of CO_2 conversion. Furthermore, the simulations indicate that there is still room for improvement by exploiting even more the non-equilibrium character of the GAP, for example, by operating at conditions in which the temperature inside the arc can be reduced, so that the vibrational distribution function of CO_2 becomes more non-thermal.

References

1 T. Nunnally, K. Gutsol, A. Rabinovich, A. Fridman, A. Gutsol and A. Kemoun, *J. Phys. D. Appl. Phys.*, 2011, **44**, 274009.

2 M. Ramakers, G. Trenchev, S. Heijkers, W. Wang and A. Bogaerts, *ChemSusChem*, 2017, **10**, 2642–2652.

3 R. Aerts, W. Somers and A. Bogaerts, *ChemSusChem*, 2015, **8**, 702–716.

4 T. Kozák and A. Bogaerts, *Plasma Sources Sci. Technol.*, 2014, **23**, 045004.

5 A. Bogaerts, T. Kozák, K. van Laer and R. Snoeckx, *Faraday Discuss.*, 2015, **183**, 217–232.

6 W. Wang, A. Berthelot, S. Kolev, X. Tu and A. Bogaerts, *Plasma Sources Sci. Technol.*, 2016, **25**, 065012.

7 T. Kozák and A. Bogaerts, *Plasma Sources Sci. Technol.*, 2015, **24**, 015024.

8 A. Berthelot and A. Bogaerts, *Plasma Sources Sci. Technol.*, 2016, **25**, 045022.

9 R. I. Asisov, A. K. Vakar, V. K. Jivotov, M. F. Krotov, O. A. Zinoviev, B. V Potapkin, A. A. Rusanov, V. D. Rusanov and A. A. Fridman, *Proc. USSR Acad. Sci.*, 1983, **271**.

10 V. D. Rusanov, A. a. Fridman and G. V. Sholin, *Sov. Phys. Usp.*, 1981, **24**, 447–474.

11 L. F. Spencer and A. D. Gallimore, *Plasma Sources Sci. Technol.*, 2013, **22**, 015019.

12 A. Fridman, *Plasma Chemistry*, Cambridge University Press, New York, 2008.

13 G. J. van Rooij, D. C. M. van den Bekerom, N. den Harder, T. Minea, G. Berden, W. A. Bongers, R. Engeln, M. F. Graswinckel, E. Zoethout and M. C. M. van de Sanden, *Faraday Discuss.*, 2015, **183**, 233–248.

14 W. Bongers, H. Bouwmeester, B. Wolf, F. Peeters, S. Welzel, D. van den Bekerom, N. den Harder, A. Goede, M. Graswinckel, P. W. Groen, J. Kopecki, M. Leins, G. van Rooij, A. Schulz, M. Walker and R. van de Sanden, *Plasma Process. Polym.*, 2016, DOI: 10.1002/ppap.201600126.

15 L. F. Spencer and A. D. Gallimore, *Plasma Chem. Plasma Process.*, 2011, **31**, 79–89.

16 S. Y. Savinov, H. Lee, H. K. Song and B.-K. Na, *Korean J. Chem. Eng.*, 2002, **19**, 564–566.

17 F. Brehmer, S. Welzel, M. C. M. Van De Sanden and R. Engeln, *J. Appl. Phys.*, 2014, **116**, 123303.

18 K. Van Laer and A. Bogaerts, *Energy Technol.*, 2015, **3**, 1038–1044.

19 Q. Yu, M. Kong, T. Liu, J. Fei and X. Zheng, *Plasma Chem. Plasma Process.*, 2012, **32**, 153–163.

20 S. Paulussen, B. Verheyde, X. Tu, C. De Bie, T. Martens, D. Petrovic, A. Bogaerts and B. Sels, *Plasma Sources Sci. Technol.*, 2010, **19**, 034015 1-6.

21 A. Ozkan, T. Dufour, T. Silva, N. Britun, R. Snyders, F. Reniers and A. Bogaerts, *Plasma Sources Sci. Technol.*, 2016, **25**, 055005.

22 M. S. Bak, S. K. Im and M. Cappelli, *IEEE Trans. Plasma Sci.*, 2015, **43**, 1002–1007.

23 J. L. Liu, H. W. Park, W. J. Chung and D. W. Park, *Plasma Chem. Plasma Process.*, 2015, **36**, 437–449.

24 A. Indarto, D. R. Yang, J. W. Choi, H. Lee and H. K. Song, *J. Hazard. Mater.*, 2007, **146**, 309–315.

25 K. Yoshikawa, H. Kawasaki, K. Konishi, D. Adachi, H. Uzu, T. Irie, K. Yoshikawa, K. Nakano, T. Uto, W. Yoshida, K. Yamamoto and M. Kanematsu, *Nat. Energy*, 2017, **2**, 17032.

26 E. C. Neyts, K. Ostrikov, M. K. Sunkara and A. Bogaerts, *Chem. Rev.*, 2015, **115**, 13408–13446.

27 M. Schreier, F. Héroguel, L. Steier, S. Ahmad, J. S. Luterbacher, M. T. Mayer, J. Luo and M. Grätzel, *Nat. Energy*, 2017, **2**, 17087.

28 S. C. Roy, O. K. Varghese, M. Paulose and C. A. Grimes, *ACS Nano*, 2010, **4**, 1259–1278.

29 G. P. Smestad and A. Steinfeld, *Ind. Eng. Chem. Res.*, 2012, **51**, 11828–11840.

30 J. R. Scheffe and A. Steinfeld, *Mater. Today*, 2014, **17**, 341–348.

31 A. H. McDaniel, E. C. Miller, D. Arifin, A. Ambrosini, E. N. Coker, R. O'Hayre, W. C. Chueh and J. Tong, *Energy Environ. Sci.*, 2013, **6**, 2424.

32 P. Furler, J. R. Scheffe and A. Steinfeld, *Energy Environ. Sci.*, 2012, **5**, 6098–6103.

Appendix

1 Gas expansion factor

The CO_2 signals with and without plasma were obtained with gas chromatography by sampling a small volume of the gas stream. Subsequently, the concentrations were deduced from a calibration curve, which was obtained for a constant gas flow rate. However, the number of molecules and thus the volumetric flux increases along the reactor, as CO_2 is converted into CO and O_2 molecules. As can be seen in Equation (A1), two CO_2 molecules split into three molecules, which increases the volume by 50 %.

$$2\ CO_2 \rightarrow 2\ CO + O_2 \qquad \text{(A1)}$$

This gas expansion effect was not taken into account in the gas chromatography approach above, which up to now is used by almost all authors. However, depending on the gas mixture, it can be quite significant.[1,2] Indeed, the CO_2 conversion would be overestimated by a factor 1.5 for pure CO_2 in case of 100 % CO_2 conversion. Hence, in this chapter the gas expansion factor has been taken into account as explained below.

CO_2 is split into CO and ½ O_2, which gives rise to an expansion of the volume by up to a factor 1.5 (in case of 100 % conversion). The gas expands, but a sample loop with a fixed volume was used, so the pressure increases. However, the GC used in this work samples at atmospheric pressure, so part of the gas was lost due to depressurization in the GC system before injection. As a result, fewer molecules were present in the sample volume in comparison with the outlet flow. Since there were less CO_2 molecules in the sample, the CO_2 conversion will appear higher. The "faulty" conversions obtained from GC measurements were corrected by performing an iterative back

calculation. X_{GC} was calculated by solving the following equation for different (fixed) values of X_{Real} until X_{GC} matches the CO_2 conversion measured by the GC.

$$X_{GC} = 1 - \left(\frac{1 - X_{Real}}{1 + \left(\frac{X_{Real}}{2} \right)} \right) \quad \text{(A2)}$$

In this formula, X_{GC} is the calculated conversion measured by the GC after gas expansion for a certain value of X_{Real}, which is the real conversion. Hence, by doing this calculation for a range of different (fixed) X_{Real} values and matching X_{GC} to the "faulty" conversion measured by the GC, the real CO_2 conversion (X_{Real}) can be determined. More details about this method can be found in the paper published by Snoeckx et al.[3]

2 Detailed experimental results

2.1 Effect of power and flow rate on CO_2 conversion, energy cost and energy efficiency

The trends we have seen for the configuration with anode diameter 14.20 mm can also be observed for the configurations with anode diameter of 7.08 and 17.50 mm. For that reason, we will discuss the results of these two configurations together. Only the exact numbers change.

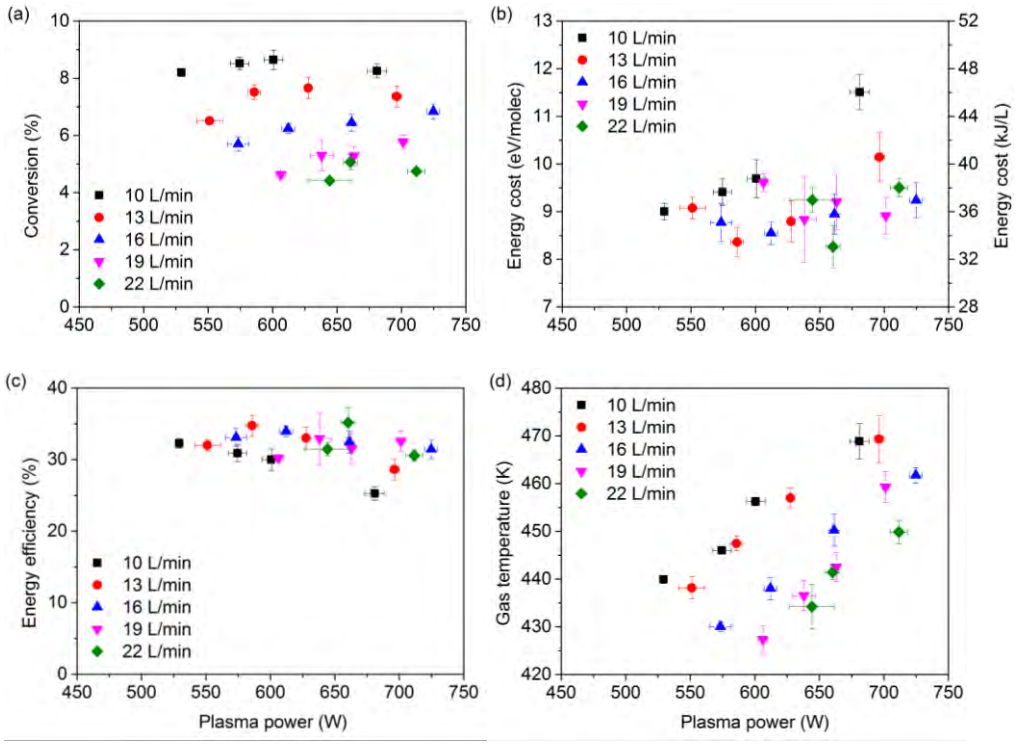

Figure A1 Conversion (a), energy cost (b), energy efficiency (c) and gas temperature of the effluent stream (d) as a function of plasma power for five different flow rates, for the configuration with anode diameter of 7.08 mm.

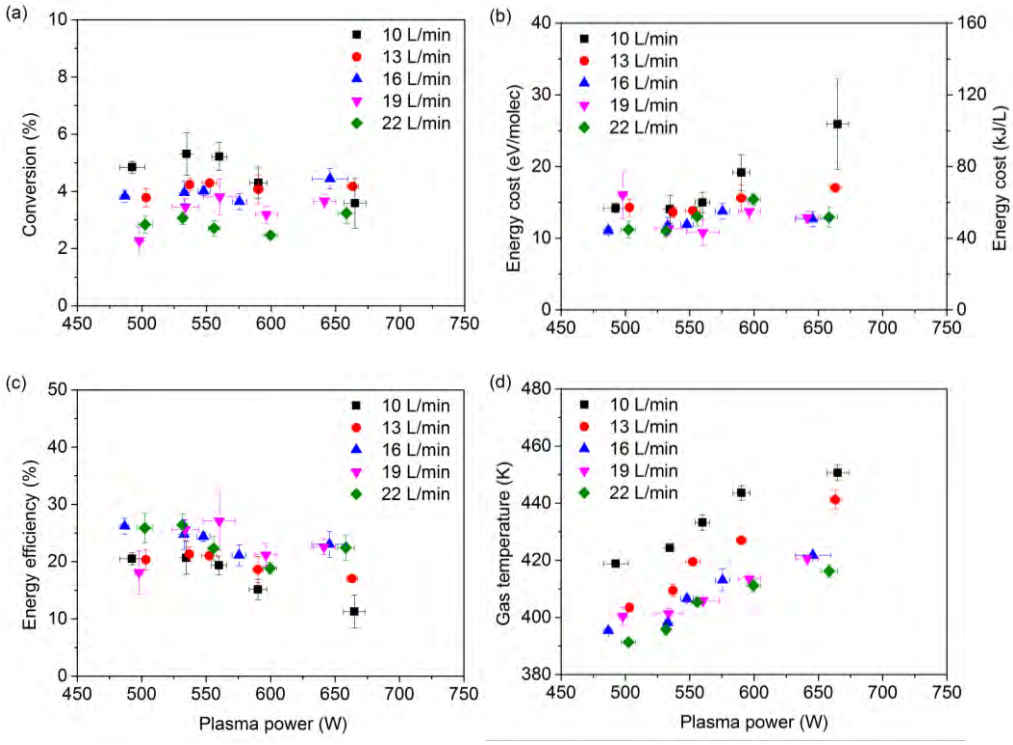

Figure A2 Conversion (a), energy cost (b), energy efficiency (c) and gas temperature of the effluent stream (d) as a function of plasma power for five different flow rates, for the configuration with anode diameter of 17.50 mm.

The conversion (Figure A1(a) and A2(a)) is higher at lower flow rate due to the longer residence time. There is, however, no significant influence of the plasma power on the conversion. The energy cost is plotted as a function of the plasma power in Figure A1(b) and A2(b). In these figures we can see that the energy cost follows the same trends as the conversion. The energy cost is higher at lower flow rate and there is no significant influence of the plasma power. In Figure A1(c) and A2(c) we see no clear dependence of the energy efficiency as a function of flow rate or plasma power. The gas temperature is higher at lower flow rate due to the longer residence time, as well as at higher plasma power, because of more significant gas heating. From Figure A1(a), A2(a) and A1(d), A2(d) it is clear that increasing the plasma power will not lead to an increase in conversion but will mainly be used to heat the gas.

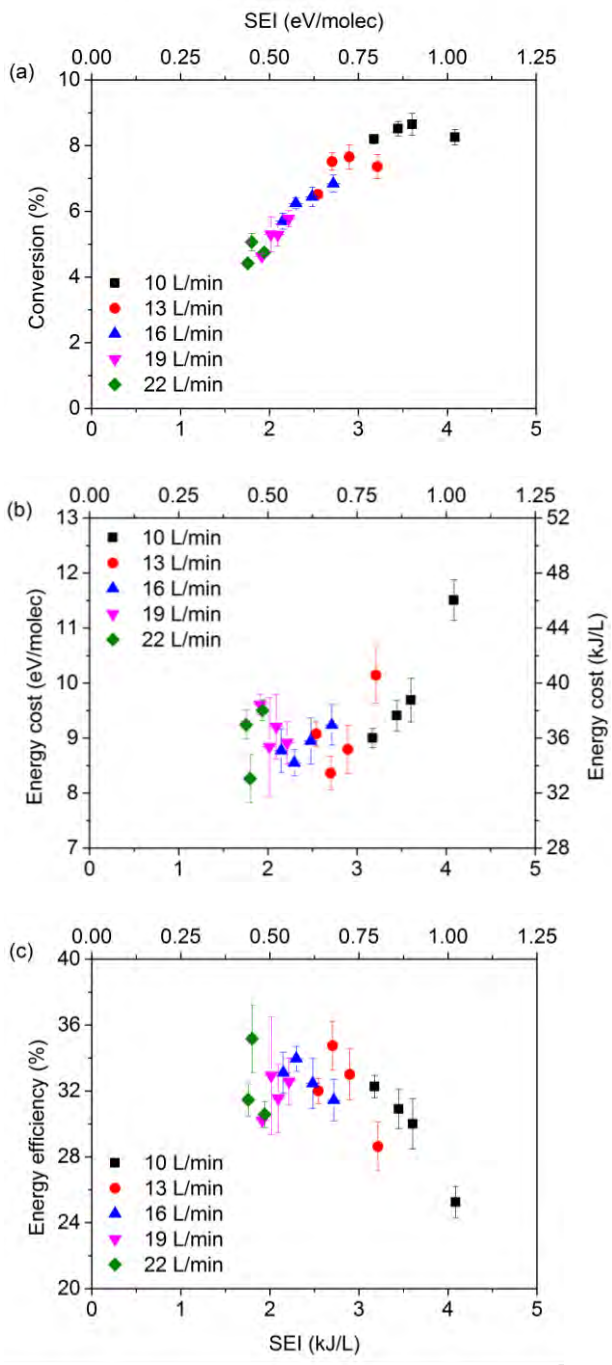

Figure A3 Conversion (a), energy cost (b) and energy efficiency (c) as a function of the SEI for five different flow rates, for the configuration with anode diameter of 7.08 mm.

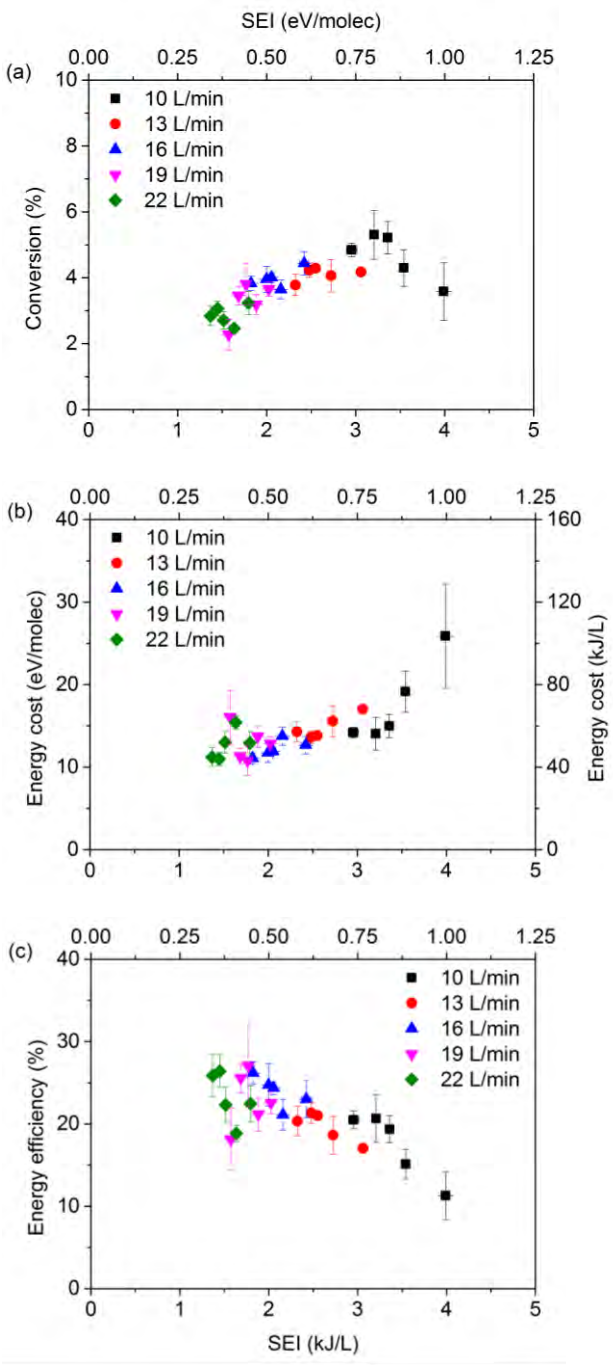

Figure A4 Conversion (a), energy cost (b) and energy efficiency (c) as a function of the SEI for five different flow rates, for the configuration with anode diameter of 17.50 mm.

The conversion increases with rising SEI, as seen in Figure A3(a) and A4(a). This is logical since more energy per molecule is available to convert CO_2. In Figure A3(b) and A4(b) the energy cost is plotted as a function of SEI. The energy cost rises with increasing SEI. Figure A3(c) and A4(c) show that the energy efficiency slightly decreases as a function of the SEI, which can be explained from the formula used to calculate the energy efficiency (Equation (5) in section 1.2).

2.2 Effect of the anode diameter on the vortex flow

To understand the effect of the anode diameter on the conversion, energy cost and energy efficiency, Georgi Trenchev (also PhD student within PLASMANT) performed gas flow simulations for the different configurations, showing how the vortex flow patterns are formed for different reactor outlet diameters. The results are depicted in Figure A5.

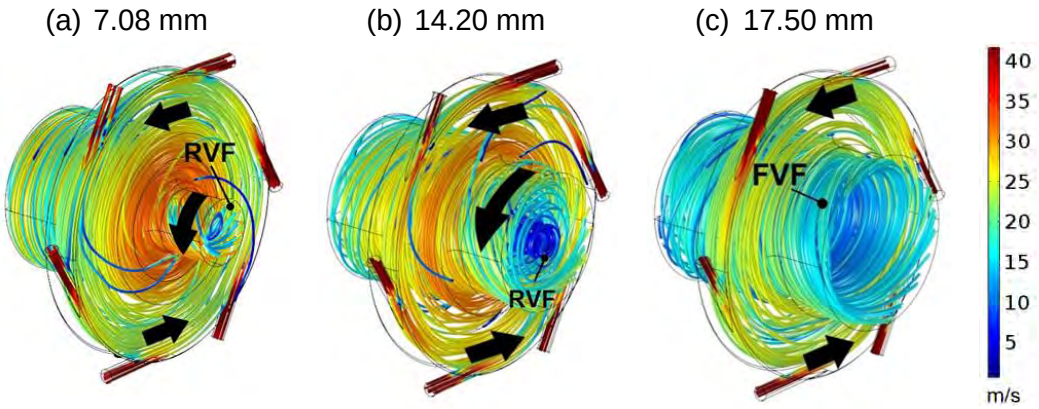

Figure A5 Flow pattern simulations in the three different configurations, with different anode diameters, as indicated above each figure. The legend on the right shows the axial velocity magnitude (in m/s). Calculations performed by G. Trenchev within PLASMANT.

The gas enters the reactor in a tangential stream through 6 inlets, i.e., they act as a swirl generator. Then it creeps along the walls in a spiral motion. When the anode and cathode diameter are equal (Figure A5(c)), the gas will move in this way towards both ends of the reactor (i.e., cathode and anode), and leave the reactor through the outlet at the anode end, in a

so-called forward vortex flow (FVF). However, when the anode diameter is smaller than the cathode diameter, the gas will only move in this spiral motion in the cathode region of the reactor. When the gas stream reaches the cathode cap, or end of the reactor, it will redirect to the reactor center, sustaining the circular motion, and finally exit the reactor through the other (i.e., anode) side. Indeed, a secondary, so-called reverse vortex flow (RVF) is formed with a smaller diameter (as the gas will lose rotational speed due to friction and inertia), being approximately equal to the outlet diameter.[4] The reverse vortex is best pronounced in the configuration with outlet diameter of 7.08 mm (Figure A5(a)), for two reasons: first, the gas is blocked from leaving the reactor directly from the outlet. Instead, it travels all the way to the cathode cap and back to the outlet. Second, the velocity magnitude is higher compared to the other configurations, because of the narrow outlet channel. A similar tendency can be noticed for the outlet diameter of 14.20 mm (Figure A5(b)), where the reverse vortex is still formed, but at lower velocity magnitude (see color table). A significant part of the gas leaves the reactor early, directly through the outlet. When the outlet diameter is 17.50 mm, i.e., the same as the reactor body diameter, the gas travels freely in both directions, as mentioned above, and almost no RVF is formed. Numeric data can be read from Figure A5 (see color table): in case (a), the reverse vortex shows a rather high magnitude of up to 20 m/s. In case (b), this velocity is much lower (2 – 5 m/s), and in case (c) it is almost 0, meaning that the reverse vortex is almost absent.

The main advantage of the RVF is clear: it forces a higher residence time of the gas in the reactor, and thus, in the arc discharge. Also, it provides thermal insulation of the discharge from the side walls, as the mass transfer always takes place from the walls to the plasma. This improves the ionization, excitation and dissociation efficiency in the plasma, as it lowers the thermal losses due to cooling by the walls. All these effects can explain the higher CO_2 conversion in the reactor configuration with the smallest anode diameter, where the RVF effect is most pronounced.

To further clarify that only the fraction of the gas which actually flows in RVF can pass through the arc, we plot in Figure A6 the calculated electron density profile in the reactor, as obtained from the 3D fluid model simulations.

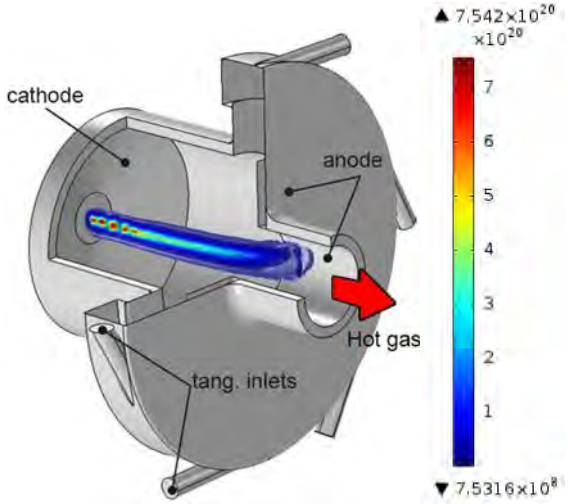

Figure A6 Calculated electron density profile at the inside of the reactor, in units of m^{-3}, for the reactor configuration with anode diameter of 7.08 mm, illustrating how the arc is concentrated in the center of the reactor. Calculations performed by G. Trenchev within PLASMANT.

As depicted in Figure A6, the arc is stabilized in the reactor center by the flow. This process can be followed through observing the time-dependent position of the arc in the model. The RVF configuration forces the gas to follow a path through the arc body, essentially forcing a longer residence time in the plasma for the gas molecules. Integrating the flow velocity over the arc surface results in a total flow of 96 L/min for the outlet diameter of 7.08 mm. Clearly, the gas is forced not only to move though the arc, but also to recirculate around it, effectively multiplying the amount of gas that is treated by the plasma. The actual effect might be even higher, as in the experiment the arc exhibits a spiral shape, while in the model it has to be approximated by a column due to the discretization mesh (see Figure A6). While computing the real arc shape might be theoretically possible, it is currently out of reach for our

calculation methods. Taking into account the axial gas flow velocity in the arc center, the average discharge residence time can be evaluated as 7 ms. This value is used as input in the 0D plasma chemistry model.

2.3 Calculated vibrational distribution function

As vibrationally excited CO_2 plays an important role in the CO_2 conversion, with a relative contribution of about 50 – 65 %, we plot in Figure A7 the vibrational distribution function (VDF) of the asymmetric stretch mode of CO_2, calculated by Stijn Heijkers (also PhD student within PLASMANT), for 4 different values of the SEI. The VDF exhibits a Boltzmann-like distribution, with a large vibrational temperature in the order of 2630 – 2840 K. When we compare this with the gas temperature inside the arc (i.e., maximum values up to 3000 K), we can conclude that the VDF is more or less thermal, which is as expected at this relatively high gas temperature. Earlier in the plasma, however, where the gas temperature is still somewhat lower, the VDF will also be somewhat more non-thermal. We observed a similar behavior in a microwave plasma[5] at high temperature and pressure and in a classical GA.[6] We believe that there is still room for improvement in the energy efficiency of CO_2 conversion in the GAP if we can somewhat reduce the temperature in the arc, so that vibration-translation relaxation processes, which depopulate the vibrational levels, can be reduced and the VDF becomes more non-thermal, with higher populations of the higher vibrational levels. On the other hand, the vibrational levels are clearly more populated than in other types of plasmas, such as a DBD, where the VDF dramatically drops for the higher vibrational levels.[7,8] This explains why the vibrational levels play an important role in CO_2 dissociation, and why the CO_2 conversion is quite energy efficient, compared to other plasma types.

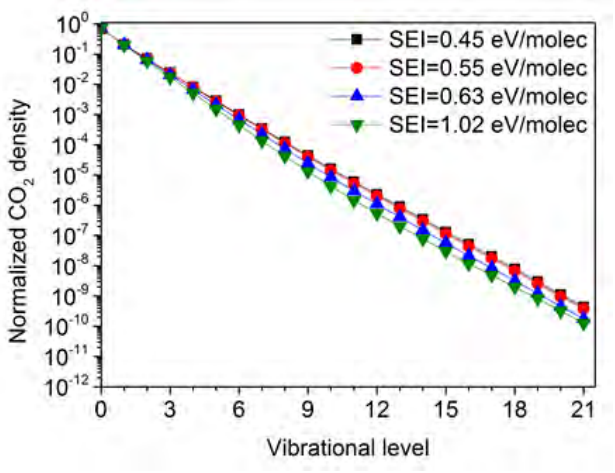

Figure A7 Calculated vibrational distribution function (VDF) of the asymmetric stretch mode of CO_2, for 4 different values of the SEI, as specified by the legend. Calculations performed by S. Heijkers within PLASMANT.

References

1 N. Pinhão, A. Moura, J. B. Branco, J. Neves, *Int. J. Hydrogen Energy*, 2016, **41**, 9245–9255.

2 N. R. Pinhão, A. Janeco, J. B. Branco, *Plasma Chem. Plasma Process.*, 2011, **31**, 427–439.

3 R. Snoeckx, S. Heijkers, K. Van Wesenbeeck, S. Lenaerts, A. Bogaerts, *Energy Environ. Sci.*, 2016, **9**, 30–39.

4 A. Gutsol, J. A. Bakken, *J. Phys. D. Appl. Phys.*, 1998, **31**, 704.

5 A. Berthelot, A. Bogaerts, Plasma Sources Sci. Technol. 2016, **25**, 45022.

6 W. Wang, A. Berthelot, S. Kolev, X. Tu, A. Bogaerts, *Plasma Sources Sci. Technol.*, 2016, **25**, 65012.

7 A. Bogaerts, T. Kozák, K. van Laer, R. Snoeckx, *Faraday Discuss.*, 2015, **183**, 217–232.

8 T. Kozák, A. Bogaerts, *Plasma Sources Sci. Technol*,. 2014, **23**, 45004

CHAPTER 3

Arc dynamics

This chapter is published as

Marleen Ramakers, Jose A. Medrano, Georgi Trenchev, Fausto Gallucci, and Annemie Bogaerts, Revealing the arc dynamics in a gliding arc plasmatron: a better insight to improve CO_2 conversion, *Plasma Sources Sci. Technol.* **2017**, *26*, 125002.

From the previous chapter we saw that a gliding arc plasmatron (GAP) is very promising for CO_2 conversion into value-added chemicals. Yet, to further improve this important application, a better understanding of the arc behavior is indispensable. Therefore, we study here for the first time the dynamic arc behavior of the GAP by means of a high-speed camera, for different reactor configurations and in a wide range of operating conditions. This allows us to provide a complete image of the behavior of the gliding arc. More specifically, the arc body shape, diameter, movement and rotation speed are analyzed and discussed. Clearly, the arc movement and shape rely on a number of factors, such as gas turbulence, outlet diameter, electrode surface, gas contraction and buoyance force. Furthermore, we also compare the experimentally measured arc movement to a state-of-the-art 3D-plasma model, which predicts the plasma movement and rotation speed with very good accuracy, to gain further insight in the underlying mechanisms. Finally, we correlate the arc dynamics with the CO_2 conversion and energy efficiency, at exactly the same conditions, to explain the effect of these parameters on the CO_2 conversion process.

1 Description of the experiments

The arc dynamics in the GAP were investigated by means of a CMOS high-speed camera. The main objective of this study was to reveal the movement of the arc as a function of different operating conditions, like the anode diameter, the feed flow rate and input current, as reported in Table 1. A photo and a schematic drawing of the GAP are illustrated in Figure 1. For these experiments, we used the same electrodes as in Chapter 2. A more detailed description can be found in the previous chapter. For all the experiments CO_2 is used as feed gas. Therefore, the results allow an assessment of the influence of the arc dynamics on CO_2 conversion.

Table 1 Experimental conditions selected for the plasma dynamics investigation.

Anode diameter (mm)	Feed flow rate (L/min)	Input current (A)	Different views recorded
7.08	10, 16, 22	0.35	Frontal, 90 ° angle
14.20	10, 16, 22	0.35	Frontal, 90 ° angle, 45 ° angle
14.20	10, 16, 22	0.05	Frontal, 90 ° angle
17.50	10, 16, 22	0.35	Frontal, 90 ° angle

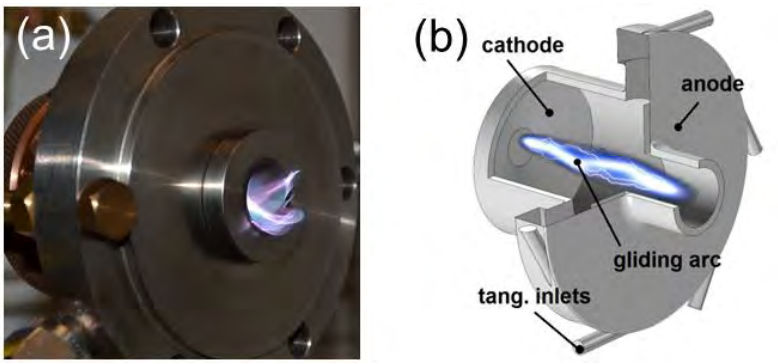

Figure 1 Photograph of the gliding arc plasmatron (GAP) (a) and schematic drawing of the internal structure (b).

The high-speed camera (Phantom SpeedSense 341 model) from DantecDynamics gives a maximum resolution of 2560 by 1600 pixels at a frame rate of 800 Hz, with the possibility to go up to 500 kHz at lower resolutions. For each experiment, the camera settings were first optimized in order to enhance the detection of the rotating arc. More specifically, the frame rate was selected to properly identify the arc rotation, and the exposure time of the detector was optimized to increase the contrast between the arc and the reactor. Since the arc rotation speed depends mostly on the anode diameter and the feed flow rate, it is important to optimize the recording frequency, so that the arc can be tracked while rotating inside the anode disk. In general, a frame rate of 3.4 kHz was selected for an image resolution of 800 × 800 pixels. Only for those cases where higher frequencies are demanded, like for high rotation speeds, the image resolution was decreased to 288 × 288 pixels, thus leading to recordings with a frame rate of 14 kHz. Similarly, the exposure time of the detector was optimized in order to find the best compromise between the following two properties: on one hand, it should be high enough to achieve sufficient contrast between the plasma and the reactor, so that it is possible to identify and track the plasma movement. On the other hand, since the plasma velocity is rather high, the exposure time should be low enough to avoid the plasma to become blurred due to the plasma movement during the image acquisition. For most of the cases, an exposure time of 5 – 10 μs was selected. Only in the case of reduced input current (0.05 A) an exposure time of 25 μs was selected.

To better understand the plasma dynamics inside the reactor, different views of the anode disk were recorded (see Figure 2). In particular, the arc rotation speed was calculated from a frontal view of the anode, based on the number of turns measured through the recordings as a function of the recording time. Since the plasma arc can rotate either inside the anode disk or in the outer part of the anode, two other views were recorded as well for selected cases. A 45 ° view was recorded for

the particular case of an anode diameter of 14.20 mm and a feed flow rate of 16 L/min to provide more information on the plasma behavior and also to obtain a better description for the comparison to the plasma dynamics modeling. The third view corresponds to the lateral recordings of the anode disk. In this case, the camera was aligned perpendicular to the feed gas, leading to a 90 ° view of the anode. Through these experiments, it was possible to visualize the end of the arc in the anode side and to discuss differences observed between the experiments.

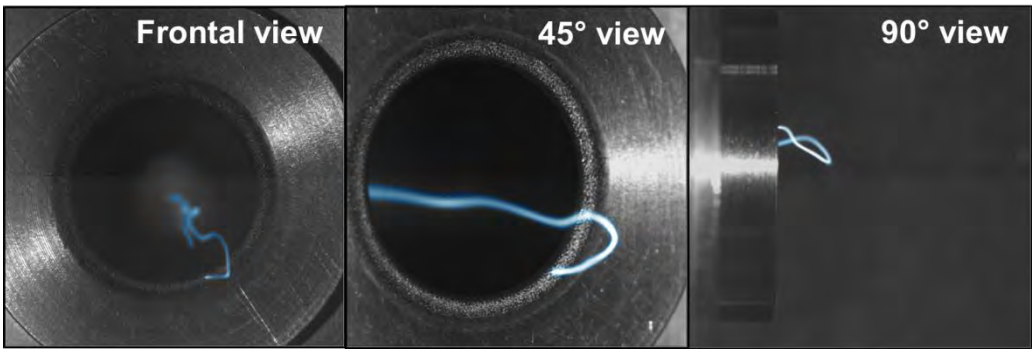

Figure 2 Snapshots of the different views for an anode diameter of 14.20 mm and a feed flow rate of 16 L/min.

The sequence followed for the recordings and post-processing of the data is similar for all the experiments and can be described as follows. At first, the camera was aligned and the lens was focused to the anode disk. Subsequently, the exposure time was selected accordingly to fulfill the two characteristics for a good recording, as mentioned above. Since the exposure time in that case was rather low, the reactor could hardly be identified. Therefore, a second recording was performed with a much higher exposure time (and absence of the arc) to overlap the arc movement with the reactor as background. To do so, the camera was kept aligned to the reactor and the recording was done with external (and homogeneous) illumination provided by two LED lights. The recorded images were analyzed using the commercial software Davis 8.0 from LaVision. The arc diameter and the distance of the plasma to

the anode disk in the 90 ° view were measured by converting first the image pixels into metric units.

In order to gain more insights in the plasma dynamics, statistical analysis of the experimental recordings has been carried out. In particular, a sufficiently long recording sequence (0.5 – 1 s) was applied for all the experiments listed in Table 1, which ensures a realistic representation of time-average results. Statistical analysis was carried out on the rotation speed by splitting the long-recording sequence into shorter ones. To do so, each recording was divided into 10 – 20 shorter recordings, which allows to elucidate better the arc rotation dynamics, especially in those cases where the arc moves from the inner to the outer part of the anode disk as discussed in the results section.

The average diameter of the arc was measured in the in-focus region, thus next to the anode, for random images at different positions within the anode disk. If the measurement was to be done in the out of focus region, the method would lead to less accurate results since the arc is not well defined. The analysis itself consists in the measurement of the number of pixels perpendicular to the arc direction. These pixels were subsequently converted into metric units by a calibration of the image size. The arc behavior in a GAP is a very dynamic process, thus it is important to repeat these measurements over time and at different positions in the anode side to get representative results of the arc properties. Statistics have been obtained by measuring the arc diameter of a minimum of 50 individual images in every experimental condition. Similarly, the average and standard deviation of the arc elongation from the inner to the outer part of the anode were obtained by measuring the longest perpendicular distance of the arc to the anode surface for more than 50 individual images of each recording.

2 Description of the modeling work

Complementary to the experiments, a 3D plasma model was developed by my colleague Georgi Trenchev within PLASMANT, for the purpose of studying the dynamic characteristics of the GAP. The model geometry was directly taken from the experimental setup. Only the internal structure of the reactor was simulated (see Figure 1(b)). The model was developed in 3D for argon, because a 3D model in CO_2 would yield an excessively long computation time. However, from 2D modeling in both argon and CO_2, we observed no difference in the arc shape, although the plasma characteristics were different (i.e., lower plasma density and higher gas temperature in CO_2). Thus, we may assume that the arc behavior in the argon and CO_2 GAP is quite similar.

The gas flow simulation was performed using the computational fluid dynamics module of the COMSOL software package.[1] A Reynolds-averaged-Navier–Stokes (RANS) turbulent model was used, as the rather high flow velocity promotes significant turbulence. More specifically, the model used for the gas flow was the shear stress tensor (SST) model.[2] The details of the model are described in the supporting information of reference 3.

3 Results and discussion

3.1 Arc behavior at different conditions

As mentioned in Table 1 above, we investigated the arc behavior for three different anode diameters, which give rise to different gas flow vortex patterns. Figure 3 shows snapshots of the arc in the different configurations (i.e., with different anode diameters). The results for the configuration with anode diameter of 14.20 mm are presented at both low (0.05 A) and high (0.35 A) electric current. In general, the arc can be seen as a thin wire with a spiral-like form. However, the arc behaves differently for the three different anode diameters. More specifically, we see a difference in arc diameter, elongation of the arc and rotation speed, as will be elaborated in more detail below.

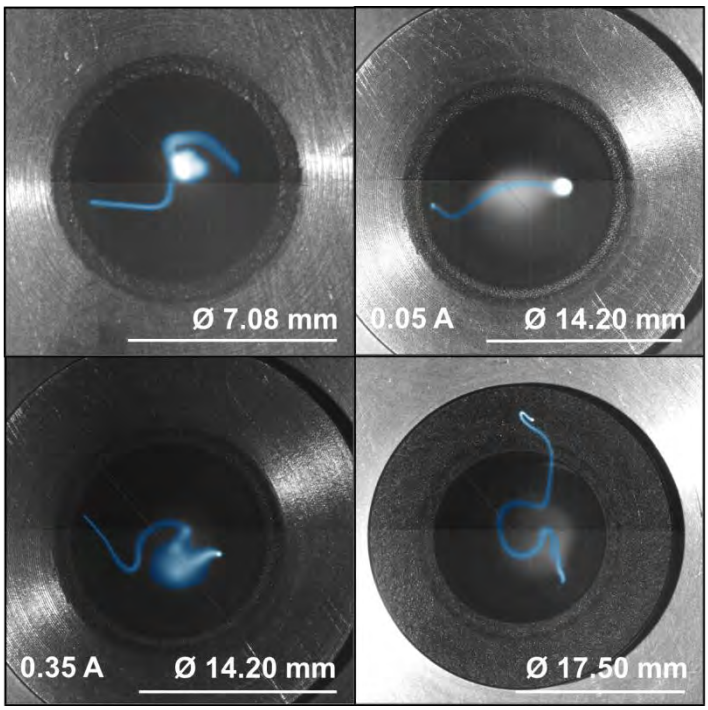

Figure 3 Snapshots of the arc discharge for the three different anode diameters investigated in this work. The top right and bottom left pictures correspond to an input current of 0.05 A and 0.35 A, respectively. The results for the two other anode diameters are at 0.35 A. The gas flow rate is 16 L/min in all cases.

In Figure 4, the arc diameter is plotted for the three different anode diameters, and in the case of 14.20 mm diameter also for two different electric currents. It is clear that when the anode diameter increases, the arc diameter rises as well. The arc diameter appears to be rather independent of the electric current in case of the anode diameter of 14.20 mm, but it was visible in the experiment that the arc is less bright for 0.05 A than for 0.35 A. This can be seen in Figure 3 as the soft white glow in the center for the 0.05 A case, while for 0.35 A, the glow around the arc is much brighter. The lower electric current will lead to less excitation and thus less bright plasma. We can conclude that these two cases correspond to different regimes of the arc, as was also demonstrated in Chapter 2. Furthermore, our experiments also revealed that changing the gas flow rate will not change the arc diameter.

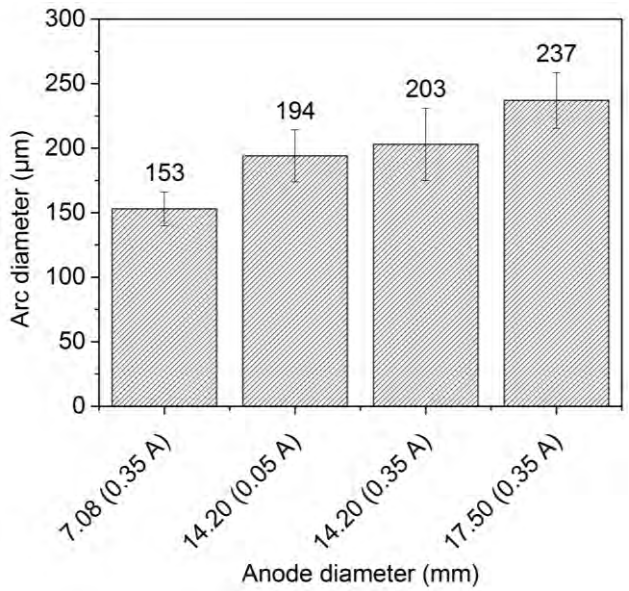

Figure 4 Arc diameter for the three different anode diameters, and in the case of 14.20 mm also for two different electric currents. The arc diameter does not depend on the feed flow rate for each anode diameter.

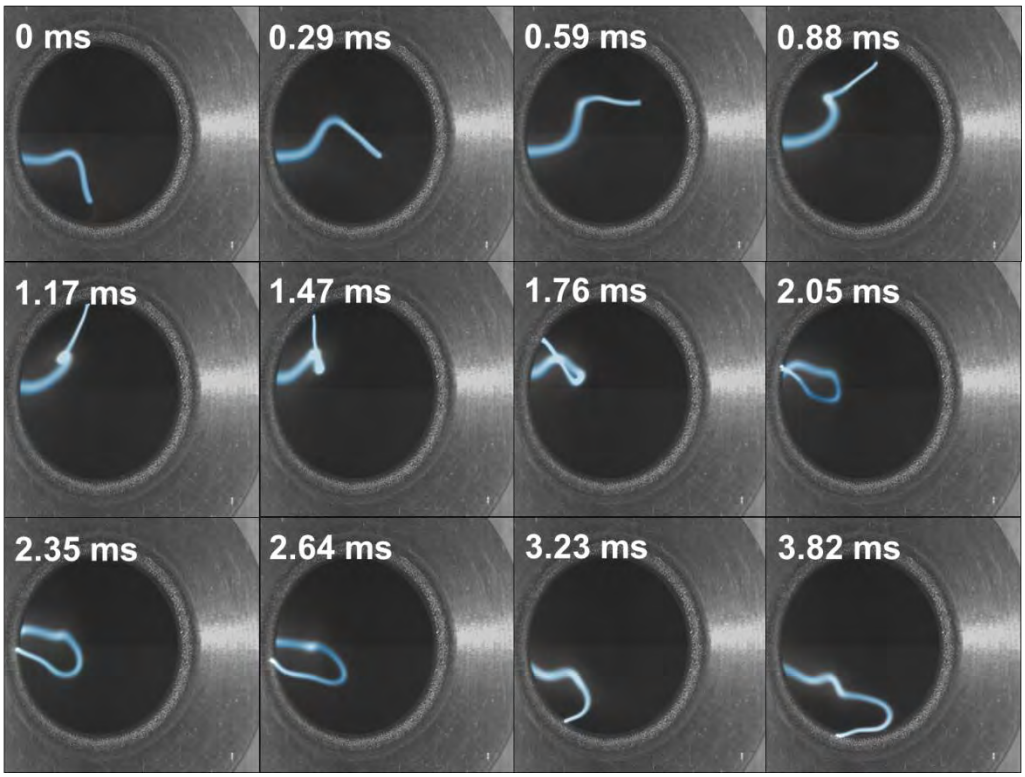

Figure 5 Snapshots at different times in the arc rotation for an anode diameter of 14.20 mm and a feed flow rate of 16 L/min from a side view of 45°. It is observed how the arc moves from the inner part of the anode to the external face of the anode disk.

Figure 5 shows snapshots at different times in the arc rotation for an anode diameter of 14.20 mm and a gas flow rate of 16 L/min from a side view of 45°. It can be observed that the arc moves from the inner part of the anode to the external face of the anode disk. This is also the case for the other configurations. However, we observe another phenomenon in the case of the configurations with anode diameter of 14.20 and 17.50 mm, that is not present in the configuration with anode diameter of 7.08 mm. In the first two cases, the anchor point of the arc at the anode moves along the external face of the anode disk towards the outer diameter of the anode, which has the same dimension for all the configurations. When the inner anode diameter increases, the arc moves further away from the inner diameter for the configurations with anode

diameter of 14.20 and 17.50 mm, respectively (see Movies 1 and 2 in the appendix or in the supporting information of reference 3). In these cases, the arc not only elongates from the inner part of the anode to the external face of the anode disk (as illustrated in Figure 5) but also along the external face of the anode disk towards the outer diameter of the anode. This can have consequences for the gas mixing and therefore also for the CO_2 conversion, which will be explained below.

Because of the movement of the anchor point of the arc along the external face of the anode disk, the arc comes out of the reactor, which can be seen in Figure 6. This is only the case for the configurations with anode diameters of 14.20 and 17.50 mm. In the configuration with anode diameter of 7.08 mm, the arc does not leave the reactor. In Figure 6, the length of the arc that comes out of the anode is also plotted as a function of the gas flow rate. When the gas flow rate is increased from 10 to 16 L/min in the configuration with anode diameter of 14.20 mm, the length of the arc coming out of the reactor also increases. However, if we increase the gas flow rate even further to 22 L/min, the arc length does not change anymore. If we compare the configurations with anode diameter of 14.20 and 17.50 mm, we see that for a gas flow rate of 16 L/min, the length of the arc is smaller for a larger anode diameter. Moreover, if we compare the case with an anode diameter of 14.20 mm at a gas flow rate of 10 L/min with the case with an anode diameter of 17.50 mm at a gas flow rate of 16 L/min, the length of the arc is similar. These observations can both be explained by the fact that for the configuration with anode diameter of 17.50 mm, the arc elongates more towards the outer diameter of the anode instead of lengthwise.

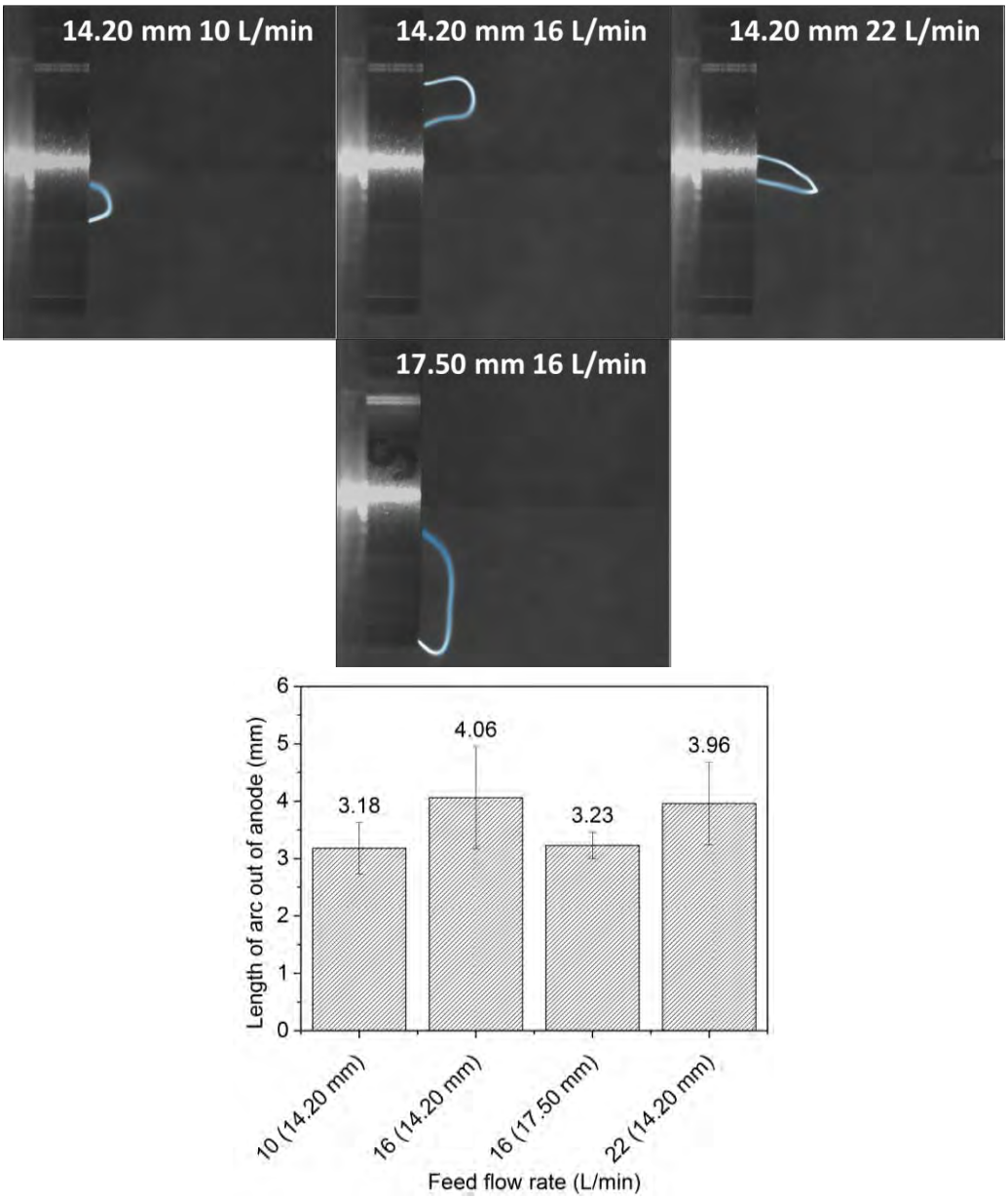

Figure 6 Snapshots of the arc discharge for an anode diameter of 14.20 mm (and gas flow rate of 10, 16, 22 L/min) and 17.50 mm (16 L/min) from a side view of 90°, as well as a graph with the length of the arc out of the anode, plotted as a function of the gas flow rate.

Besides the difference in arc diameter and elongation of the arc, also the rotation speed depends on the anode diameter. Snapshots at different times in the arc rotation for an anode diameter of 14.20 mm at a gas flow rate of 16 L/min are shown in Figure 7. The rotation is also visualized in Movie 3 in the appendix or in the supporting information of reference 3, where it is clearly observed that the arc 'hops' around the electrodes. It seems that the arc movement is dominated by reattachment on the electrodes and it does not follow a stable rotation. Therefore, the calculated rotation speed is only indicative. In Figure 8, the rotation speed is plotted as a function of the gas flow rate, for the three different anode diameters, as well as two different currents in case of the 14.20 mm anode diameter. The rotation speed significantly increases upon smaller anode diameter. Furthermore, in the case of 7.08 mm anode diameter, the rotation speed clearly increases with increasing gas flow rate, while this trend is less pronounced in the configurations with anode diameter of 14.20 and 17.50 mm. In case of 14.20 mm anode diameter at an input current of 0.05 A, we even see a decrease of rotation speed with increasing gas flow rate. The reason is that at 10 L/min, the arc rotates more smoothly as compared to the other gas flow rates, where we observed that the arc jumps backwards with a corresponding decrease in the rotation speed.

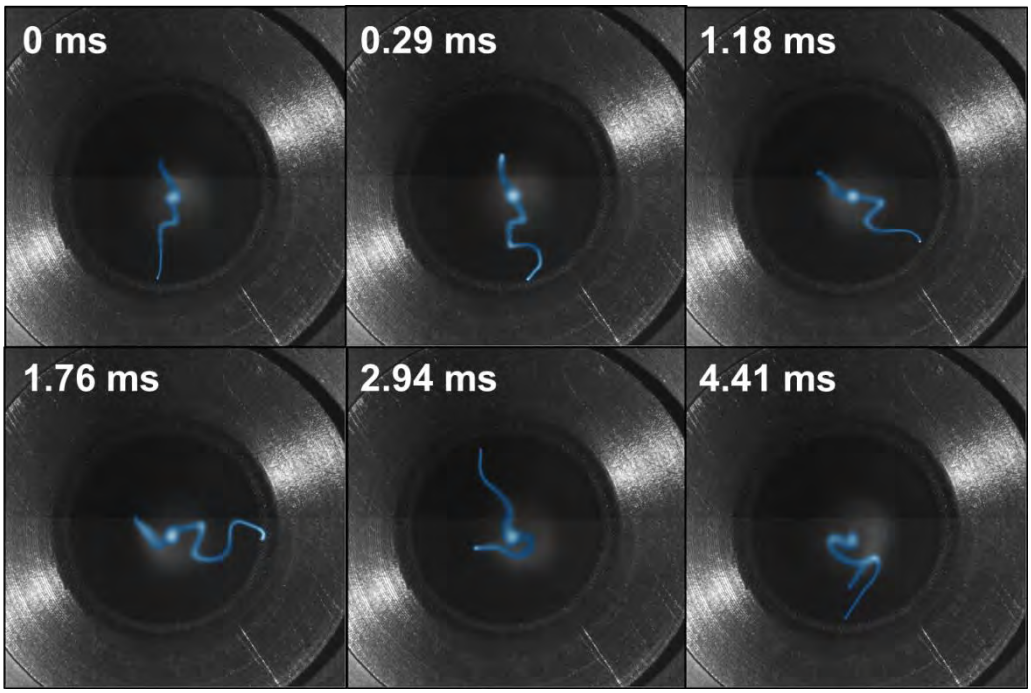

Figure 7 Snapshots at different times in the arc rotation for an anode diameter of 14.20 mm and a feed flow rate of 16 L/min.

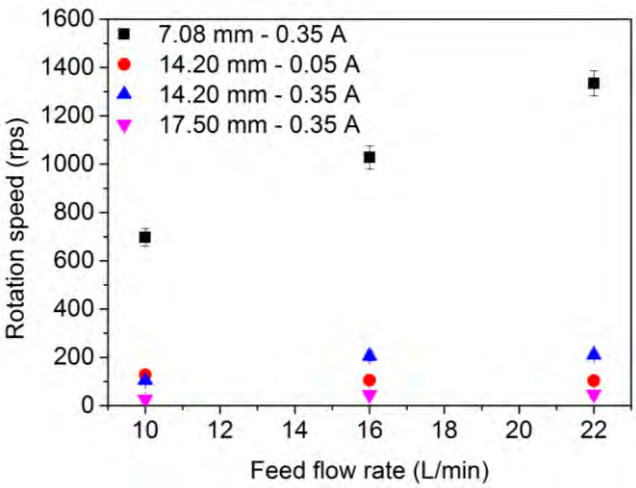

Figure 8 Rotation speed plotted as a function of gas flow rate, for the three different anode diameters, as well as two different currents for the anode diameter of 14.20 mm.

The dependence of the arc behavior on the different parameters can be explained based on the gas flow dynamics. First, gas flow rates and flow speed are directly linked to flow turbulence. Turbulence stands for small, local oscillations in flow speed, pressure and density, accompanied with turbulent 'vortices'.[4] These vortices are an essential part of the gas flow and will directly affect the arc shape by bending it into complex forms. Clearly, this has an impact on the arc length, which is linked with the overall dynamics of the arc, as the plasma conducts the electricity in the circuit, i.e., voltage, current and power will depend on the fluid dynamics. Using different anode diameters has a clear impact on the gas flow speed, and therefore, on the arc movement, and this is evident in the experiments. Furthermore, the mechanics of the arc also depend on factors such as electrode surface and temperature. Small bumps and scratches on the electrode caused by machining and natural wear can cause a local increase of the electric field, and attract the arc. Random arc jumps are indeed visible in the experiments, and they are attributed to this very factor. Moreover, as the arc remains at one spot for a longer time period, it will 'drill' even more holes on the electrode surface, eventually making a 'hot spot'. Normally, the arc will remain attached there in an 'anchored' state, causing damage to the cathode. When this was observed in our experiments, the cathode was replaced. We were thereby able to ensure that the effect of the cathode wear was minor in our experiments, compared to the effect of the arc current, gas flow rate and anode diameter. The arc current can also cause numerous changes in the arc behavior. First, higher current will contribute to higher Joule heating of the arc, and affect its temperature and contraction. This effect is observed in the experiments, where the low-current arc shows a wider, less defined arc body (see Figure 3). In addition, higher current can also increase the heating and therefore, 'anchoring' the arc to a certain point or a 'hot spot'.[5]

3.2 Arc dynamics—modeling results

To explain the behavior of the gliding arc, the results from the 3D plasma model are presented and compared with the experiments. The main motivation is to gain insight into the arc movement and its shape and position.

The gas flow pattern, simulated by G. Trenchev with the SST model, is illustrated in Figure 9. The results are represented as a streamline of the flow vector (Figure 9(a)) and an arrow plot of a 2D cut-plane (Figure 9(b)), for the configuration with anode diameter of 7.08 mm and a gas flow rate of 22 L/min. It is clear that the gas, when entering the reactor, first moves upward in the cathode part (which has a larger diameter than the anode part) in an outer vortex, and when it arrives at the closed end of the cathode part (= top in Figure 9(b)), it starts to flow downwards in a so-called reverse inner vortex with smaller diameter, because the gas has lost some rotational speed due to friction and inertia. This allows the gas to leave the reactor through the outlet (= anode part with smaller diameter).

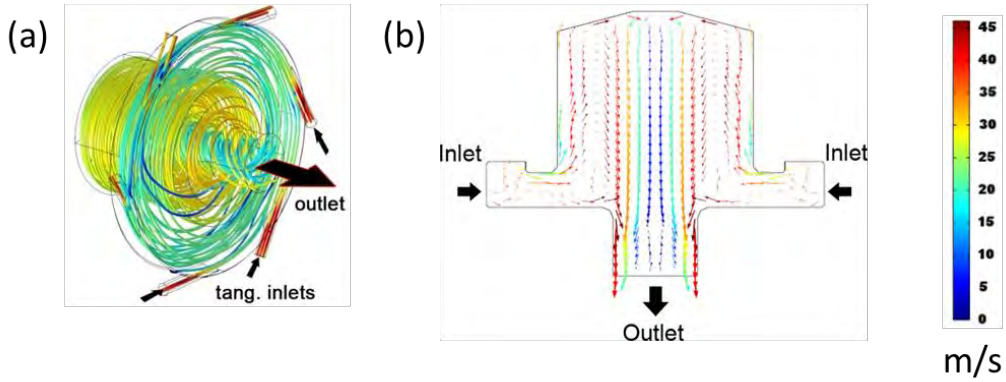

Figure 9 Streamline plot of the gas velocity and direction (a) and 2D arrow plot (b) illustrating the gas flow pattern. Calculations performed by G. Trenchev within PLASMANT.

The plasma simulation is performed using the gas flow data shown in Figure 9 as a stationary solution and an arc current of 0.24 A. The convection coefficients from the particle and heat balance equations are

directly derived from the flow vector, i.e., the arc moves in accordance with the gas flow. This can be clearly seen by visualizing the plasma density as a function of time.

As can be seen in Figure 10, the arc is ignited at the shortest distance between the anode and the cathode (Figure 10(a)), and it rotates in the reactor until it is stabilized in the reactor center by the flow (Figure 10(b)). The plasma density has a value around 10^{20} m^{-3}, which is typical for non-thermal arc plasmas in argon. The main features of the arc shape are resolved—it is a bent column, with characteristic hook-like attachment at the outlet (compare to Figure 7). Nevertheless, we have to keep in mind that the arc shape in the model is only approximate, as it is limited by the resolution of the computational mesh.

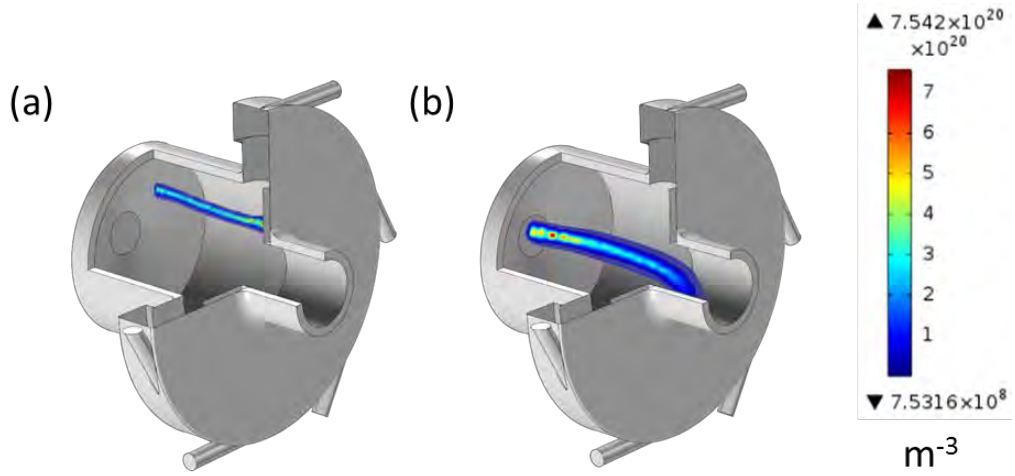

Figure 10 Calculated plasma density at an early stage of the arc at 2 ms (a) and a later stage at 4.6 ms (b). Calculations performed by G. Trenchev within PLASMANT.

The arc rotation can also be traced over time, after stabilization. In Figure 11, this process is illustrated in frontal view for a full (360 °) revolution. The calculated rotation period in the model is 0.7 ms for a gas flow rate of 22 L/min, which is in reasonable agreement with the experimental rotation period of 0.77 ms (i.e., rotation speed of 1300 rps; see Figure 8).

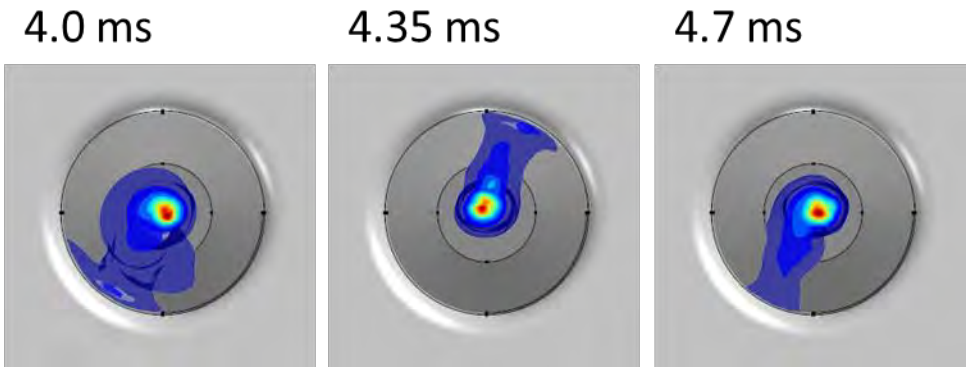

Figure 11 Arc position in frontal view, after stabilization in the reactor center, for a full rotation. Calculations performed by G. Trenchev within PLASMANT.

It is clear that several of the geometrical features of the arc, as observed in the high-speed photographs (see experimental section) are still missing from this simulation. In the model, the arc demonstrates a much simpler shape, resembling a bent column, while in the experiments many crooks and twists are present along its body, resembling a spiral spring. Computational limitations are the reason for this. First, the RANS flow model averages many of the turbulent vortices normally resulting in the flow, yielding a much smoother flow vector. This issue has been discussed before,[5] and it can only be solved by significantly higher computational power, which is not available at the moment for the method in use, i.e., COMSOL. Second, the discrete mesh density is limited, in order to provide reasonable computation times, which also leaves out many of the arc body details. Third, the boundary condition for the electrodes is adiabatic, meaning that they do not transfer heat. This effect can have an important influence, as already discussed in the experimental results section.

3.3 Influence of arc behavior on CO_2 conversion

To elucidate how the arc behavior can influence the CO_2 conversion, we plot in Figure 12 the CO_2 conversion (a), plasma power (b), SEI (c) and energy efficiency (d) for the different configurations at various operating conditions, as obtained from Chapter 2.

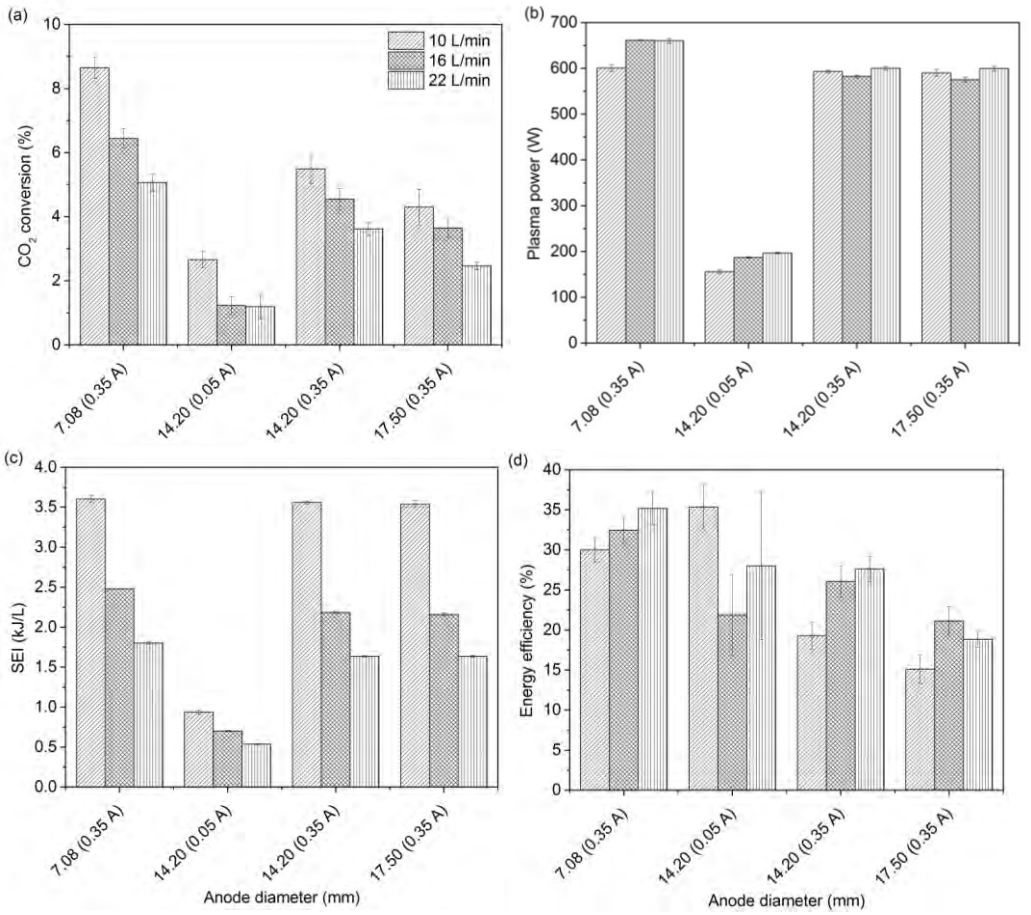

Figure 12 CO_2 conversion (a), plasma power (b), SEI (c) and energy efficiency (d) for the different configurations at various operating conditions, as obtained from Chapter 2.

We showed before that the arc diameter increases with increasing anode diameter (see Figure 4). This can lead to a drop in electron density as the same power is distributed over a larger volume, which can result in a lower conversion. Furthermore, when the anode diameter increases, the

gas velocity and therefore also the rotation speed will decrease (see Figure 8). Thus, there will be less mixing of plasma with the gas to be treated, so that less CO_2 can be converted. Another fact that indicates poor mixing in the configuration with larger anode diameter is the arc leaving the reactor. For the configuration with anode diameter of 7.08 mm the arc does not go outside of the reactor. However, as illustrated in Figure 6, in the case of 14.20 and 17.50 mm the arc leaves the reactor lengthwise, as well as along the external face of the anode disk. The length of the arc that comes out of the reactor is similar for both cases, but the elongation along the external face of the anode disk clearly differs. In the configuration with anode diameter of 17.50 mm, the arc moves all the way to the outer diameter of the anode, while in the case of 14.20 mm this elongation is limited. The arc leaving the reactor both lengthwise as well as towards the outer diameter of the anode has a negative effect on the conversion as there is less interaction of the plasma with the gas. All these effects, together with the fact that a smaller anode diameter leads to a more pronounced reverse vortex flow effect,[6] explain why the reactor with smaller anode diameter gives rise to a higher CO_2 conversion and energy efficiency, as is indeed obvious from Figure 12. The obtained CO_2 conversion is around 5.1 % - 8.6 % (rising with decreasing flow rate), while the energy efficiency is 30 % - 35 % (rising with increasing flow rate).

Figure 12 indeed illustrates, also for the other configurations, that a lower gas flow rate gives rise to a higher conversion, but a lower energy efficiency. This is merely attributed to the longer residence time of the gas in the plasma (for the conversion) and to the higher SEI (for the energy efficiency), and not so much to the arc dynamics itself. Indeed, the arc diameter does not change as a function of the gas flow rate. Furthermore, the effect of gas flow rate on the rotation speed and length of the arc coming out of the reactor for the configurations with anode diameter of 14.20 and 17.50 mm is also negligible. For the configuration with anode diameter of 7.08 mm, the rotation speed increases with

increasing gas flow rate. In this respect, we would expect that the conversion would increase because of a better mixing. However, the results indicate that the effect of the residence time has a larger contribution than the latter effect, which leads to a lower conversion for a higher flow rate. Since the plasma power is rather constant for each gas flow rate (see Figure 12(b)), it is logical that the SEI decreases with increasing gas flow rate (Figure 12(c)). As a consequence, the energy efficiency rises with increasing gas flow rate (Figure 12(d)).

Finally, if we compare the effect of electric current, for the configuration with anode diameter of 14.20 mm, it is clear from Figure 12 that a higher electric current results in more CO_2 conversion. The arc diameter is more or less the same for both cases (see Figure 4), while the rotation speed increases only slightly upon rising electric current (see Figure 8). However, these two currents form a different regime, as discussed in Chapter 2. Figure 3 clearly shows that the arc is less bright for an electric current of 0.05 A compared to 0.35 A. Hence, there is less excitation, due to the lower electron density, and therefore also a lower conversion, as indeed illustrated in Figure 12(a). This last phenomenon is also observed for the plasma power (Figure 12(b)). The plasma power is lower at an input current of 0.05 A compared to 0.35 A. This can be correlated with the observation that the arc is less bright for an input current of 0.05 A, and it supports our assumption that there is less excitation in this plasma regime. For some flow rates, the energy efficiency is higher at an input current of 0.05 A compared to 0.35 A. However, the corresponding conversion in these cases is quite low (Figure 12(a)). Therefore, these cases are overall not so interesting for CO_2 conversion.[6]

The CO_2 conversion and energy efficiency obtained in these experiments are quite promising, also when compared to other plasma reactors, including other types of gliding arcs. A detailed comparison of these results with data from literature for other plasma reactors was presented in the previous chapter.

4 Conclusions

We present here the arc dynamics of a novel type of gliding arc discharge, i.e., the GAP, which has reverse vortex flow stabilization, and we also discuss the effects of the gliding arc dynamics on the CO_2 conversion capabilities. We present for the first time high-speed camera images, which illustrate the arc stabilization process and the arc geometrical features in a GAP. Clearly, the arc movement and shape rely on a number of factors, such as gas turbulence, outlet diameter, electrode surface, gas contraction and buoyance force. We present results for different gas flow rates, arc currents and anode (outlet) diameters, showing how these parameters affect the arc diameter, rotation speed and elongation. In addition, we compare the experimental images to a state-of-the-art 3D-plasma model, which predicts the plasma movement and rotation speed with very good accuracy. Finally, we correlate the arc dynamics with the CO_2 conversion and energy efficiency, at exactly the same conditions, to explain the effect of these parameters on the CO_2 conversion process. This work is important for understanding and optimizing the GAP for CO_2 conversion.

References

1 COMSOL 5.0 https://comsol.com

2 F. R. Menter, M. Kuntz and R. Langtry, *Turbul. Heat Mass Transf. 4*, 2003, **4**, 625–632.

3 M. Ramakers, J. A. Medrano, G. Trenchev, F. Gallucci and A. Bogaerts, *Plasma Sources Sci. Technol.*, 2017, **26**, 125002.

4 D. C. Wilcox, *Turbulence Modeling for CFD*, DCW Industries, Third Edit., 2006.

5 G. Trenchev, S. Kolev and A. Bogaerts, *Plasma Sources Sci. Technol.*, 2016, **25**, 035014.

6 M. Ramakers, G. Trenchev, S. Heijkers, W. Wang and A. Bogaerts, *ChemSusChem*, 2017, **10**, 2642–2652.

Appendix

1 Movies

Movie 1: the arc rotates along the outside anode disk for an anode diameter of 14.20 mm.

Movie 2: the arc rotates along the outside anode disk for an anode diameter of 17.50 mm.

Movie 3: the arc 'hops' around the anode for an anode diameter of 14.20 mm.

CHAPTER 4

Combining CO_2 conversion and N_2 fixation

In this chapter, we provide a detailed experimental and computational study of the combined CO_2 and N_2 conversion in a GAP. The experiments and simulations reveal that N_2 actively contributes to the process of CO_2 conversion, through its vibrational levels. In addition, NOx are formed, with concentrations around 7000 ppm, which is slightly too low for valorization, but by improving the reactor design it must be possible to further increase their concentrations. We also compare our results with those obtained in other plasma reactors to clarify the differences in underlying plasma processes, and to demonstrate the superiority of the GAP. Finally, we also analyze the mechanisms to find out how we can enhance the NOx concentration to create opportunities for N_2 fixation or how we can inhibit the NOx formation when this has to be avoided for emission standards.

1 Description of the experiments

1.1 Gliding arc setup

The experiments were performed with the same GAP, which was developed at Drexel University by Nunnally et al.[1] and was described in detail in the previous chapters. As mentioned before, the reactor body acts as cathode (high voltage electrode), while the gas outlet is grounded (anode). The cathode (reactor body) has a length of 10.20 mm and a diameter of 17.50 mm, while the anode has a length of 16.30 mm and a diameter of 7.08 mm. These dimensions give rise to a reactor volume of 6.22 cm^3, but the arc volume is only about 0.13 cm^3. Indeed, it takes place only in the center of the reactor, thereby isolating the reactor walls from the hot plasma. A photograph and diagram of the entire experimental system used for this study is shown in Figure 1. It is slightly different from Figure 1 from Chapter 2, in the product analysis.

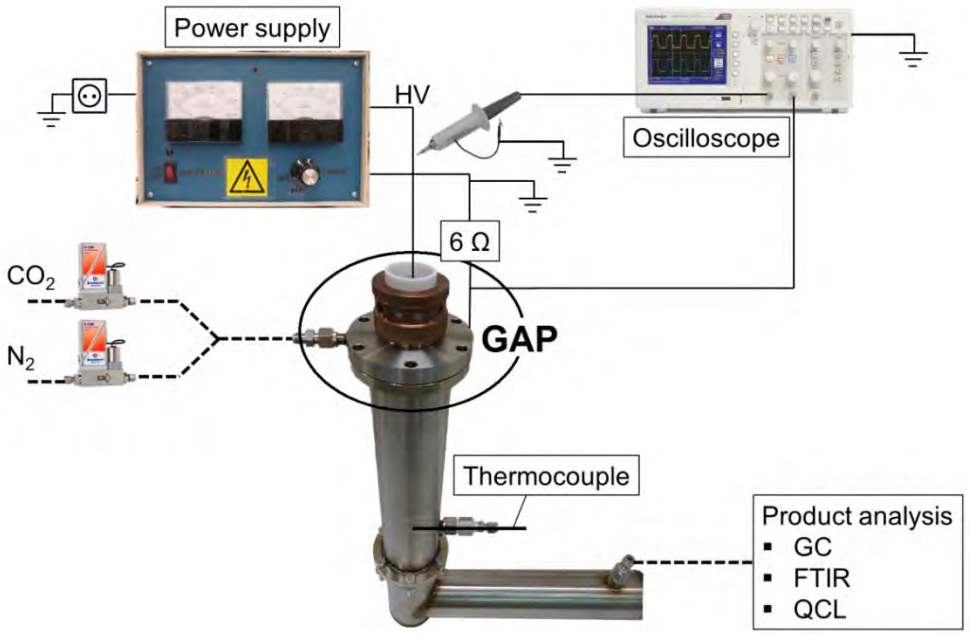

Figure 1 The plasma in the gliding arc plasmatron (GAP) is initiated by applying a high voltage over two electrodes with a power supply. The setup is completed by Mass Flow Controllers for gas input and measuring equipment, i.e., electrical (oscilloscope), temperature (thermocouple) and product analysis.

Mass Flow Controllers (Bronkhorst) were used to insert CO_2 and N_2 into the GAP. The total flow rate was kept constant at 10 L/min. The N_2 concentration was varied between 5 and 95 %. The pressure in the reactor is slightly higher than atmospheric pressure (1.25 bar). The reactor was powered by a DC current source type power supply. The plasma voltage and current were measured by a high-voltage probe (Tektronix P6015A) and a current sense resistor of 6 Ω, respectively. The electrical signals were sampled by a two-channel digital storage oscilloscope (Tektronix TDS2012C). The current was set at 0.23 A. The plasma power was calculated as the product of the plasma voltage and current over a certain time. All the experiments were performed three times. Subsequently, a propagation of uncertainty was applied to the results, to calculate the error bars.

1.2 Product analysis

The output gas composition was analyzed with three different gas analysis techniques: gas chromatography (GC), Fourier Transform Infrared spectroscopy (FTIR) and Quantum Cascade Laser (QCL) technology. The feed and main product gases (CO_2, N_2, CO, O_2) were analyzed by a three-channel compact gas chromatograph (CGC) from Interscience. Besides CO and O_2, we can expect that some other products, like O_3 and NOx compounds (i.e., NO, NO_2, N_2O, N_2O_3 and N_2O_5) are formed from the reaction of the active plasma species originating from CO_2 and N_2. We used a Nicolet 380 Fourier-Transform Infrared (FTIR) spectrometer (Thermo Fischer Scientific, Waltham, MA) and a CT5800 Analyzer (Emerson, Stirling, UK) based on Quantum Cascade Laser (QCL) technology to qualitatively and quantitatively analyze these products, respectively. These techniques, as well as the associated formulas to calculate the conversion, energy cost and energy efficiency, are described in more detail in the appendix.

2 Description of the model

Similar to Chapter 2, my colleague Stijn Heijkers within PLASMANT again simulated the chemical reactions in the GAP by a 0D chemical kinetics model. This model was briefly described in section 2 of Chapter 2. An extensive chemistry set, containing 18,180 reactions and 134 species, was included in the model. These species interact with each other through various chemical reactions, including: electron impact reactions, electron-ion recombination reactions, ion-ion, ion-neutral and neutral-neutral reactions, as well as vibration-translation (VT) and vibration-vibration (VV) relaxation reactions.

3 Results and discussion

3.1 CO_2 conversion, energy cost and energy efficiency

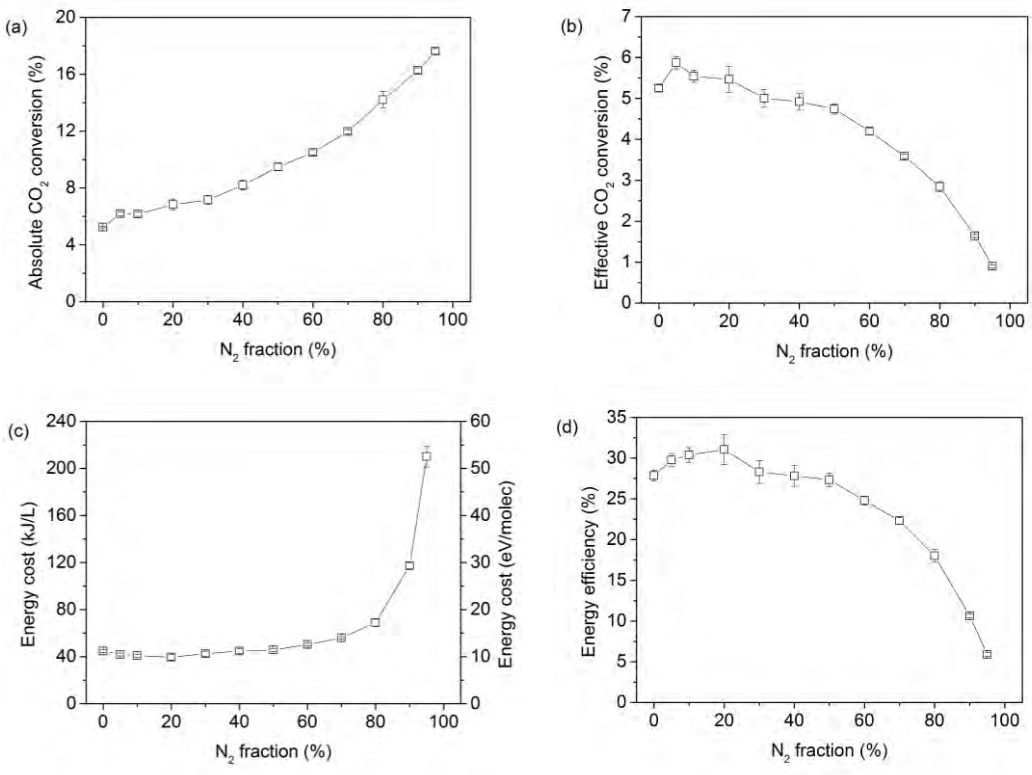

Figure 2 The addition of N_2 has a positive effect on the absolute CO_2 conversion (a). Up to a N_2 fraction of 50 % it does not (largely) affect the effective CO_2 conversion (b), energy cost (c) and energy efficiency (d), while a higher N_2 fraction causes a more pronounced drop in effective CO_2 conversion and energy efficiency, and a strong rise in energy cost. The experiments were performed with a total flow rate of 10 L/min and a plasma power of 350 W. The error bars are included in the graphs, but are sometimes too small to be visible.

Figure 2(a) shows that the absolute CO_2 conversion rises from 5 to 18 % with increasing fraction of N_2 in the mixture. Hence, N_2 helps to convert CO_2, by the transfer of energy from vibrationally excited N_2 molecules towards vibrationally excited CO_2, as explained in section 3.3 below. Indeed, it is known that CO_2 conversion in a GAP is most effective through the vibrational levels,[2,3] and the N_2 vibrational levels help to populate these CO_2 vibrational levels. The same mechanism was also

found for a microwave (MW) plasma,[4] while in a DBD plasma, another mechanism was found to be more prominent, i.e., energy transfer from the electronically excited N_2 molecules.[5]

The effective CO_2 conversion is obtained by accounting for the initial fraction of CO_2 in the mixture (see Equation (A1) in the appendix). At 5 % N_2 we observe a small increase in the effective CO_2 conversion, followed by a drop with increasing N_2 fraction. This can be explained from Figure 2(a) where the addition of 5 % N_2 gives a larger increase in absolute conversion than larger N_2 fractions. This strong increase is due to the fact that all the N_2 vibrational energy goes into the conversion of CO_2, while at higher N_2 fractions, some of this N_2 vibrational energy is also kept stored in these levels, or used for N_2 dissociation, or lost to translation (i.e., heating). Until a N_2 fraction of 50 %, the effective conversion only slightly decreases, while above 50 %, the effective conversion drops quite fast from 5 to 1 % (see Figure 2(b)). Thus, at N_2 fractions below 50 %, the increase in absolute CO_2 conversion can more or less compensate for the lower CO_2 concentration in the mixture, but at higher N_2 fractions, this is not true anymore. Indeed, not all the energy of the vibrationally excited N_2 is transferred into CO_2 dissociation, and part of it also remains stored in the N_2 vibrational levels or gets lost by collisions with ground state molecules (so-called vibration-translation (VT) relaxation). Thus, at higher N_2 fractions in the mixture, a larger portion of the applied power is used to activate the N_2 molecules, without converting all this energy into CO_2 dissociation.

The energy cost of CO_2 conversion is calculated according to Equation (4) from Chapter 2, and is shown in Figure 2(c). Until a N_2 fraction of 70 %, the energy cost has a value of about 40 kJ/L (or 10 eV/molec). At higher N_2 fractions, the energy cost rises dramatically to 210 kJ/L (or 52.5 eV/molec). The energy efficiency of CO_2 conversion (see Figure 2(d)) more or less follows the trend of the effective CO_2 conversion, since it is directly proportional to it. The fact that it does not exhibit exactly the same trend is due to a small drop in specific energy

input (SEI) upon N_2 addition (see Figure A1 in the appendix), and because the energy efficiency is inversely proportional to the SEI (see Equation (5) from Chapter 2). The energy efficiency remains more or less constant around 28 % until a N_2 fraction of 50 %, after which it decreases rapidly to a value of 5 %. Thus, upon increasing N_2 fraction in the mixture, more energy is consumed by the N_2 molecules, which cannot be used anymore for CO_2 conversion.

From these results we can conclude that up to a N_2 fraction of 50 %, the amount of N_2 has little effect on the effective (i.e., overall) CO_2 conversion, its energy cost and energy efficiency. In this respect, there is no need to separate N_2 from CO_2 in waste streams containing at maximum 50 % N_2.

The energy cost and energy efficiency reached in our GAP are very good compared to other plasma reactors, i.e., DBD and MW plasma.[4,5] This is clearly demonstrated from Figure 3, where the energy efficiency is plotted against CO_2 conversion in GAP, DBD and MW plasma. In general, most studies for CO_2 conversion are indeed carried out in these three plasma types,[6] but studies with addition of N_2 are still limited to these two references and our current work. From Figure 3 it is clear that the best energy efficiency is reached in the GAP. However, if we look at the CO_2 conversion, there is still room for improvement, and the MW plasma reaches higher conversion. Nevertheless, we have to note that the experiments with MW plasma were performed at reduced pressure (2660 Pa), while the GAP and DBD both operate at atmospheric pressure. If the pressure in the MW plasma would be increased, the conversion and energy efficiency would drop,[6–8] and in addition the plasma would become less stable.[6,8] When operating at reduced pressure, the energy cost of the pumping system should also be accounted for, and this would lower the overall energy efficiency of the process (not yet included in Figure 3). For industrial application of this technology, it would be beneficial to work at atmospheric pressure or higher.

However, not only the conversion and energy efficiency are important for evaluation of this technology. We also need to take into account the formation of byproducts, which will be elaborated in more detail in the next section. In addition, a detailed comparison between our results and the results obtained in a DBD reactor, also in terms of byproduct formation, are presented further in this chapter.

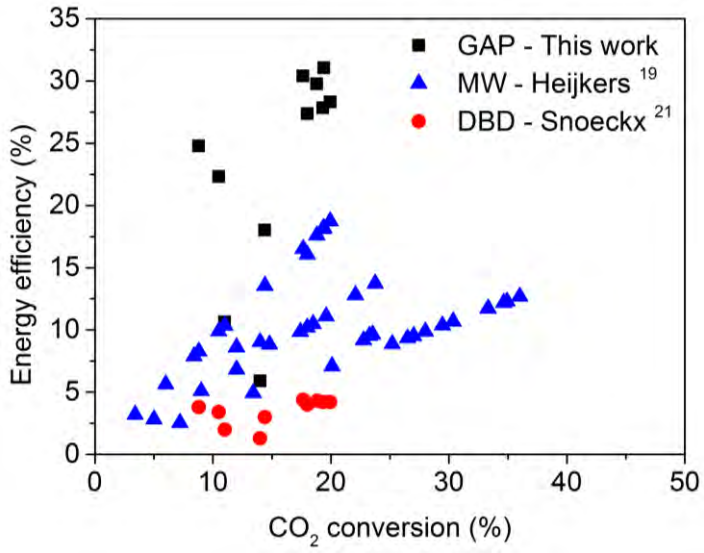

Figure 3 Comparison of the energy efficiency versus CO_2 conversion in three different types of plasma reactors mostly studied for CO_2 conversion: gliding arc plasmatron (GAP; this work), microwave plasma (MW; Heijkers[4]) and dielectric barrier discharge (DBD; Snoeckx[5]).

3.2 Analysis of the byproducts - NOx concentrations

Besides the main products of CO_2 splitting, i.e., CO and O_2, some other compounds were formed due to the presence of N_2 in the gas mixture. We used FTIR as a qualitative analysis method for the byproducts formed, such as O_3 and NOx compounds (i.e., NO, NO_2, N_2O, N_2O_3 and N_2O_5). The components that could be clearly distinguished from the FTIR-spectrum are CO, NO and NO_2. There were no signals visible for other components, like O_3, N_2O, N_2O_3 and N_2O_5. The influence of N_2 fraction on the NO and NO_2 concentration in arbitrary units is plotted in Figure A2 of the appendix.

To quantitatively analyze the NOx compounds, we used a CT5800 Analyzer based on Quantum Cascade Laser (QCL) technology. This allows us to quantify the concentrations of CO_2, CO, N_2O, NO and NO_2. However, we only focused on the NOx compounds, because the CO_2 and CO concentrations were far above the detection range and these compounds were already quantified with GC analysis. Furthermore, the QCL could not detect any N_2O, in agreement with the FTIR analysis. This means that the concentration of N_2O was never higher than 1 ppm. The concentrations of NO and NO_2 as well as the total NOx concentration, which can be expressed as the sum of the NO and NO_2 concentration, are plotted in Figure 4 as a function of N_2 fraction. The error bars are too small to be visible, as they were typically below 1 % of the actual concentrations, but the actual values of the concentrations, along with their absolute errors, are also listed in Table A1 in the appendix. All curves show a maximum around 50 - 70 % N_2. This is logical, because in this range, both CO_2 and N_2 split into the reactive species needed for NO and NO_2 formation. At very low or high N_2 fractions, either N_2 or CO_2 will act as limiting reactant. The fact that the maximum NO concentration is reached around 60-70% N_2 indicates that CO_2 dissociation occurs easier than N_2 dissociation, which is explained by the C=O vs. N≡N bond dissociation energy (i.e., 749 kJ/mol vs. 946 kJ/mol). The maximum NO_2 concentration is reached at 50% N_2, which is also logical, because its formation is favored when there is less N_2 in the mixture. If we look at the absolute values, the NO concentration is about 20 times higher than the NO_2 concentration, with maximum values of 6453 and 317 ppm, respectively.

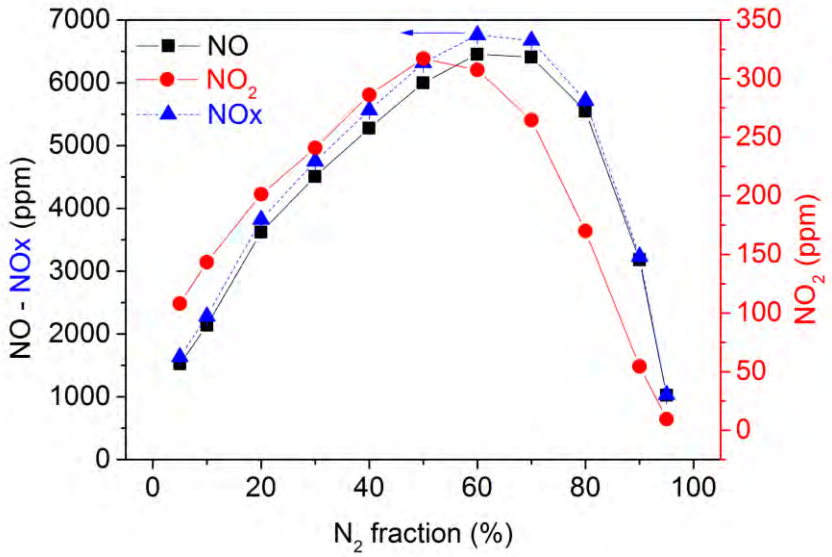

Figure 4 The NO (left axis), NO_2 (right axis) and total NOx (left axis) concentration follow a parabolic trend and reach a maximum at 50 - 70 % of N_2 in the initial gas mixture. The error bars are too small to be visible, as they were typically below 1 % of the actual concentrations, but the actual values of the concentrations, along with their absolute errors, are also listed in Table A1 in the appendix.

The highest total NOx concentration in our setup is reached at a N_2 fraction of 60 % with a total flow rate of 10 L/min and has a value of 6761 ppm. Patil et al. investigated NOx formation in a pulsed power milli-scale classical (planar) gliding arc reactor.[9,10] They reported the highest NOx concentration at a flow rate of 1 L/min and a 1/1 N_2/O_2 ratio of 2 %, with about 9470 ppm NO and 10,653 ppm NO_2. The formation of NO_2 from dry air in a classical gliding arc plasma was investigated by Bo et al.[11] in the context of VOC decomposition. The highest amount of NO_2 produced was 6982 ppm. Compared to our reactor, where we form 6453 and 317 ppm NO and NO_2, the NO_2 concentration lies much higher in the abovementioned studies. The reason is the higher temperature in our GAP, which favors NO above NO_2 formation, as revealed by computer simulations. Moreover, these studies were for NOx formation from N_2/O_2 as a starting mixture, where simply more O_2 is available to form NO_2, while in our case it depends on the CO_2 conversion. Indeed, we investigate for the first time

the possibilities for NOx formation from CO_2/N_2 as starting mixture. If this is feasible, we do not only fixate N_2 but also convert CO_2 at the same time. In this way we accomplish two goals at once.

A possible downside, however, can be the more complicated separation of CO from the mixture, compared to pure CO_2 splitting. Nevertheless, there are already technologies available today for the purification of CO-containing streams with an emphasis on CO/N_2 separation, such as cryogenic distillation and absorption.[12] However, the associated energy consumption of such approach and/or the poor stability of the absorbents have led researchers to concentrate on adsorption technologies, which are currently under development. Examples of adsorbents are zeolites (particularly Zeolites X and Y), modified activated carbons (particularly via impregnation with copper), as well as metal-organic frameworks.[12] In another approach, the produced NOx could be catalytically converted into HNO_3 first. Subsequently, the CO can be separated in a similar way by for example PSA as in the case of pure CO_2 splitting. Hence, for this approach, the catalytic conversion of NOx into HNO_3 represents an extra step for the separation. This should be taken into account when investigating whether the combined CO_2/N_2 conversion is economically feasible or not. However, this is outside the scope of the present study, because it requires an extensive techno-economic analysis, taking into account also the extra product that is produced.

Plasma-based NOx formation from N_2/O_2 mixtures has also been studied in a large number of other plasma types.[9,10,13–26] An overview of the measured values for NOx yield and energy consumption for these various plasma types is given in Table 1. Note that in our work and that of Snoeckx et al.[5] the starting mixture is CO_2/N_2, whereas in all other cases it is N_2/O_2.

Table 1 Overview of measured values for NOx yield and energy consumption for various plasma types[a].

plasma type	NOx yield	energy consumption	ref
gliding arc plasmatron (GAP) (*)	0.7 % NOx	7.02 MJ/mol NOx	this work
DBD (*)	0.06 % NOx	442 MJ/mol NOx	5
DBD with y-Al_2O_3 catalyst	0.5 % NOx	18 MJ/mol NOx	9,19
milliscale GA with pulsed power	2 % NOx	7.2 MJ/mol NOx	9,10
milliscale GA with pulsed power	0.8 % NOx	2.8 MJ/mol NOx	9,10
pulsed arc discharge	–	10.6 MJ/mol NOx	13
plasma arc jet	6.5 % NO	4.0 MJ/mol NO	14
laser-produced plasma	–	8.96 MJ/mol NO	15
exploding water jet discharge	1 % NOx	47.2 MJ/mol NOx	16
negative pulsed corona discharge	–	1638 MJ/mol NOx	17
positive pulsed corona discharge	–	1060 MJ/mol NOx	17
spark discharge	–	20.2 MJ/mol NOx	17
spark discharge	1 % NOx	2.41 MJ/mol NOx	18
MW discharge with MoO_3 catalyst	6 % NO	0.84 MJ/mol NO	20
pulsed MW discharge	6 % NO	0.60 MJ/mol NO	21
MW discharge with magnetic field	14 % NO	0.30 MJ/mol NO	22
MW discharge	0.6 % NOx	4.05 MJ/mol NOx	23
shielded sliding discharge	0.1 % NOx	15.4 MJ/mol NOx	24
electric arc (original Birkeland-Eyde process)	1 – 2 % NO	2.41 MJ/mol NO	25
electric arc with water injection	4.7 % NO	3.50 MJ/mol NO	26

[a] In some references, the NOx yield was not mentioned, and only the energy consumption was mentioned.
(*) CO_2/N_2 as starting mixture.

The results reported in literature vary depending on the plasma parameters. The NOx yield ranges from 0.06 to 14 %, while the energy consumption ranges from 0.3 to 1638 MJ/mol NOx. Thus, the GAP seems to perform at the lower limit for the NOx yield. In this respect, it is clear we still need to improve its performance, as also mentioned above. On the other hand, if we look at the energy consumption the GAP performs better, with a moderate value around 7 MJ/mol NOx. To make a fair comparison, however, we have to take into account that the starting mixture is CO_2/N_2. Therefore, the NOx yield is limited by the CO_2 conversion, which supplies the oxygen for NOx formation. In addition, this also affects the energy consumption, since part of the energy supplied to the plasma will also be used for CO_2 conversion and not only for NOx production. The real energy consumption for NOx formation in the GAP will thus be lower than 7 MJ/mol NOx.

For a DBD reactor with[9,19] and without catalyst[5], the NOx yield is lower with considerably higher energy consumption than for MW and GA discharges. The energy consumption of 442 MJ/mol NOx from reference 5 is again overestimated, for the same reason as in our work. The reason is that MW and GA plasmas are characterized by a reduced electric field (i.e., ratio of electric field over gas number density) between 5 and 100 Td, where the dominant electron-induced process is vibrational excitation of N_2,[27] similar as for CO_2.[6] Thus, in GA and MW discharges large amounts of vibrationally excited N_2 molecules are present, which provide more energy-efficient N_2 dissociation. DBDs are characterized by higher reduced electric fields, above 100 – 200 Td, and are therefore less efficient in vibrational excitation of N_2. Indeed, in a DBD mostly electronically excited species are involved in NOx production, which is thus limited by the higher energy cost for the formation of these species. A more detailed comparison between our results and the results obtained in a DBD reactor are presented further in this chapter.

If we compare our results with the results of the milliscale GA with pulsed power from Patil et al.[9,10], their NOx yield is more than twice as high, while the energy consumption is more or less the same. They also obtained results with similar NOx yield but lower energy consumption. However, we have to take into account the different starting mixture. The NOx yield in our GAP is lower because we produce NOx from CO_2/N_2 instead of N_2/O_2, and part of the energy will be consumed by CO_2 so the energy consumption that we calculated for NOx production is overestimated. Despite the lower NOx yield, we can conclude that NOx production starting from a CO_2/N_2 mixture in a GAP is worth investigating further, since it has similar energy consumption than starting from an N_2/O_2 mixture and it can solve two problems at the same time. Some ways to increase the NOx yield in our GAP are suggested below.

The best results up to now were obtained in MW plasmas[20–22] but they were operated at reduced pressure. As already mentioned, this requires pumping installations, which makes it less attractive for industrial implementation, and it should be accounted for in the calculation of the energy consumption, so the values listed in Table 1 would be higher if this was accounted for.

To make the process effective for N_2 fixation, the NOx concentration should increase above 1 %.[28,29] Indeed, it is stated by Ingels et al.[29] that low concentrations of about 1 % can already be used to make high concentrations of HNO_3. In this respect, plasma processes in general have to make efforts to increase the conversion and as a result increase the NOx concentrations. The CO_2 conversion in our GAP is still limited to 8 – 18 %, which is due to the limited amount of gas passing through the actual arc plasma column.[2,30,31] If this fraction can be further enhanced by optimizing the reactor design or the gas inlet system, it would yield higher CO_2 conversions, and thus the NOx concentration could also rise further. From previous calculations we know that the

fraction of gas passing through the arc is 14.8 %.[30] Based on this, we calculated that the conversion inside the arc is about 71 %. This means we have to increase the fraction of gas passing through the arc up to minimum 22 %, which results in a CO_2 conversion of 16 %, if we want to reach a NOx concentration above 1 % (see more details in the appendix). A way to increase this fraction is by decreasing the radius of one or more tangential inlets in order to create a higher flow velocity so that more gas is forced into the central vortex. Besides this approach, we also want to change the cathode design to increase the electric field, which also increases the plasma production and arc stability. Other approaches are also possible, but this will need dedicated fluid dynamics simulations, which are currently planned in the research group PLASMANT.

The selectivity towards NO and NO_2 (see Equation (A5) and (A6) in the appendix) are plotted as a function of N_2 fraction in Figure 5. The NO selectivity rises from 93 to 99 % with increasing N_2 fraction, while the NO_2 selectivity decreases from 7 to 1 %. These opposite trends are logical since the sum of both selectivities has to be equal to 100 %. It can also be explained by the fact that with increasing N_2 fraction, the NO_2 production by NO oxidation becomes less important.

Our results exhibit similar trends as in the paper of Wang et al.[27], who studied NOx formation from a N_2/O_2 mixture in a milli-scale classical (planar) gliding arc reactor, but the absolute values are clearly different. Indeed, Wang et al.[27] obtained more or less equal selectivities of 50 % for NO and NO_2, except at very high or low N_2 concentrations, while in our GAP the selectivity towards NO is much higher than towards NO_2. This difference is attributed to the much higher temperature in our GAP (i.e., nearly 3000 K,[31] vs. 1000 – 1500 K in the classical gliding arc[27]), favoring NO above NO_2 formation, as well as the different starting mixture, and hence the different reaction mechanisms for the formation of NO and NO_2, as will be explained in section 3.3.

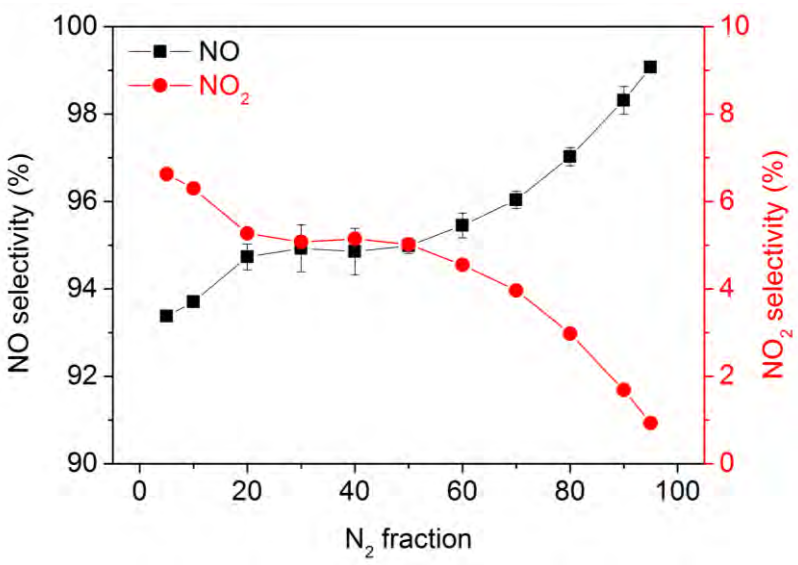

Figure 5 The NO selectivity (left axis) rises from 93 to 99 % with increasing N_2 fraction, while the NO_2 selectivity (right axis) decreases from 7 to 1 %. The error bars are included in the graph, but for some conditions they are too small to be visible.

When the NOx concentrations will still be a bit higher and thus effective for N_2 fixation, NO and NO_2 can be separated from the unconverted fraction by taking part in the Ostwald process, thereby producing nitric acid.[29] This can be used as precursor for the synthesis of more complex molecules, such as mineral fertilizers.

In the industrial Ostwald process, NH_3 is first oxidized to NOx and then absorbed by H_2O to form HNO_3. The typical yield from NH_3 to NOx is about 98 %. In our case, HNO_3 would also be made from NOx absorption by H_2O, but the yield from N_2 to NOx is considerably lower than in the industrial Ostwald process, so our process is by far not yet competitive with the Ostwald process. However, overall, producing HNO_3 from NH_3 is less sustainable, because the production of NH_3 is enormously energy intensive and produces a lot of CO_2. Hence, alternatives for the Haber-Bosch (HB) process must be investigated, and plasma technology is very promising in this respect, exactly because it can easily be combined with renewable energy, and it is thus a

sustainable alternative, especially for distributed production and in combination with renewable energy. Furthermore, the energy efficiency is very good, due to the selective activation of the molecules, as explained in this chapter. The potential of plasma technology was also recognized in a recent Science paper: "Nearly all nitric acid is manufactured by oxidation of NH_3 through the Ostwald process, but a more direct reaction of N_2 with O_2 might be practically feasible through further development of nonthermal plasma technology".[32] Furthermore, if we can produce HNO_3 from N_2 and CO_2 (without producing NH_3 as an intermediate step), this can be seen as a surplus in the CO_2 conversion reaction.

Currently, the oxidation of NO to NO_2 occurs in tubing and heat exchangers, cooling down the reaction mixture to shift the equilibrium towards NO_2 formation.[33] Subsequently, NO_2 is absorbed in water to form nitric acid.[34] Furthermore, the homogeneous non-catalytic nitric oxide oxidation can be transformed into a faster catalytic step by using a Pt/Al_2O_3 catalyst.[33,34] In addition, the selective oxidation of NOx into HNO_3 could also be made even more sustainable with photo catalysis, with for example TiO_2 as photo catalyst.[35–37] In this case, renewable energy (light) is used. If a selective catalyst is used, it is not necessary to separate NOx from the mixture.

It is worth to mention that several green technologies for NH_3 production from N_2 are being developed to replace the energy-intensive HB process, by using renewable energy,[38–42] and this NH_3 can then be further converted to HNO_3. However, the goal of our plasma process is different: it is mainly used for CO_2 conversion, and by making use of a waste stream which contains N_2, our process is also able to produce NOx, which can be further converted to HNO_3. In other words, our plasma process is a CO_2 conversion route, which has the added value of producing NOx by avoiding N_2 separation (if the current process can

still be improved of course). Hence, we believe our plasma process is a unique concept.

Although the current NOx concentrations are still somewhat too low for valorization, these high values, when released in the atmosphere, would cause environmental problems. Indeed, NO and NO_2 can react with VOC's in air, forming smog and acid rain.[43] This will have a negative effect on the air quality, with consequences for both human health and the environment. Therefore, if the NOx production cannot yet be valorized, the NOx emission must be avoided. This can be realized either by purifying the waste stream before CO_2 conversion, or by separating the NOx compounds after formation. As the NOx compounds have low concentrations, this can make the purification process more complicated compared to separating the CO_2 from the waste stream, because of low concentrations in the presence of other compounds. However, this depends on the actual waste stream and has to be evaluated separately for every process. Purely looking at the performance of the overall reaction, i.e., CO_2 conversion efficiency, we can conclude that up to 50 % N_2 fraction, we do not need pre-purification, but post-purification will be necessary, because the NOx amounts formed are not yet high enough to be effective for N_2 fixation. For a N_2 fraction above 50 %, pre-purification as well as post-purification is necessary, since a higher fraction of N_2 will reduce the reaction performance.

3.3 Underlying mechanisms as revealed by computer simulations

My colleague Stijn Heijkers developed a chemical kinetics model to investigate which mechanisms are important in the combined conversion of CO_2 and N_2 in our GAP (see brief explanation in section 2 of Chapter 2). The model has been validated against the experimental data for conversion, energy efficiency and NOx concentrations. In all cases, the trends and absolute values predicted by the model were in very good agreement with the experimental results, as illustrated in

Figure A3 and A4 in the appendix. Therefore, we can use the model to predict the underlying mechanisms.

In Figure 6, 7 and 8, we present the net time-integrated rates of the most important reactions for the loss and formation of CO_2, NO and NO_2, respectively. For additional insight, we also plotted the net contributions of these reactions in Figure A5, A6 and A7 in the appendix.

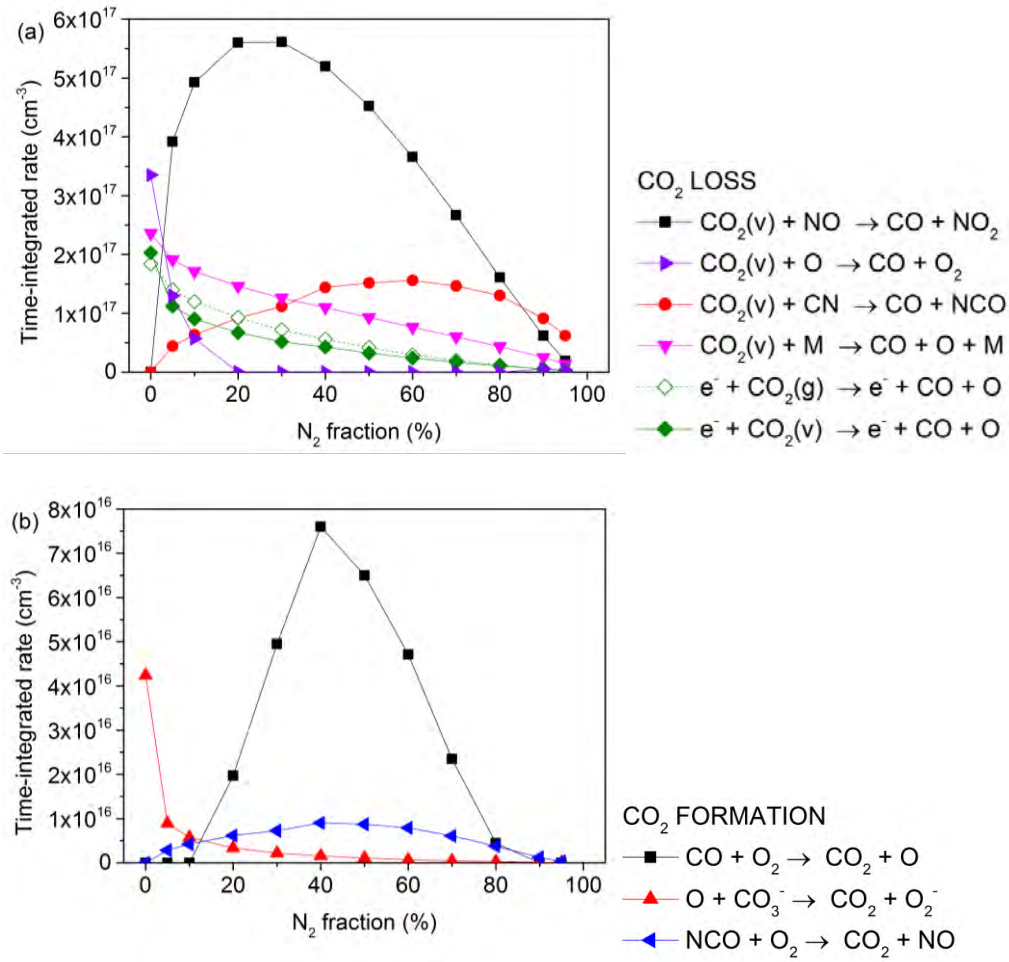

Figure 6 CO_2 mainly dissociates through reaction of its vibrational levels with NO (a), while the most important formation reaction is the recombination of CO and O_2 (b). Note that the time-integrated formation rate is an order of magnitude lower than the time-integrated loss rate. Calculations performed by S. Heijkers within PLASMANT.

For pure CO_2 the most important loss mechanism is the reaction of vibrationally excited CO_2 with O atoms, see Figure 6(a). This agrees well with earlier model predictions[2]. However, as soon as N_2 is added, the importance of this process quickly drops and the reaction of vibrationally excited CO_2 with NO becomes dominant, with an overall contribution of 50 – 60 % (see Figure A5 in the appendix). Other reactions, such as the collision of vibrationally excited CO_2 with CN or any molecule M in the plasma, and electron impact dissociation of both CO_2 ground state and vibrationally excited levels, also play a role, but their contribution is only 5 – 20 % (see Figure A5 in the appendix). The formation of CO_2 is mainly caused by recombination of CO and O_2 (see Figure 6(b)), with contributions up to 80% (see Figure A5 in the appendix). To prevent this recombination and thus enhance the CO_2 dissociation we should separate O_2 from the mixture. This might be possible with membrane technology or oxygen scavengers; however, this is outside the scope of this research.

Figure 7 and 8 illustrate the formation and loss mechanisms of NO and NO_2, respectively. NO is initially formed upon reaction of vibrationally excited N_2 molecules with O atoms, i.e., the so-called Zeldovich mechanism, in agreement with the observations for a milli-scale classical gliding arc reactor.[27] This is, however, not reflected in Figure 7(a), where the major NO formation mechanism is the reaction of O with NO_2, but of course, NO_2 first needs to be formed out of NO. Indeed, the most important loss mechanism for NO is its reaction with vibrational excited CO_2, forming CO and NO_2, which contributes for about 80 – 90%, except at very high N_2 fractions (see Figure A6 in the appendix). Hence, initially NO will be formed through the Zeldovich mechanism, but as soon as NO_2 is formed out of it, the reaction of NO_2 with O atoms will further produce NO. If we take a look at Figure 8, we see that the most important formation mechanism of NO_2 is indeed the most important loss mechanism of NO and vice versa. This indicates they are strongly

linked, mainly by their reaction with vibrational excited CO_2 and O atoms.

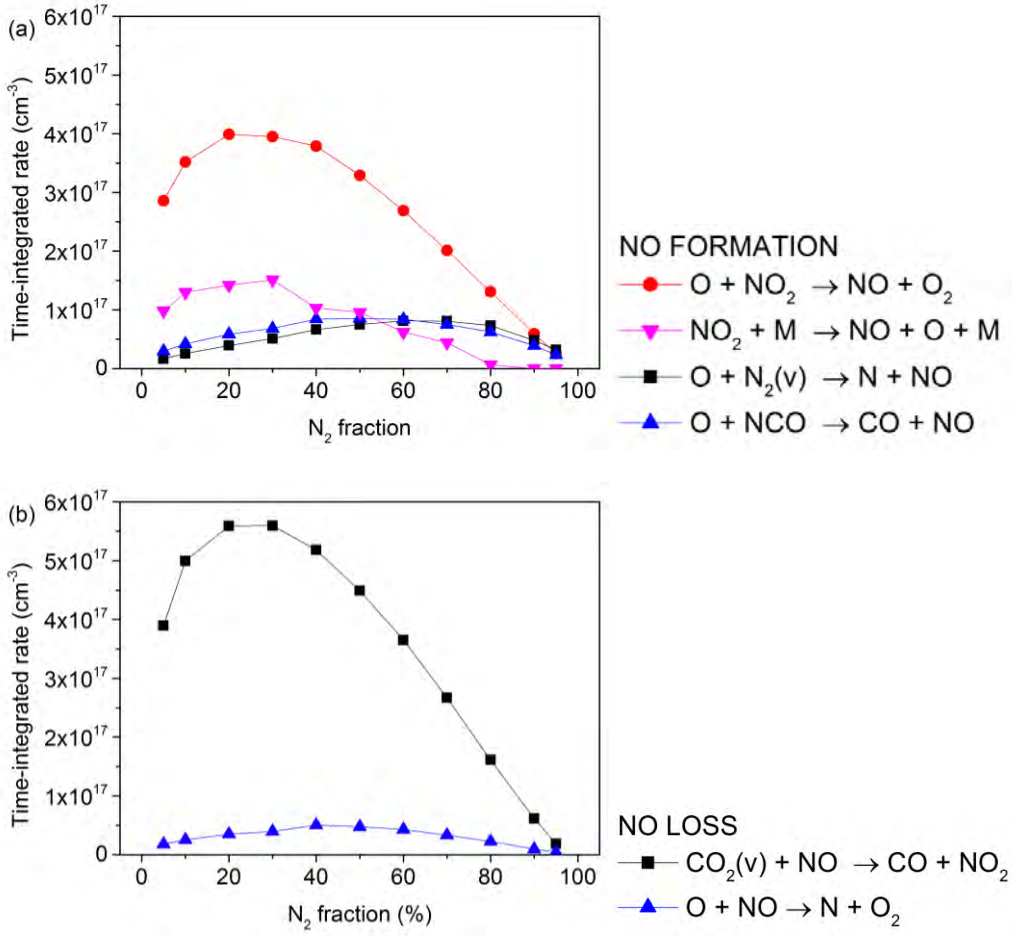

Figure 7 NO is initially formed upon reaction of $N_2(v)$ with O atoms, but is also further converted into NO_2, which is in turn converted back into NO. Indeed, overall NO is mainly formed from NO_2 upon reaction with O atoms, while reaction with vibrationally excited CO_2 predominantly transforms NO into NO_2. Calculations performed by S. Heijkers within PLASMANT.

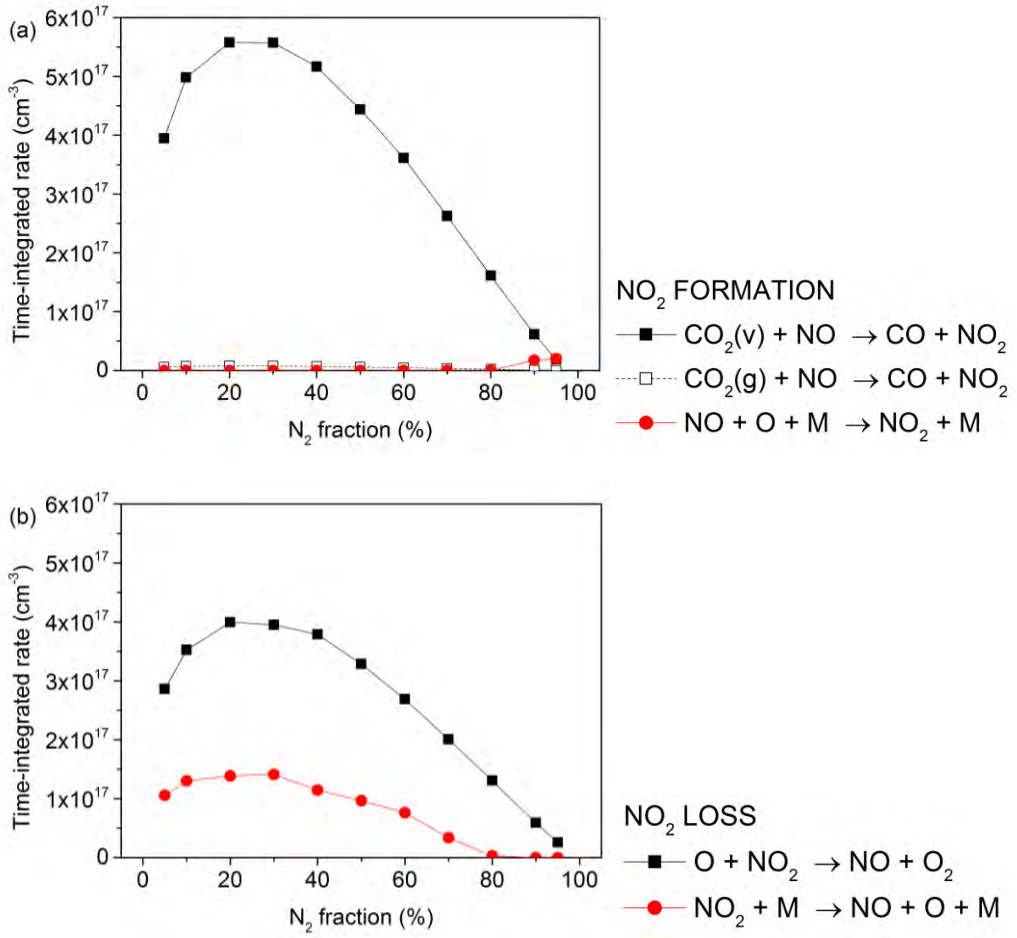

Figure 8 NO_2 is almost exclusively formed by reaction of NO with vibrationally excited CO_2, while reaction with O atoms transforms NO_2 back into NO. Calculations performed by S. Heijkers within PLASMANT.

We summarize the most important reaction pathways, as predicted by the model, in Figure 9. Reactants are indicated in color according to the time-integrated rate of their reaction (red ≥ 10^{17} cm^{-3}; green ≥ 10^{16} cm^{-3}; blue ≥ 10^{15} cm^{-3}) while the thickness of the arrow lines corresponds to the overall importance of the reaction. The most important reactions, ranked by importance based on the average time-integrated rates, are listed in Table A2 in the appendix.

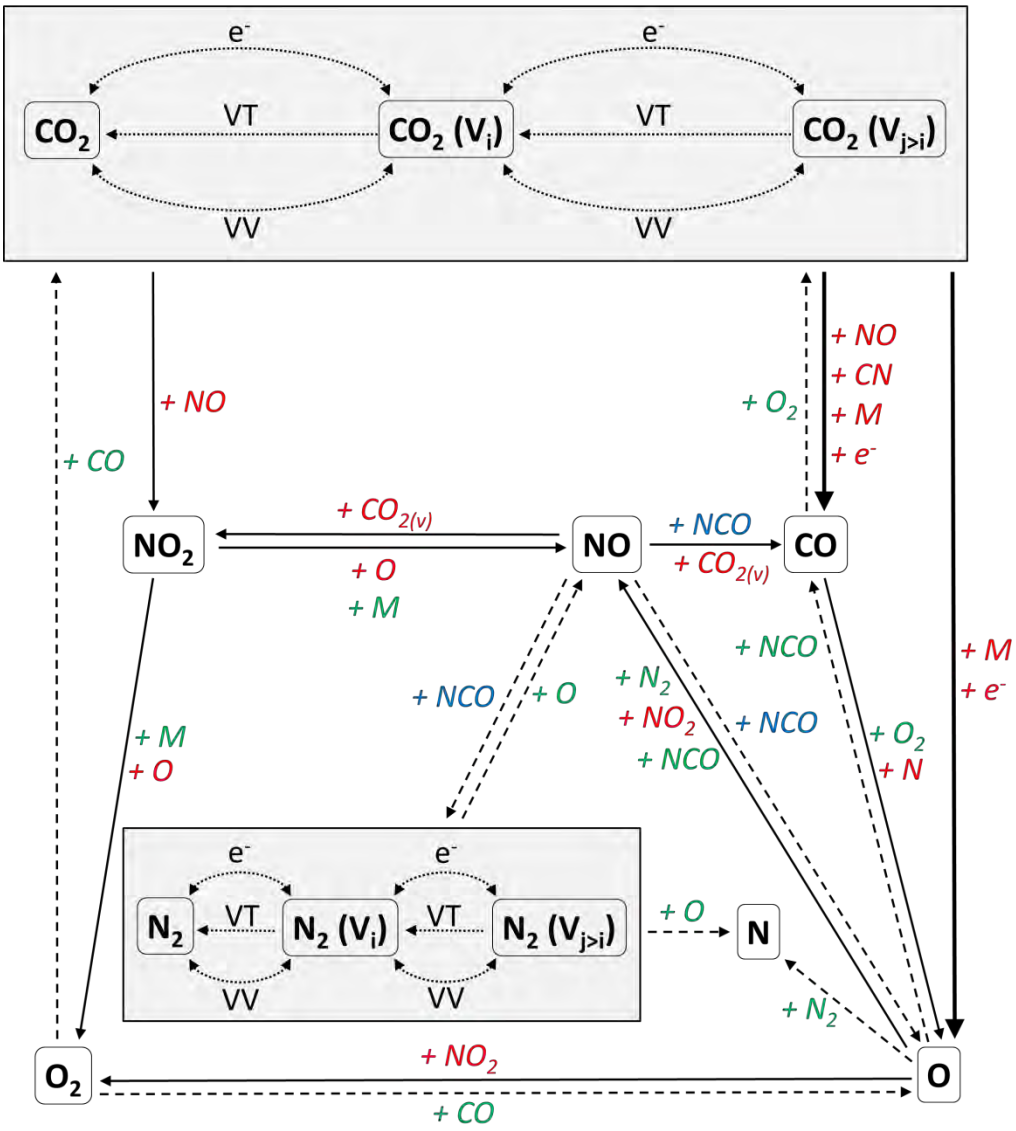

Figure 9 Reaction pathways for the conversion of CO_2 and N_2 into CO, O, O_2, N, NO and NO_2, as predicted by the model of S. Heijkers. Both CO_2 and N_2 are easily excited from ground state to vibrational levels and vice versa (dotted lines). The color of the reactants indicates the time-integrated rate of their reaction (red ≥ 10^{17} cm^{-3}; green ≥ 10^{16} cm^{-3}; blue ≥ 10^{15} cm^{-3}) while the thickness of the arrow lines corresponds to the total importance of the reactions (--- < — < ▬).

Both CO_2 and N_2 are easily excited from ground state to vibrational levels, and vice versa, upon electron impact (de)excitation, vibration-vibration (VV) and vibration-translation (VT) relaxation. The vibrational distribution functions (VDFs) of both CO_2 and N_2 are plotted in Figure A8 in the appendix. Overall, the VDF of both molecules is thermal, with the vibrational temperature more or less equal to the gas temperature. The latter is calculated to be 3140 K, while the average vibrational temperature of CO_2 and N_2 are 3174 K and 3333 K, respectively (see Figure A9 in the appendix). We should be able to increase the energy efficiency of CO_2 conversion and N_2 fixation if the VDFs of both CO_2 and N_2 would be more non-thermal, with higher populations of the higher vibrational level.[2,3] To realize this, the temperature in the arc should be reduced, so that vibration-translation relaxation processes, which depopulate the vibrational levels, can be reduced. Lowering the gas temperature should practically be realized in the GAP by cooling the cathode, which is planned as future work. Furthermore, it would protect the cathode from weathering. Another approach would be to reduce the outlet radius even further, in order to quench the gas through rapid expansion. On the other hand, the vibrational levels in our GAP are clearly more populated than in other types of plasmas, such as a DBD, where the VDF dramatically drops for the higher vibrational levels.[44–46] This explains why the vibrational levels play an important role in CO_2 dissociation (and NOx formation), and why the CO_2 conversion and N_2 fixation are quite energy efficient, compared to other commonly studied plasma types (see above).

CO_2 is mainly converted into CO and O (right arrows in the figure), and it also helps in producing NO_2 upon reaction with NO. CO is in turn mainly converted into O by reaction with N or O_2. Reaction of O with NO_2, N_2 or NCO forms NO.

NO reacts further into NO_2, mainly by reaction with vibrationally excited CO_2 (see also Figure 7 and 8 above). Vice versa, NO_2 also stimulates the formation of NO, by reaction with O atoms or any

molecule (M) in the plasma (again, see Figure 7 and 8). The fact that the most important loss mechanism of NO_2 is the most important formation mechanism of NO, and vice versa, shows that they are easily converted into each other. Still, the selectivity of NO is much higher in our GAP than the selectivity of NO_2. The reason is that, besides these processes, which virtually cancel out each other, NO is also formed upon reaction of O atoms with vibrationally excited N_2 (Zeldovich mechanism; cf. above) and with NCO, which have no reverse reaction (see Figure 7). Thus, by taking the sum of the time-integrated rates of all formation processes and reducing this with the sum of the time-integrated rates of all loss processes, the resulting concentration of NO is 20 times higher than that of NO_2 (see Figure 4), which explains the higher NO selectivity.

We can in general conclude from Figure 9 that the NOx molecules are mainly formed through reactions with O atoms. If we want to avoid NOx formation, we would have to avoid the formation of these O atoms. However, since the O atoms are an important product of CO_2 dissociation, we cannot simply avoid it. Therefore, if we want to avoid NOx formation, we have to make sure that the O atoms formed by CO_2 dissociation can quickly react with a scavenger, before they get the chance to form NO or NO_2. The addition of CH_4 or H_2 is a possibility, since these molecules produce H atoms, which react very fast with O to form OH and subsequently to H_2O, as demonstrated by simulations and experiments.[47,48]

On the other hand, if we want to stimulate NOx production to make it effective for N_2 fixation, we have to stimulate the formation of O atoms. Since they are mainly formed upon CO_2 dissociation, we have to enhance the CO_2 conversion. The latter is currently restricted due to the limited fraction of gas passing through the arc in our GAP. As mentioned before, if we can improve the design of the reactor in order to enhance this fraction, it is possible to increase the conversion and thus also the formation of O atoms and NOx products.

3.4 Comparison of gliding arc plasmatron with dielectric barrier discharge

Snoeckx et al.[5] have also analyzed the byproducts formed in a CO_2/N_2 mixture, but for a dielectric barrier discharge (DBD) plasma, which has completely different plasma properties than a GAP.[6] This clearly affects the plasma chemistry, as elaborated in the next section. Therefore, we compare here both plasma reactors in terms of conversion efficiency and byproduct formation, at typical GAP and DBD operating conditions, i.e., a specific energy input (SEI) of around 2 kJ/L and 12 kJ/L, respectively. These values originate from a plasma power of 350 W and a total flow rate of 10 L/min for the GAP, while the plasma power and total flow rate in the DBD reactor are around 120 W and 611 mL/min, respectively.

3.4.1 CO_2 conversion, energy cost and energy efficiency

In Figure 10(a), the absolute CO_2 conversion is plotted for both plasma reactors as a function of N_2 fraction. The GAP shows a slightly more than linear trend with increasing N_2 fraction, while the trend of the DBD is more exponential. The absolute values in the GAP are somewhat higher than in the DBD, even at much lower SEI (2 kJ/L in the GAP compared to 12 kJ/L in the DBD). Only at the highest N_2 fractions, the values are higher in the DBD (i.e., 22 % vs. 18 %). This indicates that in general the CO_2 conversion is higher in the GAP, but the addition of large amounts of N_2 to a CO_2 plasma in a DBD enhances the CO_2 conversion more compared to in a GAP. To explain this, we should compare the main dissociation mechanisms of CO_2 in a DBD and GAP. In a DBD the main dissociation mechanism is electron impact dissociation of ground state CO_2. The importance of this mechanism decreases with increasing N_2 fraction in the mixture, while the reaction of CO_2 with metastable N_2 molecules becomes more important and is the most important dissociation mechanism of CO_2 in a DBD above 70% N_2 addition.[5] In our GAP, the reaction of vibrationally excited CO_2 with dissociated N_2 products, i.e., mainly NO but also CN (see Figure 6(a)), is

the most important CO_2 dissociation process. The reaction with NO is dominant up to 80% N_2, while above 80 %, the reaction with CN becomes most important, but its absolute reaction rate is quite low (see Figure 6(a)), because CN also needs C to be formed, which is low at low CO_2 fractions and thus high N_2 fractions in the mixture. Thus, at high N_2 fractions, the contribution of N_2 is more important in a DBD than in a GAP, because the main dissociation mechanism in a DBD goes through metastable N_2 molecules, while in a GAP also a contribution of C is necessary, of which the concentration is lower.

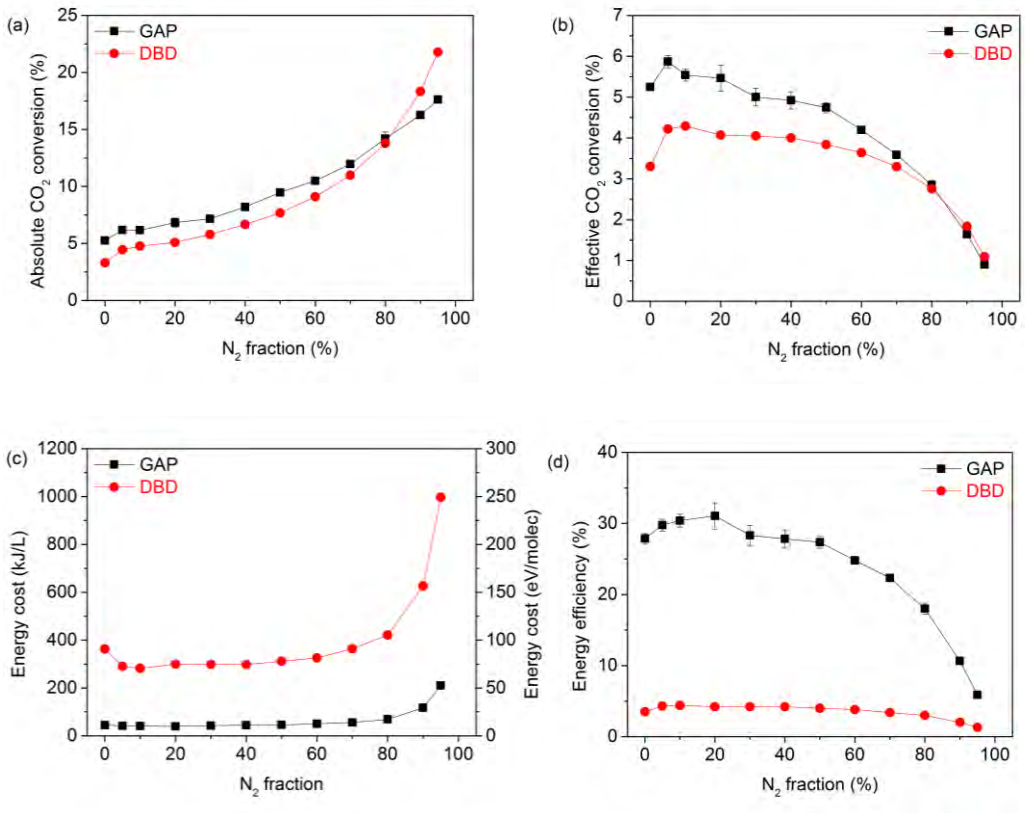

Figure 10 The absolute CO_2 conversion (a) rises slightly more than linearly with N_2 fraction in the GAP, while the trend in the DBD is more exponential. Up to a N_2 fraction of 80 %, the effective CO_2 conversion (b) is higher in the GAP than in the DBD. The energy cost (c) is significantly lower and the energy efficiency (d) significantly higher in the GAP than in the DBD. The error bars are included in the graphs, but are sometimes too small to be visible.

As is clear from Figure 10(b), the effective CO_2 conversion is higher in the GAP than in the DBD, except again at N_2 fractions above 80 %, where the values are comparable, and they follow more or less the same trend, which has been explained above.

From Figure 10(c), it is remarkable that the energy cost in the DBD is on average 6 times higher than in the GAP. This can easily be understood, as the effective conversion is slightly lower, but the SEI in the plasma is much higher (12 kJ/L vs. 2 kJ/L). For this reason, our GAP is much more promising than a DBD for plasma-based CO_2 conversion.[6]

The energy efficiency in both plasma reactors decreases with increasing N_2 fraction (see Figure 10(d)). In addition, the energy efficiency is 7 times higher in the GAP than in the DBD, for N_2 fractions up to 50 %, i.e., around 27 – 31 % for the GAP vs. 4% for the DBD. At N_2 fractions above 50 %, the difference becomes smaller, as the values drop to 5.9 % for the GAP and 1.3 % for the DBD, at 95 % N_2. We can conclude that in the GAP the contribution of vibrationally excited CO_2 is crucial for the CO_2 conversion, while this is not the case in a DBD reactor, where the main mechanism of CO_2 dissociation is electron impact dissociation from ground state CO_2 molecules.[5] Because the latter process requires much more energy, this explains why the energy efficiency is better in the GAP than in the DBD.

Based on these numbers, we can conclude that the GAP is definitely superior for CO_2 conversion in the presence of N_2, in terms of conversion efficiency, compared to a DBD. However, for industrial application of this technology, not only the conversion efficiency is important, but also the formation of byproducts, since the latter can have both economic and environmental consequences. Therefore, we will evaluate the byproduct formation for both plasma reactors in the next section.

3.4.2 Byproduct formation

The major reaction products of CO_2 splitting are CO and O_2 molecules in both the GAP and DBD. However, the addition of N_2 also leads to the formation of NOx compounds, as shown above. The concentrations of NO and NO_2, obtained in the GAP and DBD, are compared in Figure 11, as a function of N_2 fraction in the mixture.

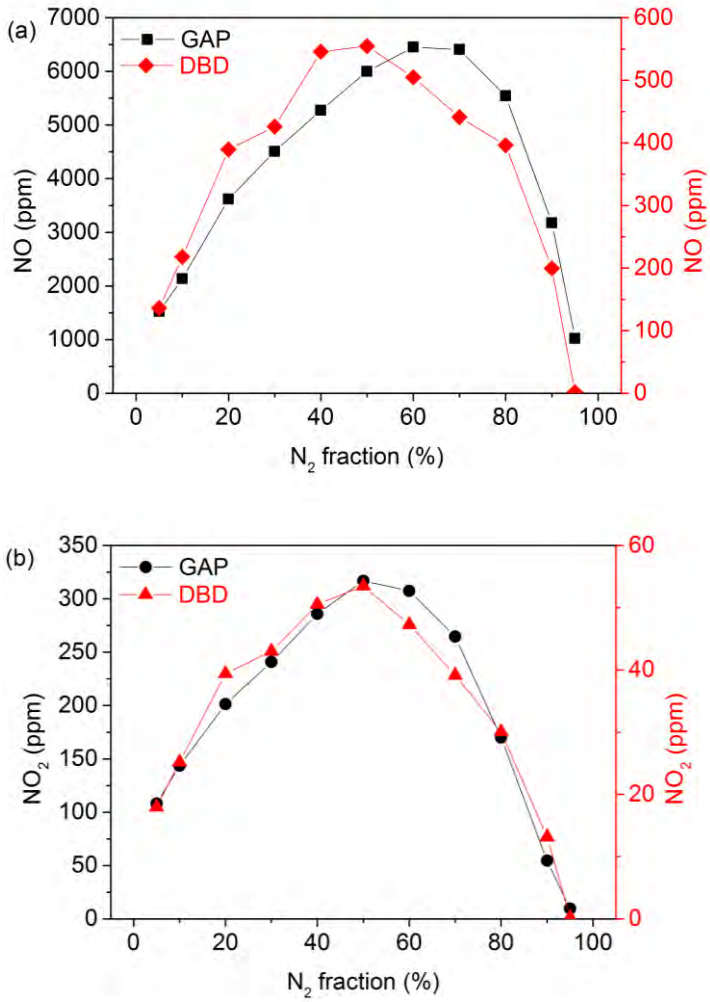

Figure 11 The concentrations of NO (a) and NO_2 (b) are more than 10 times and about 6 times higher, respectively, in the GAP than in the DBD. The error bars are included in the graphs, but are too small to be visible.

Both the NO and NO_2 concentrations follow the same trend as a function of N_2 fraction in the GAP and DBD, and the explanation for this trend was given above. However, the concentrations of NO and NO_2 are more than 10 times and about 6 times higher, respectively, in the GAP than in the DBD reactor. Maximum values of NO and NO_2 of 6453 and 317 ppm are reached in the GAP, while the maximum values of NO and NO_2 in the DBD are 555 and 54 ppm. This can only partly be explained by the higher effective CO_2 conversion in the GAP (see Figure 10(b) above), because the difference in NO and NO_2 concentrations is much larger than for the effective CO_2 conversion. Indeed, the N_2 dissociation – also needed for NOx formation – is a factor 4 higher in the GAP than in the DBD (i.e., 4 % vs. 1%). In addition, the selectivity towards NO and NO_2 seems to be significantly higher in the GAP than in the DBD, where also other NOx compounds were formed.[5]

It is indeed remarkable that in our GAP no N_2O, N_2O_3 and N_2O_5 could be detected experimentally, while they were clearly detected in the DBD experiments, with the same measuring equipment (FTIR).[5] Our simulation results also indicate that the major byproducts of CO_2 and N_2 conversion in the GAP are NO and NO_2, in agreement with our experiments, while N_2O (0.1 – 3 ppm), N_2O_3 (10^{-8} – 10^{-7} ppm), N_2O_4 (10^{-11} - 10^{-9} ppm) and N_2O_5 (10^{-12} – 10^{-10} ppm) have much lower concentrations (see Figure 12(a)). In comparison, in a DBD next to NO and NO_2 also N_2O and N_2O_5 are formed in relatively high concentrations, i.e., calculated up to 115 ppm for NO, 34 ppm for NO_2, 55 ppm for N_2O, and even up to 1000 ppm for N_2O_5; see Figure 12(b) and also reference 5. The N_2O_3 and N_2O_4 concentrations are calculated to be much lower.

The reason we only detected NO and NO_2 in our experiments, while in the DBD experiments also N_2O, N_2O_3 and N_2O_5 were detected, is attributed to the different plasma temperature. It is predicted to be around 3000 K inside the arc[31] in our GAP (for a pure CO_2 plasma), which is too high to form N_2O, N_2O_3 and N_2O_5. Indeed, at higher

temperatures the formation rates of these species increase but the loss rates are even higher (see Figure A10 in the appendix), which results in lower net concentrations (see Figure 12(a); obtained from calculations of S. Heijkers). On the other hand, in a DBD the temperature is around room temperature. At this condition, the formation rates of these species will be higher than the loss rates (see Figure A10 in the appendix), resulting in higher net concentrations (see Figure 12(b); also obtained from calculations of S. Heijkers). Furthermore, DBD plasmas are characterized by streamers, with short lifetime (order of 30 ns[49]), in which mainly electron impact reactions occur, but in between these streamers, NO_2 can interact with NO or NO_3 to form N_2O_3 and N_2O_5 respectively.[5] This is not the case in a GAP reactor, because the arc is continuously stabilized in the center of the reactor, which explains why only NO and NO_2 are detected in our experiments.

Taking into account that N_2O is a very potent greenhouse gas, with a global warming potential (GWP) of 298 $CO_{2,equivalent}$, it is highly beneficial that its concentration in the GAP does not exceed the detection limit of 1 ppm. After all, the production of N_2O would void the greenhouse gas mitigation potential of plasma technology if no denox purification step would be added.

Overall we can conclude that the GAP is far superior for CO_2 conversion in the presence of N_2 than the DBD reactor, due to the higher conversion, but especially the absence of N_2O, N_2O_3, N_2O_5 formation, and the significantly higher energy efficiency. Nevertheless, the higher NOx formation, when it is too low for valorization, would have a negative impact on air quality if released in the air, which leads to restriction of their emissions, and therefore, denox installations will be necessary. However, the higher NOx concentrations, on one hand, and less other byproducts (N_2O, N_2O_3, N_2O_5), on the other hand, will give rise to an easier separation afterwards compared to the DBD.[50] In addition, if we can further stimulate the NOx formation, this will give opportunities for N_2 fixation, as described above.

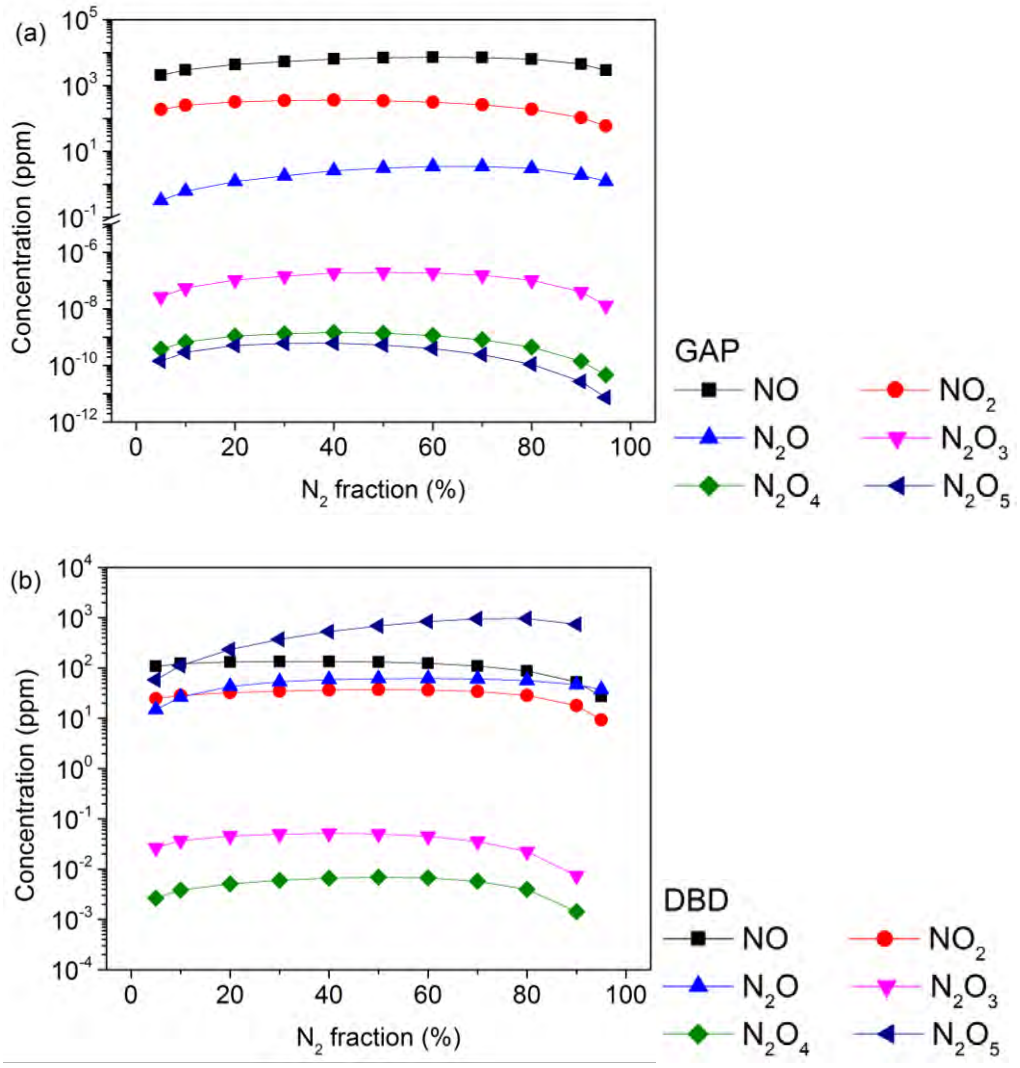

Figure 12 NO and NO_2 are the major byproducts of CO_2 and N_2 conversion in the GAP (a), while in the DBD also N_2O and N_2O_5 are formed in considerable concentrations (b). Calculations performed by S. Heijkers within PLASMANT.

4 Conclusions

We have investigated the effect of N_2 on the CO_2 conversion in a GAP, by combining experiments and simulations. The addition of N_2 has a positive effect on the absolute CO_2 conversion up to 50 %, while at higher N_2 fractions, the effective CO_2 conversion and energy efficiency of this process drop. The simulations reveal that the CO_2 conversion mainly proceeds through the vibrational levels, which are populated through collision with the N_2 vibrational levels. In addition, NO and NO_2 are formed in the CO_2/N_2 mixture, initiated by the reaction between N_2 vibrational levels and O atoms (so-called Zeldovich mechanism[27]). NO and NO_2 are easily converted into each other, but still the NO concentration is about 20 times higher than the NO_2 concentration in our GAP.

Combining CO_2 and N_2 in a GAP thus can lead to combined CO_2 conversion and N_2 fixation. The highest amount of NOx obtained is 6761 ppm, which is still below the minimum threshold of 1 % to make it effective for N_2 fixation. Computer simulations reveal that we will have to improve our reactor and gas inlet design to enhance the gas fraction that passes through the arc, as the latter will increase the CO_2 conversion, and thus also the NOx production. By changing the design so that a fraction of minimum 22 % of the gas can pass through the arc (compared to 14.8 % in the present reactor), we expect that the CO_2 conversion rises up to 16 %, yielding NOx concentrations above 1%. A way to increase this fraction is by decreasing the radius of one or more tangential inlets in order to create a higher flow velocity, so that more gas is forced into the central vortex. Besides this approach, we also want to change the cathode design to increase the electric field, which will increase the plasma production and arc stability. Other approaches might also be possible, but this optimization study will need dedicated fluid dynamics simulations, which will be performed by the research group PLASMANT in the future.

We compared the performance of our GAP reactor with other plasma types. Regarding CO_2 conversion, the best energy efficiency is reached in our GAP, while the conversion itself still needs further improvement. In terms of NOx production, the NOx yield is still quite low (which is attributed to the limited CO_2 conversion), but the energy consumption is reasonable compared to other plasma types, certainly if we take into account that our energy consumption also includes the cost for CO_2 conversion.

Finally, we made a more detailed comparison with a dielectric barrier discharge (DBD) plasma, which is the only other work in literature where NOx production was also studied from a CO_2/N_2 mixture. Remarkably, the energy efficiency was 7 times higher in our GAP than in the DBD, next to a somewhat higher CO_2 conversion. Indeed, CO_2 dissociation in the GAP proceeds through vibrationally excited states of CO_2, while in a DBD it occurs mainly by electronic excitation, which is less efficient.[6] Furthermore, our GAP only produces NO and NO_2, while N_2O, N_2O_3 and N_2O_5 are also formed in a DBD. Keeping in mind that N_2O is a very potent greenhouse gas, with a global warming potential (GWP) of 298 $CO_{2,equivalent}$, it is highly beneficial that its concentration in the GAP does not exceed the detection limit of 1 ppm. Overall we can conclude that the GAP is superior for CO_2 conversion in the presence of N_2 compared to a DBD, due to its higher conversion, but especially the absence of N_2O, N_2O_3, N_2O_5 formation and the much higher energy efficiency.

References

1 T. Nunnally, K. Gutsol, A. Rabinovich, A. Fridman, A. Gutsol and A. Kemoun, *J. Phys. D. Appl. Phys.*, 2011, **44**, 274009.

2 M. Ramakers, G. Trenchev, S. Heijkers, W. Wang and A. Bogaerts, *ChemSusChem*, 2017, **10**, 2642–2652.

3 S. Heijkers and A. Bogaerts, *J. Phys. Chem. C*, 2017, **121**, 22644–22655.

4 S. Heijkers, R. Snoeckx, T. Kozák, T. Silva, T. Godfroid, N. Britun, R. Snyders and A. Bogaerts, *J. Phys. Chem. C*, 2015, **119**, 12815–12828.

5 R. Snoeckx, S. Heijkers, K. Van Wesenbeeck, S. Lenaerts and A. Bogaerts, *Energy Environ. Sci.*, 2016, **9**, 30–39.

6 R. Snoeckx and A. Bogaerts, *Chem. Soc. Rev.*, 2017, **46**, 5805–5863.

7 L. F. Spencer and A. D. Gallimore, *Plasma Sources Sci. Technol.*, 2013, **22**, 015019.

8 A. Fridman, *Plasma Chemistry*, Cambridge University Press, New York, 2008.

9 B. S. Patil, *PhD thesis*, 2017.

10 B. S. Patil, F. J. J. Peeters, J. A. Medrano, F. Gallucci, W. Wang, A. Bogaerts, Q. Wang, G. Van Rooij, J. Lang and V. Hessel, *Appl. Energy*, 2018, Submitted.

11 Z. Bo, J. Yan, X. Li, Y. Chi and K. Cen, *J. Hazard. Mater.*, 2009, **166**, 1210–1216.

12 A. Evans, R. Luebke and C. Petit, *J. Mater. Chem. A*, 2018, **6**, 10570–10594.

13 T. Namihira, S. Katsuki, R. Hackam, H. Akiyama and K. Okamoto, *IEEE Trans. Plasma Sci.*, 2002, **30**, 1993−1998.

14 J. F. Coudert, J. M. Baronnet, J. Rakowitz and P. Fauchais, in *Synthesis of nitrogen oxides in a plasma produced by a jet arc generator*, 1977.

15 M. Rahman and V. Cooray, *Opt. Laser Technol.*, 2003, **35**, 543−546.

16 W. Bian, X. Song, J. Shi and X. Yin, *J. Electrost.*, 2012, **70**, 317−326.

17 N. Rehbein and V. Cooray, *J. Electrost.*, 2001, **51−52**, 333−339.

18 V. M. Shmelev, A. V. Saveliev and L. A. Kennedy, *Plasma Chem. Plasma Process.*, 2009, **29**, 275−290.

19 B. S. Patil, N. Cherkasov, J. Lang, A. O. Ibhadon, V. Hessel and Q. Wang, *Appl. Catal., B*, 2016, **194**, 123−133.

20 B. Mutel, O. Dessaux and P. Goudmand, *Rev. Phys. Appl.*, 1984, **19**, 461−464.

21 L. S. Polak, A. A. Ovsiannikov, D. I. Slovetsky and F. B. Vurzel, *Theoretical and Applied Plasma Chemistry*, Nauka (Science), Moscow, 1975.

22 R. I. Asisov, V. K. Givotov, V. D. Rusanov and A. Fridman, *Sov. Phys. High Energy Chem. (Khimia Vysok. Energ.*, 1980, **14**, 366.

23 T. Kim, S. Song, J. Kim and R. Iwasaki, *Jpn. J. Appl. Phys.*, 2010, **49**, 126201.

24 M. A. Malik, C. Jiang, R. Heller, J. Lane, D. Hughes and K. H. Schoenbach, *Chem. Eng. J.*, 2016, **283**, 631−638.

25 K. Birkeland, *Trans. Faraday Soc.*, 1906, **2**, 98−116.

26 J. Krop and I. Pollo, *Chemia*, 1981, **678**, 51−59.

27 W. Wang, B. Patil, S. Heijkers, V. Hessel and A. Bogaerts, *ChemSusChem*, 2017, **10**, 2145–2157.

28 B. S. Patil, Q. Wang, V. Hessel and J. Lang, *Catal. Today*, 2015, **256**, 49–66.

29 R. Ingels, D. Graves, S. Anderson and R. Koller, *Int. Fertil. Soc. Conf.*, 2015, 1–27.

30 E. Cleiren, S. Heijkers, M. Ramakers and A. Bogaerts, *ChemSusChem*, 2017, **10**, 4025–4036.

31 G. Trenchev, S. Kolev, W. Wang, M. Ramakers and A. Bogaerts, *J. Phys. Chem. C*, 2017, **121**, 24470–24479.

32 J. G. Chen, R. M. Crooks, L. C. Seefeldt, K. L. Bren, R. Morris Bullock, M. Y. Darensbourg, P. L. Holland, B. Hoffman, M. J. Janik, A. K. Jones, M. G. Kanatzidis, P. King, K. M. Lancaster, S. V. Lymar, P. Pfromm, W. F. Schneider and R. R. Schrock, *Science*, 2018, **360**.

33 R. Salman, B. Christian, X. Auvray, R. Lødeng and M. Menon, *Appl. Catal. A, Gen.*, 2018, **564**, 142–146.

34 C. A. Grande, K. A. Andreassen, J. H. Cavka, D. Waller, O. Lorentsen, H. Øien, H. Zander, S. Poulston, S. Garc and D. Modeshia, *Ind. Eng. Chem. Res.*, 2018, **57**, 10180–10186.

35 S. Devahasdin, C. Fan, K. Li and D. H. Chen, *J. Photochem. Photobiol. A Chem.*, 2003, **156**, 161–170.

36 A. Martinez-oviedo, S. K. Ray, H. P. Nguyen and S. W. Lee, *J. Photochem. Photobiol. A Chem.*, 2019, **370**, 18–25.

37 J. Lasek, Y. Yu and J. C. S. Wu, *J. Photochem. Photobiol. C Photochem. Rev.*, 2013, **14**, 29–52.

38 L. Wang, M. Xia, H. Wang, K. Huang, C. Qian, C. T. Maravelias and G. A. Ozin, *Joule*, 2018, **2**, 1055–1074.

39 R. Lan, K. A. Alkhazmi, I. A. Amar and S. Tao, *Appl. Catal. B Environ.*, 2015, **152–153**, 212–217.

40 P. Peng, P. Chen, C. Schiappacasse, N. Zhou, E. Anderson, D. Chen, J. Liu, Y. Cheng, R. Hatzenbeller, M. Addy, Y. Zhang, Y. Liu and R. Ruan, *J. Clean. Prod.*, 2018, **177**, 597–609.

41 A. J. Martín, T. Shinagawa and J. Pérez-Ramírez, *Chem*, 2018, https://doi.org/10.1016/j.chempr.2018.10.010.

42 N. Cherkasov, A. O. Ibhadon and P. Fitzpatrick, *Chem. Eng. Process. Process Intensif.*, 2015, **90**, 24–33.

43 C. Baird and M. Cann, *Environmental Chemistry*, W.H. Freeman and company, New York, 4th edn., 2008.

44 T. Kozák and A. Bogaerts, *Plasma Sources Sci. Technol.*, 2014, **23**, 045004.

45 A. Bogaerts, T. Kozák, K. van Laer and R. Snoeckx, *Faraday Discuss.*, 2015, **183**, 217–232.

46 A. Berthelot and A. Bogaerts, *Plasma Sources Sci. Technol.*, 2016, **25**, 045022.

47 R. Aerts, R. Snoeckx and A. Bogaerts, *Plasma Process. Polym.*, 2014, **11**, 985–992.

48 R. Snoeckx, A. Ozkan, F. Reniers and A. Bogaerts, *ChemSusChem*, 2017, **10**, 409–424.

49 A. Ozkan, T. Dufour, T. Silva, N. Britun, R. Snyders, F. Reniers and A. Bogaerts, *Plasma Sources Sci. Technol.*, 2016, **25**, 055005.

50 A. Jess, P. Kaiser, C. Kern, R. Unde and C. Von Olshausen, *Chemie-Ingenieur-Technik*, 2011, **83**, 1777–1791.

Appendix

1 Description of the experiments

1.1 Product analysis

The feed gases and main product gases (CO_2, N_2, CO, O_2) were again analyzed by a three-channel compact gas chromatograph (CGC) from Interscience, as explained in section 1.2 of Chapter 2. As the method mentioned above does not account for the gas expansion due to CO_2 splitting, a correction factor was used, which is explained in the appendix of Chapter 2.

The effective conversion, X_{eff,CO_2}, accounts for the fraction of CO_2 in the initial gas mixture:

$$X_{eff,CO_2}(\%) = X_{abs,CO_2}(\%) \times fraction_{CO_2} \quad \text{(A1)}$$

The specific energy input (SEI), energy cost (EC) and energy efficiency (η) were calculated in a similar way as in section 1.2 of Chapter 2.

During the experiments, the concentrations of NO, NO_2, and other NOx compounds were monitored almost in real-time using a Nicolet 380 Fourier Transform Infrared (FTIR) Spectrometer (Thermo Fischer Scientific, Waltham, MA) equipped with a 2 m heated gas cell with ZnSe windows and a DTGS detector. Based on the height of the bands, different species were monitored at the following wavenumbers: NO with ν(NO) at 1900 cm^{-1} and NO_2 with $\nu_{as}(NO_2)$ at 1597 cm^{-1}. Note that N_2O with ν(NN) at 2234 cm^{-1}, N_2O_3 with $\nu_s(NO_2)$ at 1309 cm^{-1}, N_2O_5 with $\nu_s(NO_2)$ at 1245 cm^{-1}, O_3 with ν_s at 1054 cm^{-1} were never detected with the FTIR spectrometer. To quantify these results, the concentrations were determined using a CT5800 Analyzer (Emerson, Stirling, UK) based on Quantum Cascade Laser Technology, allowing to accurately measure different N-containing molecules simultaneously. The

monitored compounds were NO, NO_2, N_2O and NH_3, with the following detection limits: 1.5 ppm, 0.5 ppm, 1 ppm and 1 ppm, respectively.

2 Results and discussion

2.1 Specific energy input as a function of N_2 fraction

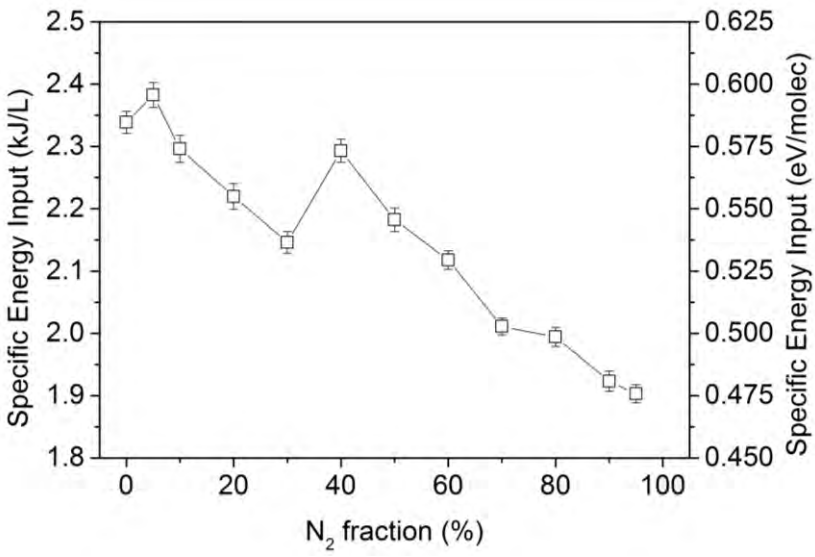

Figure A1 There is a small drop in specific energy input (SEI) upon N_2 addition.

2.2 Analysis of the byproducts - NOx concentrations

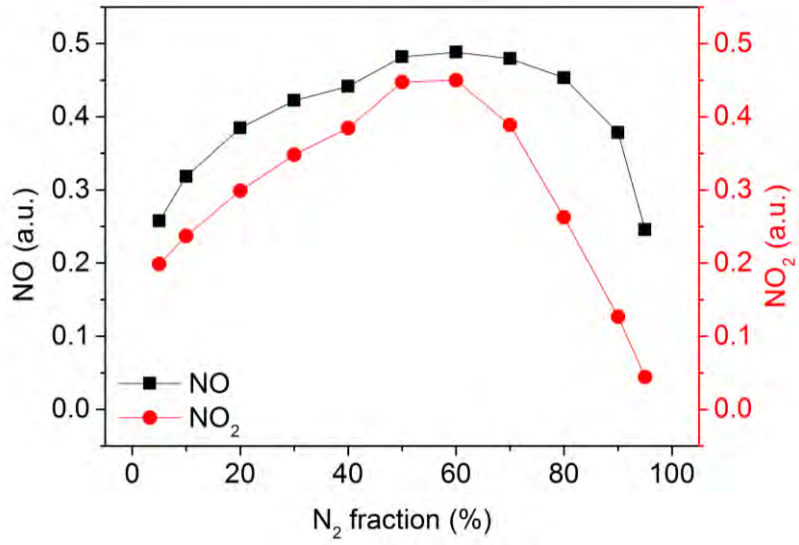

Figure A2 NO and NO_2 concentration in arbitrary units as a function of N_2 fraction, as obtained from the FTIR measurements.

Table A1 NO and NO_2 concentration and calculated error, in parts per million, as obtained from the QCL measurements.

N_2 fraction (%)	**NO (ppm)**		**NO_2 (ppm)**	
	Value	Error	Value	Error
5	1524.4	0.8	108.17	0.09
10	2136	1	143.5	0.2
20	3620	8	201.3	0.4
30	4507	19	241	1
40	5275	21	286	1
50	5998	8	316.9	0.5
60	6453	14	307.3	0.7
70	6408	10	264.6	0.4
80	5545	9	170.1	0.3
90	3178	7	54.6	0.1
95	1023.1	0.3	9.60	0.02

The maximum total NOx concentration obtained is 6761 ppm at 60 % N_2. To make the process effective for N_2 fixation, the NOx concentration should be above 1%, as stated in chapter 4. For this purpose, we should enhance the CO_2 conversion in the GAP. To realize the latter, the fraction of gas passing through the arc should be increased to 22%. This can be explained as follows: from previous fluid dynamics calculations we know that the fraction of gas passing through the arc is 14.8 % (used in Equation (A2)).[1] Based on this number, we calculated that the conversion inside the arc is about 71 % (Equation (A3)).

$$X_{CO_2}^{Absolute}(\%) = X_{CO_2,arc}(\%) \times 0.148 \quad \text{(A2)}$$

$$X_{CO_2,arc}(\%) = \frac{X_{CO_2}^{Absolute}(\%)}{0.148} = \frac{10.5\ \%}{0.148} = 71\ \% \quad \text{(A3)}$$

As we now obtain a maximum NOx concentration of 6761 ppm at 60 % N_2, and when this must be increased up to 1 %, we need an increase of $X_{CO_2}^{Absolute}$ up to 16 %. Assuming that we have 71 % CO_2 conversion in the arc and we need an absolute CO_2 conversion of 16 %, we need a fraction of 22 % passing through the arc (Equation (A4)).

$$fraction_{arc} = \frac{X_{CO_2}^{Absolute}(\%)}{X_{CO_2,arc}(\%)} = \frac{16\ \%}{71\ \%} = 0.22 \quad \text{(A4)}$$

The selectivity towards NO and NO_2 can be calculated as follows:

$$NO\ selectivity\ (\%) = \frac{NO\ concentration}{concentration\ of\ (NO + NO_2)} \times 100\ \% \quad \text{(A5)}$$

$$NO_2\ selectivity\ (\%) = \frac{NO_2\ concentration}{concentration\ of\ (NO + NO_2)} \times 100\ \% \quad \text{(A6)}$$

2.3 Underlying mechanisms as revealed by computer simulations

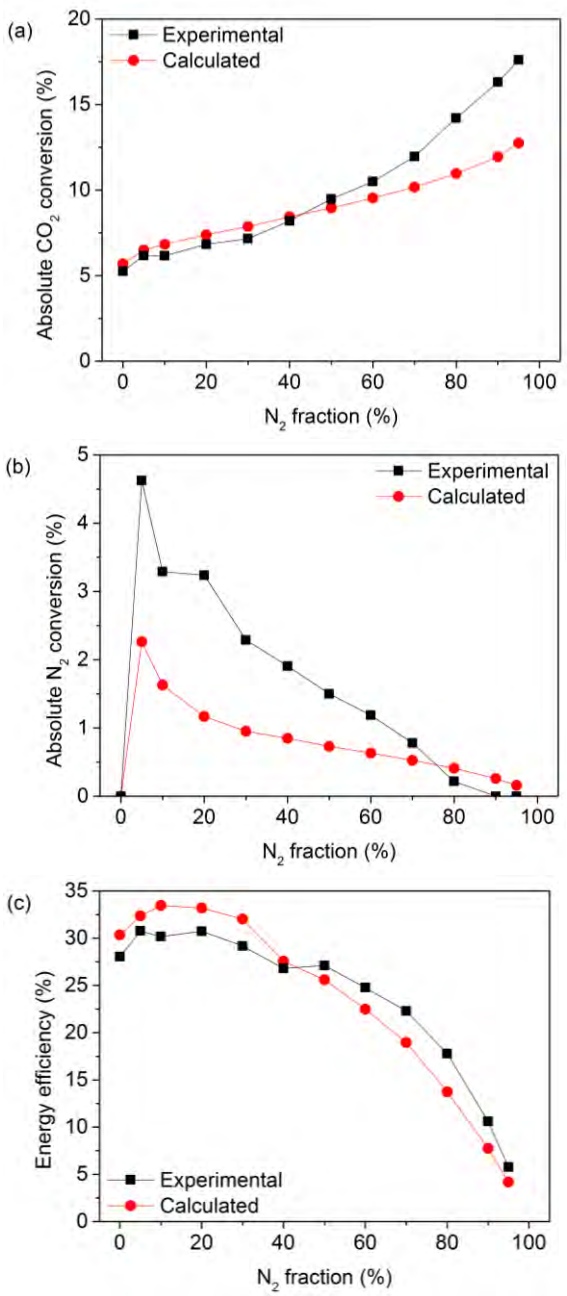

Figure A3 Experimental and calculated results for CO_2 conversion (a), N_2 conversion (b) and energy efficiency (c). Calculations performed by S. Heijkers within PLASMANT.

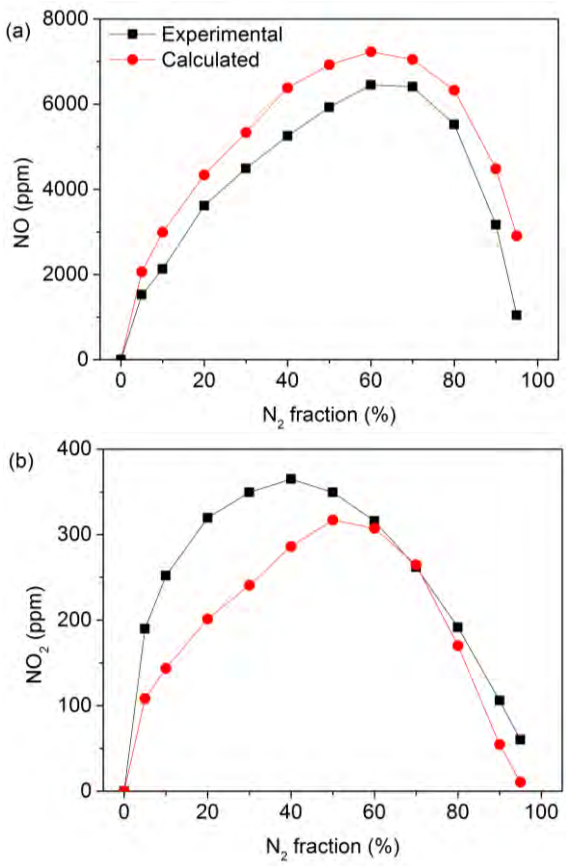

Figure A4 Experimental and calculated results for NO (a) and NO_2 (b) concentration (in parts per million). Calculations performed by S. Heijkers within PLASMANT.

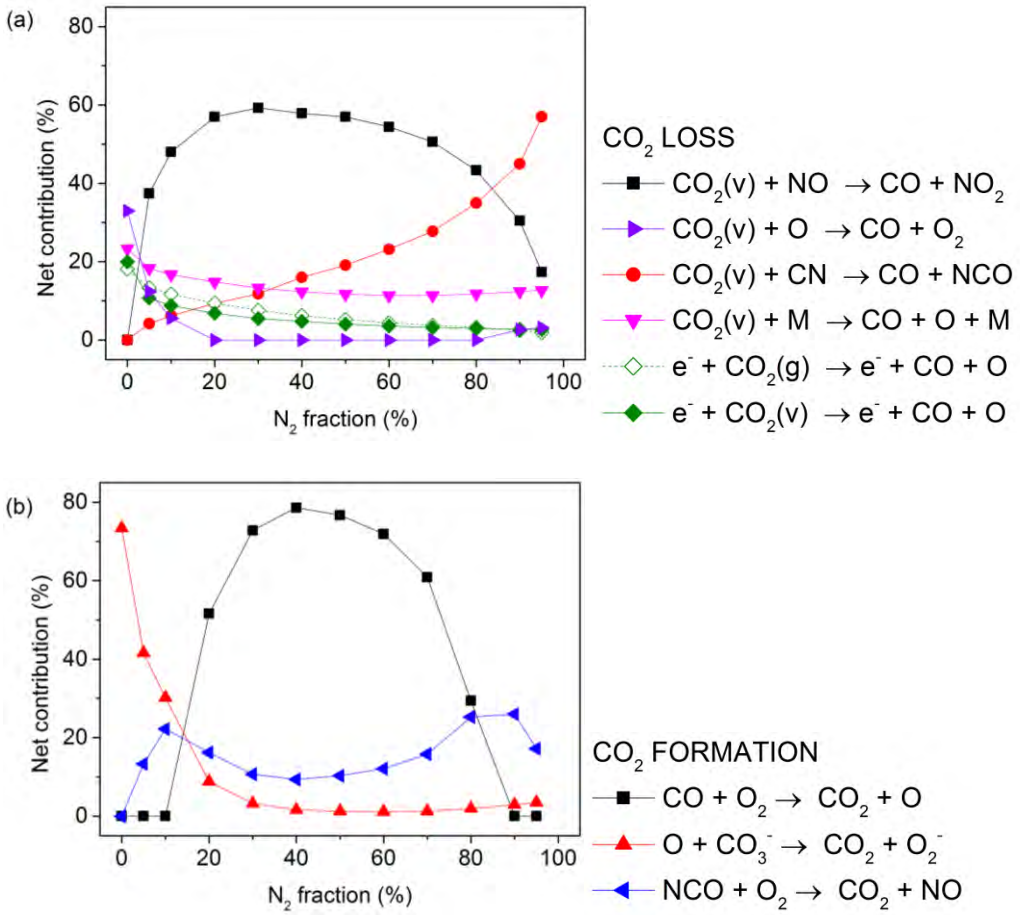

Figure A5 Net contribution of the most important loss (a) and formation (b) reactions of CO_2. Calculations performed by S. Heijkers within PLASMANT.

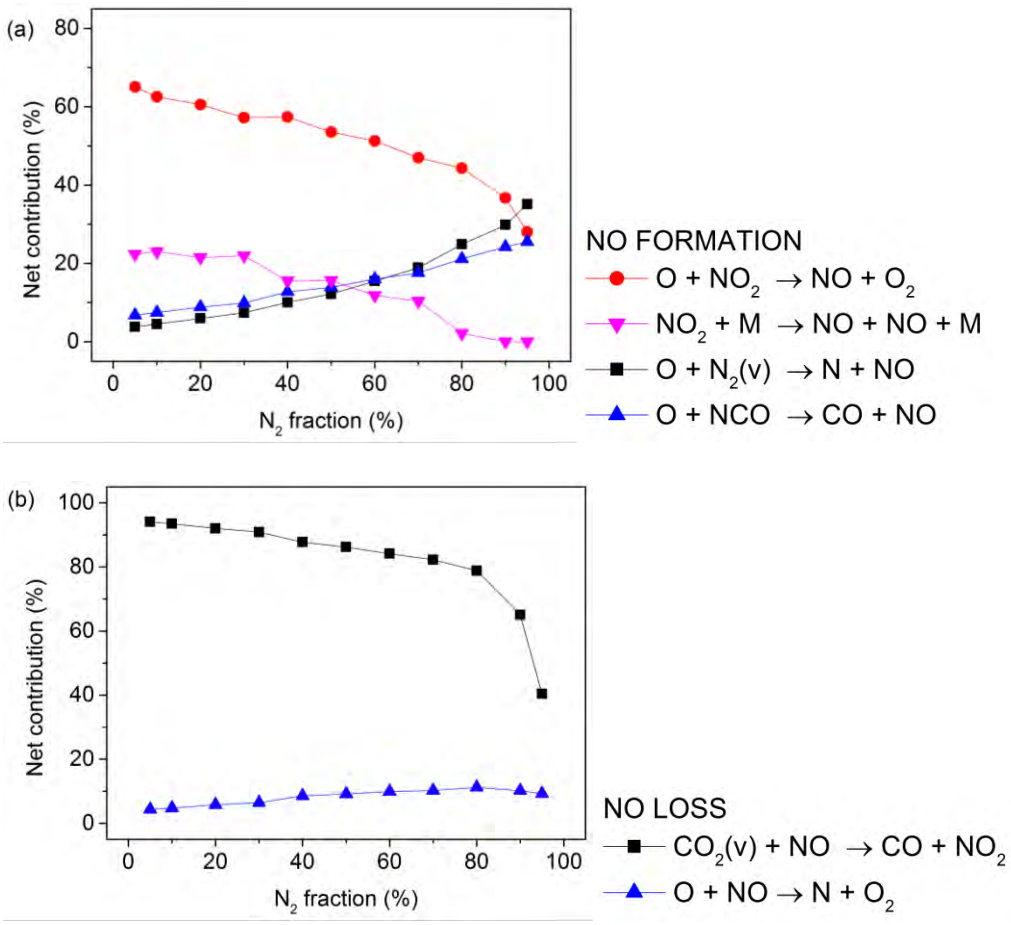

Figure A6 Net contribution of the most important formation (a) and loss (b) reactions of NO. Calculations performed by S. Heijkers within PLASMANT.

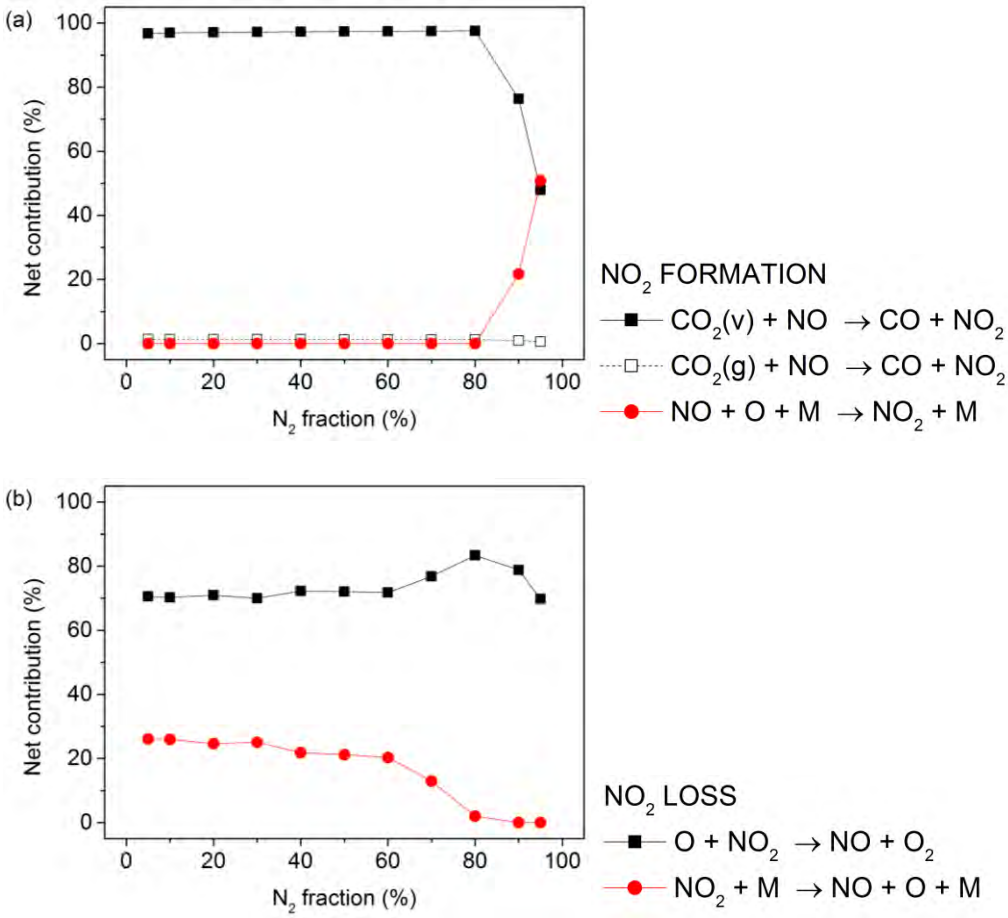

Figure A7 Net contribution of the most important formation (a) and loss (b) reactions of NO_2. Calculations performed by S. Heijkers within PLASMANT.

Table A2 Most important reactions, ranked by importance based on the average time-integrated rate. Obtained from the calculations performed by S. Heijkers within PLASMANT.

Reactions	Average time-integrated rate (cm^{-3})
$CO_2 + NO \rightarrow CO + NO_2$	3.55×10^{17}
$O + NO_2 \rightarrow NO + O2$	2.57×10^{17}
$CO + N \rightarrow CN + O$	1.38×10^{17}
$e^- + CO2 \rightarrow e^- + CO + O$	1.19×10^{17}
$CO_2 + M \rightarrow CO + O + M$	1.16×10^{17}
$CO_2 + CN \rightarrow CO + NCO$	1.15×10^{17}
$NO_2 + M \rightarrow NO + O + M$	7.63×10^{16}
$NCO + M \rightarrow N + CO + M$	5.96×10^{16}
$O + N_2 \rightarrow N + NO$	5.93×10^{16}
$O + NCO \rightarrow CO + NO$	5.92×10^{16}
$CO + O_2 \rightarrow CO_2 + O$	3.17×10^{16}
$NCO + NO \rightarrow CO + N_2 + O$	6.61×10^{15}
$N_2O + M \rightarrow N_2 + O + M$	6.49×10^{15}
$N + NO_2 \rightarrow N_2O + O$	3.78×10^{15}
$NCO + NO \rightarrow N_2O + CO$	3.13×10^{15}
$NO_2 + NO_3 + M \rightarrow N_2O_5 + M$	6.88×10^{13}
$NO_2 + NO_2 + M \rightarrow N_2O_4 + M$	9.34×10^{8}
$NO + NO_2 + M \rightarrow N_2O_3 + M$	4.28×10^{7}

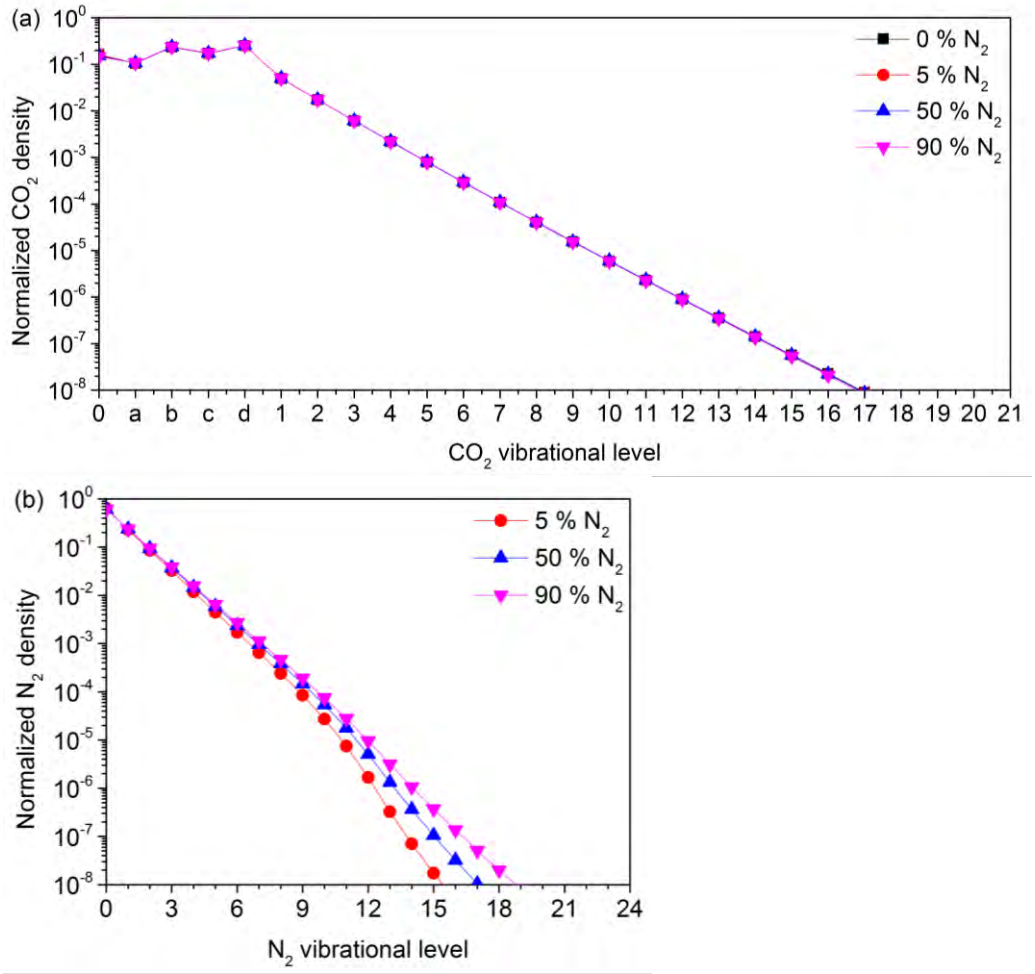

Figure A8 The calculated vibrational distributions of CO_2 (a) and N_2 (b) are nearly thermal, in the entire range of N_2 fractions in the mixture. Calculations performed by S. Heijkers within PLASMANT.

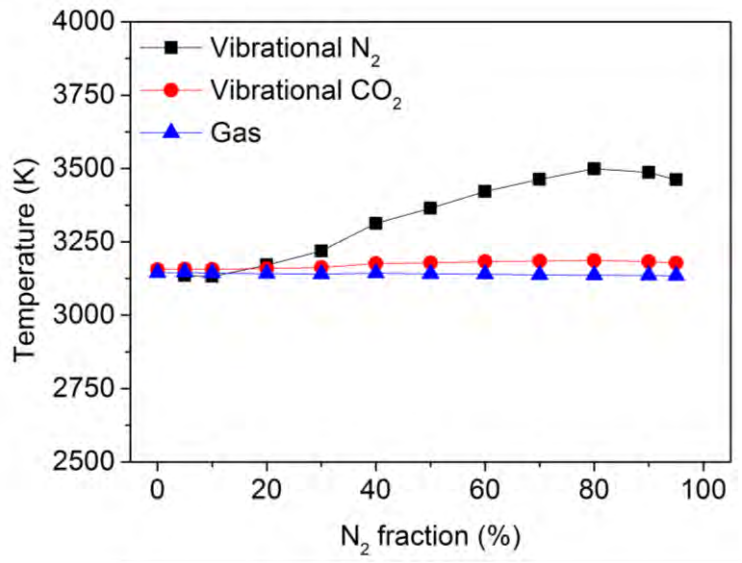

Figure A9 The average gas temperature is 3140 K, while the average vibrational temperature of CO_2 and N_2 are 3174 K and 3333 K, respectively. Calculations performed by S. Heijkers within PLASMANT.

2.4 Comparison of gliding arc plasmatron with dielectric barrier discharge

In Figure A10, we plot the total time-integrated net formation (a) and loss (b) rates of N_2O, N_2O_3, N_2O_4 and N_2O_5, in both a GAP and DBD. It is clear that the total formation rate is lower than the total loss rate in the GAP, while it is higher in the DBD, explaining why these species have a much higher concentration in the DBD than in the GAP.

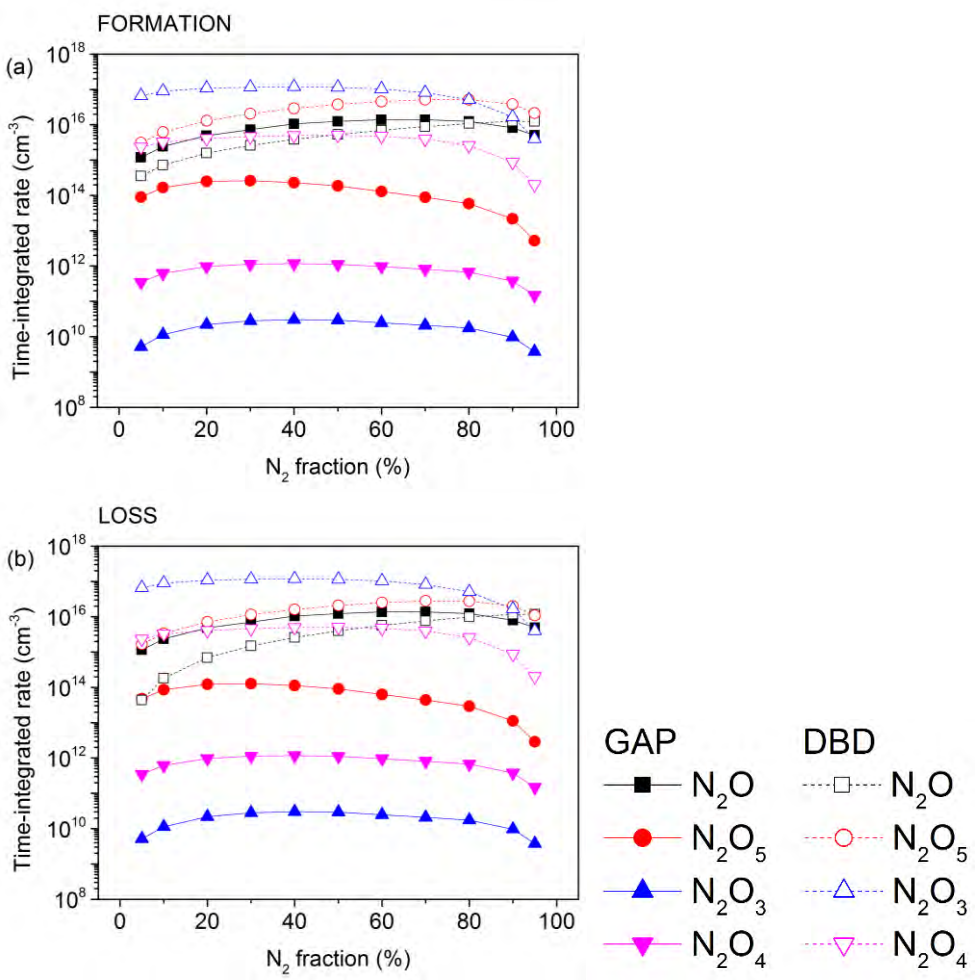

Figure A10 Total time-integrated net formation (a) and loss (b) rates of N_2O, N_2O_3, N_2O_4, N_2O_5, in both a GAP and DBD. Calculations performed by S. Heijkers within PLASMANT.

References

1 E. Cleiren, S. Heijkers, M. Ramakers and A. Bogaerts, *Chem. Sus. Chem.*, 2017, **10**, 4025–4036.

CHAPTER 5

Dry reforming

This chapter is published as

Emelie Cleiren, Stijn Heijkers, Marleen Ramakers, and Annemie Bogaerts, Dry Reforming of Methane in a Gliding Arc Plasmatron: Towards a Better Understanding of the Plasma Chemistry, *ChemSusChem* **2017**, *10*, 4025 – 4036.

In order to form more complex molecules and fuels, a source of hydrogen is needed. Methane, which is also a greenhouse gas, is a good candidate. The reaction of CO_2 with methane is called dry reforming of methane (DRM). In this chapter we study the DRM in a GAP for different CH_4 fractions in the mixture. The CO_2 and CH_4 conversion reach their highest values of approximately 18 and 10 %, respectively, at 25 % CH_4 in the gas mixture, corresponding to an overall energy cost of 10 kJ/L (or 2.5 eV/molec) and an energy efficiency of 66 %. CO and H_2 are the major products, with the formation of smaller fractions of C_2H_x (x = 2, 4, or 6) compounds and H_2O. A chemical kinetics model, developed by S. Heijkers, is used to investigate the underlying chemical processes. The calculated CO_2 and CH_4 conversion and the energy efficiency are in good agreement with the experimental data. The model calculations reveal that the reaction of CO_2 (mainly at vibrationally excited levels) with H radicals is mainly responsible for the CO_2 conversion, especially at higher CH_4 fractions in the mixture, which explains why the CO_2 conversion increases with increasing CH_4 fraction. The main process responsible for CH_4 conversion is the reaction with OH radicals. The excellent energy efficiency can be explained by the non-equilibrium character of the plasma, in which the electrons mainly activate the gas molecules, and by the important role of the vibrational kinetics of CO_2. The results demonstrate that a GAP is very promising for DRM.

1 Description of the experiments

The experimental setup for the experiments in this chapter is similar to the setup in Chapter 2. For these experiments we used a cathode with a diameter of 17.50 mm and a length of 10.20 mm, whereas the length and diameter of the anode were 16.30 and 7.08 mm, respectively. In addition, the inlet region had a width of 3 mm. This yielded a reactor volume of 3.82 cm^3. The setup can be used with different anode diameters, but the present configuration yielded the most pronounced reverse vortex flow, as revealed in Chapter 2, and provided the best CO_2 conversion and energy efficiency.

A high voltage was applied to the GAP by means of a direct current power source. The voltage was measured by a high-voltage probe (Tektronix P6015A). The current was obtained by measuring the voltage over a 10 Ω resistor. All electrical signals were recorded by a digital oscilloscope with two channels (Tektronix TDS2012C). The current and voltage inside the GAP were 0.27 – 0.33 A and 0.8 – 1.0 kV, respectively. The plasma power was calculated from the product of the plasma voltage and current over a certain time.

The gas flowed into the reactor through six tangential inlets, each with a diameter of 1.6 mm, giving rise to a vortex flow profile. The experiments were performed with a total gas flow rate of 10 L/min controlled by thermal mass flow controllers (Bronkhorst), and different fractions of CH_4 in the mixture (i.e., 0, 5, 10, 15, 20, and 25 %). The pressure in the reactor is slightly higher than atmospheric pressure (1.25 bar). The outlet of the GAP was connected to a tube in which a thermocouple was used to measure the temperature of the outlet gas. The gas was further analyzed in a gas chromatograph. All experiments were performed in triplicate. Details on the gas analysis, including more information on the gas chromatograph, how to correct for gas expansion, the formulas to calculate the CO_2 and CH_4 conversion, the product selectivities, energy efficiency, and energy cost, are provided in the appendix.

2 Description of the model

To support the experiments, computer simulations were again performed by S. Heijkers within PLASMANT, by means of the same 0D chemical kinetics model, as explained in Chapter 2. More details about the model can be found in the supporting information of reference 1. In principle, the model can also be used to calculate the gas temperature by a heat conservation equation. However, in this case, a certain temperature profile was applied as input in the model starting from room temperature at the inlet of the arc column up to 3500 K. This was based on reported 3D fluid dynamics simulations[2,3] and experimental values.[4] 134 different plasma species, including 20 neutral molecules, 37 charged species (i.e., positive and negative ions as well as the electrons), 24 radicals, and 53 excited species, were included in the model. A complete list of these species is provided in the supporting information of reference 1. These species interacted with each other through various chemical reactions, including: electron impact reactions; electron–ion recombination reactions; ion–ion, ion–neutral, and neutral–neutral reactions; vibration–translation (VT) relaxations; and vibration-vibration (VV) relaxations.

3 Results and discussion

3.1 Measured conversion, energy efficiency, and energy cost

We investigated the CO_2 and CH_4 conversion, energy efficiency, and energy cost, as well as the product selectivities (see next section) as a function of the CH_4 fraction in the gas mixture (from 0 to 25%) for a gas flow rate of 10 L/min. We were limited to a maximum CH_4 fraction of 25 % in the current setup because the plasma became unstable for larger fractions, owing to limitations of the power supply. The plasma power was approximately 500 W in the entire range of CH_4 fractions, yielding a specific energy input (SEI) of approximately 3 kJ/L (or 0.75 eV/molec; Figure A1 in the appendix).

Figure 1(a) and (b) illustrate the measured CO_2 and CH_4 conversion as a function of CH_4 fraction in the mixture. The absolute CO_2 conversion increases from 7.5 to 24 % upon increasing CH_4 fraction, whereas the absolute CH_4 conversion drops from 61 to 42 % (Figure 1(a)). The CH_4 conversion is much higher than the CO_2 conversion, which is attributed to the lower bond dissociation energy of C—H (4.48 eV) compared to C=O (5.52 eV), making the dissociation of CH_4 easier than for CO_2.

The effective conversion of CO_2 and CH_4 in the mixture was obtained by multiplying the absolute conversion with the fraction of the component in the initial mixture (Figure 1(b)). The effective CO_2 and CH_4 conversion both increase with increasing CH_4 fraction. Indeed, the rising CH_4 fraction compensates for the lower absolute CH_4 conversion, whereas the lower CO_2 fraction in the mixture is not important enough to compensate for the higher absolute CO_2 conversion upon the addition of CH_4 to the mixture. Consequently, the overall conversion also increases from 7.5 to approximately 30 % upon the addition of CH_4 to the mixture. These trends agree well with results obtained in a tornado-type GA plasma.[5]

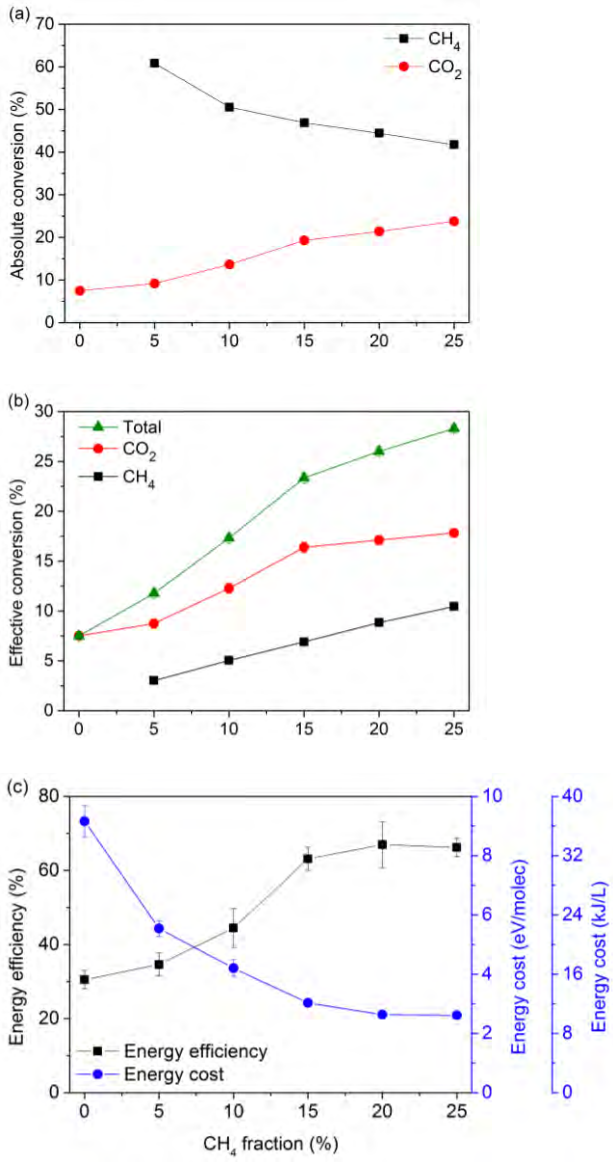

Figure 1 Absolute (a) and effective (b) conversion of CO_2 and CH_4, as well as the total conversion (b), and overall energy efficiency and energy cost (c), as a function of CH_4 fraction in the mixture. The error bars are included in the graphs, but are too small to be visible in (a) and (b).

The energy efficiency and energy cost upon increasing CH_4 fraction are plotted in Figure 1(c). The energy efficiency follows the rising trend of the overall conversion, whereas the energy cost follows the opposite trend. This is logical because the energy efficiency and energy cost are

linearly and inversely proportional to the overall conversion, respectively, and they are further determined by the SEI (see Equation (A7) and (A8) in the appendix); the SEI is more or less constant in the entire range of CH_4 fractions (Figure A1). The rising trend in energy efficiency is most striking up to 15% CH_4 fraction, increasing from 30 % in pure CO_2 to above 60 % between 15 and 25 % CH_4. The energy cost drops from 37 to 10 kJ/L (or from 9.3 to 2.6 eV/molec), upon increasing the CH_4 fraction. The trends of rising energy efficiency and decreasing energy cost are accompanied by a slight drop in temperature of the gas flowing out of the GAP reactor, from 120 °C to 103 °C at 0 % and 25 % CH_4 fraction, respectively. Clearly, less energy is lost to gas heating and more energy can effectively be used for the conversion.

The combined values of the conversion, energy efficiency, and energy cost are much better than the typical values obtained in DBDs, which are the most commonly used plasmas for DRM. Indeed, DBDs typically yield maximum conversions of a few % up to 60 % (with a few exceptions up to 80 % for packed-bed DBDs), but the corresponding energy cost is between 20 and 100 eV/molec (with some lower and higher exceptions for packed bed DBDs).[6–33] We compare the literature values for the energy cost instead of the energy efficiency because for the latter we need to account for all formed products (and their enthalpy of formation; cf. Equation (A7) in the appendix); in the literature, typically, only the selectivity towards the syngas components (and sometimes light hydrocarbons) is reported, making a comparison based on energy efficiencies not very reliable. However, comparison based on the energy cost can provide the same insights in the performance of our GAP compared to other results in the literature.

Microwave (MW) plasmas are quite promising for pure CO_2 splitting, with energy efficiencies of up to 50 % at a conversion of up to 26 %;[34,35] however, these values are typically reached at reduced pressure, which is less convenient for industrial applications, and the energy cost of

vacuum systems would have to be added to the overall energy cost. Moreover, the number of studies on DRM in a MW plasma is very limited. A pulsed MW plasma was able to demonstrate an absolute CH_4 and CO_2 conversion of 71 % and 69 %, respectively, with an energy cost of 6.5 eV/molec.[36] Comparing these results with our GAP, for which we obtained an absolute CH_4 and CO_2 conversion of up to 61 % and 24 %, respectively (cf. Figure 1(a) above), the conversion was higher in this MW plasma but the energy cost was also double the best value reached in our experiments. Another study of continuous MW plasma yielded similar maximum conversions as in the pulsed MW plasma, but with a higher power (1.5 kW), and thus a very high energy cost of up to 343 eV/molec.[37]

For GA plasmas, maximum conversions in the range of 30 – 50 % have been reported, with energy costs as low as 1 – 2 eV/molec.[5,38–48] The best reported result was obtained for a rotating GA reactor, which yielded a total conversion of 39 % with an energy cost of 1 eV/molec,[38] which is somewhat better than our results.

Other types of plasmas have also been investigated for DRM. In corona discharges, maximum conversions between 10 and 90 % have been reached, with energy costs between 4 and 100 eV/molec.[49–56] The best combined result was a conversion of 44 % with an energy cost of 5.2 eV/molec.[50] In spark discharges, the minimum energy cost has been reported to be approximately 3 – 10 eV/molec for conversions between 10 and 85 %,[57–64] with the best total conversion of 85 % with an energy cost of 3.2 eV/molec.[57] Atmospheric pressure glow discharges also seem to be promising for DRM, with maximum conversions of 35 – 85 % and energy costs of 1 - 60 eV/molec.[65–67] The best result is a total conversion of 89 % with an energy cost of only 1.2 eV/molec.[66] Finally, nanosecond-pulsed plasmas provided conversions between 1 and 60 % for energy costs between 3 and 100 eV/molec.[68–72]

Clearly, the GAP is among the most promising types of plasmas for DRM in terms of energy cost or energy efficiency. In reference 73, a maximum energy cost of 4.27 eV/molec corresponding to a minimum energy efficiency of 60 % (assuming that syngas was the only product formed) was proposed as the target for plasma-based DRM to become industrially competitive with classical and other novel conversion technologies. Figure 1(c) illustrates that we reached this target with our GAP if the CH_4 fraction in the gas mixture was sufficiently high. This good result was attributed to the important role of the vibrational levels of CO_2 for energy-efficient conversion.

3.2 Measured product selectivities

The major DRM products detected in our GAP are CO and H_2, alongside, to a much lower extent, O_2, H_2O, and C_2H_x (x = 2, 4, or 6) hydrocarbons. The model calculations of S. Heijkers reveal that other products can also be formed in this gas mixture. Figure 2(a) illustrates the (H- and O-based) selectivities of H_2 and O_2 as a function of the CH_4 fraction. The remaining H and O atoms give rise to higher hydrocarbons (C_2H_x) and H_2O, and to CO and H_2O, respectively, and maybe to some minor oxygenated compounds that could not be detected. The strong drop in O-based selectivity of O_2 (S_{O,O_2}) upon addition of 5 % CH_4 indicates that the O atoms, which are mainly converted into O_2 (and CO) in pure CO_2 splitting, are converted into other compounds upon addition of a H-source, so that almost no O_2 is formed anymore. Furthermore, it is clear from Figure 2(a) that the selectivity towards H_2 increases, which is desirable as H_2 is a component of syngas. At a low CH_4/CO_2 ratio, the H-based selectivity towards H_2O will be higher.[73]

Figure 2(b) presents the C-based selectivities as well as the C-balance, which is 100 %. The fact that the C-based selectivity of CO ($S_{C,CO}$) is sometimes higher than the C-balance is probably due to the error associated with this selectivity. CO is clearly the dominant product. The slight drop in $S_{C,CO}$ upon increasing CH_4 fraction is due to a rise in the

formation of other C-based products such as C_2 components. However, the rise in S_{C,C_2} from 2 to 4 % (Figure 2(b)) is not sufficient to compensate for the drop of 13 % (with an uncertainty of 6 %) in $S_{C,CO}$, which indicates that other C-based compounds that were not detected by GC are formed.

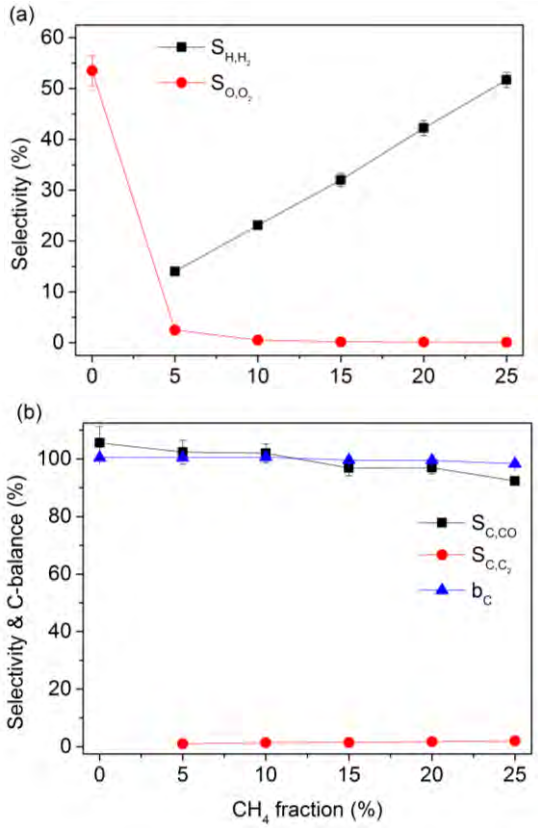

Figure 2 H- and O-based selectivities (a) and C-based selectivities (where C_2 is the sum of C_2H_6, C_2H_4 and C_2H_2) as well as the C-balance (b), as a function of CH_4 fraction in the mixture.

The two main components formed are H_2 and CO (syngas). The H_2/CO ratio increases slightly more than linearly upon increasing CH_4 fraction, from 0.08 at 5 % CH_4 to 0.44 at 25 % CH_4 (Figure A2). This is logical because CH_4 is the only source of H in the mixture. The H_2/CO ratio is strongly affected by the gas mixing ratio and can be easily tuned by this parameter to reach optimum values for subsequent Fischer–Tropsch

(FT) or methanol synthesis. However, the current CO and H_2 yields might still be too low for FT or methanol synthesis, which require high yields of CO and H_2 feed gas, as obtained from DRM. This is because the conversion in our current setup is still rather low. As mentioned before, the research group PLASMANT aims to optimize the setup in the future, to improve the conversion.

3.3 Comparison of measured and calculated conversion and energy efficiency

Stijn Heijkers and Emelie Cleiren (both within PLASMANT) developed a chemical kinetics model to investigate the underlying mechanisms of DRM in our GAP, as explained in reference 1 and its supporting information. Before we use this model for a deeper analysis, it is validated against the experimental data for conversion and energy efficiency. Figure 3 illustrates the CO_2 (Figure 3(a)) and CH_4 (Figure 3(b)) conversion as a function of the CH_4 fraction in the mixture for an input power of 500 W (SEI = 0.75 eV/molec) and gas flow rate of 10 L/min. As explained in Chapter 2, the arc is stabilized in the center of the GAP reactor, and only a fraction of the gas (i.e., 14.8 %; for details, see the supporting information of reference 1) passes through this arc column. However, the model not only considers the conversion inside the arc column but also in a certain region around the actual arc column that is still at a rather high temperature, thus allowing some thermal conversion to take place. Both contributions are indicated in Figure 3(a) and (b) with dashed lines. Adding both contributions yields the total conversion, which is compared with the measured conversion. Both the rising trend in CO_2 conversion (Figure 3(a)) and the drop in CH_4 conversion (Figure 3(b)) are correctly predicted by the model and the absolute values are in very good agreement.

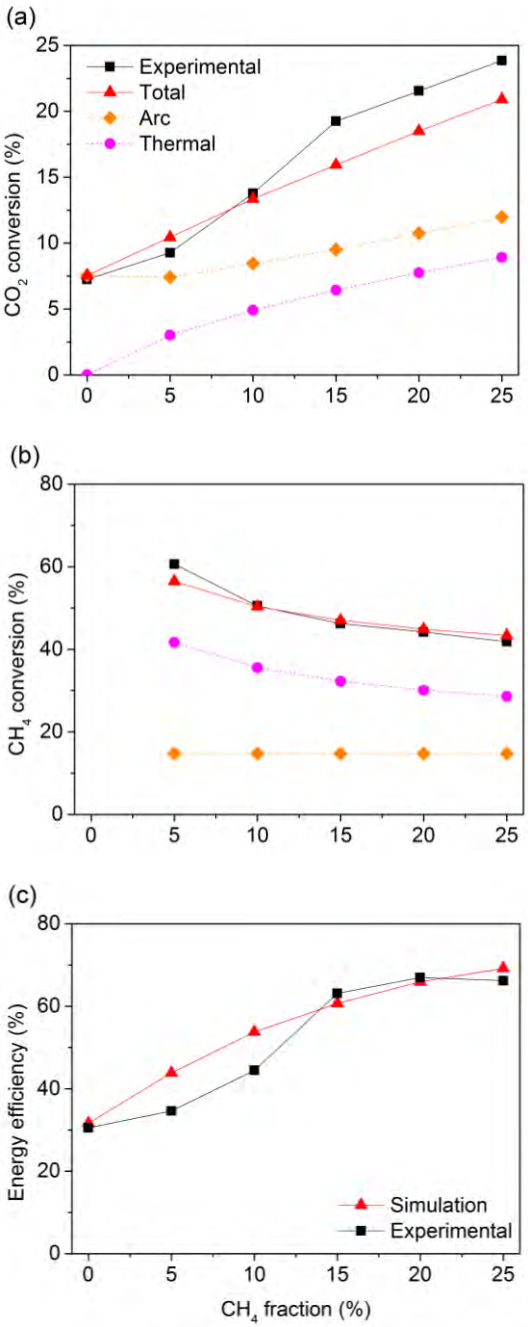

Figure 3 Measured and calculated CO_2 conversion (a) and CH_4 conversion (b), as well as energy efficiency (c) as a function of the CH_4 fraction in the mixture. The individual contributions of the conversion inside the arc and in the thermal area around the arc are indicated in dashed lines in (a) and (b). Calculations performed by S. Heijkers and E. Cleiren within PLASMANT.

As evident from Figure 3(a) and (b), only accounting for the conversion in the arc column will underestimate the total conversion, especially for CH_4, for which the thermal conversion outside the arc column appears to be even higher than the plasma conversion. This is attributed to the lower C—H bond dissociation energy, which allows thermal conversion to occur at lower temperatures.

Furthermore, Figure 3(b) indicates that the CH_4 conversion inside the arc was constant at 14.8 %, independent from the CH_4 fraction in the mixture. The reason is that the CH_4 conversion inside the arc is in fact 100 %, but the overall contribution of the arc is limited by the fraction of gas that passes through the arc, which was predicted to be 14.8 % (more details in the supporting information of reference 1).

Figure 3(c) illustrates the measured and calculated values of the energy efficiency as a function of the CH_4 fraction. Again, the agreement is very good, with relative differences between 1.5 and 27 % and an average difference of 10 % between the values. The rising trend is not exactly the same at low CH_4 fraction, which may indicate that the thermal conversion is somewhat overestimated at 5 and 10 % CH_4 in the mixture. Indeed, the model simply assumes the same area around the arc column at which thermal conversion can take place, but this area will most probably be smaller at low CH_4 fractions because CH_4 gives rise to a somewhat higher temperature. Of course, the assumptions made about the thermal conversion in a fixed area around the arc are somewhat rough, owing to the inherent nature of the 0D chemical kinetics model. A more accurate description would require full 3D calculations;[2,3] however, this would result in excessively long calculation times when incorporating the complex CO_2/CH_4 chemistry. Nevertheless, despite the approximations that need to be made in the 0D model, the agreement is quite satisfactory. In general, the model provides quite realistic predictions of the CO_2 and CH_4 conversion and the energy efficiency, which can be used to investigate the underlying mechanisms.

4 Conclusions

We have investigated the dry reforming of methane (DRM) in a gliding arc plasmatron for different CH_4 fractions in the mixture by experiments, supported by chemical kinetics modeling. The CO_2 and CH_4 conversion reached their highest values of approximately 18 and 10 %, respectively, at 25 % CH_4 in the gas mixture, which corresponded to an overall energy cost of 10 kJ/L (or 2.5 eV/molec) and an energy efficiency as high as 66 %. The latter was above the required energy efficiency target reported in literature to be competitive with classical thermal DRM (i.e., 60%)[73]. CO and H_2 were the major products, with some smaller fractions of C_2H_x compounds formed, as well as H_2O, which could not be quantified by GC.

The results demonstrate that the GAP is very promising for DRM, also in comparison with other plasma types, certainly when considering the energy efficiency (or energy cost). However, the conversion needs to be further improved. To date, the conversion has been limited by the fraction of gas that passes through the plasma column. Indeed, the conversion inside the arc plasma column itself was calculated to be between 51 and 81 % for CO_2 and was already 100 % for CH_4; however, a significant fraction of the gas (ca. 85 %) does not pass through the plasma column, therefore lowering the overall conversion in the GAP. We should be able to enhance the gas fraction treated by the arc by modifying the reactor design (i.e., anode and cathode configuration), enabling the arc to be developed and extended in a larger region of the reactor, or by modifying the gas inlet configuration, enabling a larger gas fraction to pass through the arc. To realize such modifications, more insight is needed in the gas flow dynamics, which will be studied in the future by PLASMANT.

References

1 E. Cleiren, S. Heijkers, M. Ramakers and A. Bogaerts, *ChemSusChem*, 2017, **10**, 4025–4036.

2 G. Trenchev, S. Kolev and A. Bogaerts, *Plasma Sources Sci. Technol.*, 2016, **25**, 035014.

3 G. Trenchev, S. Kolev, W. Wang, M. Ramakers and A. Bogaerts, *J. Phys. Chem. C*, 2017, **121**, 24470–24479.

4 T. P. Nunnally, *PhD dissertation*, Drexel University, 2011.

5 J. L. Liu, H. W. Park, W. J. Chung and D. W. Park, *Plasma Chem. Plasma Process.*, 2015, **36**, 437–449.

6 R. Snoeckx, Y. X. Zeng, X. Tu and A. Bogaerts, *RSC Adv.*, 2015, **5**, 29799–29808.

7 X. Tu and J. C. Whitehead, *Appl. Catal. B Environ.*, 2012, **125**, 439–448.

8 N. R. Pinhão, A. Janeco and J. B. Branco, *Plasma Chem. Plasma Process.*, 2011, **31**, 427–439.

9 H. K. Song, H. Lee, J. W. Choi and B. K. Na, *Plasma Chem. Plasma Process.*, 2004, **24**, 57–72.

10 W. C. Chung, K. L. Pan, H. M. Lee and M. B. Chang, *Dry reforming of methane with dielectric barrier discharge and ferroelectric packed-bed reactors*, 2014, vol. 28.

11 Y. Zeng, X. Zhu, D. Mei, B. Ashford and X. Tu, *Catal. Today*, 2015, **256**, 80–87.

12 Q. Wang, Y. Cheng and Y. Jin, *Catal. Today*, 2009, **148**, 275–282.

13 S. K. Mahammadunnisa, P. Manoj Kumar Reddy, B. Ramaraju and C. H. Subrahmanyam, *Energy and Fuels*, 2013, **27**, 4441–4447.

14 X. Zheng, S. Tan, L. Dong, S. Li and H. Chen, *J. Power Sources*, 2015, **274**, 286–294.

15 D. Mei, X. Zhu, C. Wu, B. Ashford, P. T. Williams and X. Tu, *Appl. Catal. B Environ.*, 2016, **182**, 525–532.

16 Q. Wang, B. H. Yan, Y. Jin and Y. Cheng, *Energy and Fuels*, 2009, **23**, 4196–4201.

17 X. Tu, H. J. Gallon, M. V Twigg, P. A. Gorry and J. C. Whitehead, *J. Phys. D. Appl. Phys.*, 2011, **44**, 274007.

18 A. Ozkan, T. Dufour, G. Arnoult, P. De Keyzer, A. Bogaerts and F. Reniers, *J. CO2 Util.*, 2015, **9**, 74–81.

19 X. Zheng, S. Tan, L. Dong, S. Li and H. Chen, *Int. J. Hydrogen Energy*, 2014, **39**, 11360–11367.

20 K. Zhang, T. Mukhriza, X. Liu, P. P. Greco and E. Chiremba, *Appl. Catal. A Gen.*, 2015, **502**, 138–149.

21 M. H. Pham, V. Goujard, J. M. Tatibouët and C. Batiot-Dupeyrat, *Catal. Today*, 2011, **171**, 67–71.

22 J. Sentek, K. Krawczyk, M. Młotek, M. Kalczewska, T. Kroker, T. Kolb, A. Schenk, K. H. Gericke and K. Schmidt-Szałowski, *Appl. Catal. B Environ.*, 2010, **94**, 19–26.

23 K. Krawczyk, M. Młotek, B. Ulejczyk and K. Schmidt-Szałowski, *Fuel*, 2014, **117**, 608–617.

24 H. J. Gallon, X. Tu and J. C. Whitehead, *Plasma Process. Polym.*, 2012, **9**, 90–97.

25 B. Eliasson, C. Liu and U. Kogelschatz, *Ind. Eng. Chem. Res.*, 2000, **39**, 1221–1227.

26 J. J. Zou, Y. P. Zhang, C. J. Liu, Y. Li and B. Eliasson, *Plasma Chem. Plasma Process.*, 2003, **23**, 69–82.

27 V. Goujard, J. M. Tatibouët and C. Batiot-Dupeyrat, *Appl. Catal. A Gen.*, 2009, **353**, 228–235.

28 X. Zhang and M. S. Cha, *J. Phys. D. Appl. Phys.*, 2013, **46**, 415205.

29 Q. Wang, B. H. Yan, Y. Jin and Y. Cheng, *Plasma Chem. Plasma Process.*, 2009, **29**, 217–228.

30 H. K. Song, J.-W. Choi, S. H. Yue, H. Lee and B.-K. Na, *Catal. Today*, 2004, **89**, 27–33.

31 A. J. Zhang, A. M. Zhu, J. Guo, Y. Xu and C. Shi, *Chem. Eng. J.*, 2010, **156**, 601–606.

32 Y. Li, C. J. Liu, B. Eliasson and Y. Wang, *Energy and Fuels*, 2002, **16**, 864–870.

33 Y. P. Zhang, Y. Li, Y. Wang, C. J. Liu and B. Eliasson, *Fuel Process. Technol.*, 2003, **83**, 101–109.

34 G. J. van Rooij, D. C. M. van den Bekerom, N. den Harder, T. Minea, G. Berden, W. A. Bongers, R. Engeln, M. F. Graswinckel, E. Zoethout and M. C. M. van de Sanden, *Faraday Discuss.*, 2015, **183**, 233–248.

35 W. Bongers, H. Bouwmeester, B. Wolf, F. Peeters, S. Welzel, D. van den Bekerom, N. den Harder, A. Goede, M. Graswinckel, P. W. Groen, J. Kopecki, M. Leins, G. van Rooij, A. Schulz, M. Walker and R. van de Sanden, *Plasma Process. Polym.*, 2016, DOI: 10.1002/ppap.201600126.

36 J. Q. Zhang, Y. J. Yang, J. S. Zhang and Q. Liu, *Acta Chim. Sin.*, 2002, **60**, 1973–1980.

37 W. Cho, W. S. Ju, S. H. Lee, Y. S. Baek and Y. C. Kim, *Proc. 7th Int. Conf. Carbon Dioxide Util.*, 2004, 205–208.

38 A. Wu, J. Yan, H. Zhang, M. Zhang, C. Du and X. Li, *Int. J. Hydrogen Energy*, 2014, **39**, 17656–17670.

39 N. Rueangjitt, T. Sreethawong and S. Chavadej, *Plasma Chem. Plasma Process.*, 2008, **28**, 49–67.

40 Y. N. Chun, Y. C. Yang and K. Yoshikawa, *Catal. Today*, 2009, **148**, 283–289.

41 Z. A. Allah and J. C. Whitehead, *Catal. Today*, 2015, **256**, 76–79.

42 J. L. Liu, H. W. Park, W. J. Chung, W. S. Ahn and D. W. Park, *Chem. Eng. J.*, 2016, **285**, 243–251.

43 K. Li, J. L. Liu, X. S. Li, X. Zhu and A. M. Zhu, *Chem. Eng. J.*, 2016, **288**, 671–679.

44 Y. N. Chun, H. W. Song, S. C. Kim and M. S. Lim, *Energy and Fuels*, 2008, **22**, 123–127.

45 Z. Bo, J. Yan, X. Li, Y. Chi and K. Cen, *Int. J. Hydrogen Energy*, 2008, **33**, 5545–5553.

46 X. Tu and J. C. Whitehead, *Int. J. Hydrogen Energy*, 2014, **39**, 9658–9669.

47 A. Indarto, J. W. Choi, H. Lee and H. K. Song, *Energy*, 2006, **31**, 2986–2995.

48 N. Rueangjitt, C. Akarawitoo, T. Sreethawong and S. Chavadej, *Plasma Chem. Plasma Process.*, 2007, **27**, 559–576.

49 M. W. Li, C. P. Liu, Y. L. Tian, G. H. Xu and F. C. Zhang, *Energy & Fuels*, 2006, **20**, 1033–1038.

50 A. Aziznia, H. R. Bozorgzadeh, N. Seyed-Matin, M. Baghalha and A. Mohamadalizadeh, *J. Nat. Gas Chem.*, 2012, **21**, 466–475.

51 M. W. Li, G. H. Xu, Y. L. Tian, L. Chen and H. F. Fu, *J. Phys. Chem. A*, 2004, **108**, 1687–1693.

52 N. Seyed-Matin, A. H. Jalili, M. H. Jenab, S. M. Zekordi, A. Afzali, C. Rasouli and A. Zamaniyan, *Plasma Chem. Plasma Process.*, 2010, **30**, 333–347.

53 M. A. Malik and X. Z. Jiang, *Plasma Chem. Plasma Process.*, 1999, **19**, 505–512.

54 S. L. Yao, M. Okumoto, A. Nakayama and E. Suzuki, *Energy and Fuels*, 2001, **15**, 1295–1299.

55 Y. Yang, *Ind. Eng. Chem. Res.*, 2002, **41**, 5918–5926.

56 C. J. Liu, R. Mallinson and L. Lobban, *Appl. Catal. A Gen.*, 1999, **178**, 17–27.

57 W. C. Chung and M. B. Chang, *Energy Convers. Manag.*, 2016, **124**, 305–314.

58 M. M. Moshrefi, F. Rashidi, H. R. Bozorgzadeh and M. Ehtemam Haghighi, *Plasma Chem. Plasma Process.*, 2013, **33**, 453–466.

59 V. Shapoval and E. Marotta, *Plasma Process. Polym.*, 2015, **12**, 808–816.

60 B. Zhu, X. S. Li, J. L. Liu, X. Zhu and A. M. Zhu, *Chem. Eng. J.*, 2015, **264**, 445–452.

61 X. S. Li, B. Zhu, C. Shi, Y. Xu and A. M. Zhu, *AlChE J.*, 2011, **57**, 2854–2860.

62 S. Kado, K. Urasaki, Y. Sekine and K. Fujimoto, *Fuel*, 2003, **82**, 1377–1385.

63 B. Zhu, X. S. Li, C. Shi, J. L. Liu, T. L. Zhao and A. M. Zhu, *Int. J. Hydrogen Energy*, 2012, **37**, 4945–4954.

64 K. Li, J. L. Liu, X. S. Li, X. B. Zhu and A. M. Zhu, *Catal. Today*, 2015, **256**, 96–101.

65 A. Huang, G. Xia, J. Wang, S. L. Suib, Y. Hayashi and H. Matsumoto, *J. Catal.*, 2000, **189**, 349–359.

66 D. Li, X. Li, M. Bai, X. Tao, S. Shang, X. Dai and Y. Yin, *Int. J. Hydrogen Energy*, 2009, **34**, 308–313.

67 H. Long, S. Shang, X. Tao, Y. Yin and X. Dai, *Int. J. Hydrogen Energy*, 2008, **33**, 5510–5515.

68 M. Scapinello, L. M. Martini, G. Dilecce and P. Tosi, *J. Phys. D. Appl. Phys.*, 2016, **49**, 075602.

69 A. M. Ghorbanzadeh, S. Norouzi and T. Mohammadi, *J. Phys. D. Appl. Phys.*, 2005, **38**, 3804–3811.

70 S. L. Yao, F. Ouyang, A. Nakayama, E. Suzuki, M. Okumoto and A. Mizuno, *Energy & Fuels*, 2000, **14**, 910–914.

71 A. M. Ghorbanzadeh, R. Lotfalipour and S. Rezaei, *Int. J. Hydrogen Energy*, 2009, **34**, 293–298.

72 X. Zhang, B. Dai, A. Zhu, W. Gong and C. Liu, *Catal. Today*, 2002, **72**, 223–227.

73 R. Snoeckx and A. Bogaerts, *Chem. Soc. Rev.*, 2017, **46**, 5805–5863.

Appendix

1 Gas analysis

The same compact gas chromatograph (CGC) of Interscience as in Chapter 2 was used. The CGC is equipped with three different ovens, each with a separate column and detector. The first channel has a Rtx-1 column and a flame ionization detector (FID), which can be used to measure alkanes, alkenes and alkynes. The other two channels make use of thermal conductivity detectors (TCDs). The middle channel has two columns, a molecular sieve (Molsieve 5A) and a RT-QBond, and the TCD measures the permanent gases, like O_2, N_2, CO, H_2 and CH_4. The last channel has two RT-QBond columns, which allow the separation of CO_2 and lower hydrocarbons (up to C_3).

First a calibration was performed for the compounds to be detected, namely CO_2, CO, O_2, CH_4, H_2, C_2H_2, C_2H_4 and C_2H_6. C_2H_2 and C_2H_4 could not be separated with the CGC. However, because of their low concentrations, the C_2 compounds (C_2H_n; n = 2, 4 or 6) were considered as one compound. H_2O was detected as a broad band, which could not be quantified. Higher hydrocarbons and oxygenated compounds could not be detected with this CGC.

2 Determination of the CO_2 and CH_4 conversion

By analyzing the gas mixture with and without plasma, we could calculate the CO_2 and CH_4 conversion by Equation (A1). $C_{i\,(in)}$ and $C_{i\,(out)}$ are the concentrations of component i (CO_2 or CH_4) measured after passing through the GAP without plasma (blank measurement) and with plasma, respectively. α is a correction factor, explained in the next section.

$$\chi_i(\%) = \frac{C_{i\,(in)} - \alpha \cdot C_{i\,(out)}}{C_{i(in)}} \cdot 100\ \% \quad with\ i = CO_2\ or\ CH_4 \tag{A1}$$

Besides this (absolute) conversion, we also determined the effective conversion for both CO_2 and CH_4, accounting for the fraction of this component present in the initial gas mixture:

$$\chi_{eff,i}(\%) = \chi_i(\%) \cdot fraction_i \quad with\ i = CO_2\ or\ CH_4 \tag{A2}$$

The total conversion is the sum of both effective conversions, and is of interest to compare mixtures with different CO_2/CH_4 ratios.

3 Correction factor for the gas expansion

The correction factor α in Equation (A1) accounts for gas expansion taking place during the reaction. Indeed, both in pure CO_2 splitting and dry reforming of methane (DRM), the number of molecules rises during reaction, so the volumetric flux will rise as well. Because the GC always samples the same volume of the gas flow, neglecting this correction factor, which is done in most papers on plasma-based gas conversion, would overestimate the conversion.[1] Indeed, the sample loop of the GC has a fixed volume, so that gas expansion will yield a pressure rise. However, the GC always samples at atmospheric pressure, so part of the gas will be lost before being injected in the GC. Hence, the number of molecules that will arrive in this sample volume is lower than the original number in the outlet flow. Thus, less molecules will be measured in the sample, which manifests itself as a higher conversion.

To account for this gas expansion, we added an internal standard (N_2) to the outlet gas flow. Using an internal standard has several advantages: (i) it is easy to implement; (ii) no extra calibration is needed; (iii) it has no effect on the reaction processes; (iv) it can be used with every gas mixture.[1]

By comparing the peak surface area of N_2 in the chromatogram with and without plasma, we could obtain the correction factor α (Equation (A3))[1] assuming that the ratio of the surface areas is proportional with the ratio of the fluxes.

$$\alpha = \frac{A_{N_2,blank}}{A_{N_2,plasma}}(1+\beta) - \beta \tag{A3}$$

β is equal to the ratio of the gas flow rate of the internal standard with respect to the total gas flow rate in the GAP (Equation (A4)). In this work we always used 10 % of the total gas flow rate as internal standard (β = 0.1), hence for a total gas flow rate of 10 L/min, we added 1 L/min N_2 as internal standard.

$$\beta = \frac{\Phi_{standard}}{\Phi_{effluent}} = \frac{gas\ flow\ rate_{N_2}}{gas\ flow\ rate_{CO_2+CH_4}} \tag{A4}$$

By adding the internal standard, we needed to correct the measured concentrations (C_m) by means of Equation (A5) and (A6), for the blank measurements and the plasma measurements, respectively.[1]

$$C^{blank} = C_m^{blank}(1+\beta) \tag{A5}$$

$$C^{plasma} = C_m^{plasma}\left(1+\frac{\beta}{\alpha}\right) \tag{A6}$$

In the following, we always use the corrected concentrations.

4 Determination of the specific energy input (SEI), energy efficiency and energy cost

The SEI was calculated from the plasma power and the gas flow rate according to Equation (3) from Chapter 2.

The energy efficiency (η) was calculated as follows:

$$\eta = \frac{\alpha \cdot C_{CO(out)} \cdot H_{f,CO} - (\chi_{CH_4} \cdot C_{CH_{4(in)}} \cdot H_{f,CH_4} + \chi_{CO_2} \cdot C_{CO_{2(in)}} \cdot H_{f,CO_2})}{SEI\ (kJ/L) \cdot V_{mol}\ (L/mol)} \tag{A7}$$

H_f is the enthalpy of formation ($H_{f,CO}$ = - 110,5 kJ/mol; H_{f,CH_4}= - 74,8 kJ/mol; H_{f,CO_2}= - 393,5 kJ/mol). The SEI was converted into kJ/mol by means of the molar volume. This definition yields the chemical energy efficiency. For the sake of completeness, the enthalpy of formation of C_2H_n (n = 2, 4 of 6), and of other possible (oxygenated) compounds, should be accounted for in the numerator. However, due to the nearly negligible concentrations of these products, these terms could be neglected here.

Finally, the total energy cost (EC) was expressed as:

$$EC_{total}(eV/molec) = \frac{SEI\ (eV/molec)}{\chi_{total}} \quad \text{(A8)}$$

5 Determination of the product selectivities and carbon balance

The C-, H- and O-based selectivities of CO, the C_2-based hydrocarbons (C_2H_n ; n = 2, 4 or 6, expressed as C_2), H_2 and O_2, were calculated as follows:

$$S_{C,CO} = \frac{\alpha \cdot C_{CO(out)}}{(C_{CO_2(in)} - \alpha \cdot C_{CO_2(out)}) + (C_{CH_4(in)} - \alpha \cdot C_{CH_4(out)})} \quad \text{(A9)}$$

$$S_{C,C_2} = \frac{2 \cdot \alpha \cdot C_{C_2(out)}}{(C_{CO_2(in)} - \alpha \cdot C_{CO_2(out)}) + (C_{CH_4(in)} - \alpha \cdot C_{CH_4(out)})} \quad \text{(A10)}$$

$$S_{H,H_2} = \frac{\alpha \cdot C_{H_2(out)}}{2 \cdot (C_{CH_4(in)} - \alpha \cdot C_{CH_4(out)})} \quad \text{(A11)}$$

$$S_{O,O_2} = \frac{\alpha \cdot C_{O_2(out)}}{C_{CO_2(in)} - \alpha \cdot C_{CO_2(out)}} \quad \text{(A12)}$$

Finally, to determine the ratio of the total number of C atoms in the products vs. in the reactant, we calculated the carbon balance:

$$b_C = \frac{\alpha \cdot (C_{CO(out)} + C_{CO_2(out)} + C_{CH_4(out)} + 2 \cdot C_{C_2(out)})}{C_{CO_2(in)} + C_{CH_4(in)}} \quad \text{(A13)}$$

6 Extra information on the experimental results

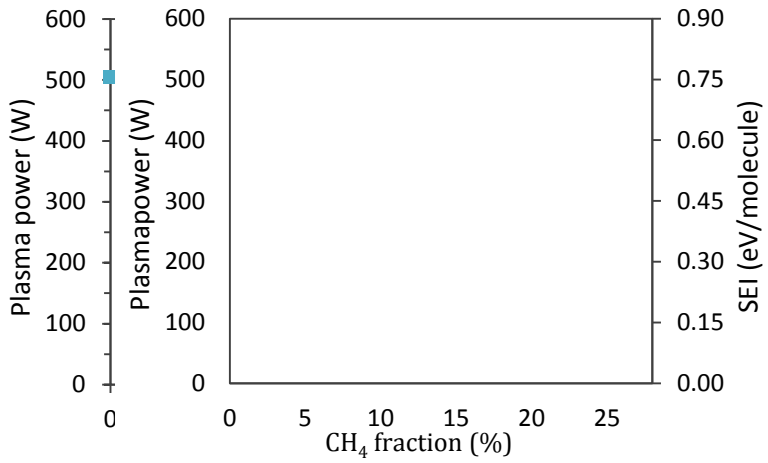

Figure A1 Plasma power (left axis) and specific energy input (SEI; right axis) as a function of the CH_4 fraction in the mixture, showing that they are more or less constant in the entire gas mixing ratio.

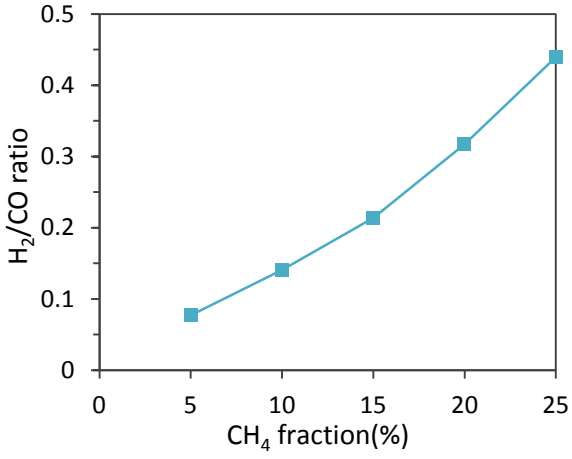

Figure A2 H_2/CO ratio as a function of the CH_4 fraction in the mixture, showing a slightly more than linear increase.

References

1 N. Pinhão, A. Moura, J. B. Branco, J. Neves, *Int. J. Hydrogen Energy*, 2016, **41**, 9245–9255.

CHAPTER 6

Multi-reforming

As already mentioned in Chapter 4 waste streams from industry are rarely pure CO_2 but often contain a series of other compounds. To enhance the industrial application of the GAP, it is important to understand the influence of these other compounds on the CO_2 conversion. In this chapter, we experimentally study the effect of N_2 on the DRM. More specifically, we investigate the effect of the applied current and gas flow rate in a mixture with 80 % of N_2 and 10 % of CO_2 and CH_4, respectively. The experimental setup and formulas used in this chapter are similar as in Chapter 5.

Similarly as with pure CO_2, a higher applied current leads to a higher absolute and effective conversion, due to an increasing SEI. A higher gas flow rate, on the other hand, leads to a lower absolute and effective conversion due to the shorter residence time. A higher SEI had a slightly negative effect on the energy efficiency for pure CO_2 (see Chapter 2). However, in this study we do not see a significant effect of the change in applied current and gas flow rate on the energy efficiency. Addition of N_2 has a positive effect on the absolute conversion of both CO_2 and CH_4 but a negative effect on the effective conversion and energy efficiency due to the dilution. However, due to the energy efficient vibrational excitation and dissociation of CO_2 in the GAP, the energy efficiency is still high.

1 Results and discussion

1.1 Effect of applied current and gas flow rate

The experiments were performed for the same GAP setup as shown in Chapter 2, at three different applied currents (0.20 – 0.25 – 0.30 A) and gas flow rates (10 – 15 – 20 L/min). The $CO_2/CH_4/N_2$ ratio was kept constant at 1/1/8. The pressure in the reactor is slightly higher than atmospheric pressure (1.25 bar). The cathode used in these experiments had a length and diameter of 10.20 and 17.50 mm, respectively. The length and diameter of the anode were 16.30 and 7.08 mm. Every experiment was performed three times. Subsequently, a propagation of uncertainty was applied to the results to calculate the error bars.

In Figure 1 we show the absolute conversion of CO_2 (a) and CH_4 (b) for the different values of applied current and gas flow rate. If we multiply the absolute conversion with the fraction of these compounds in the initial gas mixture, we obtain the effective conversion. This is shown in Figure 2 for CO_2 (a) and CH_4 (b). From Figure 1 and 2 it is clear that the CO_2 conversion is always lower than that of CH_4. This is logical since the dissociation energy of a C–H bond (4.48 eV) is lower than that of a C=O bond (5.52 eV).[1] This makes it easier to convert CH_4 compared to CO_2.

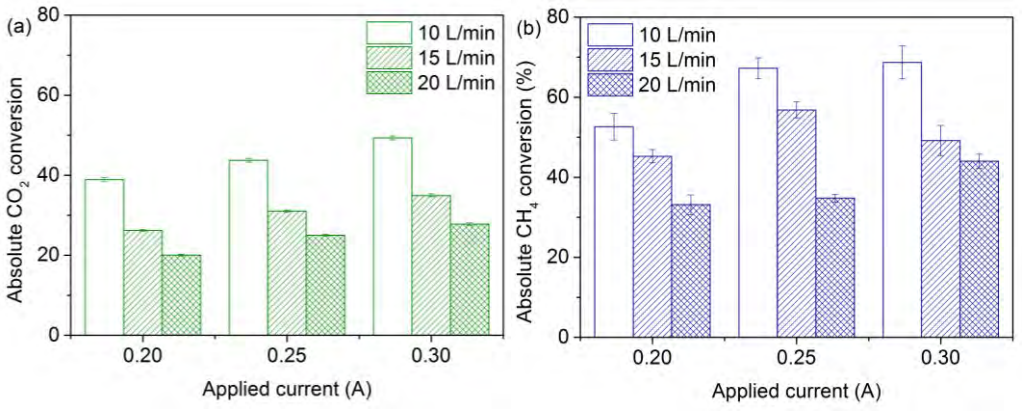

Figure 1 The absolute conversion of CO_2 (a) is always lower than that of CH_4 (b).

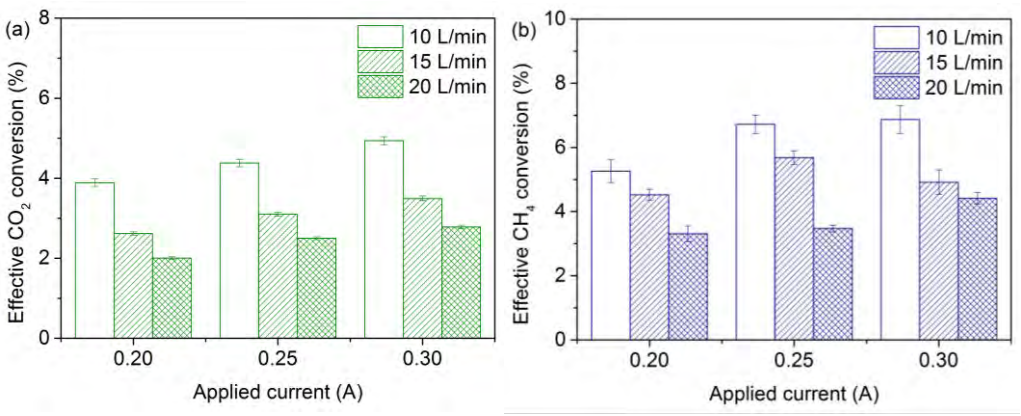

Figure 2 The effective conversion of CO_2 (a) and CH_4 (b) is obtained by multiplying its absolute conversion with its fraction in the initial gas mixture.

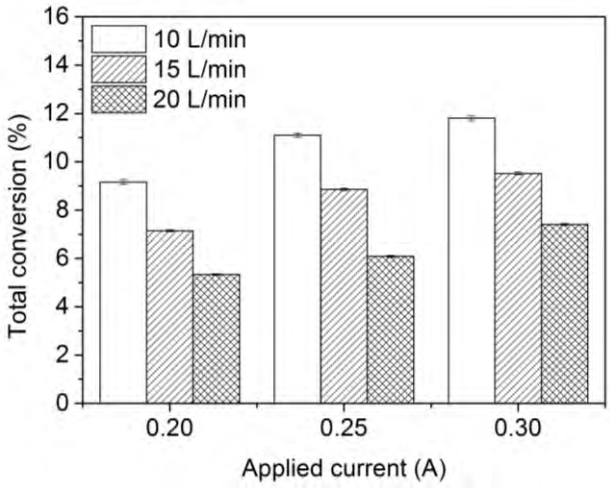

Figure 3 The total conversion is the sum of the effective conversion of CO_2 and CH_4. It decreases with increasing gas flow rate and increases when increasing the applied current.

The total conversion is shown in Figure 3 as a function of the applied current. This is the sum of the effective CO_2 and CH_4 conversion. The total conversion increases when increasing the applied current. This is the same trend as seen in the previous chapters. Increasing the applied current leads to an increase in power, which in turn leads to a higher SEI. The higher the SEI, the higher the conversion. The corresponding plasma power and SEI for the different conditions are shown in the

appendix (see Figure A1 and A2). Increasing the gas flow rate leads to a drop in conversion (see Figure 1, 2 and 3). This trend also coincides with the previous chapters. It can be explained by the fact that a higher gas flow rate leads to a lower residence time of the gas in the plasma and to a lower SEI.

The drop in conversion has an effect on the H_2/CO ratio, which is shown in Figure 4. There is a small increase of the H_2/CO ratio with increasing gas flow rate. We expect a lower H_2 formation, due to the lower CH_4 conversion, as well as a lower CO formation, due to both the lower CO_2 and CH_4 conversion. Because of this, the CO formation experiences a larger effect than the H_2 formation, causing a small increase in H_2/CO ratio upon increasing gas flow rate.

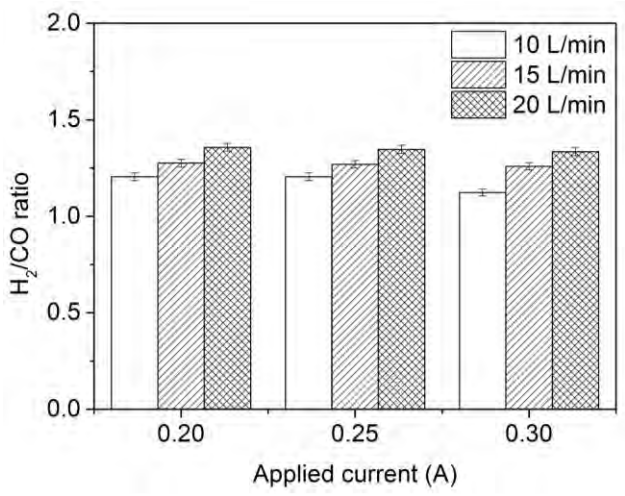

Figure 4 The H_2/CO ratio slightly increases with increasing gas flow rate, while there is no clear effect of the applied current.

Figure 5 shows the energy cost for CO_2 (a) and CH_4 (b) conversion as a function of the applied current. The energy cost for CO_2 conversion is always higher than that for CH_4 conversion, which can again be explained by the lower dissociation energy of the CH_4 bonds. Indeed, as is clear from the definition of the energy cost (see Equation (1)), a higher effective conversion leads to a lower energy cost.

$$EC_i(kJ/L) = \frac{SEI\ (kJ/L)}{X_{eff,i}} \qquad with\ i = CO_2\ or\ CH_4 \tag{1}$$

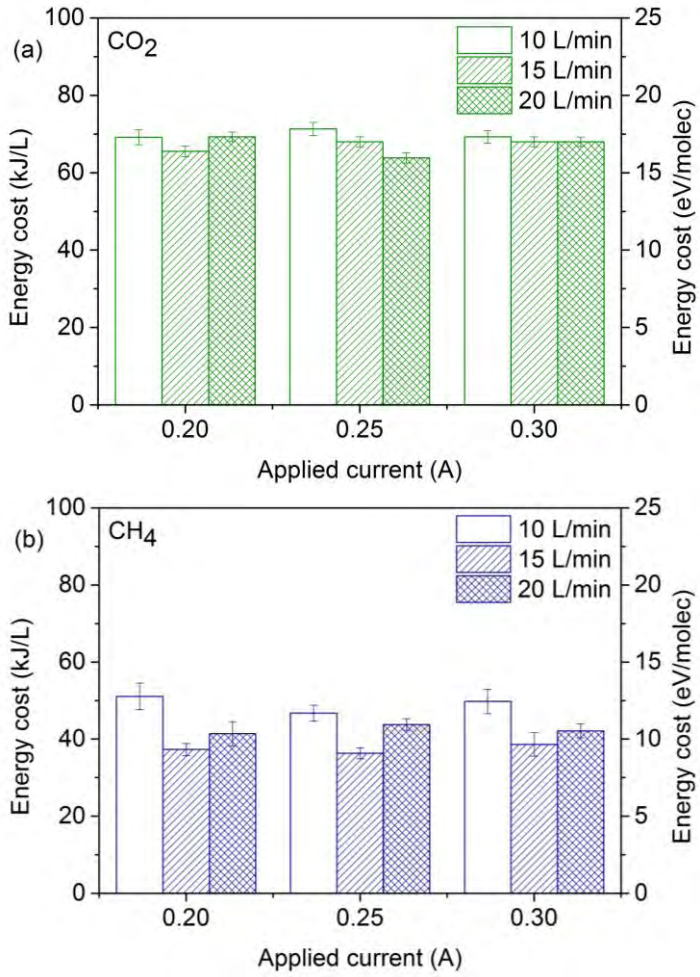

Figure 5 The energy cost for CO_2 (a) conversion is always higher than that for CH_4 (b) conversion. The energy cost is expressed in kJ/L (left axis) and eV/molec (right axis).

The total energy cost is again the sum of the energy cost for CO_2 conversion and that of CH_4 conversion, which is shown in Figure 6. Neither Figure 5 nor Figure 6 reveals a clear increasing or decreasing trend. The energy cost stays more or less constant when varying the applied current and gas flow rate. This is logical if we take a look at the following equation:

$$SEI = \frac{Plasma\ power\ (kW)}{Gas\ flow\ rate\ (L/min)} \times 60\ s/min \quad (2)$$

Both the plasma power (which depends on the applied current) and the gas flow rate determine the SEI. Equation (1) shows that the energy cost in turn depends on the SEI and the effective conversion. In summary, the energy cost is determined by three variables: the plasma power, the (total) effective conversion and the gas flow rate. This is summarized in Equation (3):

$$EC\ (kJ/L) = \frac{Plasma\ power\ (kW)}{Gas\ flow\ rate\ (L/min) \cdot X_{eff}} \times 60\ s/min \quad (3)$$

When increasing the applied current, the plasma power will also increase. This leads to a higher effective conversion, as already mentioned above. Depending on the relative increase in plasma power and conversion, the energy cost will slightly increase or decrease at the different conditions. The same reasoning can be made for an increase in gas flow rate, which causes a drop in effective conversion, so that the energy cost stays more or less the same.

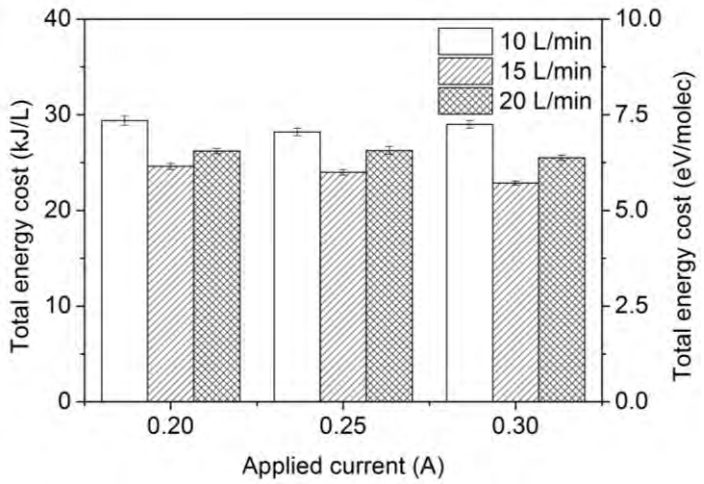

Figure 6 The total energy cost is the sum of the energy cost for CO_2 conversion and that of CH_4 conversion. It stays more or less constant when changing the applied current and gas flow rate.

The same trend as for the energy cost can be seen in Figure 7 for the energy efficiency. This is logical since the energy efficiency depends on the same three variables (see Equation (4)). Hence, it will also slightly rise or drop, depending on the relative rise/drop of the effective conversion, gas flow rate and applied power/current.

$$\eta = \frac{X_{eff} \cdot \Delta H_R(kJ/mol)}{SEI\ (kJ/mol)} \quad (4)$$

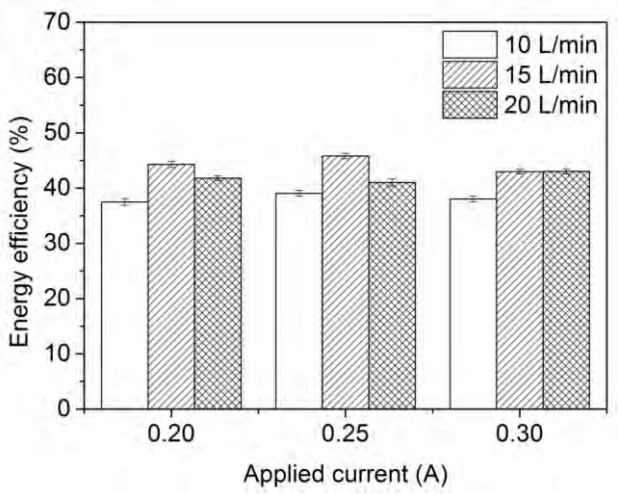

Figure 7. The energy efficiency stays more or less constant when changing the applied current and gas flow rate.

It can thus be concluded that the applied current and gas flow rate have no clear influence on the energy cost and energy efficiency. This is in contrast to the results obtained in Chapter 2, where a slight decrease was observed when increasing the applied current or decreasing the gas flow rate.

1.2 Effect of N_2 addition

We compare here the present results with those of the previous chapter, in order to find out the effect of N_2 addition on DRM; see Table 1.

Table 1 Comparison of the experimental results from this chapter (10/10/80 % $CO_2/CH_4/N_2$) with the results of the previous chapter (75/25 % CO_2/CH_4) to study the effect of N_2 addition on DRM.

	$CO_2/CH_4/N_2$	**CO_2/CH_4**
Absolute CO_2 conversion (%)	43.8 ± 0.5	23.8 ± 0.5
Absolute CH_4 conversion (%)	67 ± 3	41.73 ± 0.01
Effective CO_2 conversion (%)	4.38 ± 0.09	17.8 ± 0.4
Effective CH_4 conversion (%)	6.7 ± 0.3	10.5 ± 0.1
Total conversion (%)	11.1 ± 0.3	28.3 ± 0.4
Energy efficiency (%)	39.1 ± 0.5	66 ± 3
Energy cost CO_2 (eV/molec)	16.6 ± 0.4	4.1 ± 0.1
Energy cost CH_4 (eV/molec)	10.9 ± 0.5	7.1 ± 0.1
Total energy cost (eV/molec)	6.56 ± 0.09	2.61 ± 0.05
SEI (kJ/L)	3.14 ± 0.04	3.18 ± 0.04
Plasma power (W)	523 ± 5	531 ± 6
H_2/CO ratio	1.21 ± 0.02	0.439 ± 0.2

As seen in Table 1, the absolute conversion of both CO_2 and CH_4 is 20 - 25 % higher in the experiments with N_2 addition. Thus, N_2 has a positive effect on the absolute conversion. This trend was also seen for CO_2 splitting in a DBD reactor,[2] MW reactor,[3] as well as in Chapter 4 of this thesis. In each of these studies, the addition of N_2 had a positive effect on the absolute conversion of CO_2. The positive effect of N_2 on pure CH_4 conversion was also observed by Indarto et al. in a GA[4] and by Snoeckx et al in a DBD.[5] For pure CO_2 splitting, the positive effect of N_2 can be explained as follows: when adding N_2, these molecules get

vibrationally excited by electron impact. The energy can then be transferred to CO_2 through vibrational energy transfer, which causes the vibrational levels of CO_2 to be filled up more quickly.[3] This leads to the (more efficient) dissociation of CO_2. The fact that N_2 also has a positive effect on the absolute CO_2 conversion in DRM, suggests a similar mechanism as with pure CO_2 splitting. Vibrational excitation of N_2 as well as the electronically excited metastable states of N_2 also have a positive effect on the conversion of CH_4. This has been studied by Indarto et al. in a GA[4] and by Snoeckx et al. in a DBD[5] for pure CH_4 conversion. The exact mechanisms are however not yet known for DRM and should be further explored with theoretical modeling.

Both the effective and total conversion are lower in the presence of N_2. This was also the case for CO_2 splitting in a DBD and MW reactor;[2,3] and for the results in Chapter 4. This is indeed logical since the total fraction of CO_2 and CH_4 is lower upon addition of N_2. In the current experiments, the concentrations of CO_2 and CH_4 were each 10 %. This is the reason why the effective CH_4 and especially CO_2 conversion are lower than the effective conversions from Chapter 5, where the CO_2 and CH_4 concentrations were 75 % and 25 %, respectively.

Another difference can be noticed in the H_2/CO ratio. This is however not the result of the presence of N_2. In Chapter 5 a mixture with 25 % CH_4 was used, which of course causes less H_2 and more CO to be formed. In the experiments from this chapter, the CO_2 and CH_4 concentrations are equal, causing a H_2/CO ratio close to 1. To find out the possible influence of N_2 on the H_2/CO ratio, more research is needed, e.g., at the same CO_2 and CH_4 concentrations in the mixture with and without N_2. However, as mentioned in Chapter 5, we could not attain a stable plasma for CH_4 fractions above 25% in DRM without N_2 addition.

Since the energy efficiency and energy cost are dependent on the effective (total) conversion, these values logically are lower and higher,

respectively, compared to DRM without N_2 addition. A part of the energy input in the plasma will be used to excite, ionize and dissociate N_2 molecules. This energy cannot all be used for CO_2 and CH_4 conversion and this effect increases when adding more N_2.[2] A higher N_2 fraction has thus a negative effect on the energy efficiency. However, from the experiments within this chapter, we still obtain an energy efficiency of about 40 %, which is still high compared to the average energy efficiency in for example a DBD reactor (typically 2.6 – 12.8 %).[6]

2 Conclusions

To realize DRM on an industrial level, the conversion of CO_2 and CH_4 as well as the energy efficiency of the process has to be optimized in the presence of N_2, as N_2 is often present in industrial waste streams.

The influence of the applied current, gas flow rate and the addition of 80 % N_2 have been studied in this chapter. From these experiments, we can conclude that a higher applied current leads to a higher absolute and effective conversion. The influence of the applied current on the energy cost and energy efficiency is limited. An increase of the gas flow rate has a negative effect on the absolute and effective conversion, while the energy cost and energy efficiency experience little influence from a change in gas flow rate. N_2 has a positive effect on the absolute CO_2 and CH_4 conversion. However, a high fraction of N_2 has a negative effect on the effective (total) conversion. Consequently, this has a negative effect on the energy cost and energy efficiency. Nevertheless, the obtained energy cost and efficiency are still very reasonable, due to the specific properties of a GAP.

Before the GAP can be introduced on industrial level, there are many other aspects that should be investigated. An overview of these aspects is given in the next chapter: “The road to industry?”.

References

1 E. Cleiren, S. Heijkers, M. Ramakers and A. Bogaerts, *ChemSusChem*, 2017, **10**, 4025–4036.

2 R. Snoeckx, S. Heijkers, K. Van Wesenbeeck, S. Lenaerts and A. Bogaerts, *Energy Environ. Sci.*, 2016, **9**, 30–39.

3 S. Heijkers, R. Snoeckx, T. Kozák, T. Silva, T. Godfroid, N. Britun, R. Snyders and A. Bogaerts, *J. Phys. Chem. C*, 2015, **119**, 12815–12828.

4 A. Indarto, J. W. Choi, H. Lee and H. K. Song, *Energy*, 2006, **31**, 2986–2995.

5 R. Snoeckx, M. Setareh, R. Aerts, P. Simon, A. Maghari and A. Bogaerts, *Int. J. Hydrogen Energy*, 2013, **38**, 16098–16120.

6 R. Snoeckx and A. Bogaerts, *Chem. Soc. Rev.*, 2017, **46**, 5805–5863.

Appendix

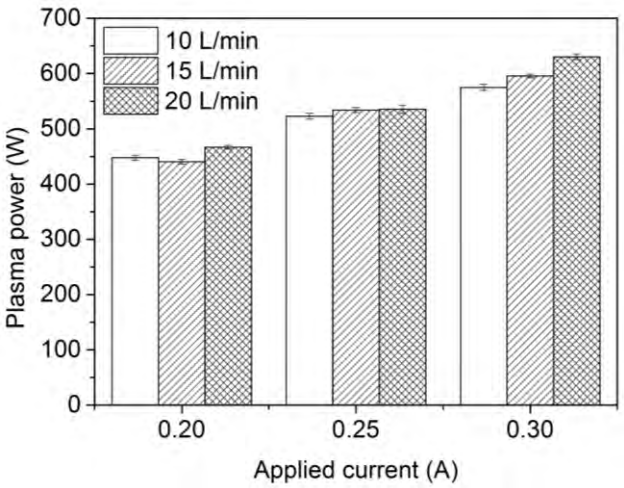

Figure A1 The plasma power increases when increasing the applied current but stays more or less constant when varying the gas flow rate.

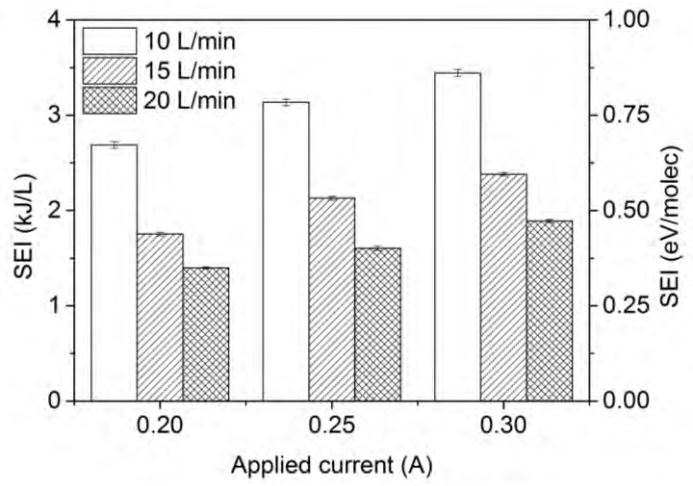

Figure A2 The specific energy input (SEI) increases when increasing the applied current while it decreases with increasing gas flow rate. The SEI is expressed in kJ/L (left axis) and eV/molec (right axis).

CHAPTER 7

The road to industry?

In this last chapter we evaluate the performance of the GAP for CO_2 conversion, based on a techno-economic analysis (TEA), using the results from the previous chapters. The TEA can predict the minimum selling price (MSP) of the products and how this MSP changes when different parameters are adjusted. It thus allows to estimate how competitive is the GAP compared to existing processes and how it could be improved. In this way, we obtain a quantitative analysis. Further in this chapter, we also suggest in a qualitative manner some other investigation routes for possible industrialization of the GAP.

1 Techno-economic analysis

The calculations within the techno-economic analysis (TEA) were performed by Dr. Hakan Olcay (Hasselt University), with input from our experiments for pure CO_2 splitting. Based on these calculations, we made the interpretations as explained below. First the methods will be explained step-by-step. Subsequently, we will discuss the results.

1.1 Methods

The objective of the TEA is to estimate the minimum selling price (MSP) of the products formed by pure CO_2 splitting, and to analyze the sensitivity of the key parameters, in order to propose further improvements in the development of this GAP. The MSP is the minimum price at which the product should be sold to recover the costs made to build and maintain the production plant (hence here the GAP plant, which includes the reactors and gas separation section; see below). The tools used are Aspen Plus (a) and Aspen Process Economic Analyzer (APEA) (b). The followed approach can be divided into eight steps:

(1) Determine the plant capacity, maximum reactor size and number of reactors needed.

(2) Model[(a)] the process units based on experimental data.

(3) Simulate[(a)] steady-state operation of the units to evaluate material and energy flows, and associated costs.

(4) Choose construction material for each process unit[(b)].

(5) Determine size and cost of each process unit[(b)].

(6) Estimate costs from available cost data by scaling.

(7) Determine economic parameters.

(8) Estimate minimum selling prices (MSPs), using a discounted cash flow rate of return (DCFROR) model.

1.2 Results and discussion

The TEA starts with determining the plant capacity. This is set at 20,000 ton CO/year, in analogy to a study performed by Van Rooij et al. for a MW discharge.[1] Our GAP reactor is small-scale, but the same design has also been built at somewhat larger scale by the company Advanced Plasma Solutions (APS), where we ordered our GAP reactor as well. The size of our lab-scale GAP and the largest GAP that is currently available are presented in Figure 1.

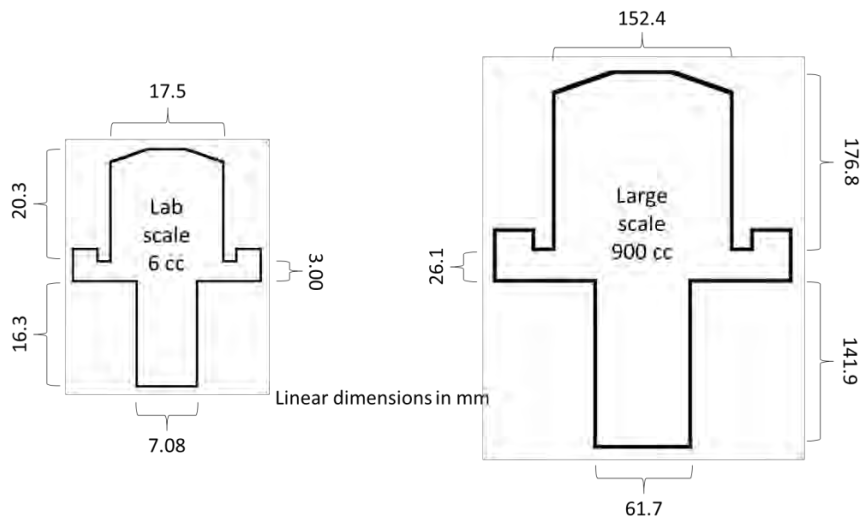

Figure 1 Size of our lab-scale GAP and the largest scale GAP that is currently available.

The model uses our lab-scale data (see section 1 of the appendix) and calculates the mass and energy balances for a steady-state plant operation. It assumes the same conversion (i.e., 8.6 % for pure CO_2 splitting) as obtained in our experiments, due to the lack of experimental data in a large-scale GAP. However, this approximation is standard in such TEA studies, and we assume the value will indeed be very similar. Using this conversion of 8.6 % and plant capacity of 20,000 ton CO/year (see above), the number of (large-scale) reactors needed to reach this capacity is calculated to be 256. To obtain this

value, first the amount of CO produced by one large-scale reactor is calculated based on the conversion of 8.6 % (~ 78 ton/year). Subsequently, the number of reactors needed is simply obtained by dividing the plant capacity by the amount of CO produced by a single large-scale reactor (see appendix for the detailed calculation). We consider here the large-scale GAP reactors, as they can treat a larger volume (i.e., about 1400 L/min instead of 10 L/min for the lab-scale GAP).

The second step in the TEA is to model the process units with Aspen Plus. The GAP plant can be divided into two sections: a reactor section and a gas separation section. A schematic representation of such a GAP plant is showed in Figure 2. The reactor section is straightforward and consists of 256 reactors placed in parallel. These parallel units share the same installation (i.e., electrical, piping, etc.), so the total installation costs are less than the costs for installing them individually.[2] In these reactors, CO_2 is converted into CO and O_2. We did not observe any carbon deposition in our experiments.

The separation of the unconverted CO_2 from the product stream relies on an existing commercial process, i.e., the Benfield process.[3] The treated gas stream (including products and unconverted CO_2) goes to the CO_2 absorber where it enters up-flow. This absorber is a packed bed of Pall rings, which create an interfacial mass transfer area between the gas and liquid phase. The absorbent liquid consists of K_2CO_3 in water at a pH > 7 and enters the absorber in down-flow. In this manner, the acidic CO_2 gas dissolves completely into the liquid phase by chemically enhanced mass transfer:

$$K_2CO_3 + CO_2 + H_2O \rightarrow 2HCO_3^- + 2K^+$$

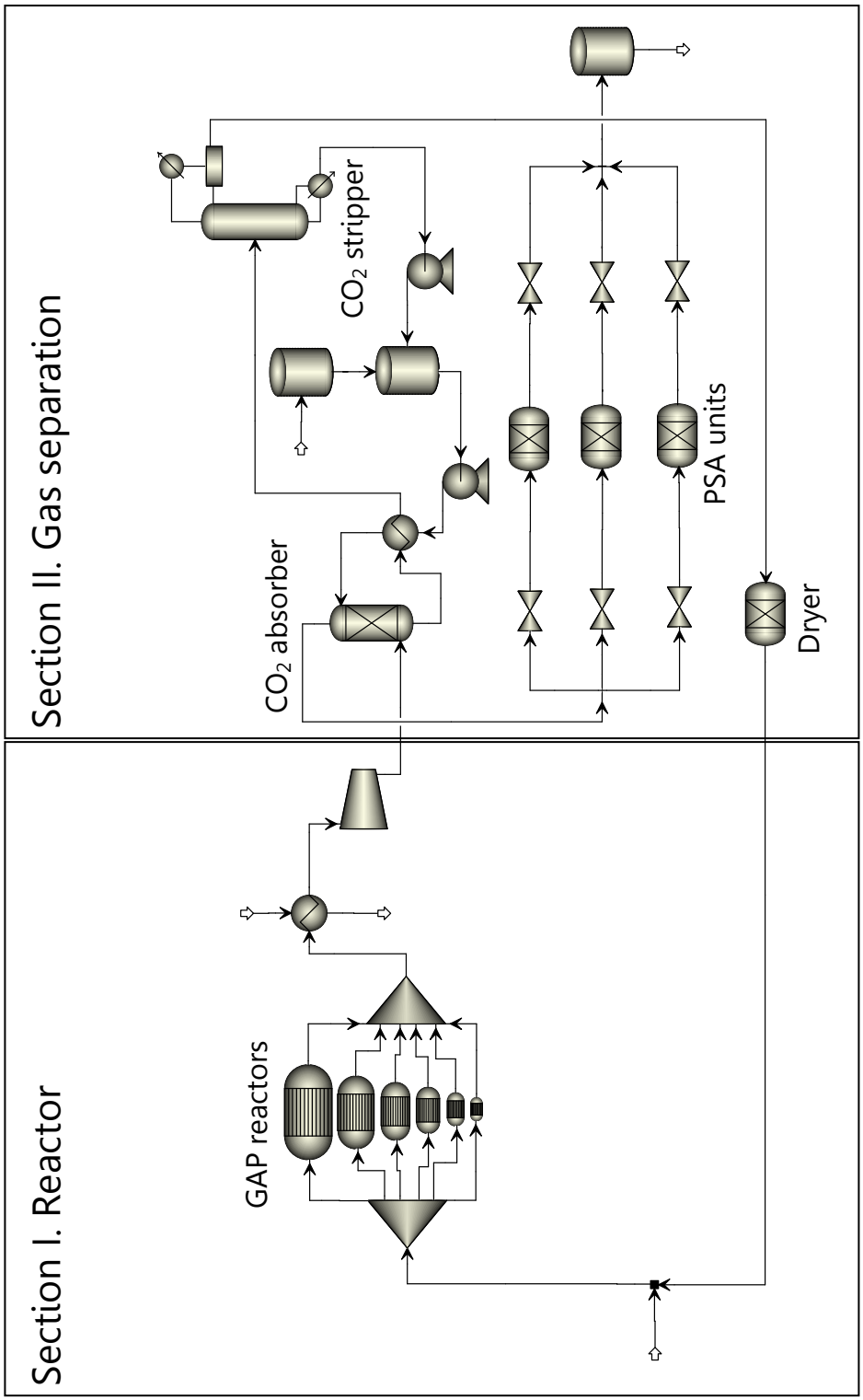

Figure 2 Schematic representation of a GAP plant.

The unconverted CO_2 is now separated from CO and O_2, which is sent to the pressure swing adsorption (PSA) units. One unit adsorbs CO, yielding an O_2 stream that is sent to flare. At the same moment, a second unit is regenerated by desorbing the adsorbed CO, yielding a pure CO stream that can either be stored or used directly. The third unit is on standby in case one of the other units malfunctions.

The liquid flow with unconverted CO_2 from the CO_2 absorber enters the CO_2 stripper in down-flow. A low pressure (LP) steam reboiler is installed at the bottom of the CO_2 stripper. The produced steam flows up and comes in contact with the down-flowing liquid absorbent flow rich in CO_2. Similar to the CO_2 absorber, the CO_2 stripper also contains a packed bed of Pall rings to enlarge the liquid/gas interfacial area. The up-flowing steam effectively strips the CO_2 out of the liquid phase during the interfacial contact on the packed bed elements. At the top of the CO_2 stripper, a wet recycle CO_2 flow leaves to a condenser to remove as much water as possible. The condensed water flow is lead back to the CO_2 stripper. The semi-dry recycled CO_2 flow is passing through a dryer, whereafter it can be recycled again as input in the process.

The simulation for the reactor section is carried out in Aspen Plus, to obtain the steady-state operation of the units and to evaluate material and energy flows. This data is then transferred to Aspen Process Economic Analyzer (APEA). The plant capacity determines the number of units beforehand. With this data as input and by specifying the construction materials, the APEA software calculates the individual capital expenditures (CAPEX) for the reactor section, which includes the GAP reactors, a heat exchanger and a compressor. The cost for the gas separation section (including PSA units) is not simulated in Aspen but is estimated by scaling the available data from the MW plant of reference 1. The formulas used for scaling can be found in the appendix. The capital costs of the plant (both the reactor and gas separation section) are listed in Table 1. The capital costs for each individual unit

can be found in Table A2 in the appendix. Both the costs in k$ and the percentage (%) of the total cost are presented.

Table 1 Capital costs in k$ and percentage (%) of the total cost.

CAPEX (rounded values)		
	k$	%
GAP reactors	15,336	69
Pumps, compressors	2,370	11
Packing materials	2,047	9
Heat exchangers	1,303	6
Process vessels	1,099	5
Columns	173	1
TOTAL	**22,328**	**100**

The total capital cost for a 20,000 ton/year CO plant is about 22 M$ - with 18 M$ for the reactor section and 4 M$ for the separation section. This is similar to the total capital cost required for a CO-plant based on conventional technology and feedstock.[1] The total CAPEX for a MW plasma reactor plant was estimated by Van Rooij et al. to be 30 M$, with the largest part (23 M$) for the plasma generators.[1] Compared to that study, the CAPEX of the GAP is lower, because there is no need for expensive microwave tubes. The largest part of the capital costs for the GAP plant (i.e., almost 70 %) originates from the 256 GAP reactors. This cost includes the cost of the material for the reactors as well as the power supply, which encompasses the biggest part of the cost (94 %). Pumps and compressors, which enable all flows in the plant, contribute for 11 % of the capital costs. Packing materials, which create the interfacial mass transfer area between the liquid and gas phase in the CO_2 absorber and CO_2 stripper, have a similar cost (contribution of 9 %). Heat exchangers (used after the GAP reactors and in the CO_2 absorption

and CO_2 stripper unit), process vessels (i.e., other than the GAP reactors) and columns (used in the CO_2 absorber and CO_2 stripper) each contribute for a smaller fraction of the costs.

The operating expenditures (OPEX) are calculated based on assumed feedstock/input/utility prices and the material/energy balances from Aspen Plus. These are listed in Table 2 as the sum of both the reactor and gas separation section. The operating costs for each individual unit can be found in Table A3 in the appendix.

Table 2 Operating costs in k$/year and percentage (%) of the total cost.

OPEX (rounded values)		
	k$/year	%
Electricity	10,262	76
LP steam	1,521	11
Cooling water	635	5
CO_2	629	5
K_2CO_3	307	2
Others	112	1
TOTAL	**13,466**	**100**

The total operating cost is about 13 M$ - with 11 M$ for the reactor section and 2 M$ for the separation section. This is similar to the operating costs of a MW plasma reactor plant (14 M$).[1] It is clear from Table 2 that electricity represents the largest fraction (i.e., 76 %) of the total operating cost. This is mainly the electricity to power the GAP reactors. Indeed, the PSA units only use 3.5% of the total electricity costs. Note that the efficiency of the GAP power supply is not taken into account here. The latter was measured to be 80%, so taking this into account will increase the electricity cost to some extent. However, efforts should be made to develop more efficient power supplies, so that the

applied power can all be introduced in the plasma, but this is outside the scope of plasma research.

Within this calculation, the electricity price is set to 50 $/MWh, which is the current industrial rate.[1] It is expected that the cost for electricity will go down significantly[1] and therefore the effect of the electricity price is included in the sensitivity analysis below. Low pressure (LP) steam, which is used to regenerate CO_2 in the CO_2 stripper, contributes for 11 % of the operating costs. Cooling water used for cooling down the process streams and the costs for CO_2 as input gas each contribute for 5 %. The cost for K_2CO_3 (i.e., the CO_2 absorbent used in the CO_2 absorber) and other costs (i.e., maintenance costs, such as regeneration of zeolite (used in the PSA units) and silica gel (used in the dryer)) contribute for a small fraction of the costs.

The manufacturing costs (i.e., the sum of CAPEX and OPEX) for the reactor section and the separation section are about 29 M$ and 7 M$, respectively. The total manufacturing cost is about 36 M$. From the manufacturing cost and the fixed capital investment (FCI; see details in section 5 of the appendix), the minimum selling price (MSP) of CO can be estimated using a discounted cash flow rate of return (DCFROR) model.[2] This is a way to amortize the total cost over the lifetime of the plant. A plant lifetime of 20 years has been taken, as this is what most TEA studies would consider as plant lifetime. The heuristics and economic parameters used in this DCFROR model can be found in section 5 of the appendix. The MSP of CO is estimated in this way to be 1102 $/ton.

It is very interesting to know the effect of various possible price reductions and process improvements on the MSP of CO. Therefore, the MSP of CO for different scenarios is presented in Figure 3. To judge the economic viability of the process, a market price for bulk and specialty CO, taken from reference 1, is also indicated in Figure 3. The specialty price (3150 $/ton) is based on various price offers for 40 - 100 L gas

cylinders. The bulk price had to be estimated, since there is no bulk market for CO regarding the safety issues. Bulk CO is only produced to be immediately converted into less hazardous and more valuable products. Mostly, CO is synthesized from methane and converted into methanol, which means that the price of CO has to be within the price bracket of methane and methanol. From their market prices, a bulk CO price of 228 $/ton can be estimated.

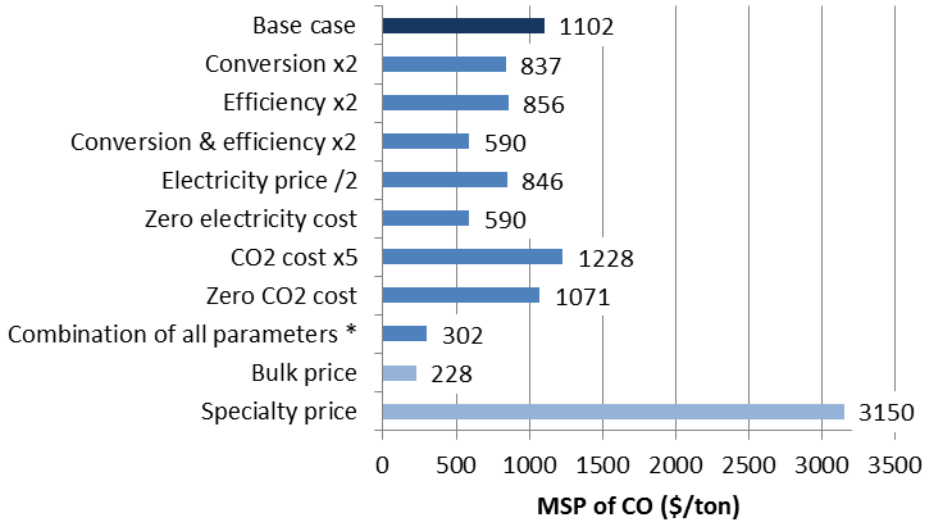

Figure 3 Sensitivity analysis for the main cost factors in the minimum selling price of CO produced by the GAP. An estimate of the present CO bulk and specialty price is shown as a reference. * Combination of a zero electricity cost with zero CO_2 cost, in addition to a rise in CO_2 conversion and energy efficiency by a factor two.

As mentioned above, the MSP of CO for the base case is 1102 $/ton. This is slightly lower than the MSP of CO estimated for the base case of the MW plasma reactor plant (i.e., 1228 $/ton) described by Van Rooij et al.[1] This can be explained by the fact that the CAPEX are also slightly lower for the GAP plant than for the MW plasma reactor plant (see above). However, the difference is not very substantial.

If we could double the conversion from 8.6 % to 17.2 % in the GAP, keeping the same energy efficiency, the MSP of CO would decrease to 837 $/ton. Likewise, if we could double the energy efficiency of the

plasma conversion process (keeping the conversion constant), the MSP of CO would decrease to 856 $/ton. Increasing the conversion thus has a similar but slightly larger effect on the MSP of CO compared to increasing the energy efficiency. On one hand, the conversion is strongly linked to both the separation costs and capital costs. Indeed, when a higher conversion is reached, the separation costs can be reduced. Likewise, a higher conversion also requires less GAP reactors to produce the same amount of product, thus reducing the capital costs. On the other hand, the energy efficiency is strongly linked to the electricity consumption and it was already mentioned above that the electricity is a large part of the operating costs, which will thus be reduced when the energy efficiency can be increased.

However, if the conversion could be increased by a factor two, for the same SEI (e.g., by smart reactor design), the energy efficiency would increase accordingly by a factor two. This would yield a MSP of CO of 590 $/ton. Therefore, to make the GAP-based CO_2 conversion into CO economically viable, it will be necessary to enhance the CO_2 conversion at constant SEI, so that the energy efficiency rises accordingly.

Besides the process parameters, we also study the effect of external parameters, such as the CO_2 and electricity price. If the electricity price would halve, the MSP of CO would decrease to 846 $/ton. When we assume that the electricity price is equal to zero (for example in case when the company produces its own electricity with renewable energy sources), the MSP of CO would go down even further to 590 $/ton. In the base case the CO_2 price was set to 20 $/ton. This price is based on different external economic and tax factors.[1] If this price would rise by a factor 5 (i.e., the CO_2 price is equal to 100 $/ton), the MSP of CO would rise up to 1228 $/ton. In contrast, if we could directly use pure CO_2 from effluent gases, we could assume a zero cost and this gives a MSP of CO of 1071 $/ton. It is thus clear that the CO_2 cost is not a major factor in the MSP of CO.

Finally, if we would be able to combine a zero electricity cost with zero CO_2 cost, in addition to a rise in CO_2 conversion and energy efficiency by a factor two, this would yield a MSP of CO of 302 $/ton. Hence, this would be only 74 $/ton more than the bulk CO price. However, we have to note that this scenario might not be very realistic.

1.3 Conclusions

To produce 20,000 ton CO/year in a GAP plant with a current conversion of 8.6 %, 256 GAP reactors need to be placed in parallel. The manufacturing costs (i.e., the sum of CAPEX and OPEX) for the reactor section and the separation section are about 29 M$ and 7 M$, respectively. The total manufacturing cost is about 36 M$. Based upon the calculated costs, we obtain a MSP for CO of 1102 $/ton. Compared to the bulk CO price (228 $/ton), we have to conclude that a GAP reactor for CO_2 conversion into CO with the current electricity price is not yet competitive. From the sensitivity analysis it is clear that both the conversion and efficiency of the process have to be improved. A zero electricity cost would also make the GAP more competitive for CO production. The base case CO MSP is about three times less than the specialty CO price (3150 $/ton). However, the risks of product handling, storage and transport should still be taken into account.

If we could combine a zero electricity cost with zero CO_2 cost, in addition to a rise in CO_2 conversion and energy efficiency by a factor two, this would yield a MSP of CO of 302 $/ton, which is only slightly higher than the bulk CO price, hence making the GAP for CO_2 conversion almost competitive with traditional CO production processes. In addition, some optimization in the separation process can decrease the manufacturing costs. Indeed, instead of pure CO_2 splitting, other compounds (such as CH_4) can be added in order to produce easily separable end products, such as methanol or a pure CO/H_2 mixture, which can also improve the economic viability of the GAP reactor.

2 Investigation routes for industrialization

In this thesis we first studied the splitting of CO_2 as a benchmark (Chapter 2). We also investigated the influence of the reactor design (forward vs. reverse vortex flow). Subsequently, we visualized the arc dynamics through imaging with a high-speed camera, and we linked these results to the CO_2 conversion (Chapter 3). In Chapter 4, we studied the influence of N_2 on the CO_2 conversion, and we evaluated the combined CO_2 conversion and N_2 fixation. For the formation of value-added chemicals, such as hydrocarbons and oxygenates, or even syngas, a hydrogen-source must be added to the CO_2 plasma. This can be CH_4, which is also a major greenhouse gas. Therefore, we investigated the combined CO_2 + CH_4 conversion (or dry reforming of methane; DRM) in the GAP (Chapter 5) and additionally also the influence of N_2 on this reaction (Chapter 6). Although the results from these studies are quite promising, before the GAP can be introduced at industrial level, a number of aspects should be further investigated.

We studied the influence of N_2 on CO_2 splitting and DRM, but in industry, waste streams often contain much more components. For example, H_2O is a common component in waste streams of industrial processes. The effect of H_2O on CO_2 conversion was already studied in a GA discharge at atmospheric pressure,[4,5] and it was reported to have a rather unwanted effect, since H_2O quenches the CO_2 vibrational levels and the formation of OH from H_2O can cause a back reaction with CO to form CO_2 again.[4–8] However, in a MW plasma at reduced pressure (30 - 60 Torr), the addition of H_2O yielded better CO_2 conversion.[9] Introducing H_2O ensures a cooling effect which could explain the better conversion in that case. Moreover, quenching of the CO_2 vibrational levels by H_2O molecules might be less effective at reduced pressure. Another component of interest could be O_2, to realize a combination of DRM and POX (partial oxidation of methane), i.e., a multi-reforming process. Liu et al.[10] have shown that the addition of O_2 has a positive effect on the CO_2 and CH_4 conversion and on the energy cost in a GA.

For a $CH_4/CO_2/O_2$ mixture with ratio 3/2/1.8 they obtained a CH_4 and CO_2 conversion of 77 % and 27 % at an energy cost of 32 kJ/mol. When they used air instead of pure O_2, a slight drop in conversion and a higher energy cost were obtained, due to the dilution. The addition of both N_2 and O_2, in different ratios, is clearly an interesting topic for further research. Finally, the influence of other gases (i.e., higher hydrocarbons, NOx, SO_2, etc.) that might be present in effluent streams can also provide useful information.

Furthermore, the experiments in this thesis and the modeling work of PhD students within PLASMANT (Georgi Trenchev and Stijn Heijkers) revealed that currently the GAP still has some limitations. Three main features should still be improved.[7] The first is the gas conversion. Although the 3D design of the GAP is already an improvement over a classical GA, the fraction of gas that passes through the active arc plasma is still limited, which limits the overall gas conversion. For this purpose, the reactor design should be modified, to increase the fraction of gas passing through the arc. Another option that can be studied to increase the conversion is lowering the pressure. We have seen before that a lower pressure typically gives a higher conversion. However, the lower throughput and the efficiency of the pumping installation should be taken into account. It might be though that a small reduction of the pressure could already give a large increase in conversion. This has to be investigated further, as well as the stability of the plasma at lower pressure. A second feature is the energy efficiency. This is already quite high in the GAP but we believe there is still room for improvement. In the current GAP reactor, the gas temperature is rather high, which stimulates vibration-translation (VT) relaxation. More specifically, there is not enough overpopulation of the high vibrational levels to obtain the most energy-efficient gas conversion. The key is thus to reduce the gas temperature, but maintaining a high power density, so that the non-equilibrium character of the GAP can be exploited, with a higher vibrational temperature than gas temperature. The third and last feature

is the selectivity of the plasma process. A plasma is typically very reactive as many reactive species are created, but therefore it is not selective. Catalysts can be used to selectively create products. In theory, the combination of plasma and catalysis will offer the best of both worlds. The plasma activates inert molecules under mild conditions, while the activated species can selectively recombine at the catalyst surface to yield the desired products. This is especially important for the direct formation of liquids from CO_2. The most convenient way for introducing a catalyst in the GAP setup is by placing it at the reactor outlet, either in a packed bed or fluidized bed configuration. In this way it is possible to make use of the hot gas with the presence of reactive plasma species leaving the reactor, depending on the distance from the outlet. Since the plasma already activates the gas, the preferred catalysts are not necessarily the same as in classical catalysis processes. Therefore, tailored design of suitable catalysts is needed. On the other hand, when the catalysts are placed downstream of the GAP reactor, thermal catalysts might also perform well, being thermally activated by the hot gas leaving the reactor (heat recovery).

Besides these three major features, also stability tests should be carried out to see how the reactor performs after a long running time. Even at shorter running times it is recommended to further investigate the plasma stability. From our experiments it is clear that not in every gas mixture and for every reactor dimensions a stable plasma can be created, depending on the power supply. It is thus necessary to match the power supply with the exact reactor geometry and the desirable gas mixture. We especially faced difficulties when adding CH_4 to the CO_2 gas. In the current setup, we were limited to a maximum CH_4 fraction of 25 %, because the plasma became unstable for larger fractions (see Chapter 5). Linked to these necessary stability tests, we should also evaluate when is the best time to replace the electrodes, since they erode where the plasma is attached. In order to avoid or reduce erosion, other materials could be employed as electrode material. However, it is

important to take into account the cost of the material itself, the number of replacements necessary and the material's influence on the process, to evaluate what is the best choice.

In all these aspects, modeling can be of great help to develop a better design and process. However, to verify whether the model predictions are realistic, experiments must be performed, since they are essential for industrialization. Sometimes a process might work in theory but not in practice. Therefore, cooperation between modeling and experiments is the best manner to find the way to industry.

References

1 G. J. van Rooij, H. N. Akse, W. A. Bongers and M. C. M. van de Sanden, *Plasma Phys. Control. Fusion*, 2018, **60**, 014019.

2 H. Olcay, R. Malina, A. A. Upadhye, J. I. Hileman, G. W. Huber and S. R. H. Barrett, *Energy Environ. Sci.*, 2018, **11**, 2085–2101.

3 *Benfield Process*, https://uop.com/?document=benfield-process-datasheet&download=1.

4 A. Indarto, J.-W. Choi, H. Lee and H. K. Song, *Environ. Eng. Sci.*, 2006, **23**, 1033–1043.

5 T. Nunnally, K. Gutsol, A. Rabinovich, A. Fridman, A. Gutsol and A. Kemoun, *J. Phys. D. Appl. Phys.*, 2011, **44**, 274009.

6 A. Fridman, *Plasma Chemistry*, Cambridge University Press, New York, 2008.

7 A. Bogaerts and E. C. Neyts, *ACS Energy Lett.*, 2018, **3**, 1013–1027.

8 R. Snoeckx, A. Ozkan, F. Reniers and A. Bogaerts, *ChemSusChem*, 2017, **10**, 409–424.

9 G. Chen, N. Britun, T. Godfroid, V. Georgieva, R. Snyders and M.-P. Delplancke-Ogletree, *J. Phys. D. Appl. Phys.*, 2017, **50**, 084001.

10 J. L. Liu, H. W. Park, W. J. Chung, W. S. Ahn and D. W. Park, *Chem. Eng. J.*, 2016, **285**, 243–251.

Appendix

1 Mass - energy balance and operating conditions of single lab-scale GA reactor

Table A1 Mass – energy balance and operating conditions of a single lab-scale GA reactor. Based on these experimental parameters, a 20,000 ton CO/year plant is calculated.

Input 1	Name Quantity (mol)	CO_2 0.446
Input 2	Name Quantity (kWh)	Electricity $1 \cdot 10^{-2}$
Product 1	Name Quantity (mol)	CO 0.0384
Product 2	Name Quantity (mol)	O_2 0.0192
Temperature	20 °C	
Pressure	1 atm	

2 Calculation of the number of reactors needed

The amount of CO_2 introduced in the lab-scale reactor is 0.446 mol/min, based on a CO_2 flow rate of 10 L/min and a molar volume of 22.4 L/mol. Consequently, the amount of CO produced, based on a conversion of 8.6 %, is 0.038 mol/min. This lab-scale reactor has a volume of 6.2 cc, while the large-scale reactor has a volume of 900 cc (see Figure 1). We can rescale the amount of CO produced from the lab-scale reactor to the large-scale reactor according to the following equation:

$$CO_{large-scale}\ (mol/min) = V_{large-scale}\ (cc) \times \frac{CO_{lab-scale}\ (mol/min)}{V_{lab-scale}\ (cc)}$$

$$= 900\ cc\ \times \frac{0.038\ mol/min}{6.2\ cc} =\ 5.5\ mol/min$$

Converting this amount of CO produced of 5.5 mol/min to an amount in ton/year (assuming 350 days of operation), we obtain 78 ton CO/year. Dividing the plant capacity (20,000 ton/year) by the amount of CO produced by a single large-scale reactor (78 ton/year) results in the number of reactors needed, which is 256.

3 Scaling formulas

The total cost of the reactor section is scaled with a train cost factor of 0.9:

$$Cost_{Total} = Cost_{Reactor} \times \left(Number\ of\ reactors\right)^{0.9} \quad \text{(A1)}$$

The equipment cost for the separation section is scaled with the six-tenth rule based on the MW study of Van Rooij et al.:[1]

$$Cost\ of\ equipment_{GA} = \left(Cost\ of\ equipment_{MW}\right) \times \left(\frac{Characteristic\ component\ flow_{GA}}{Characteristic\ component\ flow_{MW}}\right)^{0.6} \quad \text{(A2)}$$

The characteristic component is either CO or unreacted CO_2. The costs of packing material in the separation section (pall rings, silica gel, and zeolite) are scaled linearly.

4 Individual CAPEX and OPEX per section

Table A2 Capital costs in k$ and percentage (%) of the total cost per section.

CAPEX (rounded values)		
Reactor section		
	k$	%
GAP reactors	15,336	86
Heat exchanger	75	1
Compressor	2,350	13
TOTAL	**17,761**	**100**
Separation section		
	k$	%
CO_2 absorber	65	1.4
Pall ring loading	65	1.4
CO_2 stripper	109	2.4
Pall ring loading	19	0.4
CO_2 stripper condenser	832	18.2
CO_2 stripper condenser vessel	203	4.4
CO_2 stripper steam reboiler	133	2.9
Drying bed	61	1.3
Silica gel loading	1,478	32.3
PSA unit	24	0.5
Zeolite loading	486	10.6
Lean absorbent pump 1	10	0.2
Lean absorbent pump 2	10	0.2
Heat exchanger	265	5.8
Surge tank	91	2.0
K_2CO_3 make up vessel	40	0.9
CO storage tank	680	14.9
TOTAL	**4,571**	**100**

Table A3 Operating costs in k$/year and percentage (%) of the total cost per section.

OPEX (rounded values)		
Reactor section		
	k$/year	%
CO_2	629	6
Cooling water	99	1
Electricity	10,229	93
TOTAL	**10,957**	**100**
Separation section		
	k$/year	%
K_2CO_3	307	12
Cooling water	537	21
Electricity	33	1
LP steam	1,521	61
Others	112	5
TOTAL	**2,510**	**100**

5 Heuristics and economic parameters DCFROR model

Category	Parameter		Remarks
Total capital investment	Inside batterly limits (ISBL)	(1)	Installed equipment cost from APEA + initial catalyst cost
	Outside batter limits (OSBL)	(2)	30 % of (1)
	Direct costs	(3)	(1) + (2)
	Engineering and supervision	(4)	13 % of (3)
	Construction and fees	(5)	23 % of (3)
	Contigengency	(6)	20 % of (3) + (4) + (5)
	Indirect costs	(7)	(4) + (5) + (6)
	Fixed capital investment (FCI)	(8)	(3) + (7)
	Working capital	(9)	15 % of (8)
Operating cost	Direct operating cost	(10)	3 % of (8)
	Variable operating cost	(11)	Feedstock, material and utility costs + catalyst refurbishing cost
Discounted cash flow	Financing		100 % equity
	Depreciation method		Variable declining balance (VDB)
	Depreciation period		7 years
	Construction period		3 years
	% FCI in Year -3		8%
	% FCI in Year -2		60%
	% FCI in Year -1		32%
	Discount rate		10%
	Income tax rate		35%
	Plant lifetime		20 years
	Plant availability		350 days
	Cost year		2016
	Inflation per annum		2%

Figure A1 Heuristics and economic parameters used in the DCFROR model.

6 Plasma stability

As explained in section 2 of Chapter 7, the plasma stability depends on the reactor geometry (more specifically the cathode length and anode diameter) and the gas mixture composition. The plasma is stable when a bright rotating arc is observed and the plasma does not extinguish by itself. An overview of the minimum running time of the plasma in the different experiments is given in Table A4. The time given in the table is the time necessary for the gas analysis and it does not necessarily mean that the plasma is not stable for a longer time.

Table A4 Overview of the minimum running time of the plasma in the different experiments. The first column refers to the chapters where these gas mixtures were used.

Ch.	**Gas mixture**	**Cathode length (mm)**	**Anode diameter (mm)**	**Running time (min)**
2	CO_2	20.30	7.08, 14.20, 17.50	30
4	CO_2 – N_2	10.20	7.08	30
5	CO_2 – CH_4	10.20	7.08	30
6	CO_2 – CH_4 – N_2	10.20	7.08	15

Summary

The problems that arise from climate change can no longer be ignored by our society. They are gaining more and more attention in the media and various researchers are investigating techniques to limit climate change. The latter is caused by the increasing concentration of CO_2 in our atmosphere. It is therefore necessary to limit the emission of CO_2 as much as possible. A technology that is extensively investigated for the conversion of CO_2 into useful chemicals and fuels is plasma technology.

An introduction on plasmas is given in Chapter 1. Also, the question why plasma-based conversion might be an interesting conversion technology is answered. Subsequently, different kinds of plasma setups are described, with specific detail for the plasma setup used in this thesis, i.e., the gliding arc plasmatron (GAP).

In Chapter 2, we evaluate the performance of this GAP for the conversion of CO_2, in terms of energy cost and efficiency, for a wide range of conditions of plasma power and gas flow rate, and for different anode diameters of the setup. The best performance, in terms of both conversion and energy cost/efficiency, is reached in the configuration with the smallest anode diameter of 7.08 mm. The highest conversion of 8.6 % is obtained at an energy cost of 39 kJ/L (or 9.7 eV/molec) and an energy efficiency of 30 %, whereas the highest energy efficiency in this configuration is 35 %, corresponding to an energy cost of 33 kJ/L (or 8.3 eV/molec), but at a somewhat reduced conversion of 5.1 %. In general, we can conclude that the GAP is very promising for CO_2 conversion, but we believe there is still room for improvement. We compare our results with the conversion and energy efficiency of thermal CO_2 splitting, as well as with results of other types of plasmas and novel CO_2 conversion technologies. From model calculations, performed by S. Heijkers (also PhD student within PLASMANT), it is clear that vibrationally excited CO_2 significantly contributes to the CO_2

dissociation, and this can explain the good energy efficiency of CO_2 conversion in a GAP.

Chapter 3 presents for the first time high-speed camera images, which illustrate the arc stabilization process and the arc geometrical features in the GAP. Clearly, the arc movement and shape rely on a number of factors, such as gas turbulence, outlet diameter, electrode surface, gas contraction and buoyance force. We present results for different gas flow rates, arc currents and anode (outlet) diameters, showing how these parameters affect the arc diameter, rotation speed and elongation. The arc dynamics are correlated with the CO_2 conversion and energy efficiency, at exactly the same conditions, to explain the effect of these parameters on the CO_2 conversion process.

As N_2 is an important component in industrial waste streams, we investigate in Chapter 4 the effect of N_2 on the CO_2 conversion in the GAP, by means of experiments, supported by computer simulations, carried out by S. Heijkers. The addition of N_2 has a positive effect on the absolute CO_2 conversion up to 50 %, while at higher N_2 fractions, the effective CO_2 conversion and energy efficiency of this process drop. The simulations reveal that the CO_2 conversion mainly proceeds through the vibrational levels, which are populated through collision with the N_2 vibrational levels. In addition, NO and NO_2 are formed in the CO_2/N_2 mixture. Combining CO_2 and N_2 in a GAP thus could lead to combined CO_2 conversion and N_2 fixation. The highest amount of NOx obtained is 6761 ppm, which is however still below the minimum threshold of 1 % to make it effective for N_2 fixation. Computer simulations of G. Trenchev (another PhD student within PLASMANT) reveal that we will have to improve our reactor and gas inlet design to enhance the gas fraction that passes through the arc, as the latter will increase the CO_2 conversion, and thus also the NOx production. We compare the performance of our GAP reactor with other plasma types. Regarding CO_2 conversion, the best energy efficiency is reached in our GAP, while the conversion itself still

needs further improvement. In terms of NOx production, the NOx yield is still quite low (which is attributed to the limited CO_2 conversion), but the energy consumption is reasonable compared to other plasma types, certainly if we take into account that our energy consumption also includes the cost for CO_2 conversion. A more detailed comparison with a dielectric barrier discharge (DBD) is made, which is the only other work in literature where NOx production was also studied from a CO_2/N_2 mixture. From this comparison we can conclude that the GAP is superior for CO_2 conversion in the presence of N_2 compared to a DBD, due to its higher conversion, but especially the absence of N_2O, N_2O_3, N_2O_5 formation and the much higher energy efficiency.

To produce value-added chemicals and fuels, we investigate the dry reforming of methane (DRM) in Chapter 5 for different CH_4 fractions in the mixture, again supported by chemical kinetics modeling of S. Heijkers. The CO_2 and CH_4 conversion reach their highest values of approximately 18 and 10 %, respectively, at 25 % CH_4 in the gas mixture, which corresponds to an overall energy cost of 10 kJ/L (or 2.5 eV/molec) and an energy efficiency as high as 66 %. CO and H_2 are the major products. The CO_2 conversion clearly increases upon increasing CH_4 fraction in the mixture, which can be explained by the model. Our results demonstrate that the GAP is very promising for DRM, also in comparison with other plasma types, certainly when considering the energy efficiency (or energy cost). However, the conversion needs to be further improved.

In Chapter 6 we study the influence of the applied current, the gas flow rate and the addition of 80 % N_2 on the DRM. We can conclude that a higher applied current leads to a higher absolute and effective conversion, but its influence on the energy cost and energy efficiency is limited. A higher gas flow rate reduces the absolute and effective conversion, but its effect on the energy cost and energy efficiency is again limited. N_2, which is often present in industrial waste streams, has a

positive effect on the absolute CO_2 and CH_4 conversion. However, a high fraction of N_2 reduces the effective (total) conversion. Consequently, this has a negative effect on the energy cost and energy efficiency. Nevertheless, the obtained energy cost and efficiency are still good due to the specific properties of the GAP.

Before the GAP can be introduced on an industrial level, several aspects should be further investigated. An overview of these aspects is given in Chapter 7. In the first part of that chapter, a quantitative evaluation of the GAP for CO_2 conversion is made based on a techno-economic analysis (TEA), and using the results from the previous chapters. Subsequently, we also suggest qualitatively some further improvements needed for potential industrialization of the GAP.

Samenvatting

De problematiek rond klimaatverandering is niet meer weg te denken uit onze maatschappij. Ze krijgt steeds meer aandacht in de media en verschillende onderzoekers spitsen zich toe op technieken die de klimaatverandering binnen de perken kunnen houden. De oorzaak ligt bij de stijgende concentratie van CO_2 in onze atmosfeer. Het is dus noodzakelijk de uitstoot van CO_2 zoveel mogelijk te beperken. Een technologie die uitvoerig onderzocht wordt voor het omzetten van CO_2 in nuttige chemicaliën en brandstoffen is plasmatechnologie.

Een inleiding over plasma's wordt gegeven in Hoofdstuk 1. Ook wordt uitgelegd waarom plasma-gebaseerde conversie een interessante conversietechnologie kan zijn. Daarna worden verschillende plasma setups besproken, met in het bijzonder de plasma setup die gebruikt wordt in deze thesis, namelijk de gliding arc plasmatron (GAP).

In Hoofdstuk 2 wordt deze GAP onderzocht voor CO_2 conversie en geëvalueerd op basis van energiekost en energie-efficiëntie voor een wijde selectie van plasmavermogen en gasdebiet, en voor verschillende anode configuraties. De beste resultaten voor zowel conversie als energie kost/efficiëntie worden gehaald in de configuratie met de kleinste anode diameter (7,08 mm). De hoogste conversie van 8,6 % wordt bereikt bij een energiekost van 39 kJ/L (of 9,7 eV/molecule) en een energie-efficiëntie van 30 %. De hoogste energie-efficiëntie in deze configuratie is 35 %, overeenkomend met een energiekost van 33 kJ/L (of 8,3 eV/molecule), maar dit is bij een lagere conversie van 5,1 %. Algemeen kunnen we concluderen dat de GAP veelbelovend is voor CO_2 conversie en we geloven dat er nog ruimte is voor verbetering. We hebben onze resultaten vergeleken met thermische CO_2 splitsing, maar ook met de resultaten van andere plasmatypes en andere CO_2 conversietechnieken. Simulaties, uitgevoerd door S. Heijkers (ook een doctoraatsstudent bij PLASMANT), geven aan dat vibrationeel geëxciteerd CO_2 aanzienlijk bijdraagt aan de

splitsing van CO_2, wat ook de goede energie-efficiëntie in de GAP verklaart.

In Hoofdstuk 3 worden foto's getoond die genomen zijn met een hogesnelheidscamera, waaruit de stabilisatie en de geometrie van de boog duidelijk worden. De beweging van de boog en zijn vorm zijn afhankelijk van een aantal factoren, zoals gasturbulentie, de uitlaatdiameter, elektrode-oppervlak en gasstroming. Er worden resultaten weergegeven voor verschillende gasdebieten, stroomsterktes en anode (uitlaat) diameters. Ze laten zien hoe deze parameters de boog diameter, rotatiesnelheid en verlenging van de boog beïnvloeden. De beweging en vorm van de boog worden gecorreleerd met de CO_2 conversie en energie-efficiëntie om het effect van deze parameters op het CO_2 conversieproces te kunnen verklaren.

Als belangrijke component in industriële afvalstromen, onderzoeken we in Hoofdstuk 4 het effect van N_2 op de CO_2 conversie in een GAP, door het uitvoeren van experimenten die ondersteund worden door computersimulaties, uitgevoerd door S. Heijkers. Toevoegen van N_2 heeft een positief effect op de absolute CO_2 conversie tot 50 % N_2. Bij grotere concentraties zal de effectieve CO_2 conversie en de energie-efficiëntie echter dalen. Uit simulaties blijkt dat de CO_2 conversie voornamelijk doorgaat via de vibrationele niveaus, die worden bevolkt door botsing met vibrationeel geëxciteerde N_2 moleculen. Bovendien wordt ook NO en NO_2 gevormd. Het tegelijk omvormen van CO_2 en N_2 in een GAP kan dus leiden naar een gecombineerde CO_2 conversie en N_2 fixatie. De hoogste concentratie NOx geproduceerd is 6761 ppm. Dit is nog te laag om het effectief te gebruiken voor N_2 fixatie, waarvoor een minimum van 1 % is gedefinieerd. Computersimulaties van G. Trenchev (een andere doctoraatsstudent bij PLASMANT) voorspellen dat het design van de reactor en de gasinlaat moet aangepast worden om de fractie van het gas dat door de boog gaat te verhogen, waardoor de CO_2 conversie en dus ook de NOx productie stijgt. We vergelijken de resultaten van onze GAP

reactor met andere plasmatypes. Wat betreft CO_2 conversie, is de energie-efficiëntie in de GAP het hoogst, terwijl de conversie zelf nog verbetert dient te worden. Als we kijken naar NOx productie, zien we dat die nog te laag is (als gevolg van de gelimiteerde CO_2 conversie), maar de energieconsumptie is vergelijkbaar met andere plasma types. Een meer gedetailleerde vergelijking met een diëlektrische barrière ontlading (DBD) wordt gemaakt. Uit deze vergelijking kunnen we concluderen dat de GAP een betere kandidaat is voor CO_2 conversie in de aanwezigheid van N_2 ten opzichte van een DBD, door de hogere conversie maar vooral omdat N_2O, N_2O_3, N_2O_5 niet gevormd worden en door de zeer hoge energie-efficiëntie.

Om waardevolle chemicaliën en brandstoffen te vormen, onderzoeken we in Hoofdstuk 5 de reactie van CO_2 met CH_4, ook wel dry reforming van methaan (DRM) genoemd. Deze reactie wordt experimenteel onderzocht voor verschillende CH_4 concentraties in het startmengsel en opnieuw worden de experimenten ondersteund door simulaties uitgevoerd door S. Heijkers. De hoogst behaalde waarden voor CO_2 en CH_4 conversie zijn respectievelijk 18 en 10 % bij 25 % CH_4 in het startmengsel. Dit komt overeen met een energiekost van 10 kJ/L (of 2,5 eV/molecule) en een energie-efficiëntie van 66 %. CO en H_2 zijn de belangrijkste producten. Het is duidelijk dat de CO_2 conversie stijgt bij een stijgende hoeveelheid van CH_4 in het startmengsel, wat verklaard kan worden door de computersimulaties. Onze resultaten tonen aan dat de GAP veelbelovend is voor DRM wat betreft energie-efficiëntie, vergeleken met andere plasma types. De conversie dient echter nog verbeterd te worden.

De invloed van de stroomsterkte, het gasdebiet en een toevoeging van 80 % N_2 op DRM wordt onderzocht in Hoofdstuk 6. Uit deze experimenten kan geconcludeerd worden dat een hogere stroomsterkte leidt tot een hogere absolute en effectieve conversie. De invloed van de stroomsterkte op de energiekost en de energie-efficiëntie is beperkt. Een

toename in het gasdebiet heeft een negatief effect op de absolute en effectieve conversie. Opnieuw wordt de energiekost en energie-efficiëntie weinig beïnvloed door een verandering in gasdebiet. N_2, dat vaak aanwezig is in industriële afvalstromen, heeft een positief effect op de absolute CO_2 en CH_4 conversie. Een hoge fractie N_2 heeft echter een negatief effect op de effectieve (totale) conversie. Als gevolg heeft dit ook een negatief effect op de energiekost en de energie-efficiëntie. Toch is de bekomen energie-efficiëntie hoog door de specifieke eigenschappen van een GAP.

Voor de GAP kan gebruikt worden in de industrie zijn er vele andere aspecten die nog verder onderzocht dienen te worden. Een overzicht van deze aspecten wordt gegeven in Hoofdstuk 7. In het eerste deel van dat hoofdstuk is een kwantitatieve evaluatie van de GAP voor CO_2 conversie gemaakt op basis van een techno-economische analyse en de resultaten uit de voorgaande hoofdstukken. Vervolgens stellen we op een kwalitatieve manier een aantal verbeterpunten voor die nodig zijn voor een mogelijke industrialisatie van de GAP.

Publications

- **M. Ramakers**, I. Michielsen, R. Aerts, V. Meynen, A. Bogaerts, Plasma Process. Polym. (2015), 12, 755.

- S. Vermeylen, J. De Waele, S. Vanuytsel, J. De Backer, J. Van der Paal, **M. Ramakers**, K Leyssens, E. Marcq, J. Van Audenaerde, E. L. J. Smits, S. Dewilde, A. Bogaerts, Plasma Process Polym. (2016), 13, 1195.

- **M. Ramakers**, G. Trenchev, S. Heijkers, W. Wang, A. Bogaerts, ChemSusChem (2017), 10, 2642.

- E. Cleiren, S. Heijkers, **M. Ramakers**, A. Bogaerts, ChemSusChem (2017), 10, 4025.

- **M. Ramakers**, J. A. Medrano, G. Trenchev, F. Gallucci, A. Bogaerts, Plasma Sources Sci. Technol. (2017), 26, 125002.

- G. Trenchev, S. Kolev, W. Wang, **M. Ramakers**, A. Bogaerts, The Journal of Physical Chemistry C (2017), 121, 24470.

- S. Gröger, **M. Ramakers**, M. Hamme, J.A. Medrano, N. Bibinov, F. Gallucci, A. Bogaerts, P. Awakowicz, J. Phys. D: Appl. Phys. (2019), 52, 065201.

Conference contributions

- Poster presentations July 5 – 10, 2015

22nd International Symposium on Plasma Chemistry (ISPC 22), Antwerp, Belgium:

1. CO_2 conversion in a dielectric barrier discharge upon addition of argon or helium: How noble gases can save the world from global warming
2. Plasma treatment of melanoma cells by a He/O_2 µ-plasma jet

- Oral presentation August 1 – 5, 2016

10th International Symposium on Non-Thermal/Thermal Plasma Pollution Control Technology and Sustainable Energy (ISNTP 10), Florianopolis, Brazil: CO_2 conversion in a gliding arc plasmatron

- Oral presentation August 21 – 24, 2016

International Workshop on Plasmas for Energy and Environmental Applications (IWPEEA), Liverpool, UK: Improving the energy efficiency of CO_2 conversion by means of a gliding arc plasmatron

- Poster presentation October 24 – 26, 2016

Chemical Research in Flanders (CRF) Symposium, Blankenberge, Belgium: Using a gliding arc plasmatron for CO_2 conversion: A new method for making fuels?

- Poster presentation July 2 – 6, 2017

iPlasmaNano-VIII, Antwerp, Belgium: Using a gliding arc plasmatron for CO_2 conversion

- Poster pitch and poster presentation July 30 – August 4, 2017

23rd International Symposium on Plasma Chemistry (ISPC 23), Montreal, Canada: Converting CO_2 into value-added chemicals: Dry reforming in a gliding arc plasmatron

- Oral presentation March 15 – 16, 2018

6th Conference on Carbon Dioxide as Feedstock for Fuels, Chemistry and Polymers, Cologne, Germany: Carbon dioxide as feedstock for value-added chemicals and fuels in a gliding arc plasmatron

- Oral presentation July 1 – 5, 2018

11th International Symposium on Non-Thermal/Thermal Plasma Pollution Control Technology and Sustainable Energy (ISNTP 11), Montegrotto Terme, Italy: Dry reforming of methane in a gliding arc plasmatron

Awards

- **Best oral presentation** award at the 'International Workshop on Plasmas for Energy and Environmental Applications (IWPEEA)', Liverpool, UK, August 21 – 24, 2016, for the contribution entitled: Improving the energy efficiency of CO_2 conversion by means of a gliding arc plasmatron.

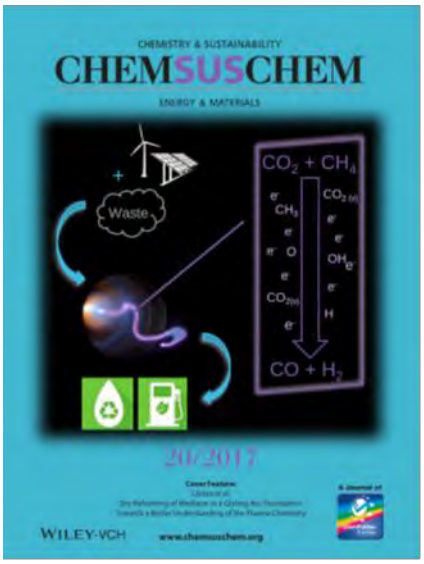

- **Cover** for publication E. Cleiren, S. Heijkers, M. Ramakers, A. Bogaerts, ChemSusChem (2017), 10, 4025.

- **Eos Pipet 2018**. Both jury- and public prize for most promising researcher of 2018.

Collaborations with other research groups (including research visit)

- Research visit, Drexel University – **Drexel Plasma Institute** (DPI), Philadelphia, United States, for the design and operation of the gliding arc plasmatron, August 3 – 8, 2014.

- Collaboration with Eindhoven University of Technology (**TU/e**), Eindhoven, The Netherlands, to study the arc dynamics in the gliding arc plasmatron with high-speed camera, 2016.

- Collaboration with Dutch Institute for Fundamental Energy Research (**DIFFER**), Eindhoven, The Netherlands, to study the plasma properties in the gliding arc plasmatron with laser scattering, 2017.

- Collaboration with Ruhr-Universität Bochum (**RUB**), Bochum, Germany, to study the plasma properties in the gliding arc plasmatron with optical emission spectroscopy, 2017.

Dankwoord - Acknowledgements

Na zowel mijn bachelor- als mijn masterproef voltooid te hebben bij PLASMANT, was het voor mij een logische stap om ook in deze onderzoeksgroep aan een doctoraat te beginnen. Het onderzoek naar CO_2 omzetting binnen de groep sprak me enorm aan door de maatschappelijke relevantie die gelinkt is aan de klimaatverandering. Dat laatste is trouwens nog altijd een onderwerp waar ik bezorgd om ben. Ik hoop dan ook om in de toekomst (al dan niet door onderzoek) nog steeds bij te dragen aan de strijd tegen klimaatverandering.

Het voltooien van een doctoraat is niet vanzelfsprekend. Voor mij is het een enorme leerschool geweest op zowel persoonlijk als professioneel vlak. Het is zeker niet iets dat je alleen doet. Daarom wil ik van deze gelegenheid gebruik maken om een aantal personen te bedanken die mij op één of andere manier geholpen hebben.

Eerst en vooral wil ik Annemie bedanken om mij als promotor de kans te geven om te doctoreren en steeds vertrouwen te hebben in mijn manier van werken en mijn beslissingen. Ik vind het enorm fijn dat ik tijdens de afgelopen jaren mijn ding heb kunnen doen en uw steun hier steeds in vond. Het leiden van zo'n grote onderzoeksgroep is bewonderingswaardig en ik vraag me vaak af hoe u zo snel feedback kan geven terwijl uw dagen altijd volgepland zijn. Het harde werk dat u levert voor zowel mij als de hele groep is alleszins iets dat ik van harte apprecieer. Ik ben dan ook oprecht blij dat ik in uw onderzoeksgroep terecht gekomen ben.

Daarnaast bedank ik ook alle(!) collega's van PLASMANT (zonder ze allemaal bij naam te noemen). Vanaf mijn masterthesis heb ik met één daarvan een speciale band, ontstaan als "team M&I". Inne, heel erg bedankt om altijd je enthousiaste zelf te zijn en mij te helpen bij problemen in het labo (en nog veel meer). Ik wens je nog heel veel succes

bij het afronden van je doctoraat en op je nieuwe job! Robby en Ramses, ik beschouw jullie als mijn leermeesters. Jullie hebben me veel geleerd over labowerk en de organisatie ervan. Yannick, ingenieur van de groep, wist ook altijd raad bij technische problemen in het labo. Ik was steeds opgelucht, na lang zelf te zitten zoeken, dat jij snel met de oplossing kwam. Dat heeft me dan ook geleerd om iets sneller hulp te vragen als je er zelf niet uit geraakt.

I'm also happy to have met Abraham in the US when I started my PhD. After seeing him again at a few conferences, it was nice that he started as a post-doc in our group. The constant smile on his face instantly makes you happy. Charlotta kwam pas in de onderzoeksgroep toen ik begon met het afronden van mijn werk maar was snel enthousiast om mij te vergezellen tijdens mijn middagwandelingen waardoor er ook snel een goede band ontstond.

Stijn en Georgi wil ik graag bedanken voor het uitvoeren van de simulaties die hielpen om mijn experimentele resultaten te verklaren. Uit deze samenwerking zijn ook een aantal mooie publicaties voortgekomen. Thank you Georgi for also helping with electrical problems in the lab and fixing the resistors many times. Your knowledge in these things really helped me in my research.

Daarnaast wil ik Emelie en Bart nog bedanken om zo goed de taken die ik hen gaf, uit te voeren. Het was heel aangenaam jullie te begeleiden tijdens jullie master- en bachelor thesis.

Niet enkel directe collega's hebben bijgedragen aan mijn thesis, maar ook een aantal externen zoals Jose en Hakan. I both want to thank you for the effort you have put into our collaboration.

De sfeer op kantoor zat altijd goed en daar wil ik zowel de vroegere (Antonin) als huidige (Maryam, Amin en Inne) kantoorcollega's voor bedanken.

Luc (en op het einde van mijn doctoraat ook Karel) stond altijd klaar om te helpen. Voor labo-gerelateerde zaken kon ik steeds bij Karen terecht. Fabiana, Ingrid en Nelly hielpen me bij de administratieve zaken. Ik wil hen allen bedanken voor hun hulp.

Gilles en Eddie (en ook de anderen) van de mechanische werkplaats wil ik bedanken om altijd zeer snel de nieuwe ontwerpen mee te ontwikkelen en te realiseren. Peter kwam me steeds uit de nood helpen bij elektrische problemen, bedankt daarvoor.

De mensen die ik heb ontmoet op congressen hebben ervoor gezorgd dat de tijd die ik in het buitenland doorbracht zeer aangenaam was. Ik heb daarnaast ook vaak nieuwe ideeën opgedaan uit de gesprekken met hun.

Mijn vrienden binnen en buiten de duikclub zorgden voor de nodige afleiding tijdens de vaak drukke periodes. Ik wil ze bedanken voor de ontspannende momenten die leuke herinneringen opleverden. Het deed me ook plezier dat ze interesse toonden in mijn onderzoek. In het bijzonder wil ik Yves bedanken om mijn idee van de cover afbeelding zo mooi uit te werken.

Mijn ouders staan steeds voor me klaar en hebben me telkens gesteund in mijn keuzes. Ik kan ze hiervoor niet genoeg bedanken. Mijn grootouders wil ik bedanken voor het duimen en kaarsjes branden bij belangrijke gebeurtenissen in mijn leven.

Als laatste wil ik mijn vriend Jasper bedanken. In dezelfde situatie als mij, begrijpt hij me beter dan geen ander. Bedankt om er steeds voor mij te zijn en me gerust te stellen wanneer ik me ergens zorgen om maak.

Faculteit Wetenschappen

Departement Chemie

Antwerpen 2019

Universiteit Antwerpen